FAKULTÄT FÜR !NFORMATIK
Faculty of Informatics

Visual Analysis of Methods for Processing 3D X-ray Computed Tomography Data of Advanced Composites

DISSERTATION

zur Erlangung des akademischen Grades

Doktor der Technischen Wissenschaften

eingereicht von

Dipl.-Ing. Johannes Weissenböck, BSc
Matrikelnummer 0325215

an der Fakultät für Informatik

der Technischen Universität Wien

Betreuung: Ao.Univ.Prof. Dipl.-Ing. Dr.techn. Eduard Gröller
Zweitbetreuung: Dipl.-Ing. (FH) Dr.techn. Christoph Heinzl

Diese Dissertation haben begutachtet:

Rüdiger Westermann

Gerik Scheuermann

Wien, 4. November 2019

Johannes Weissenböck

Die approbierte gedruckte Originalversion dieser Dissertation ist an der TU Wien Bibliothek verfügbar.
The approved original version of this doctoral thesis is available in print at TU Wien Bibliothek.
TU Bibliothek Your knowledge hub

Die approbierte gedruckte Originalversion dieser Dissertation ist an der TU Wien Bibliothek verfügbar.
The approved original version of this doctoral thesis is available in print at TU Wien Bibliothek.

FAKULTÄT FÜR !NFORMATIK
Faculty of Informatics

Visual Analysis of Methods for Processing 3D X-ray Computed Tomography Data of Advanced Composites

DISSERTATION

submitted in partial fulfillment of the requirements for the degree of

Doktor der Technischen Wissenschaften

by

Dipl.-Ing. Johannes Weissenböck, BSc
Registration Number 0325215

to the Faculty of Informatics

at the TU Wien

Advisor: Ao.Univ.Prof. Dipl.-Ing. Dr.techn. Eduard Gröller
Second advisor: Dipl.-Ing. (FH) Dr.techn. Christoph Heinzl

The dissertation has been reviewed by:

Rüdiger Westermann

Gerik Scheuermann

Vienna, 4th November, 2019

Johannes Weissenböck

Die approbierte gedruckte Originalversion dieser Dissertation ist an der TU Wien Bibliothek verfügbar.
The approved original version of this doctoral thesis is available in print at TU Wien Bibliothek.
TU Bibliothek Your knowledge hub

Die approbierte gedruckte Originalversion dieser Dissertation ist an der TU Wien Bibliothek verfügbar.
The approved original version of this doctoral thesis is available in print at TU Wien Bibliothek.

Erklärung zur Verfassung der Arbeit

Dipl.-Ing. Johannes Weissenböck, BSc

Hiermit erkläre ich, dass ich diese Arbeit selbständig verfasst habe, dass ich die verwendeten Quellen und Hilfsmittel vollständig angegeben habe und dass ich die Stellen der Arbeit – einschließlich Tabellen, Karten und Abbildungen –, die anderen Werken oder dem Internet im Wortlaut oder dem Sinn nach entnommen sind, auf jeden Fall unter Angabe der Quelle als Entlehnung kenntlich gemacht habe.

Wien, 4. November 2019

Johannes Weissenböck

Die approbierte gedruckte Originalversion dieser Dissertation ist an der TU Wien Bibliothek verfügbar.
The approved original version of this doctoral thesis is available in print at TU Wien Bibliothek.
TU WIEN Bibliothek Your knowledge hub

Die approbierte gedruckte Originalversion dieser Dissertation ist an der TU Wien Bibliothek verfügbar.
The approved original version of this doctoral thesis is available in print at TU Wien Bibliothek.

Acknowledgements

This thesis results from six years of close collaboration between the Research Unit Computer Graphics at the Institute of Visual Computing and Human-Centered Technology at the Vienna University of Technology and the Research Group Computed Tomography at the University of Applied Sciences Upper Austria – Wels Campus. I would like to thank Meister Eduard Gröller and Christoph Heinzl for their excellent supervision and guidance, especially for their dedication to the development of new ideas, for the helpful discussions and feedback, and for their ability to motivate me despite setbacks. I would also like to thank all my co-authors and colleagues from the Research Group Computed Tomography for supporting this work and for the pleasant teamwork. Moreover, I would like to thank the Research Unit Computer Graphics for their valuable advice in designing the concepts and for their suggestions and criticisms when preparing for conference talks.

The presented work has received funding from the European Union Seventh Framework Programme (FP7/2007- 2013) under grant agreement Nº314562: Quantitative Inspection of Complex Composite Aeronautic Parts Using Advanced X-ray Techniques (QUICOM), from the FFG Bridge Early Stage project Nº851249: Advanced Multimodal Data Analysis and Visualization of Composites Based on Grating Interferometer Micro-CT Data (ADAM), from the K-Project PSSP, supported by the COMET Programme of the FFG and by the federal government of Upper Austria and Styria, and from the Research Foundation Flanders (FWO) and the Austrian Science Fund (FWF) under the grant agreement NºG0F9117N and NºI3261-N36 respectively: Quantitative X-ray Tomography of Advanced Polymer Composites. This work was also partly written in collaboration with the VRVis Competence Center. VRVis is funded by BMVIT, BMWFW, Styria, SFG, and the Vienna Business Agency in the scope of COMET-Competence Centers for Excellent Technologies (Nº854174), which is managed by FFG.

Die approbierte gedruckte Originalversion dieser Dissertation ist an der TU Wien Bibliothek verfügbar.
The approved original version of this doctoral thesis is available in print at TU Wien Bibliothek.
TU WIEN Bibliothek Your knowledge hub

Die approbierte gedruckte Originalversion dieser Dissertation ist an der TU Wien Bibliothek verfügbar.
The approved original version of this doctoral thesis is available in print at TU Wien Bibliothek.

Abstract

Advanced composites have excellent mechanical properties at low weight and can be realized as complex components that can be manufactured quickly and cost-effectively. Due to these outstanding characteristics, these materials are used in many different areas of industry, such as aviation and automotive. Industrial 3D X-ray computed tomography (XCT) is used as a non-destructive testing (NDT) method to inspect the quality of components and to develop new advanced composite materials. XCT has the ability to determine the inner and outer geometries of a specimen non-destructively. For example, interesting features in fiber-reinforced polymers (FRPs) such as fibers, pores, and higher-density inclusions can be detected. The high resolutions of modern XCT devices generate large volume datasets, which reveal very fine structures. However, this high information content makes the exploration and analysis of the datasets with conventional methods very difficult and time-consuming.

In this doctoral thesis, typical NDT application scenarios of advanced composites using XCT are addressed and visual analysis methods and visualization techniques are designed to provide material experts with tools to improve their workflow and to efficiently analyze the XCT data, so that domain-specific questions can be answered easily and quickly. This work describes a novel visualization system for the interactive exploration and detailed analysis of FRPs, a tool for the visual analysis and evaluation of segmentation filters to accurately determine porosity in FRPs, and a more general system for the visual comparison of interesting features in an ensemble of XCT datasets are presented. The results of the individual visualization systems are presented using real-world and simulated XCT data. The proposed visual analysis methods support the experts in their workflows by enabling improved data analysis processes that are simple, fast, and well-founded, and provide new insights into material characterization with XCT.

Die approbierte gedruckte Originalversion dieser Dissertation ist an der TU Wien Bibliothek verfügbar.
The approved original version of this doctoral thesis is available in print at TU Wien Bibliothek.
TU WIEN Bibliothek Your knowledge hub

Die approbierte gedruckte Originalversion dieser Dissertation ist an der TU Wien Bibliothek verfügbar.
The approved original version of this doctoral thesis is available in print at TU Wien Bibliothek.

Kurzfassung

Hochleistungsverbundwerkstoffe weisen hervorragende mechanische Eigenschaften bei gleichzeitig geringem Gewicht auf und erlauben es, komplexe Bauteile zu realisieren, die relativ schnell und kostengünstig produziert werden können. Aufgrund dieser Besonderheiten werden diese Werkstoffe in vielen verschiedenen Bereichen der Industrie, wie etwa im Flugzeug- und Automobilbau verwendet. Um Bauteile in Hinblick auf ihre Qualität überprüfen beziehungsweise neue Hochleistungsverbundmaterialien entwickeln zu können, wird die industrielle 3D-Röntgencomputertomographie (XCT) als zerstörungsfreies Prüfverfahren eingesetzt. Die industrielle Röntgencomputertomographie besitzt dabei die Fähigkeit, die inneren und äußeren Geometrien einer Probe zerstörungsfrei zu bestimmen. So können interessante Merkmale in faserverstärkten Kunststoffen (FRPs), wie zum Beispiel Fasern, Poren, und Einschlüsse erfasst werden. Die hohen Auflösungen von modernen XCT-Geräten erzeugen dabei große Volumendatensätze, die sehr feine unterschiedliche Strukturen erkennen lassen. Dieser hohe Informationsgehalt führt aber dazu, dass die Exploration und Analyse der Datensätze mit herkömmlichen Methoden nur sehr schwer zu bewerkstelligen und zeitaufwendig ist.

Im Rahmen dieser Dissertation werden typische Anwendungsszenarien der zerstörungsfreien Prüfung von Hochleistungsverbundwerkstoffen mittels XCT aufgegriffen und visuelle Analysemethoden und Visualisierungstechniken entworfen. Damit werden Materialexperten Werkzeuge zur Verfügung gestellt, mit denen sie ihre Arbeitsabläufe verbessern und die XCT-Daten effizient analysieren können, sodass fach-spezifische Fragestellungen einfach und schnell beantwortet werden können. Dazu wird ein neuartiges Visualisierungssystem zur interaktiven Exploration und detaillierten Analyse von FRPs vorgestellt, ein Werkzeug zur visuellen Analyse und Evaluierung von Segmentierungsfiltern, um die Porosität in FRPs genau bestimmen zu können und ein generelles System für den visuellen Vergleich von interessanten Merkmalen in einem Ensemble von XCT-Datensätzen. Dabei werden die Ergebnisse der einzelnen Visualisierungssysteme anhand von realen und simulierten XCT-Daten vorgestellt. Die vorgeschlagenen visuellen Analysemethoden unterstützen die Experten in ihren Arbeitsabläufen, indem sie verbesserte Datenanalyseprozesse ermöglichen, die einfach, schnell und fundiert sind und neue Erkenntnisse auf dem Gebiet der Materialcharakterisierung mit XCT liefern.

Die approbierte gedruckte Originalversion dieser Dissertation ist an der TU Wien Bibliothek verfügbar.
The approved original version of this doctoral thesis is available in print at TU Wien Bibliothek.
TU Bibliothek WIEN Your knowledge hub

Die approbierte gedruckte Originalversion dieser Dissertation ist an der TU Wien Bibliothek verfügbar.
The approved original version of this doctoral thesis is available in print at TU Wien Bibliothek.

Contents

Abstract **ix**

Kurzfassung **xi**

Contents **xiii**

1 Introduction **1**
1.1 Advanced Composites 2
1.2 Industrial 3D X-ray Computed Tomography 6
1.3 Contributions of the Thesis 10

2 FiberScout **15**
2.1 Introduction 16
2.2 Related Work 19
2.2.1 Visualization and Analysis of Material Systems 19
2.2.2 Parameter-space Exploration 19
2.2.3 Visual Exploration 20
2.3 Dataset Description and Preprocessing 20
2.3.1 Dataset Description 20
2.3.2 Preprocessing 22
2.4 Visualization 22
2.4.1 Visual Fiber Exploration 23
2.4.1.1 Parallel Coordinates Plot (PCP) for Fibers 23
2.4.1.2 Scatter Plot Matrix (SPLOM) for Fibers 24
2.4.1.3 Fiber Class Explorer 24
2.4.2 Fiber Orientation Distribution (FOD) 26
2.4.3 Fiber Length Distribution (FLD) 27
2.4.4 Blob Visualization 28
2.4.5 Fiber Metadata Visualization 30
2.5 Results and Evaluation 32
2.5.1 Visualization Results 32
2.5.2 Evaluation and User Feedback 32
2.6 Implementation 35
2.7 Summary and Conclusion 35

Die approbierte gedruckte Originalversion dieser Dissertation ist an der TU Wien Bibliothek verfügbar.
The approved original version of this doctoral thesis is available in print at TU Wien Bibliothek.
TU WIEN Bibliothek Your knowledge hub

3 PorosityAnalyzer **37**
3.1 Introduction . . . 38
3.2 Related Work . . . 41
3.3 Dataset Description . . . 43
3.4 Setup of Segmentation Pipelines . . . 45
3.5 Visual Analysis and Evaluation of Pore Segmentation-Pipelines . . . 50
3.5.1 Prefiltering Stage . . . 51
3.5.2 Overview Stage . . . 52
3.5.3 Analysis Stage . . . 53
3.5.4 Visual Examination Stage . . . 56
3.6 Evaluation and Domain Feedback . . . 58
3.7 Case Studies . . . 61
3.7.1 Porosity Determination with Non-Parametric Segmentation Pipelines 61
3.7.2 Influence of Edge-Preserving Smoothing on Porosity Determination 63
3.8 Implementation . . . 68
3.9 Summary and Conclusion . . . 68

4 Dynamic Volume Lines **69**
4.1 Introduction . . . 70
4.2 Related Work . . . 74
4.3 Datasets . . . 75
4.3.1 Data Acquisition . . . 75
4.3.2 Dataset Description . . . 76
4.4 Dynamic Volume Lines . . . 78
4.4.1 Hilbert Space-Filling Curve Generation . . . 79
4.4.2 Nonlinear Scaling of the Hilbert Line Plots . . . 81
4.4.3 Visualization Techniques . . . 82
4.4.3.1 Interactive Histogram Heatmap Visualization . . . 83
4.4.3.2 Interactive 1D Hilbert Line Plot Visualization . . . 84
4.4.3.3 Scaling Widget Visualization . . . 86
4.5 Case Studies . . . 86
4.5.1 Artificial Specimen from Simulated XCT . . . 86
4.5.2 Real-world TLGI-XCT Foam Specimen . . . 87
4.5.3 Implementation and Performance Measurements . . . 92
4.6 Conclusion and Future Work . . . 92

5 Summary and Conclusion **93**

Bibliography **99**

Appendix **111**
FiberScout Evaluation Questionnaire . . . 112
PorosityAnalyzer Evaluation Questionnaire . . . 120

Curriculum Vitae **142**

Die approbierte gedruckte Originalversion dieser Dissertation ist an der TU Wien Bibliothek verfügbar.
The approved original version of this doctoral thesis is available in print at TU Wien Bibliothek.
TU WIEN Bibliothek Your knowledge hub

Die approbierte gedruckte Originalversion dieser Dissertation ist an der TU Wien Bibliothek verfügbar.
The approved original version of this doctoral thesis is available in print at TU Wien Bibliothek.

CHAPTER 1

Introduction

The quest for greater efficiency, environmental protection, safety, and comfort is the driving force in industrial research for the development of new cost-effective, functional and lightweight components. Advanced composite materials, such as fiber-reinforced polymers (FRPs), meet these requirements and are of great interest for today's industry due to their impressive mechanical properties and their versatile processing and application possibilities. Components that are currently manufactured from conventional materials such as aluminum or steel can be replaced by these new high-performance materials. The functionality of such components is not impaired, but they have increased strength and stiffness with lower weight at the same time [FL96, FA13].
The industrial sectors aerospace, automotive, wind energy, electrical engineering, and sport and leisure have recognized the potential of FRPs and will rely on these material systems in the coming years. As reported by Sauer et al. [SKW17], the global demand for carbon fiber-reinforced polymers (CFRPs) is growing at an annual rate between 10 and 13%. The global demand for carbon fiber-reinforced polymers was 59,000 tons in 2011 and is forecasted at 194,000 tons for 2022. At 60% (US$ 11.66 billion), the aerospace industry accounts for the largest share of total worldwide turnover for the carbon composite market due to high quality standards and approval costs. This can be attributed to developments in civil aviation. For example, the share of fiber-reinforced composite materials in newly developed commercial aircrafts such as the A350 (Airbus) and the 787 Dreamliner (Boeing) has increased to more than 52% in recent years [Hes14, Giu15]. In addition, the carrier rockets Ariane 6 (ESA/ASL) [Bla18] as well as the Falcon9 (SpaceX) [Mil18] are designed in large proportions with the aid of carbon composites.

Due to the increasing share of advanced composites and respective components, the demand for non-destructive testing (NDT) is also growing rapidly, as it covers the topics of defect analysis and material characterization. A method of NDT is industrial 3D X-ray computed tomography (XCT). It has the ability to determine the inner and outer

geometries of a component non-destructively [DCCK+14]. Currently available XCT systems are capable of resolving structures of less than one micrometer [KPR12]. With these high-resolution measurements, it is possible to resolve internal material features such as individual fibers, pores, and inclusions and to determine their orientation and length. These possibilities are decisive for materials research and development, as the mechanical processes within a specimen can be deduced and important component properties in terms of stiffness, strength, and ductility can be determined. In addition, XCT is increasingly used in quality control and dimensional metrology to check the material qualities and tolerances required by industry.

Since the resolution of XCT systems is constantly being improved and as a result the information content of a volume dataset increases, the areas of NDT, i.e., error analysis and material characterization, are confronted with new challenges in order to reasonably explore and analyze the immense amount of data. Therefore, suitable and meaningful visualization techniques and image processing algorithms are necessary, for example to answer questions regarding material fatigue of a component or simply to improve the workflows of the experts.

1.1 Advanced Composites

Composite materials in general consist of two or more components, a reinforced agent or a selected filler and a compatible matrix binder (or resin). The components remain separated within the final structure, but nevertheless act together and provide improved material properties compared to conventional materials, which cannot be achieved by any of the components alone [Lub82]. The components are mostly fibers surrounded by a matrix. The fibers serve as the actual reinforcement, have a high tensile strength, but a low shear strength (i.e., they are brittle). They are made for instance of glass, carbon, aramid, boron, silicon carbide, alumina, high-density polyethylene, basalt, or cellulose. The matrix helps to distribute the load from the reinforcement, absorbs energy, reduces stress concentrations and prevents crack propagation. At the same time, the matrix should have a relatively high shear strength in order to make the fibers resistant to abrasion and other external environmental influences. The matrix consists of a material that can be assigned to one of four categories: polymers, metals, ceramics, and carbon [Zwe06, Che12].

In this thesis we concentrate on fiber-reinforced polymers (or fiber-reinforced plastics), a group of composite materials consisting of a polymer matrix (resin) reinforced by fibers. The polymer is usually a thermosetting epoxy, vinyl ester, or polyester plastic. The fibers are typically made of carbon or glass. Due to their low weight, corrosion resistance, high strength and stiffness, fiber-reinforced polymers are ideal for designs that require weight savings, precision engineering, tight tolerances, and simplification of components in production and operation. For example, carbon fiber-reinforced polymers (CFRPs) have five times the relative stiffness of steel, and glass fiber-reinforced polymers allow weight savings of up to 60% over aluminum. In addition, fiber-reinforced polymers can

Die approbierte gedruckte Originalversion dieser Dissertation ist an der TU Wien Bibliothek verfügbar.
The approved original version of this doctoral thesis is available in print at TU Wien Bibliothek.
TU Bibliothek Your knowledge hub WIEN

be produced cost-effectively because the expensive and scarce resins can be stretched with inexpensive and readily available fillers. For example, an injection molded polymer part can be produced cheaper, faster, easier, with more accurate tolerances, and higher material strength than a similar aluminum or steel part [Mas13].

In order to produce a composite structure, a large number of fibers are incorporated into a thin layer of the matrix, which forms a lamina (or ply). A lamina can be constructed from continuous (long) fibers or discontinuous (short) fibers. If continuous (long) fibers are used, their orientation can be unidirectional (i.e., all fibers are oriented in one direction, see Figure 1.1 A), bidirectional (i.e., fibers are oriented in two directions, typically perpendicular to each other, see Figure 1.1 B) or multi-directional (i.e., fibers are oriented in more than two directions, see Figure 1.1 C). A composite material with a lamina having unidirectionally oriented fibers, has the highest strength in the longitudinal direction of the fibers and a very low strength in the transverse direction. For a lamina having bi- and multi-directional fibers, the strength in the longitudinal and transverse directions can be changed by varying the fiber quantity and architecture. This means that forces acting simultaneously in several directions can be absorbed by fibers aligned in several different directions. Bi- and multi-directional fibers can be produced in two or three dimensions using weaving, knitting, braiding, and stitching processes commonly used in the textile industry (see Figure 1.2 A–D). This improves the interlaminar properties and prevents delamination. The discontinuous (short) fibers can be oriented either unidirectionally (see Figure 1.1 D) or randomly (see Figure 1.1 E). Discontinuous fiber-reinforced composites have lower strength than continuous fiber composites. However, if the fibers are randomly oriented, the same mechanical and physical properties can be achieved in all directions (in the plane of the lamina). In order to support a certain load or to maintain deflection in a fiber-reinforced composite structure, several laminas are stacked in a specified sequence and consolidated into a laminate. Different laminas in a laminate can contain fibers either all in one direction or in different directions. By properly orienting the fibers in various layers (see Figure 1.1 F), the difference in strength in different directions can be reduced [Mal07].

The process of introducing fibers into a polymer matrix can be divided into two categories. In the first category, the fibers and matrix are processed directly into the final product or structure, e.g., by using filament winding or pultrusion. In the filament winding process, machines pull fiber bundles through a wet resin bath and wind them in a specific orientation over a rotating steel mandrel. The components are cured either at room temperature or at elevated temperatures. In the pultrusion process, continuous strand rovings and mats are pulled through a resin bath, a series of preformers and finally through a long preheated die. The preformers evenly distribute the fiber bundles, squeeze out the excess resin and bring the material to its final configuration. The final shaping, compaction, and curing takes place in the die. A series of tension rollers or blocks then pull the cured pultruded structural form (e.g., beam) out of the die. In the second category, fibers are incorporated into the matrix to prepare ready-to-mold sheets, which are available in two basic forms, prepregs and sheet-molding compounds

Die approbierte gedruckte Originalversion dieser Dissertation ist an der TU Wien Bibliothek verfügbar.
The approved original version of this doctoral thesis is available in print at TU Wien Bibliothek.
TU WIEN Bibliothek Your knowledge hub

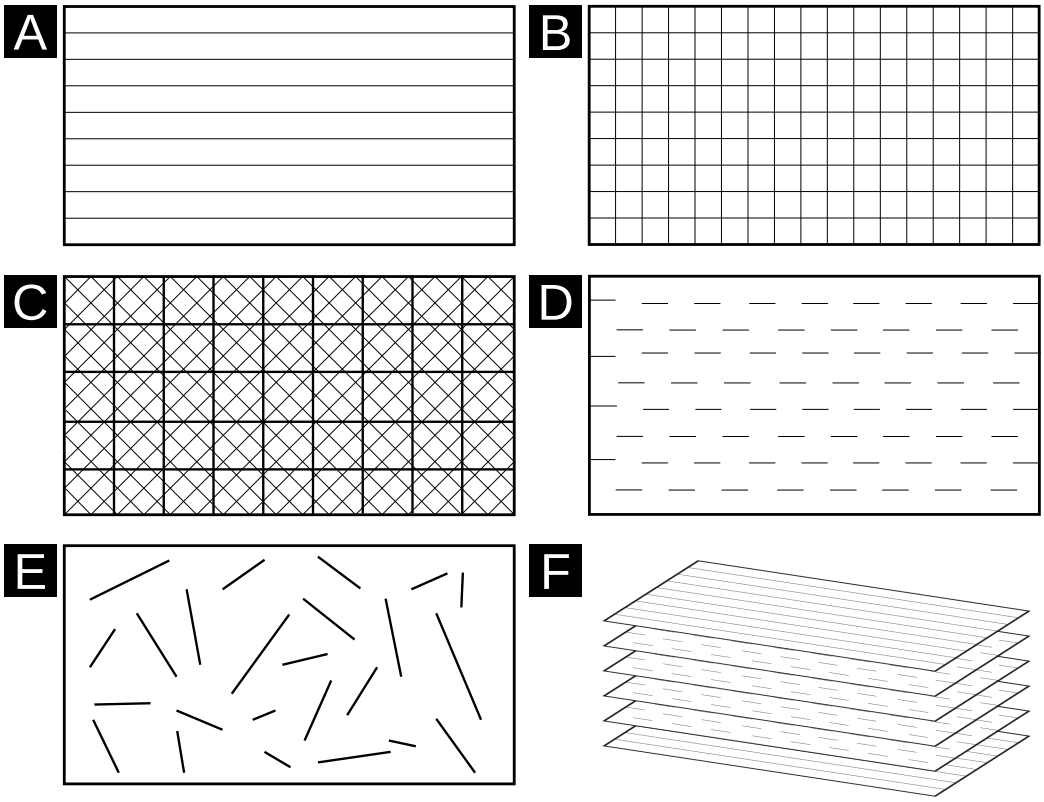

Figure 1.1: The different orientation configurations of continuous fibers and discontinuous fibers in a lamina (or ply): (A) Unidirectional continuous fibers, (B) bidirectional continuous fibers, (C) multi-directional continuous fibers, (D) unidirectional discontinuous fibers, and (E) random discontinuous fibers. (F) A laminate is formed by stacking several various laminas. Adapted from [Mal07].

(SMCs). Prepregs are thin fiber sheets (continuous rovings, mats, or fabrics) impregnated with predetermined amounts of an evenly distributed polymer matrix, usually epoxy. These impregnated sheets can be stored and later processed to form laminated structures. Prepregs are primarily used in the aerospace industry to manufacture components, e.g., winglets. For this purpose, prepreg plies are stacked with the desired fiber orientation angle as well as with the desired sequence in an open mold. The material is covered with release film, bleeder material and a vacuum bag. A vacuum is built up on the component and the entire mold is placed in an autoclave (heated pressure vessel). The component is cured with a continuous vacuum to remove trapped gases from the laminate. This process takes several hours, but enables precise control of the molding process to achieve the required material quality in the aerospace industry. SMCs are thin sheets of fibers precompounded with a thermoset resin and mainly used in the compression molding process. The SMC sheets are produced on a sheet-molding compound machine. The resin

Die approbierte gedruckte Originalversion dieser Dissertation ist an der TU Wien Bibliothek verfügbar.
The approved original version of this doctoral thesis is available in print at TU Wien Bibliothek.
TU Bibliothek Your knowledge hub WIEN

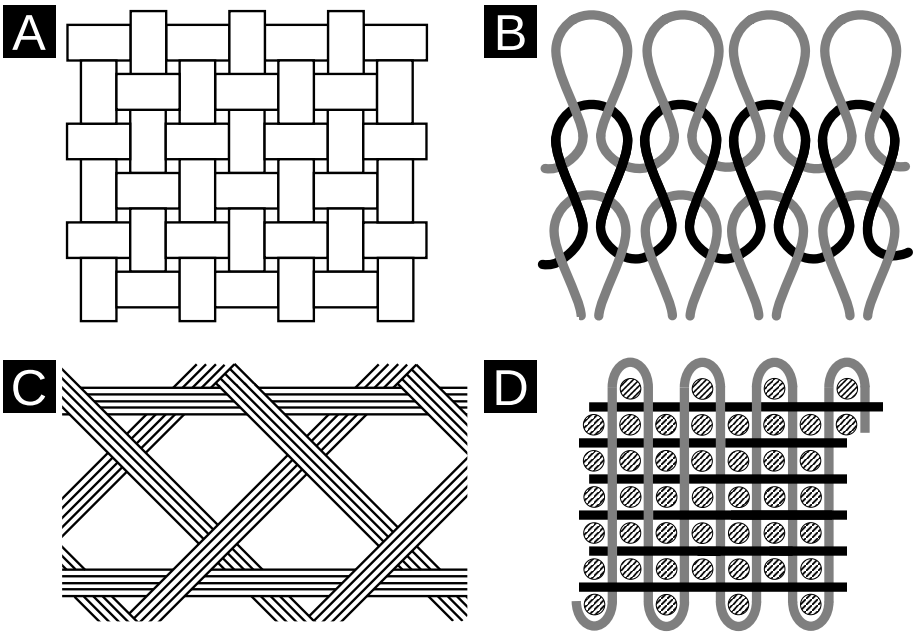

Figure 1.2: Different arrangements of continuous fibers in a composite (fiber architecture). (A) 2D bidirectional woven fabric. (B) 2D weft-knitted fabric. (C) 2D biaxial braided fabric. (D) stitching threads and woven fabrics create a 3D architecture. Adapted from [Mal07].

paste is applied to a polyethylene carrier film. This carrier film runs under a chopper that randomly cuts the continuous fiber rovings onto the bottom resin paste. After covering the fibers with the top resin paste, another polyethylene carrier film is applied. The carrier films are compacted by multiple rolls to form a sheet, which is wound around a take-up roll and allowed to mature between one to seven days at 30° C [Mal07].

During the production of advanced composite materials, irregularities occur in the manufacturing process, which cause the mechanical material properties to deviate from the designed specifications. These irregularities can be divided into matrix, fiber, or interface defects. The most significant type of defects are voids (or pores), i.e., areas that are not filled with resin and fibers (matrix defects). Other defects that may occur during the manufacturing process concern the fibers or the interface between fibers and matrix. Fiber defects are, e.g., misaligned fibers or broken fibers due to excessive fiber curvature during production or excessive friction in the textile machine. Interface defects are for example fiber/matrix debondings and interlaminar delaminations. Another matrix defect is incomplete resin hardening. Irregularities in the material caused by loading are referred to as damage and are, e.g., matrix cracks, fiber fractures, and fiber pull-outs [AAS+16, MGVVL19].
In order to better understand these defect-damage mechanisms and to improve material development and production, suitable measuring and testing procedures are necessary.

Die approbierte gedruckte Originalversion dieser Dissertation ist an der TU Wien Bibliothek verfügbar.
The approved original version of this doctoral thesis is available in print at TU Wien Bibliothek.
TU WIEN Bibliothek Your knowledge hub

These allow the specialists to detect these defects and to evaluate them qualitatively and quantitatively with suitable techniques. As an example, for the determination of the porosity value in fiber-reinforced polymers (FRPs), various testing methods such as ultrasonic attenuation, acid digestion, materialography, and active thermography exist [KPSS10]. However, these methods often only achieve inaccurate results, do not provide a spatial representation of the specimen (or a look inside the specimen), introduce measuring errors, and are destructive. A measuring and testing technique that avoids these disadvantages is industrial 3D X-ray computed tomography.

1.2 Industrial 3D X-ray Computed Tomography

The first prototype of an X-ray computed tomography (CT) scanner was developed in 1968 by Godfrey Newbold Hounsfield as a medical imaging method. The experiments were performed on a human brain prepared with formalin, the brain of a living calf, and the kidneys of a pig [Cie11]. Since then, CT has been using X-ray radiation and measuring their absorption, making it suitable for studying materials with high atomic numbers. It uses X-rays to take a series of 2D projection images of an object from many positions around an axis of rotation. By using suitable computer algorithms, these images are reconstructed into a 3D model that reveals the inner and outer geometries of the scanned object [KH18, DCCK+14]. The unique ability of CT to create a holistic model of an object accurately, contact-free, and non-destructively has also been recognized by industry. In recent decades, CT as a non-destructive testing (NDT) method entered many different industrial applications such as functional testing, defect analysis, material characterization, simulation, and dimensional metrology.

Industrial 3D X-ray computed tomography (XCT) devices differ fundamentally from medical CT devices. In medical CT systems, the X-ray source and detector rotate around the patient, in XCT systems the object rotates in the X-ray beam, the source and detector remain stationary. Most XCT systems of industrial applications use a cone beam geometry in combination with a flat-panel detector. In such a setup, the specimen is placed on a rotary table between an X-ray source and a detector. The specimen is penetrated by X-rays. As X-rays pass through the specimen, radiation is absorbed by the specimen. The incident X-rays are attenuated depending on the sample thickness, the density and the atomic number of the material. The remaining part is transferred by the scintillation layer of the X-ray detector to visible light, which is finally recorded as a 2D projection image. The resolution and accuracy of XCT systems can be varied by changing the geometrical resolution between source, object, and detector. If the distance between the source and the object is small, a higher image magnification and pixel resolution is achieved to resolve small material features. If the object is closer to the detector, a larger volume can be scanned at once but at a lower resolution.
In order to generate a volumetric model of the specimen, several hundred projection images (typically 800–2400) are acquired step-wise during a 360° rotation. These projection images are finally combined with the aid of reconstruction algorithms, usually with filtered backprojection introduced by Feldkamp et al. [FDK84], to compute a 3D volume.

Die approbierte gedruckte Originalversion dieser Dissertation ist an der TU Wien Bibliothek verfügbar.
The approved original version of this doctoral thesis is available in print at TU Wien Bibliothek.
TU Bibliothek WIEN Your knowledge hub

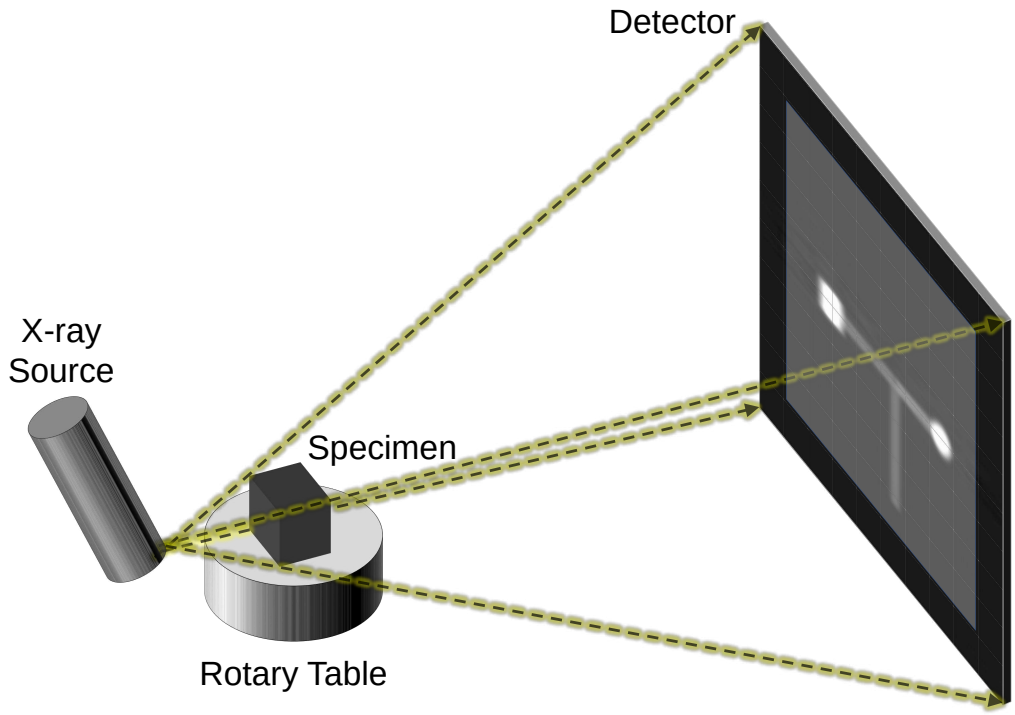

Figure 1.3: Basic principle of a cone beam XCT system. The conically emitted X-rays penetrate the specimen. The attenuation of the X-rays is converted into a 2D digital projection image at the detector.

The volumetric data thereby contain the spatial attenuation values and the corresponding information about the outer and inner microstructure of the specimen. Figure 1.3 depicts the basic principle of a cone beam XCT system.

Due to the cone beam geometry and the high X-ray doses of the XCT devices, the requirements of the industry for high resolutions and accuracies can be achieved. As a result, the scanning parameters of XCT devices differ significantly from those of medical CT devices. In the following paragraphs, two XCT devices at the University of Applied Sciences Upper Austria – Wels Campus are described, which were used to measure the specimens of this thesis. The first device is a Nanotom 180 NF (GE Phoenix|X-Ray), which has a 180 kV nanofocus X-ray source with a minimum focal spot diameter below one micrometer (see Figures 1.4 A and B). Thereby, a minimum voxel size of 0.5 µm can be achieved. The second device is a SkyScan 1294 (Brucker) desktop phase-contrast X-ray microtomograph with integrated grating Talbot-Lau X-ray interferometer for the simultaneous extraction of attenuation contrast, differential phase contrast, and dark-field contrast images (see Figures 1.4 C and D). Its microfocus X-ray source with a minimum focal spot diameter of 33 µm enables a minimum voxel size of 5.7 µm.

Die approbierte gedruckte Originalversion dieser Dissertation ist an der TU Wien Bibliothek verfügbar.
The approved original version of this doctoral thesis is available in print at TU Wien Bibliothek.
TU WIEN Bibliothek Your knowledge hub

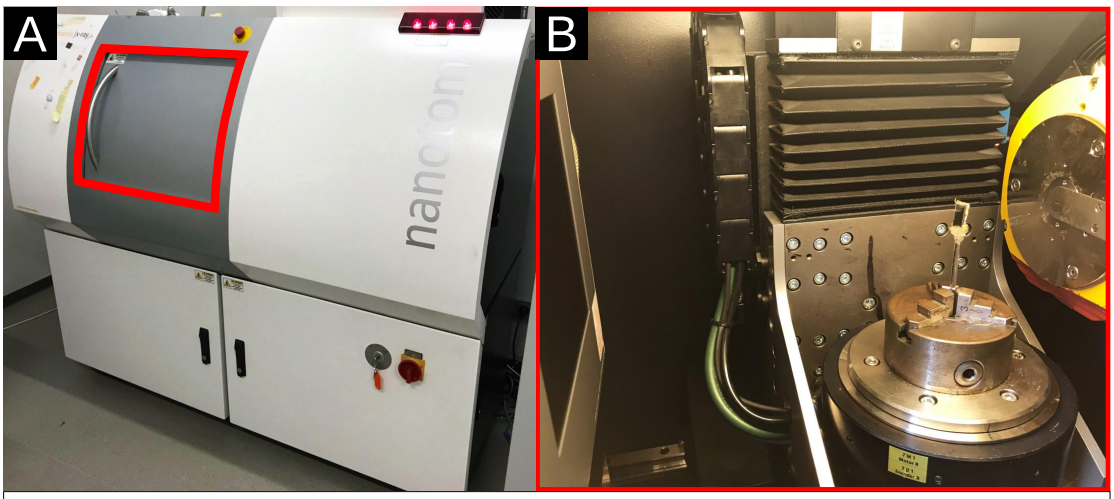

Nanotom 180 NF Technical Specifications

- 180 kV nanofocus X-ray source with a min. focal spot diameter of < 1 µm
- 2304 × 2304 pixel 12 bit detector
- Min. voxel size: 0.5 µm
- Max. specimen diameter: 68 mm
- Max. specimen height: 150 mm

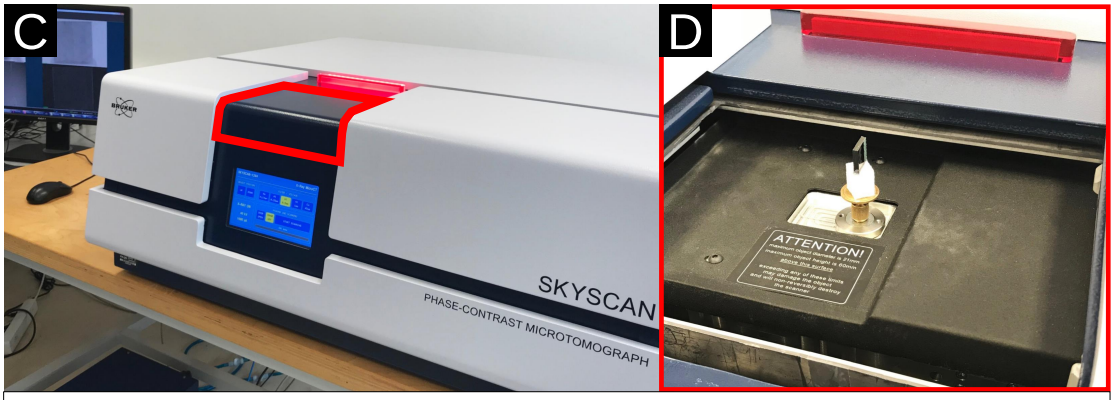

Skyscan 1294 Technical Specifications

- 60 kV microfocus X-ray source with a min. focal spot diameter of 33 µm
- 4000 × 2672 pixel 12 bit detector
- Min. voxel size: 5.7 µm
- Max. specimen diameter: 20 mm
- Max. specimen height: 60 mm

Figure 1.4: XCT devices at the University of Applied Sciences Upper Austria – Wels Campus. (A) The Nanotom 180 NF high-resolution submicro-CT system with (B) flat-panel detector, turntable with a mounted CFRP specimen, and X-ray source. (C) The Skyscan 1294 desktop phase-contrast X-ray microtomograph, which shows (D) the opened cabin with a mounted CFRP specimen.

Die approbierte gedruckte Originalversion dieser Dissertation ist an der TU Wien Bibliothek verfügbar.
The approved original version of this doctoral thesis is available in print at TU Wien Bibliothek.
TU Bibliothek Your knowledge hub WIEN

With these XCT devices it is possible to perform high-precision 3D inspections of fiber architectures, manufacturing defects, and damage accumulations non-destructively in advanced composites. Thus, it is now possible to examine cross-sections, which were previously only possible by means of time-consuming, expensive and skilled mechanical sectioning with the danger of damage or material loss [GWW18]. For example, the subtle material-determining properties, like fibers and pores in fiber-reinforced polymers, can be characterized with XCT. Figure 1.5 depicts the resulting 3D dataset of a high-resolution XCT scan of a CFRP specimen with endless carbon fiber rovings embedded in an epoxy resin matrix. The specimen was produced using the prepreg manufacturing process (see Section 1.1). The prepreg layers are stacked on top of each other. The fiber orientation of the individual layers runs alternately along the z-axis and the y-axis (see Figure 1.5 A and B). Figure 1.5 C presents a 2D cross-section of the XCT data. The fibers and the matrix (resin) appear in light gray, the pores (air) appear in dark gray. The average carbon fiber diameter is approximately seven microns.

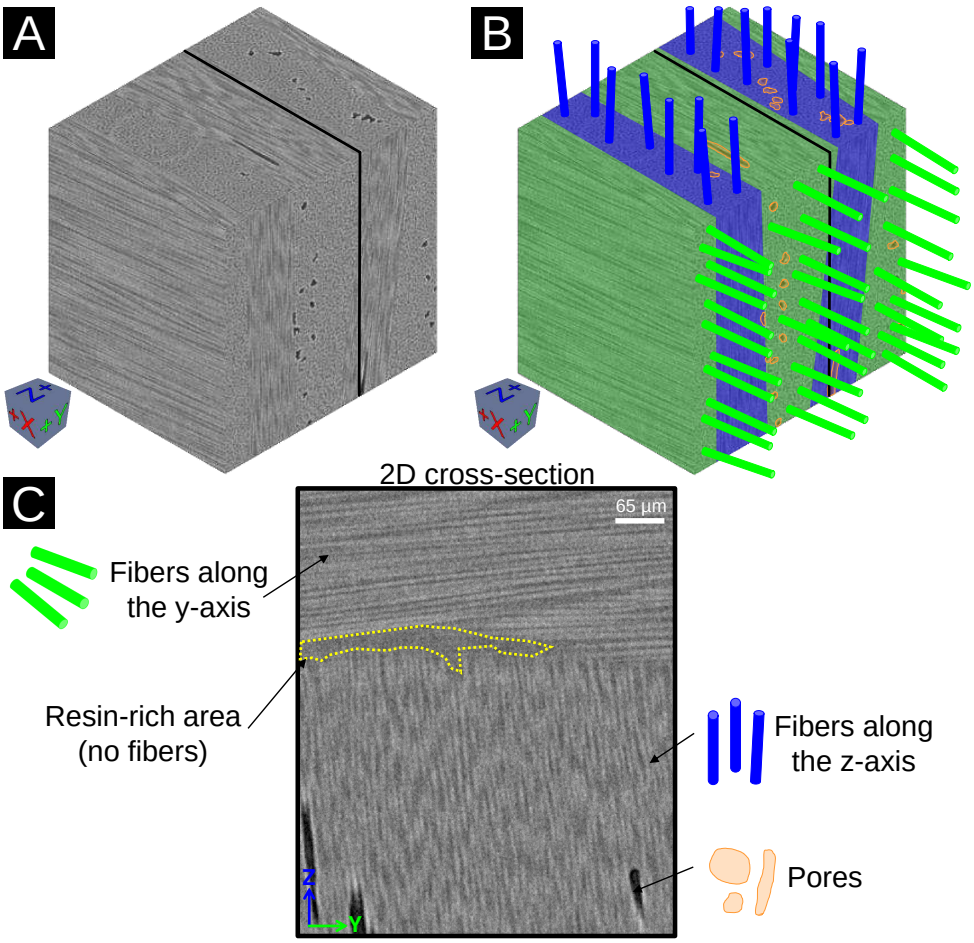

Figure 1.5: (A) An XCT dataset of a CFRP specimen with (B) stacked fiber layers showing (C) a 2D cross-section with interesting features, e.g., fibers and pores.

Die approbierte gedruckte Originalversion dieser Dissertation ist an der TU Wien Bibliothek verfügbar.
The approved original version of this doctoral thesis is available in print at TU Wien Bibliothek.

1.3 Contributions of the Thesis

Advanced composites have become increasingly important in many areas of industry (e.g., aviation and leisure) due to their high strength-to-weight ratio. XCT plays an important role in this context, as it facilitates to precisely and non-destructively acquire the outer and inner microstructures of composite materials. Therefore, significant insights are gained in the fields of material characterization, development, and inspection. For example, non-destructive testing (NDT) practitioners use these advantages of XCT to obtain a comprehensive and very detailed analysis of their test specimens. However, modern XCT devices generate large-volume datasets with very high resolution. Consequently, very fine structures can be detected. This high information content causes big challenges in the exploration and visualization of XCT datasets and limits the derivation of material properties.

The overall goal of this thesis is to improve and augment the current analysis workflow for characterizing advanced composite materials scanned with XCT through meaningful visualizations and interactive visual analysis tools. For this reason, three typical application scenarios of NDT using XCT, i.e., *fiber characterization*, *porosity-value determination*, and *feature comparison in multiple volumes*, are addressed. With the help of the following contributions, in the form of novel visualization tools, the domain-specific questions in the respective areas are answered. The contributions are based on research papers and are described in detail in the Chapters 2, 3, and 4:

- **Interactive exploration and visual analysis of fibers in advanced composites.** A typical XCT dataset of an FRP specimen contains hundreds of thousands or more fibers. In such a fiber dataset, e.g., the position, length, and orientation of each individual fiber is of interest to the domain experts. The manual analysis of a fiber dataset, e.g., with 2D slice views, is very difficult with conventional analysis tools. This poses the question of how to adequately analyze the vast amount of information to characterize an FRP specimen in detail with respect to its fiber content. In order to answer this domain-specific question, we designed the *FiberScout* research prototype. It interactively explores and visually analyzes the arrangement, length, and orientation of fibers in FRPs in detail. By using suitable overview visualizations, the individual fiber lengths, fiber orientations, as well as the shape of entire fiber layers are comprehensibly illustrated. Furthermore, the fibers can be highlighted and classified according to their different fiber characteristics in order to reveal hidden relationships in the fiber data.

- **Visual analysis and evaluation of porosity in fiber-reinforced polymers.** Unlike fibers, which are purposely introduced into FRPs and have a positive effect on the mechanical properties, pores in FRPs occur unintentionally during the manufacturing process and have a negative effect. When analyzing an FRP component scanned with XCT, the quantitative determination of the pores through the porosity-value, plays a decisive role for the experts. Various segmentation

Die approbierte gedruckte Originalversion dieser Dissertation ist an der TU Wien Bibliothek verfügbar.
The approved original version of this doctoral thesis is available in print at TU Wien Bibliothek.
TU Bibliothek Your knowledge hub WIEN

algorithms with different parameter settings are used to detect the pores in an XCT dataset. Depending on the material and the XCT scan, the one or the other algorithm segments interesting structures as pores better or worse. For the domain specialists, the question arises which segmentation algorithm with which parameter setting is best suited for a precise porosity-value determination for the respective material. Together with domain experts, we designed *PorosityAnalyzer*, a research prototype for the visual analysis and evaluation of segmentation pipelines to determine the porosity in FRPs. The tool allows the user to set up different segmentation pipelines, to sample the involved parameter spaces, and to calculate the results. The segmentation results can then be systematically evaluated and compared with each other using comprehensive visualizations. Thereby, the visual knowledge discovery follows a drill-down approach. It allows the user to perform a visual analysis from the data overview to the most detailed representations of the results by selecting the most interesting data portion on each level and then passing this on to the next level.

- **Visual comparison of interesting features in 3D volumes.** During the close collaboration with material experts, it turned out that not only fibers or pores in advanced composites are of great interest for them, but also features with arbitrary shapes such as cracks, higher-density inclusions, and material interfaces. The image quality of the features in XCT datasets depends significantly on the reconstruction and image processing algorithms and their different parameter settings. Because of this circumstance the experts try to select and develop the algorithms and their parameters in such a way that the features are represented with the highest possible image quality. To achieve this, the experts generate many XCT datasets (containing features) with different algorithms and different parameter settings and evaluate them. Usually, the numerous feature volumes are compared with 2D slice views. Finding and comparing the differences in such a volume ensemble is very difficult and insufficient due to the vast amount of data. The domain-specific question arises how to efficiently analyze an ensemble of XCT volumes with regard to image quality and features that are often only slightly different. To tackle this challenge, we developed *Dynamic Volume Lines*, a research prototype for the visual comparison of 3D volumes through Space-filling Curves. It abstracts an ensemble of XCT volumes to one-dimensional line plots. A nonlinear scaling based on the intensity variations in the ensemble is applied to the line plots to better use the available screen space. The nonlinear scaling emphasizes regions with high variations by expanding them and compressing uninteresting regions. Interactive 2D and 3D comparative visualizations allow the user to select and evaluate interesting feature regions.

The significance of the presented visualization contributions for the field of visual computing emerges from the challenges identified by Heinzl and Stappen [HS17]. In their state-of-the-art report, they point out the importance of visual computing to support research endeavors in the field of material science. Their systematic survey examines

Die approbierte gedruckte Originalversion dieser Dissertation ist an der TU Wien Bibliothek verfügbar.
The approved original version of this doctoral thesis is available in print at TU Wien Bibliothek.
TU Bibliothek Your knowledge hub WIEN

the intersection of both research domains by analyzing the existing body of literature, identifying the main tasks, and reviewing data and techniques from both disciplines. As a result, the authors summarize four open high level challenges, which future research needs to tackle for boosting research undertakings in material science. In the following, the individual high level challenges are briefly explained and it is described which of the developed visual analysis tools contribute to the respective challenges.

- *Integrated Visual Analysis Challenge:* Standard visualization tools are not sufficient to explore material science data in detail and to make the most out of all the data available. Therefore, there is a need for integrated visual analysis tools with linked views and interaction concepts that are tailored to a specific application area and support users in their exploration using simple and meaningful visualization techniques [HS17].
  The visualization contributions in this thesis were developed in close collaboration with material specialists and provide special interactive visualizations. With *FiberScout*, fiber data can be analyzed in detail using linked 2D and 3D rendering views. *PorosityAnalyzer* offers a tailored interactive system for the systematic analysis of numerous pore segmentation pipelines with linked views on different levels of detail. *Dynamic Volume Lines* enables a visual comparison of similar volumes in an ensemble by abstracting the volumes as 1D line plots.

- *Quantitative Data Visualization Challenge:* Specific visual analysis tools for extracting and analyzing derived data (e.g., calculated from features of spatial, temporal, or higher dimensional data) have to be designed and implemented. Therefore, feature extraction and clustering techniques are required to statistically evaluate the data in order to visualize the properties of the individual features and feature classes [HS17].
  In this context, *FiberScout* calculates derived outputs such as fiber orientations or fiber length distributions based on the preprocessed fiber data (e.g., start and end points of all the individual fibers). The fibers can then be analyzed and classified by their preprocessed and derived fiber characteristics using linked 2D and 3D rendering views. Thus, fiber clusters with similar characteristics can be identified. *PorosityAnalyzer* also calculates derived features from the different pore-segmentation results. These can be analyzed and statistically evaluated according to the sampled input parameters of the segmentation pipelines using overview visualizations, detailed 2D slice views, and 3D rendering views. With *Dynamic Volume Lines*, differences in an ensemble of volumes can be analyzed and compared. The spatial data of the individual volumes are depicted as 1D line plots. A nonlinear scaling based on intensity variations of the volumes, generates interactive 2D views at different levels of detail. The nonlinear scaling has the effect that regions in the 2D views with low respectively high intensity variations among the volumes are compressed (clustered) or expanded. In order to create a spatial context to the volumes, the 2D views of the 1D line plots are linked to 3D rendering views. In both views, interesting features in the volumes can be explored.

Die approbierte gedruckte Originalversion dieser Dissertation ist an der TU Wien Bibliothek verfügbar.
The approved original version of this doctoral thesis is available in print at TU Wien Bibliothek.
TU Bibliothek WIEN Your knowledge hub

- *Visual Debugger Challenge:* Similar to a code debugger, a visual debugger should visually indicate errors and identify incorrectly used algorithms and parameters in the analysis, which show only very limited benefits or lead to incorrect results. In addition, such a tool should be able to give guidance to improve an analysis and suggest appropriate algorithms or pipelines for specific tasks [HS17].
  The overview visualizations of *PorosityAnalyzer* help to identify porosity segmentation pipelines, which lead to incorrect or unsatisfying results compared to the reference segmentation. At a more detailed level, a scatter plot matrix, 2D slice views, and 3D rendering views are used to examine the results of the different parameter settings of a pore segmentation pipeline. Hereby parameterizations can be identified, which do not lead to correct pore segmentations in comparison to the reference segmentation.

- *Interactive Steering Challenge:* In this context, visual analysis tools are used to steer ongoing simulation or data acquisition systems. Such a visual analysis system would monitor a costly process and should guide users on how to continuously refine their results [HS17].
  PorosityAnalyzer uses a scatter plot matrix to present the results of a segmentation pipeline along with the corresponding input parameters. This matrix can be used to check if the parameter space of a pore segmentation pipeline has been sampled with sufficient accuracy or if the parameter settings need to be refined and new segmentations need to be calculated.

It should be noted that the software modules of the individual visualization contributions have been integrated into the open source software framework *open_iA* [FWS+19] in order to provide a unified solution.

Die approbierte gedruckte Originalversion dieser Dissertation ist an der TU Wien Bibliothek verfügbar.
The approved original version of this doctoral thesis is available in print at TU Wien Bibliothek.
TU Bibliothek Your knowledge hub WIEN

Die approbierte gedruckte Originalversion dieser Dissertation ist an der TU Wien Bibliothek verfügbar.
The approved original version of this doctoral thesis is available in print at TU Wien Bibliothek.

Die approbierte gedruckte Originalversion dieser Dissertation ist an der TU Wien Bibliothek verfügbar.
The approved original version of this doctoral thesis is available in print at TU Wien Bibliothek.

CHAPTER 2

FiberScout: An Interactive Tool for Exploring and Analyzing Fiber-Reinforced Polymers

This chapter is based on the following publication:

J. Weissenböck, A. Amirkhanov, W. Li, A. Reh, A. Amirkhanov, E. Gröller, J. Kastner, C. Heinzl, FiberScout: An Interactive Tool for Exploring and Analyzing Fiber Reinforced Polymers, *Proceedings of the IEEE Pacific Visualization Symposium (PacificVis)*, pp. 153–160, Yokohama, Japan, 2014. doi: 10.1109/PacificVis.2014.52

Follow-up publications:

A. Bhattacharya, J. Weissenböck, R. Wenger, A. Amirkhanov, J. Kastner, C. Heinzl. Interactive Exploration and Visualization using MetaTracts extracted from Carbon Fiber Reinforced Composites. *IEEE Transactions on Visualization and Computer Graphics*, Vol. 23, No. 8, pp. 1988–2002, 2017. doi: 10.1109/TVCG.2016.2582158

J. Weissenböck, A. Bhattacharya, B. Plank, C. Heinzl, J. Kastner. Visual classification of braided and woven fiber bundles in X-ray computed tomography scanned carbon fiber reinforced polymer specimens. *Case Studies in Nondestructive Testing and Evaluation*, Vol. 6, Part B, pp. 39–46, 2016. doi: 10.1016/j.csndt.2016.05.006

J. Weissenböck, A. Reh, D. Salaberger, C. Heinzl, J. Kastner. Advanced Visualization and Exploration Techniques for Fiber Reinforced Polymers. *Proceedings of 11th European Conference on Non-Destructive Testing (ECNDT)*, Prague, Czech Republic, 2014.

Advanced composites such as fiber-reinforced polymers (FRPs) are promising candidate materials for future components as they allow integrating the continuously rising demands of industry regarding cost-effectiveness, function-orientation, and lightweightness. The most important structures of fiber-reinforced polymers are the individual fibers, as their characteristics (stiffness, strength, ductility, durability, etc.) to a large extent determine the properties of the final component. The main contribution of this chapter is the introduction of a new system for interactive exploration and visual analysis of fiber properties in industrial 3D X-ray computed tomography (XCT) data of fiber-reinforced polymers. The presented tool, *FiberScout*, uses a parallel coordinates plot (PCP) to define and configure initial fiber classes. Using a scatter plot matrix (SPLOM) linked to the PCP the initial classification may be refined. This allows to analyze hidden relationships between individual fiber properties. 2D and 3D views depict the resulting fiber classifications. By using polar plots, an intuitive rendering of the fiber orientation distribution (FOD) is provided. In addition, two approaches of higher abstraction are proposed: The Blob visualization creates a hull around fibers with similar characteristics. The Fiber Metadata visualization allows the user to calculate overlays for 2D and 3D views, containing regional information of particular material characteristics. The proposed system has been evaluated by two groups of domain experts. By applying the presented concepts, the user feedback shows that the domain experts are now able to efficiently perform tasks like classification of fibers, visualization of fiber lengths and orientations, and visualization of fiber regions. The insights gained can be forwarded to the design office as well as to material development and simulation, in order to speed up the development of novel composite components.

2.1 Introduction

When analyzing an FRP specimen, the domain experts are interested in how the fibers are distributed according to length and orientation. Depending on the given lengths and how the fibers are aligned, experts can then estimate and verify the material properties. They are looking for fiber layers with different fiber orientations resulting from the manufacturing process. Furthermore, it is important for the experts to determine the fiber characteristics of a spatial sub-region. These insights can be used for subsequent simulations. In addition another question for material experts is, how the individual fiber properties relate to each other and which regularities can be derived from them. Currently, the domain experts are using specific software products, such as the VGSTUDIO MAX by Volume Graphics [Gmb], more specifically the *Fiber Composite Material Analysis Module* to examine FRP materials. With this module, local and global orientations as well as concentrations of fibers can be displayed in a 3D view and a 2D slice view. It is not possible to search for specific fiber properties within a specimen and there is no

Die approbierte gedruckte Originalversion dieser Dissertation ist an der TU Wien Bibliothek verfügbar.
The approved original version of this doctoral thesis is available in print at TU Wien Bibliothek.
TU Bibliothek Your knowledge hub WIEN

visual highlighting or classification of fibers. In addition, no dependencies between the individual fiber characteristics can be investigated. The previously mentioned software tool provides no visualizations on a higher abstraction level than on the 3D volume data itself. Based on the domain-specific requirements, the following tasks for fiber characterization and fiber visualization using XCT have been identified:

- **Task 1: Classification of fibers.** The most important task is to identify and visualize classes of fibers in XCT scans of FRP specimens. The domain experts need interactive visualization techniques to define and configure fiber classes in accordance to their specific properties and to individually render each class.
- **Task 2: Visualization of fiber lengths and orientations.** Fiber lengths and orientations contribute to a large extent to the characteristics of the final components such as strength or stiffness. Therefore, the domain experts need visualization techniques to render the fiber length and orientation distribution in the dataset.
- **Task 3: Visualization of fiber regions and fiber classes.** The domain experts require a quick and easy solution to identify and visualize regions with similar fiber characteristics. A hull has to be determined, which is enclosing regions of fibers with similar characteristics and differs significantly from other regions. The domain experts need a method to analyze the manufacturing process in order to determine modifications in the layer structure of the material. Furthermore, methods are required to quickly explore the data and to identify relationships between individual fiber characteristics.

In order to address the tasks identified by the domain experts, we introduce *FiberScout*, a system to visualize and explore XCT scans of fiber-reinforced composites. The analysis workflow starts with an XCT scan of the specimen and thus the generation of data. In a preprocessing stage, a label image is calculated from the original grey value image. Starting from the label image, the techniques designed in the following, their domain specific integration, as well as the solutions of the Tasks 1–3 constitute the main contribution of this work (see Figure 2.1):

- **Parallel coordinates plot and scatter plot matrix to classify fibers.** In order to analyze the internal microstructure of the specimen, a PCP and a SPLOM classify the fibers according to fiber characteristics. The SPLOM is used to refine the classification results from the PCP in a successive step. Furthermore, the SPLOM allows the user to reveal relationships between fiber characteristics.
- **Polar plots to render fiber orientations.** A fiber orientation distribution (FOD) is computed on a half sphere and visualized using the azimuthal projection of the northern hemisphere on a 2D plane. A spherical color map is integrated to color code the orientations of fibers in 3D as specified by the domain expert.

Die approbierte gedruckte Originalversion dieser Dissertation ist an der TU Wien Bibliothek verfügbar.
The approved original version of this doctoral thesis is available in print at TU Wien Bibliothek.
TU WIEN Bibliothek Your knowledge hub

- **Blob visualization and Fiber Metadata visualization to render fiber classes.** In order to address the problem of occlusion and clutter when rendering datasets with high fiber content, a smooth hull (blob) is extracted and rendered. It shows regions of fibers with similar characteristics or fiber bundles. Each identified region is visualized as a blob. Furthermore, regional meta information of the fiber data is computed for the Fiber Metadata visualization to quickly explore the data.

In the subsequent section (Section 2.2) we review the related work on fiber analysis and fiber visualization. In Section 2.3 the datasets and the data preprocessing are described. In Section 2.4, the visualization techniques to address Task 1–3 are introduced. Section 2.5 presents the evaluation of the visualization results. Section 2.6 provides implementation details. Finally, we conclude and point out potential future work in Section 2.7.

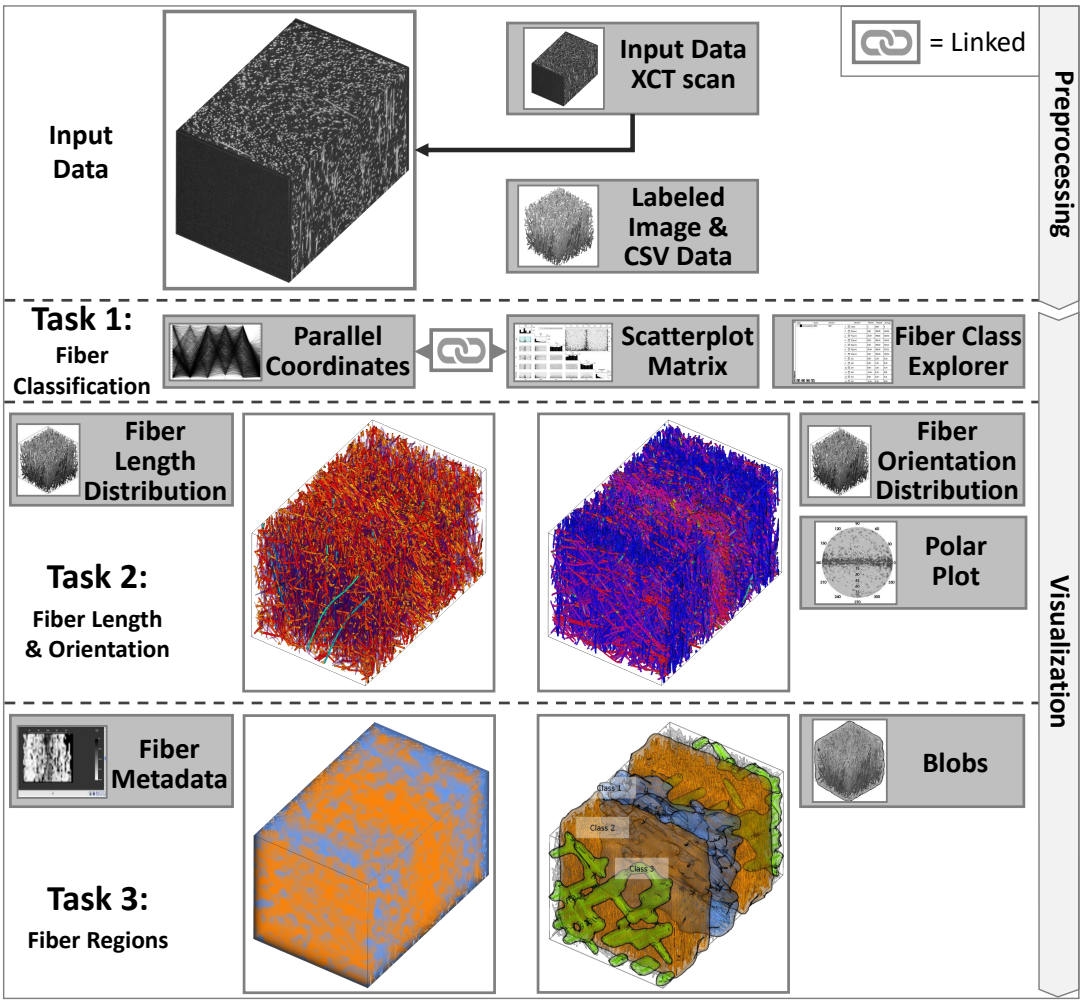

Figure 2.1: Overview of the interactive *FiberScout* visualization methods.

Die approbierte gedruckte Originalversion dieser Dissertation ist an der TU Wien Bibliothek verfügbar.
The approved original version of this doctoral thesis is available in print at TU Wien Bibliothek.

2.2 Related Work

The related work of the proposed techniques is mainly found in the visualization and analysis of material systems, the parameter-space exploration, as well as the visual data exploration techniques.

2.2.1 Visualization and Analysis of Material Systems

Initial visualization techniques for non-destructive testing using XCT data have been first introduced by Huang et al. [HMMW03]. A method for visualizing a precomputed feature volume with a time series of domain parameters using 3D transfer functions was presented by Hadwiger et al. [HLRS+08]. Based on this method, Fritz et al. [FHG+09] introduced an approach to explore steel fiber-reinforced sprayed concrete and to quantify fiber properties such as fiber orientation. They use a direction sphere histogram to visualize the FOD. Furthermore, direction transfer functions in the orientation domain are used to visualize fiber orientations with user-specified colors. The field of application of Fritz' work is, in comparison to our application area of FRPs, a completely different one. We can calculate far more individual fiber characteristics of FRPs and we can represent each characteristic in charts. Furthermore, we can search for fibers with a highly specific set of fiber features and classify them. Besides these differences, we employ several abstract representations to visualize fiber characteristics and the defined fiber classes. Regarding orientation visualization, Robb et al. [RWS07] presented a method to calculate the local orientation of a fiber using a Gaussian orientation space. Altendorf and Jeulin [AJ09] compute the local directions in continuous space by analyzing the mathematical morphology of images. A disadvantage of the local orientation analysis is that a single fiber may have various orientations, as the calculation is performed on a pixel or voxel-basis. This is not suitable for visualizing fibers as a whole object in our visualization pipeline. The algorithm described by Salaberger et al. [SKK+11] and Teßmann et al. [TMG+10] is used to extract individual fibers in our visualization pipeline. Tests included in their work demonstrate that the method produces results with accuracies of more than 95% correctly detected fibers (mainly depending on the fiber content). Based on this implementation further algorithms are applied to the calculation of fiber properties (e.g., fiber orientation, fiber length, fiber diameter, fiber volume). Fiber orientations are then visualized in 3D space with a domain specific spherical color map based on the work of Yamrom et al. [YSW94].

2.2.2 Parameter-space Exploration

The PCP [ID90] and SPLOM [WB97] are popular techniques for visualizing high-dimensional datasets. For example, Craig et al. [CKC05] use coordinated parallel views to query micro array time-course data. The queries done in the coordinated parallel view are then linked to a scatter plot. They conclude that the coordinated parallel view is more appropriate for revealing details in the data and supporting the discovery of less dominant patterns. The S-shape axis layout for PCPs are used by Qu et al. [QCX+07]

Die approbierte gedruckte Originalversion dieser Dissertation ist an der TU Wien Bibliothek verfügbar.
The approved original version of this doctoral thesis is available in print at TU Wien Bibliothek.
TU Bibliothek Your knowledge hub WIEN

to highlight wind directions for analyzing the air pollution problem in Hong Kong. This approach is suitable for revealing correlations between 1D directions and other variables. However for analyzing 3D directions together with spatial information, conventional PCPs are more convenient. Kuang et al. [KZZM12] did a comparison of scatter plots and PCPs. They found that PCPs show advantages in low dimensionality and low density datasets, while scatter plots outperform PCPs in higher dimensionality and higher density datasets. A PCP and a SPLOM are integrated in our visualization pipeline. We combine the two techniques using linking and brushing [Kei02], in order to explore the data in a more interactive way. The advantages of these two techniques are exploited and hidden correlations between individual characteristics are easier to detect.

2.2.3 Visual Exploration

Regarding clustering methods, Zhou et al. [ZCQ+09] introduced splatting of the individual lines in PCPs to reveal strong correlations between the dimensions and to detect trends. In addition, Zhao et al. [ZK10] proposed a novel method using PCPs for multi-dimensional transfer function design. Guo et al. [GXY11] present an effective transfer function design for multivariate volumes, providing tightly coupled views of PCPs. Li et al. [LZQ13] showed a novel approach for space deformation to simulate a magnification lens on versatile volume datasets and textured solid models. Tatu et al. [TMF+12] employ interestingness-guided subspace search algorithms to detect a candidate set of subspaces. The result of a k-means [KMN+02] algorithm turned out to generate robust consequences for initial automatic classifications. Therefore, in our proposed work we follow this approach for the determination of fiber classes with similar characteristics. Jackson et al. [JLS+13] present a tangible interface, which allows the user a 3D interactive exploration of thin fiber structures to understand patterns in fiber orientation inside a volume.

2.3 Dataset Description and Preprocessing

This section describes the investigated datasets (see Section 2.3.1) and how the preprocessing stage extracts fibers and calculates fiber characteristics (see Section 2.3.2).

2.3.1 Dataset Description

The two glass fiber-reinforced polymer (GFRP) specimens to test the fiber-visualization pipeline are $614 \times 961 \times 600$ and $608 \times 1411 \times 500$ voxels in size with a resolution of 2 μm and 3 μm respectively. We will subsequently call them *Dataset 1* (see Figure 2.2 A) and *Dataset 2* (see Figure 2.2 B). The carbon fiber-reinforced polymer (CFRP) specimen we investigated in this work has a size of $600 \times 500 \times 600$ voxels and is scanned with a resolution of 1 μm. We will subsequently call it *Dataset 3* (see Figure 2.2 C). All specimens are scanned with a GE phoenix|X-Ray Nanotom 180 NF XCT device.

Die approbierte gedruckte Originalversion dieser Dissertation ist an der TU Wien Bibliothek verfügbar.
The approved original version of this doctoral thesis is available in print at TU Wien Bibliothek.
TU Bibliothek WIEN Your knowledge hub

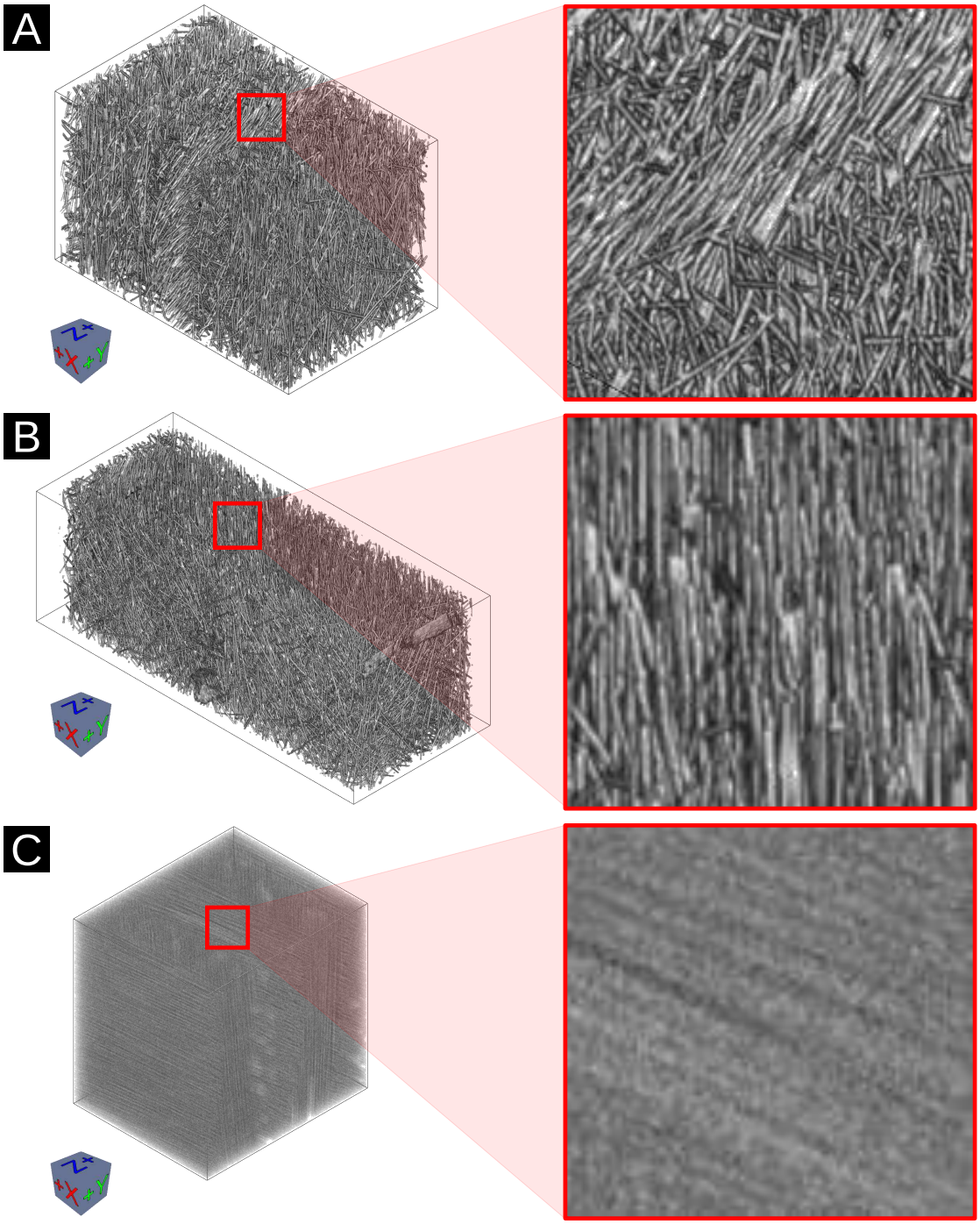

Figure 2.2: (A) *Dataset 1*: GFRP specimen with 15916 fibers. (B) *Dataset 2*: GFRP specimen with 21751 fibers. (C) *Dataset 3*: CFRP specimen with 22656 fibers.

Die approbierte gedruckte Originalversion dieser Dissertation ist an der TU Wien Bibliothek verfügbar.
The approved original version of this doctoral thesis is available in print at TU Wien Bibliothek.

2.3.2 Preprocessing

In the preprocessing stage, the fiber characterization pipeline according to Salaberger et al. [SKK+11] is applied to the scanned XCT volume data of the fiber-reinforced polymer (FRP) specimens. In the first step of this pipeline, Gaussian blurring is applied to reduce noise in the original volume data. In the second step the gradient magnitude is computed, which is used as input for the computation of the Hessian matrix at each voxel. Using the Hessian matrix, the gray value differences of a voxel compared to its neighboring voxels are detected, which permits a statement about the main orientation of the fibers. The Hessian matrix also determines the medial axis of the individual fibers as originally proposed by Teßmann et al. [TMG+10]. The intermediate results of the pipeline are the extracted individual fibers of the dataset given by their corresponding start and end points. The characteristics of the extracted fibers are computed at the same time as the individual fibers are extracted. Finally, a labeling filter is applied to all the extracted fibers. In the labeled image every voxel of an individual fiber is mapped to a unique label identification. In total, twenty-five fiber characteristics for each fiber are available. The most significant fiber characteristics for further analysis are shown in Table 2.1.

Characteristic	**Description**	**Unit**
a_{11}, a_{22}, a_{33}	The main diagonal elements of a fiber orientation tensor [SSK11]	-
φ, θ	Spherical coordinates of a fiber orientation	$^\circ$
x_i, y_i, z_i	Cartesian coordinates of the ith fiber center point, $0 \leq i \leq m-1$	μm
sL	Straight length of a fiber	μm
diameter	Diameter of a fiber	μm
volume	Volume of a fiber	μm^3

Table 2.1: The most significant fiber characteristics in the work of *FiberScout*.

2.4 Visualization

For understanding the micro structures of FRPs, visualization techniques such as direct volume rendering of the extracted fibers do not satisfy the requirements of the domain specialists. This is due to clutter and occlusion. To overcome this problem, the *FiberScout* research prototype (see Figure 2.3) with its visual fiber exploration techniques (see Section 2.4.1) has been developed, enabling interactive data exploration, clustering, and classification. A PCP (see Section 2.4.1.1) is linked to a SPLOM (see Section 2.4.1.2), the Fiber Class Explorer (see Section 2.4.1.3), as well as to 2D and 3D views. Furthermore,

Die approbierte gedruckte Originalversion dieser Dissertation ist an der TU Wien Bibliothek verfügbar.
The approved original version of this doctoral thesis is available in print at TU Wien Bibliothek.
TU Bibliothek WIEN Your knowledge hub

visualization techniques have been developed to give insight into the clustered fiber data at a higher level of abstraction. These widgets and techniques include the FOD (see Section 2.4.2), the fiber length distribution (see Section 2.4.3), the Blob visualization (see Section 2.4.4), and the Fiber Metadata visualization (see Section 2.4.5).

2.4.1 Visual Fiber Exploration

Right after loading the dataset into the visualization pipeline, an overview of the data is presented in a PCP, in a SPLOM, as well as in a 3D rendering view (see Figure 2.3 A). Following the visual information-seeking mantra described by Shneiderman [Shn96], the data is divided into subclasses (zoom and filter), which are displayed in turn with the PCP and the SPLOM. The clutter and occlusion problem of the visualization may be considerably reduced applying additional user-specified queries to the data (details on demand). Furthermore, the views of the PCP and the SPLOM are linked with each other. Changes done in the parameter space will immediately be applied to the data (3D view and 2D slice views) so that the user is able to get a real-time feedback when querying the data. This concept supports interactivity and makes the visual exploration process clear and simple.

2.4.1.1 Parallel Coordinates Plot (PCP) for Fibers

The PCP [ID90] is a powerful visualization technique using high-dimensional geometry for the analysis of multivariate data. Unlike in the Cartesian coordinate system, the axes are set up in parallel and equidistant to each other. A point in the n-dimensional space is represented by a polyline crossing the n parallel axes. The position of the intersection on the jth axis corresponds to the value of the jth coordinate of the point. In the end, each multi-dimensional point is represented by a polyline through the parallel axes.

In the proposed approach, a PCP is used to initially classify fibers according to their individual characteristics (see Table 2.1). The number of fibers in a specimen ranges from several hundreds to hundreds of thousands and more. This results in cluttering and occlusion (see Figure 2.2). As too many lines are drawn between the parallel axes, the exploration process becomes very inefficient. Following the nested model for visualization design and validation [Mun09], we examined our implementation and explored *axis order selection* for PCPs [QCX+07]. If axes representing fiber characteristics with hidden correlations are placed near to each other, the relationships between these characteristics are likely to become apparent. We then found that we will lose other potential correlations between the rest of the characteristics. Furthermore, it is a very time-consuming procedure and requires practical experience to understand the whole reorder and cluster process. After studying the coordinated parallel views for exploratory analysis of micro array time-course data [CKC05], we took an approach that links a SPLOM to enhance and refine the classification results of the PCP. Figure 2.3 D depicts the PCP with selected fiber characteristics color-coded in red.

Die approbierte gedruckte Originalversion dieser Dissertation ist an der TU Wien Bibliothek verfügbar.
The approved original version of this doctoral thesis is available in print at TU Wien Bibliothek.
TU Bibliothek WIEN Your knowledge hub

2.4.1.2 Scatter Plot Matrix (SPLOM) for Fibers

In addition to the PCP, a SPLOM [WB97] is used to visualize and reveal relationships such as dependencies, patterns, and even outliers among all fiber characteristics (see Figure 2.3 B). Furthermore, the SPLOM serves as a refinement tool for the selection obtained using the PCP. The SPLOM used in our visualization pipeline consists of $n(n-1)/2$ scatter plots organized in a matrix. n represents the number of fiber characteristics used in the SPLOM. To avoid redundancy, only the region below the main diagonal of the SPLOM is filled. A histogram of each fiber characteristic is shown in the main diagonal. Below this main diagonal, a scatter plot is drawn for each pair of the characteristics. In the upper right corner an enlarged view of the selected scatter plot is displayed. In the enlarged view and in the small charts as well, selections are performed by drawing rectangles, which will mark the selected data in red (brushing). These selections will be applied to all other scatter plots, the PCP, as well as the 3D rendering view (linking). In order to suggest initial classes of fibers, a k-means algorithm [KMN+02] is used. The fiber characteristics depicted in the enlarged view are taken as input data for the automatic clustering. The number of classes is specified by the user. Results of the classification can then be transferred to the Fiber Class Explorer or further refined in the PCP and in the SPLOM.

2.4.1.3 Fiber Class Explorer

The Fiber Class Explorer lists all created classes of fibers and allows the user to add, modify, and remove classes of interest. For each class, the user may assign individual names and colors. In addition, for each class, statistical information such as number of fibers (*Count*), the percentage of the fiber count (*Percent*), and the *minimal*, *maximal*, and *average* values of all fiber characteristics within a class are calculated (see Figure 2.3 C). By clicking on a class of interest, its elements are revealed and the individual properties of each fiber may be explored. It is also possible to check the 25 fiber characteristics individually. The checked features will be highlighted in the SPLOM, PCP, and in the 2D and 3D views immediately. Figure 2.3 C shows a manual classification of the GFRP dataset with respect to fiber orientation and the spatial position in y-direction of the fiber center point. Three classes are defined, the rest of the fibers are left as *Unclassified*.

Die approbierte gedruckte Originalversion dieser Dissertation ist an der TU Wien Bibliothek verfügbar.
The approved original version of this doctoral thesis is available in print at TU Wien Bibliothek.
TU Bibliothek WIEN Your knowledge hub

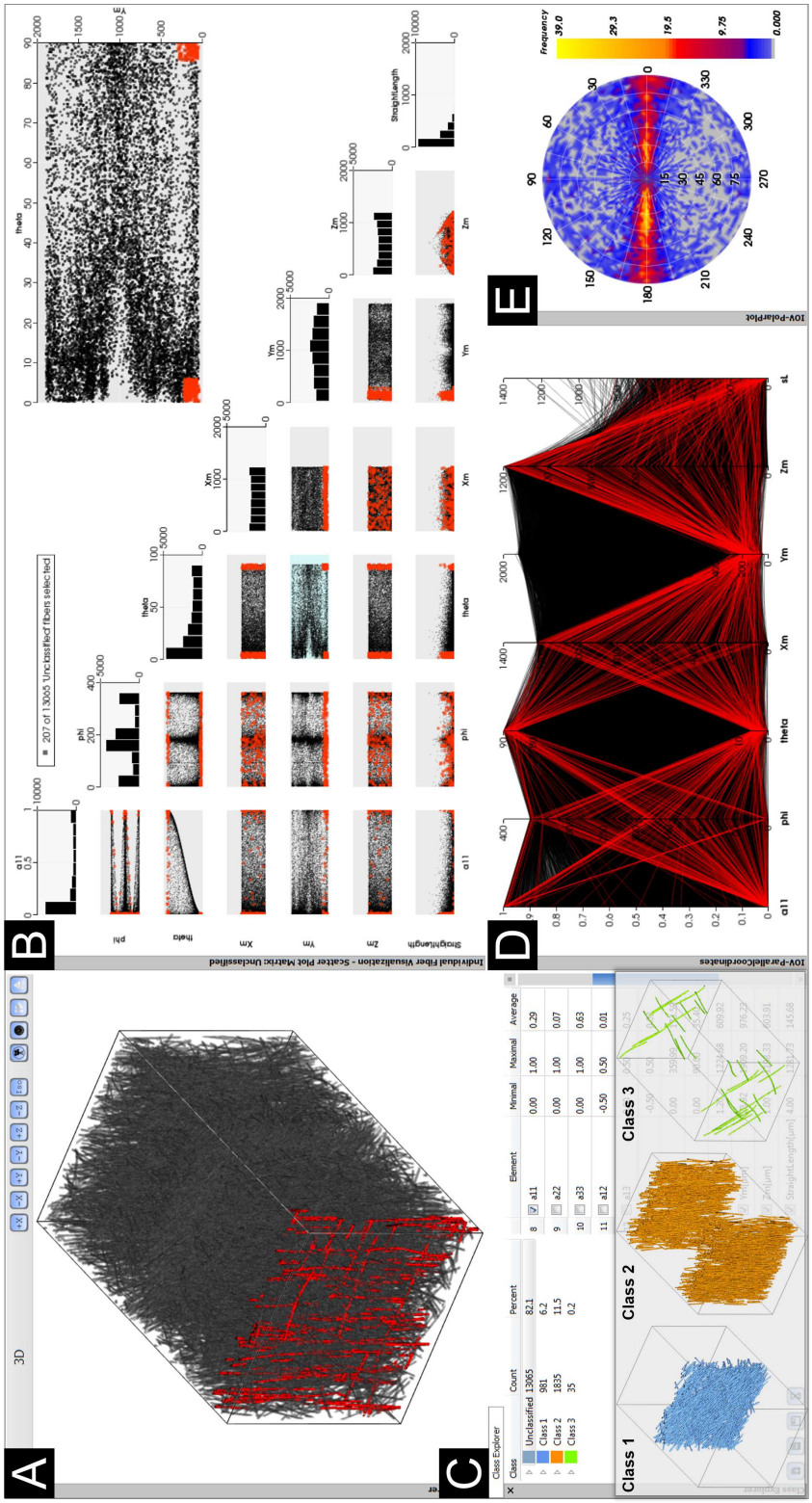

Figure 2.3: The graphical user interface (GUI) of the *FiberScout* tool depicts *Dataset 1* in (A) the 3D rendering view with selected fibers colored in red. The selection of the fibers may be performed either in (B) the SPLOM or in (D) the PCP. All the views are linked and highlight the fiber characteristics and the selected fibers receptively. (C) The Fiber Class Explorer shows three user-defined fiber classes and the *Unclassified* fiber class. (E) The polar plot exemplarily presents the FOD (see Section 2.4.2).

TU Bibliothek WIEN Your knowledge hub
Die approbierte gedruckte Originalversion dieser Dissertation ist an der TU Wien Bibliothek verfügbar.
The approved original version of this doctoral thesis is available in print at TU Wien Bibliothek.

2.4.2 Fiber Orientation Distribution (FOD)

To visualize the fiber orientations, spherical coordinates are used. Figure 2.4 A shows the construction of the fiber orientations from Cartesian coordinates. Here, θ represents the polar angle measured from the zenith z-direction. The azimuth angle φ lies in the xy-plane and is measured from the x-direction. Because of symmetry it is possible to depict all fiber orientations on a half sphere by specifying $\theta \in [0, \pi/2]$ and $\varphi \in [0, 2\pi)$. We discretize the northern half sphere with a user defined resolution and compute the frequency of each discretized direction. This builds up the FOD. The azimuthal projection is later used to generate a 2D image of the FOD. The Figures 2.4 A and 2.3 E depict the global FOD of *Dataset 1*, Figure 2.4 B shows the global FOD of *Dataset 3*. The annotations around the outer circle represent the azimuthal angle and the annotations inside represent the polar angle. The color bar ranges from gray to yellow where gray encodes low frequencies and yellow encodes high frequencies. Gray is used to depict the orientations where no fibers are headed. In addition to the global FOD, we enable the computation of the orientation distribution for each manually defined class. The main orientations in both Figures 2.4 A and B are easily visible as yellow spots. In case of *Dataset 1* (see Figure 2.2 A), a strong prevalence along the x-axis is present (see Figures 2.3 E and 2.4 A). This indicates that most fibers are aligned along the x-axis at an angle of approximately 10–50 degrees to the z-axis. In the case of *Dataset 3* (see Figure 2.2 C), the preferred direction of the fibers is along the y-axis at a angle of nearly 90 degrees to the z-axis (yellow spot in Figure 2.4 B).

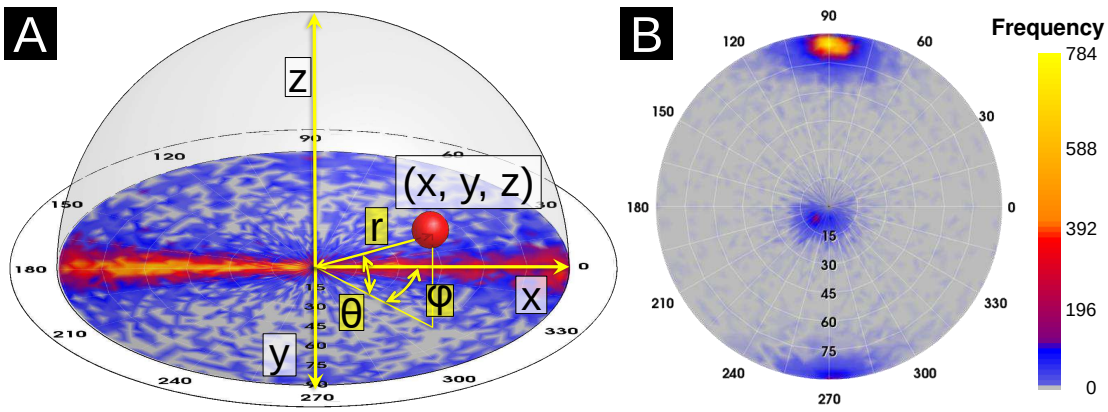

Figure 2.4: Fiber orientation distribution in the polar plot. (A) Construction of the fiber orientations from Cartesian coordinates (*Dataset 1*). (B) Global FOD of *Dataset 3*.

The visualization of the FOD, which defines the mechanical loading capacity, is of great interest to the domain experts. Therefore, we applied a spherical color map where the colors are mapped to the spatial fiber orientations. In order to highlight the x, y and z-directions of a dataset, we mapped these directions to red, green, and blue respectively. Figure 2.5 A depicts a direct volume rendering of fibers by color coding the orientations with the spherical color map (see Figure 2.5 B). This visualization allows the user an

Die approbierte gedruckte Originalversion dieser Dissertation ist an der TU Wien Bibliothek verfügbar.
The approved original version of this doctoral thesis is available in print at TU Wien Bibliothek.
TU Bibliothek Your knowledge hub WIEN

easy identification of the fiber orientations by their color.

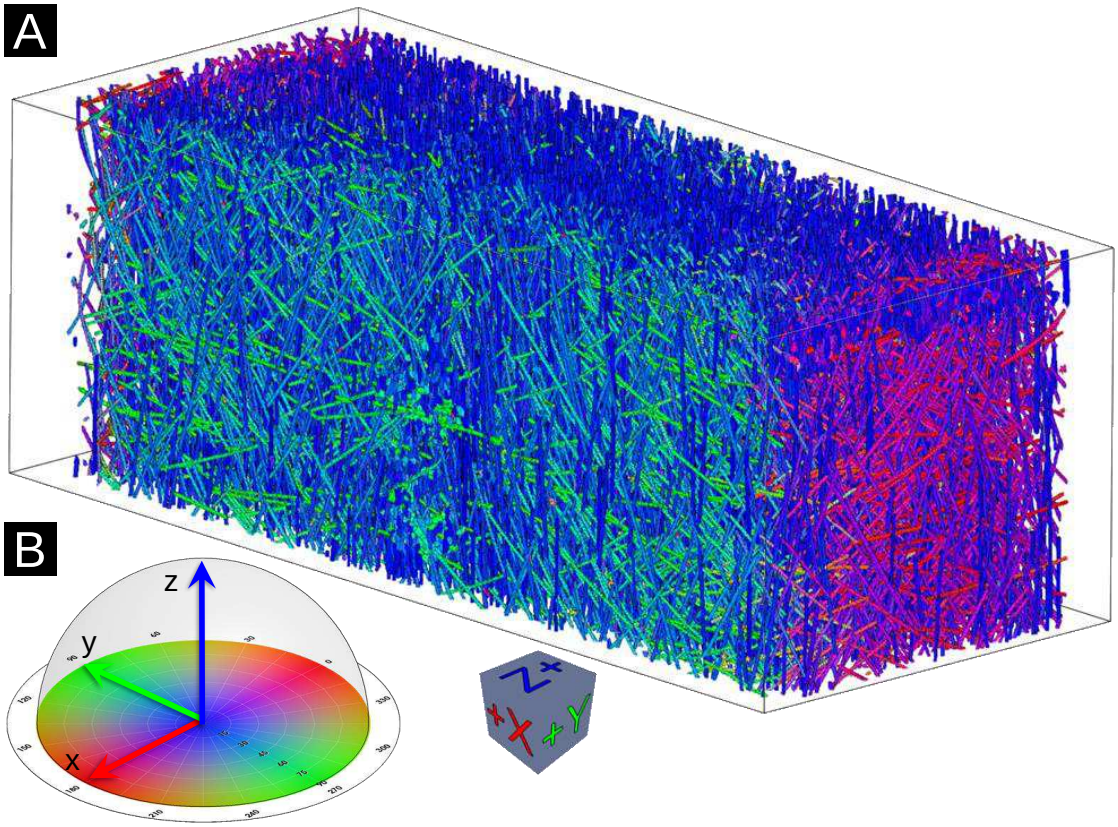

Figure 2.5: (A) Direct volume rendering of the individual fibers of *Dataset 2* using (B) a spherical color map to encode the fiber orientations.

2.4.3 Fiber Length Distribution (FLD)

In addition to fiber orientation visualization, an automatic algorithm is applied to classify and visualize the fibers according to their length. The calculation of the FLD is very important for the experts to quickly represent the layout of short and long fibers in the volume. Thus, conclusions about the loading capacity of the material can be drawn. Figure 2.6 A shows a 3D rendering of a FLD of *Dataset 2* and Figure 2.6 B depicts the corresponding histogram of the fiber lengths.

Die approbierte gedruckte Originalversion dieser Dissertation ist an der TU Wien Bibliothek verfügbar.
The approved original version of this doctoral thesis is available in print at TU Wien Bibliothek.
TU WIEN Bibliothek Your knowledge hub

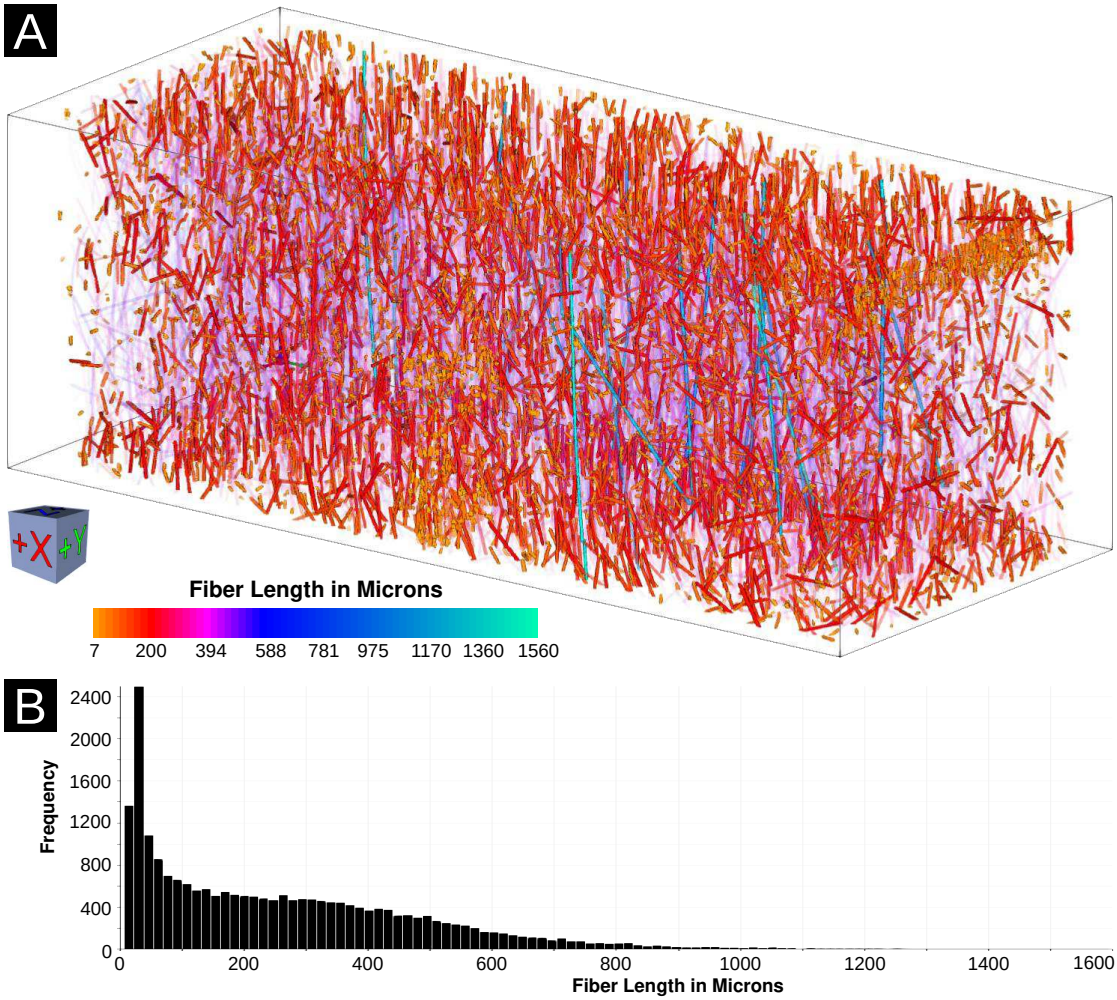

Figure 2.6: Visualization of the different fiber lengths of *Dataset 2*. (A) 3D rendering view of the color-coded FLD and (B) the corresponding histogram of the fiber lengths.

2.4.4 Blob Visualization

For the domain experts, it is important to gain a quick overview of the shape of each fiber class and the layer structure in order to analyze the material build-up of the final component. Due to the issues of overlap and occlusion, the separation of the different fiber classes is frequently problematic using techniques like direct volume rendering. This task is becoming challenging especially for datasets with a very high fiber density that contain thousands of fibers. Based on the defined fiber classes in the Fiber Class Explorer, we introduce a Blob visualization (see Figure 2.7) by applying methods of implicit modeling as proposed by Bloomenthal et al. [BW90].

A blob in our application case is defined as a closed contour surface surrounding all fibers

Die approbierte gedruckte Originalversion dieser Dissertation ist an der TU Wien Bibliothek verfügbar.
The approved original version of this doctoral thesis is available in print at TU Wien Bibliothek.
TU Bibliothek Your knowledge hub WIEN

of a class. It provides the domain experts with an enclosure of the class and shows the spatial location and shape of the class within the data. To construct the blob surface, we apply a distance-field based approach, which is remotely similar to the Metaballs method proposed by Blinn et al. [Bli82]. For every fiber of the class, we specify a line segment so that the start and the end points of a line segment correspond to the start and the end points of a fiber. This provides an approximation for straight and slightly curved fibers. Taking all line segments we can define the shape of a blob by the following distance function defined in 3D space: $\min_{i=1..m} d_i \leq threshold$, where m is the number of line segments, d_i is the Euclidean distance to the given line segment and $threshold$ is a parameter defining the blob size. To obtain a mesh of the blob surface, we uniformly sample the distance function on a grid and then apply the marching cubes algorithm by Lorensen and Cline [LC87] with a corresponding threshold value. In some cases, blobs determined from different fiber classes may overlap, which results in unclear or cluttered representations. To solve this issue we have modified the algorithm in a way that it removes overlapping by adjusting the blob shapes (see Figure 2.7 A and B). We resolve conflicts for those points belonging to more then one blob using the following approach: the point belongs to the blob with the closest fiber. For all the other blobs we set the distance function to infinity so that they do not include the point. This way the point will belong to the blob with the closest fiber and the areas where blobs overlap will become separated based on the corresponding Voronoi diagrams. We further allow the user to

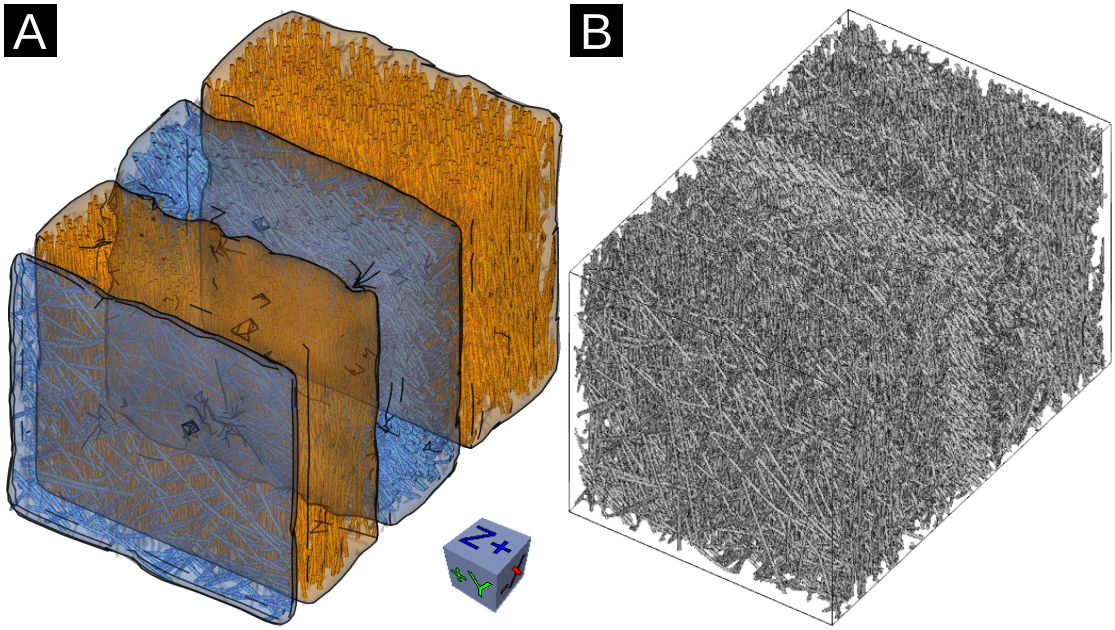

Figure 2.7: Blob visualization of *Dataset 1*. (A) Direct volume rendering of user-defined blue and orange fiber classes with semi-transparent blobs. (B) Direct volume rendering of the dataset with unclassified fibers in gray.

Die approbierte gedruckte Originalversion dieser Dissertation ist an der TU Wien Bibliothek verfügbar.
The approved original version of this doctoral thesis is available in print at TU Wien Bibliothek.

define the minimal separating distance for any pair of blobs. If the minimal separating distance is introduced, the point in an overlapping area is not assigned to any of the blobs if the difference between their distance functions in this point is smaller than the separation distance. Each blob in the 3D view is marked with a label containing the name of the class and a few class statistics: the number of fibers in the class and the percentage of the total fiber count. In order to enhance the shape perception of the blob, the user can enable a silhouette rendering mode. This mode shows the outline of the blob and highlights its sharp edges using black lines.

2.4.5 Fiber Metadata Visualization

As described in Task 3, domain users need a method to explore the data in order to find regions of interest (ROI). Due to the high information content, visualizations based on the original volume data are often not efficient. In order to provide a higher level overview of the fiber characteristics' distribution in the data, we use the Fiber Metadata visualization approach. We subsample the original volume data with a user-specified scaling-factor, which results in a "meta volume", i.e., a volume made up of larger cells, typically 5 to 20 voxels each. We then calculate local characteristic values based on the fibers, which at least partially lie in each cell of the "meta volume". The average value of each fiber characteristic is calculated from all fibers of a cell. The individual fiber characteristics are used as input data for calculating the meta volume. We visualize the "meta volume" as a context for the original volume data in the 3D view (see Figure 2.8 A) using multi-channel volume rendering as well as overlaying in the 2D slice views. Figure 2.8 B on the left, shows a "meta volume" color-coded according to the fiber orientation angle θ. An opacity indicator takes care of the overall adjustment regarding the opacity between the overlaid "meta volume" and the original volume data in the 2D slice views. Figure 2.8 B on the right, shows the 2D slice view of the meta volume overlaid on the original volume data. The Fiber Metadata visualization allows the user to pick a fiber characteristic of interest and to visualize the characteristic's distribution as a context. It enables a better visual exploration of the data by facilitating the identification of regions with similar or different fiber characteristics.

Die approbierte gedruckte Originalversion dieser Dissertation ist an der TU Wien Bibliothek verfügbar.
The approved original version of this doctoral thesis is available in print at TU Wien Bibliothek.
TU Bibliothek WIEN Your knowledge hub

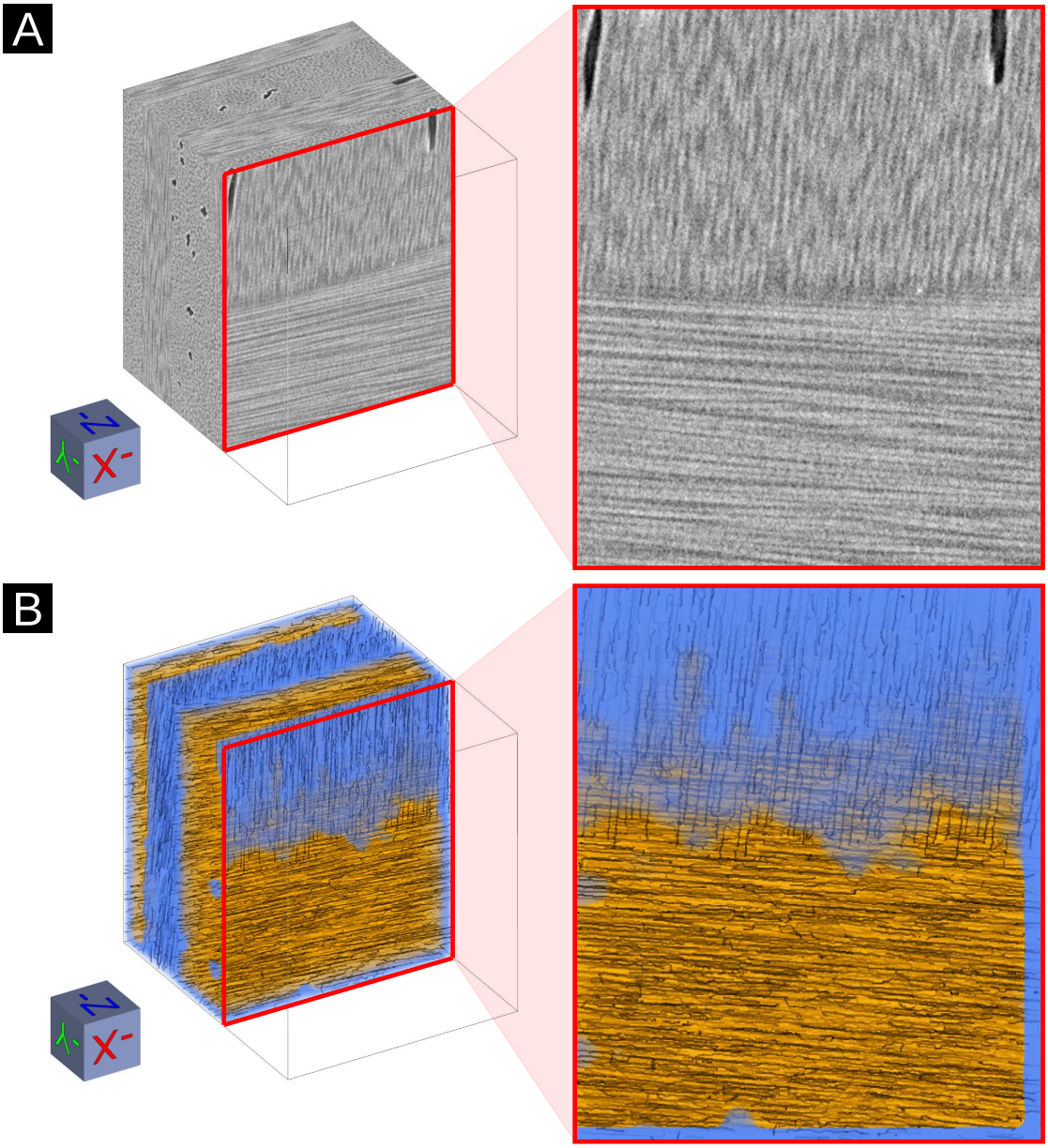

Figure 2.8: Fiber Metadata visualization of *Dataset 3*. (A) Left: Direct volume rendering of the original CFRP dataset. Right: 2D slice view with vertical fibers and pores (black areas) in the upper half and horizontal fibers in the lower half of the dataset. (B) Left: Direct volume rendering of the "meta volume" overlaid on the original CFRP data. Right: 2D slice view of the semi-transparent "meta volume" overlaid on the original data with a linear blending.

Die approbierte gedruckte Originalversion dieser Dissertation ist an der TU Wien Bibliothek verfügbar.
The approved original version of this doctoral thesis is available in print at TU Wien Bibliothek.
TU WIEN Bibliothek Your knowledge hub

2.5 Results and Evaluation

The generated results are demonstrated on different types of FRPs, i.e., one carbon fiber-reinforced polymer and two glass fiber-reinforced polymer specimens (see Section 2.5.1). A questionnaire to evaluate all presented methods was prepared and filled out by domain experts. The results outline the usability of the presented methods from the perspective of domain experts (see Section 2.5.2).

2.5.1 Visualization Results

- **Original Volume Data:** As shown in Figure 2.1 (input data), fiber classes or fiber orientations of *Dataset 1* are difficult to identify.

- **Visual Fiber Exploration Method:** After the visual exploration process, the user is able to apply a multi-class rendering process to the manually defined classes. All fibers are colored according to their specific fiber-class color in the PCP, the SPLOM, and the 3D rendering view. Figure 2.3 depicts the manually defined classes for *Dataset 1*. All the classes can be clearly identified.

- **Orientation Identification:** Figure 2.5 A depicts the 3D view of the extracted fibers (*Dataset 2*) color-coded according to the spherical color map (Figure 2.5 B). The fiber orientations can be clearly identified. The color coding is applied to the 3D view and the 2D slice view.

- **Fiber Length Distribution:** An automatic algorithm is applied to classify and visualize the fibers according to their length. Figure 2.6 shows the color-coding of the extracted fibers (*Dataset 2*) with respect to their length.

- **Blob Visualization:** To provide the domain experts with an enclosure of all their defined classes, we applied the concept of Blob visualization. This allows the domain experts to gain a quick overview of the specimens layer structure and the shape of the fiber classes. Figure 2.7 illustrates the Blob visualization based on *Dataset 1*.

- **Fiber Metadata Visualization:** A 3D view of the "meta volume" (*Dataset 3*) color coded according to the fiber characteristic θ is shown in Figure 2.8 B on the left. Blue represents a θ value between 0° and 10° and indicates that the fiber orientation is aligned along the z-axis. Orange represents a θ value between 80° and 90° and denotes fibers which are aligned orthogonally to the z-direction. The 2D slice view (see Figure 2.8 B on the right) with reduced opacity information clearly indicates the layer structure of the specimen.

2.5.2 Evaluation and User Feedback

The necessity of individual and interactive fiber-visualizations originates from requirements of non-destructive testing (NDT). During the *FiberScout* development over a

Die approbierte gedruckte Originalversion dieser Dissertation ist an der TU Wien Bibliothek verfügbar.
The approved original version of this doctoral thesis is available in print at TU Wien Bibliothek.
TU Bibliothek Your knowledge hub WIEN

period of more than 18 months, improvements of the fiber-visualization pipeline were contentiously done together with the NDT practitioners.

In order to get feedback on the *FiberScout* system, we designed an evaluation questionnaire with regard to the tasks defined by the domain experts (see Section 2.1). The questionnaire is structured so that information on the experiences of the participants with industrial 3D X-ray computed tomography are collected first. Then it is determined how suitable the PCP and the SPLOM are for classifying the fibers. In addition, the usefulness of the statistical information of the Fiber Class Explorer is queried. After that we tried to find out how the FOD is applicable for displaying fiber orientations. It is then checked if the fiber classes can be well distinguished by the Blob visualization. Finally, it is determined how well Fiber Metadata visualization suffices to indicate general fiber orientations. To evaluate the system, we choose four NDT practitioners who are familiar with X-ray computed tomography and its visual representations and four material scientists who are experienced in analyzing fiber-reinforced polymers. The averaged and weighted results of the evaluation questionnaire are depicted in Figure 2.9. The red lines represent the results of the material scientists, while the blue ones display the results of the NDT practitioners. We use a Likert scale ranging from one to five to represent the user experience, varying from poor to excellent.

The fiber-visualization pipeline on the whole received good feedback from the domain experts. The SPLOM was considered as well suited for clustering fiber characteristics. By linking the SPLOM and PCP, the relationships between the fiber characteristics can be easily revealed. Outliers in the SPLOM are obvious to be detected. In addition, the participants pointed out that further material characteristics such as porosity are easily observable. The orientation visualization is simple and self-explanatory. The main fiber orientation can be easily determined using the polar plot for the FOD. Both the NDT practitioners and the material scientists reckon that it is difficult to generate useful information of fiber characteristics using the original volume data. Blob and Fiber Metadata visualization also provide valuable results for separating fiber classes.

Die approbierte gedruckte Originalversion dieser Dissertation ist an der TU Wien Bibliothek verfügbar.
The approved original version of this doctoral thesis is available in print at TU Wien Bibliothek.
TU Bibliothek Your knowledge hub WIEN

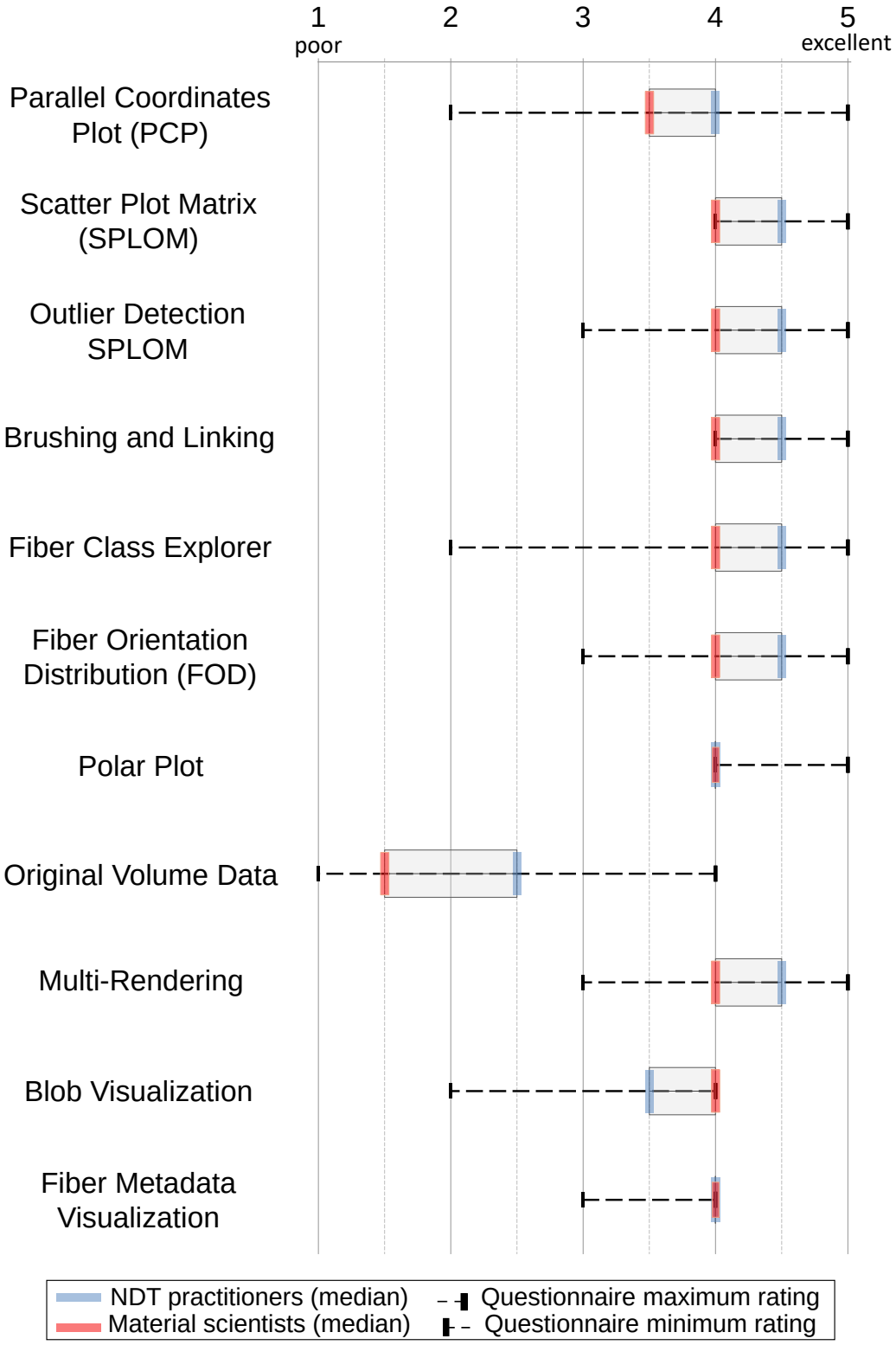

Figure 2.9: The averaged and weighted results of the *FiberScout* evaluation questionnaire with a five-point Likert scale ranging from one to five respectively, i.e., from poor to excellent.

Die approbierte gedruckte Originalversion dieser Dissertation ist an der TU Wien Bibliothek verfügbar.
The approved original version of this doctoral thesis is available in print at TU Wien Bibliothek.

2.6 Implementation

FiberScout was implemented in C++. The experiments were performed on a desktop machine with an Intel(R) Core(TM) i7-3770 CPU, 32 GB RAM and an NVIDIA GeForce GTX 1080 GPU with 8 GB RAM. ITK 4.9 [JMIC15] was used to perform basic image processing and to load the datasets. The 3D rendering views and the 2D slice views were calculated with VTK 7.0 [SML06]. The GUI was implemented in Qt 5.8 [Gro]. The research prototype is available in the open source framework *open_iA* [FWS+19].

2.7 Summary and Conclusion

In this chapter we present *FiberScout*, a system for the visual analysis of fiber characteristics in fiber-reinforced polymers. The user feedback shows overall good results from domain experts, especially concerning clustering with the help of a SPLOM with brushing and linking and the visualization of the FOD. The Fiber Metadata visualization allows the user to quickly explore the data and find regions of interest. The Blob visualization is an appreciated technique to represent regions with the same characteristics in a volume. One shortcoming of the current implementation is that the analysis is limited to approximately 100.000 fibers. In case of one million fibers, the calculation times would last much longer. This fact could be counteracted by parallelizing appropriate code sections. Another problem relates to the PCP and the SPLOM, which are cluttered if too many fiber features are selected. For future work, the calculation of additional statistics and the selection of individual fibers in the 3D view could be interesting. The experts indicated that combining the porosity information and the fiber characteristics of a specimen would be important for them as well.

Die approbierte gedruckte Originalversion dieser Dissertation ist an der TU Wien Bibliothek verfügbar.
The approved original version of this doctoral thesis is available in print at TU Wien Bibliothek.
TU Bibliothek Your knowledge hub WIEN

Die approbierte gedruckte Originalversion dieser Dissertation ist an der TU Wien Bibliothek verfügbar.
The approved original version of this doctoral thesis is available in print at TU Wien Bibliothek.

Die approbierte gedruckte Originalversion dieser Dissertation ist an der TU Wien Bibliothek verfügbar.
The approved original version of this doctoral thesis is available in print at TU Wien Bibliothek.

CHAPTER 3

PorosityAnalyzer: Visual Analysis and Evaluation of Segmentation Pipelines to Determine the Porosity in Fiber-Reinforced Polymers

This chapter is based on the following publication:

J. Weissenböck, A. Amirkhanov, E. Gröller, J. Kastner, C. Heinzl. PorosityAnalyzer: Visual Analysis and Evaluation of Segmentation Pipelines to Determine the Porosity in Fiber-Reinforced Polymers. *Proceedings of the IEEE Conference on Visual Analytics Science and Technology (VAST)*, pp. 101–110, Baltimore, United States of America, 2016. doi: 10.1109/VAST.2016.7883516

Follow-up publications:

M. Schiwarth, J. Weissenböck, B. Plank, B. Fröhler, C. Heinzl, J. Kastner. Visual Analysis of Void and Reinforcement Characteristics in X-Ray Computed Tomography Dataset Series of Fiber-Reinforced Polymers. *Proceedings of 13th International Conference on Textile Composites (TexComp-13)*, Milan, Italy, 2018. doi:10.1088/1757-899X/406/1/012014

J. Weissenböck, S. Senck, B. Plank, C. Heinzl, J. Kastner. Porosity Evaluation of Carbon Fiber-Reinforced Polymers with Porosity Analyzer. *Proceedings of the 3rd International Conference on Tomography of Materials and Structures*, Lund, Sweden, 2017.

In this chapter we present *PorosityAnalyzer*, a research prototype for detailed evaluation and visual analysis of pore-segmentation pipelines to determine the porosity in fiber-reinforced polymers (FRPs). The presented tool consists of two modules: the computation module and the analysis module. The computation module enables a convenient setup and execution of distributed offline computations on industrial 3D X-ray computed tomography (XCT) datasets. It allows the user to assemble individual segmentation pipelines in the form of single pipeline steps, and to specify the parameter ranges as well as the sampling of the parameter space of each pipeline segment. The analyzed data consists of the calculated 3D binary-segmentation mask, the resulting porosity value, and other derived results (e.g., segmentation-pipeline runtime) along with the input parameters. The analysis module presents the data at different levels of detail by drill-down filtering in order to determine accurate and robust segmentation pipelines. Overview visualizations allow the user to initially compare and evaluate the segmentation pipelines. With a scatter plot matrix (SPLOM), the segmentation pipelines are examined in more detail based on their input and output parameters. Individual segmentation-pipeline runs are selected in the SPLOM and visually examined and compared in 2D slice views and 3D rendering views by using aggregated segmentation masks and statistical contour renderings. *PorosityAnalyzer* has been thoroughly evaluated with the help of twelve domain experts. Two case studies demonstrate the applicability of our proposed concepts and visualization techniques, and show that our tool helps domain experts to gain new insights (e.g., that one segmentation algorithm does not work reliably at certain porosity values while another works across the whole range) and improve their workflow efficiency.

3.1 Introduction

In material testing and quality control the porosity value is often used for deciding whether an expensive component passes a quality-control check or whether it is rejected. The porosity value is defined as the ratio in percent of the total cumulative volume of all pores in the specimen to the specimen's volume. There exist various destructive and non-destructive testing (NDT) methods for the porosity determination in FRPs. Destructive testing methods include wet-chemical analysis using acid digestion and materialography in combination with microscopic analysis [BS04]. NDT methods, for example, are ultrasonic testing and active thermography [MPSH11]. However, these methods are often not as accurate as desired in critical areas of the specimen. In contrast, modern XCT scanning devices are capable of delivering high-resolution results down to a few microns. When XCT is used for a precise porosity determination, the scan parameters, the reconstruction methods, the image processing, and especially the segmentation algorithms play a decisive role. The porosity determination of FRPs by means of XCT is difficult, since typical industrial components are composed of various materials. The wide variety of material

Die approbierte gedruckte Originalversion dieser Dissertation ist an der TU Wien Bibliothek verfügbar.
The approved original version of this doctoral thesis is available in print at TU Wien Bibliothek.
TU Bibliothek WIEN Your knowledge hub

combinations causes differences in image quality regarding noise, sharpness, and artifacts. Therefore, the XCT experts are required to adjust the parameters of their segmentation methods for every material type.
To determine the porosity of an XCT-scanned FRP specimen, the domain experts are mainly using global-threshold segmentation algorithms to extract the pores from the rest of the specimen (fibers and matrix) [SKO+11]. The advantage of global-thresholding segmentation methods is the high processing speed and the small number of parameters to tune. A representative of this family is the Otsu segmentation algorithm [Ots79]. This histogram-based segmentation method has no parameters. Usually XCT datasets are suffering from noise, artifacts (e.g., beam hardening), and low resolution. Therefore, global-thresholding segmentation methods might produce a significant number of misclassified voxels, which leads to an incorrect porosity value of the specimen. This problem can be solved by using smoothing filters to reduce the noise and more advanced segmentation methods. These algorithms typically require additional parameters to specify. Tuning these input parameters to find an appropriate parameter preset is essential.
Typically, domain experts start this task by empirically setting initial parameters to the best of their knowledge and experience. The result is then visually compared side-by-side to a reference segmentation, which comes from the same dataset. Depending on the result, the parameters are adapted. This iterative process is terminated as soon as the domain experts considers the correspondence between result and reference as sufficient. In addition, the comparison of the results is further hampered by the different outcomes, which originate from different reference methods. During the iterative procedure of porosity determination, it is important to record the parameter combinations and the corresponding results to evaluate and compare them later. This trial-and-error approach is not only time-consuming, tiring, and often frustrating, but also generates modest results in many cases.
Taking all the factors mentioned above into account, it follows that there is a high demand for methods to set up segmentation pipelines, to perform all necessary computations in batches, to manage and organize the resulting data, and to support the visual analysis of the data. With such tools available, domain experts can be much more efficient in making a well-justified selection of the segmentation pipeline for XCT-scanned FRP specimens. Moreover, it enables the domain experts to base their decision-making on a detailed analysis of various aspects of pore-segmentation pipelines and domain-specific requirements. Based on the demands of the experts, we identified the following tasks:

- **Task 1:** Set up a segmentation pipeline where the parameter ranges of all filters are adjustable and run the segmentation pipelines in a batch process.
- **Task 2:** Analyze and evaluate the pipelines and compare them with each other.
- **Task 3:** Explore segmentation-pipeline parameter trade-offs concerning accuracy, performance, and stability.
- **Task 4:** Generate accurate, robust, and reproducible results using a specific segmentation-pipeline preset for a class of datasets.

Die approbierte gedruckte Originalversion dieser Dissertation ist an der TU Wien Bibliothek verfügbar.
The approved original version of this doctoral thesis is available in print at TU Wien Bibliothek.
TU Bibliothek WIEN Your knowledge hub

In order to fulfill these domain-specific demands we present *PorosityAnalyzer*, an interactive research prototype to visually analyze and explore segmentation pipelines for porosity determination in FRPs. The workflow of the *PorosityAnalyzer* is shown in Figure 3.1. The input data are: a list of XCT-scanned FRP datasets and a list of reference segmentations for these datasets. The datasets are described in Section 3.3.

The tool is divided into two modules: the computation module and the analysis module. The computation module allows users to set up and execute distributed offline computations of porosity segmentation pipelines (see Section 3.4). In the computation setup-phase, the parameter spaces of the segmentation algorithms for the chosen datasets are sampled and the resulting settings are stored. The computations are then performed, resulting in sets of segmentation-pipeline runs. For each run the segmentation mask, porosity value, runtime, and Dice-coefficients describing the similarity between a segmentation mask and a reference-segmentation mask [Dic45] are calculated and stored. These computation results are used as input for the analysis module (see Section 3.5), which provides methods for visualization, exploration, and visual analysis of the segmentation pipelines. The analysis module consists of four levels: prefiltering, overview, analysis, and visual examination. During a drill-down approach, the user performs a visual analysis and an examination of the data on each level by selecting the most interesting data portion and passing it on to the next level. This allows the user a thorough visual analysis from the data overview to the most detailed representations.

The main contributions of this part of the work are in the visual knowledge discovery, in the interactive visualization techniques on multiple levels-of-detail, and in the fulfillment of the domain-specific requirements for the analysis of pore segmentation-pipelines concerning XCT-scanned FRP specimens.

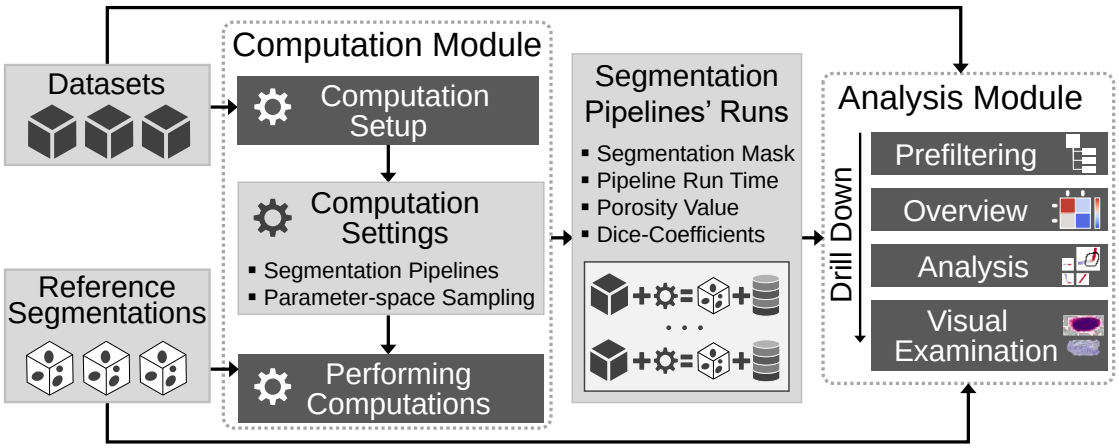

Figure 3.1: Overview of the *PorosityAnalyzer* workflow (light gray boxes: input and intermediate data, dark-gray boxes: stages of the workflow).

Die approbierte gedruckte Originalversion dieser Dissertation ist an der TU Wien Bibliothek verfügbar.
The approved original version of this doctoral thesis is available in print at TU Wien Bibliothek.

3.2 Related Work

The related work of *PorosityAnalyzer* lies in the areas of 3D image segmentation, visualization of multi-dimensional data, and visual parameter-space analysis. A broad survey of 3D image segmentation methods is presented by Wirjadi [Wir07]. Gleicher et al. [GAW+11] provide a detailed survey on methods for information visualization and visual comparison. Scatter plots are often used as a visualization method for statistical, non-spatial, and multi-dimensional data [CM88]. A SPLOM organizes all possible combinations of 2D scatter plots in one layout for providing an overview on multidimensional data, studying the correlations between data dimensions, and locating clusters of data points. Elmqvist et al. [EDF08] introduced novel SPLOM navigation techniques using transitions for an intuitive multidimensional visual data exploration. Mindek et al. [MMGB17] present a model for providing a data sensitive navigation for user interface elements. The model normalizes the user input according to the visual changes. This makes the changes in the input parameters more predictable with respect to the perceived changes in the output image and helps the user to anticipate the expected effects of the interaction. Gavrilescu et al. [GMG10] extended interface elements, such as sliders or transfer function editors, with plots showing the magnitude of change in a rendered image. This provides visual cues on the resulting effects that would occur if a certain parameter is changed. We utilized a similar approach with parameter-range sliders (see Section 3.5.3).

The related research in the area of porosity analysis and pore visualization in FRPs is given in the approaches by Reh et al. Porosity Maps [RPK+12] provide an overview of pore locations and density. The Mean Objects (MObjects) [RGK+13] visualization aggregates all the pores in the specimen in order to cluster pores by shape and size, and provides a global overview of pore shapes in the data. Ushizima et al. [UMW+12] proposed geometric and topological descriptors to enhance the estimation of material permeability in complex porous micro structures. Their analysis framework combines image processing, multi-scale topological analysis, and the visualization of pore bodies.

Visual parameter-space analysis has a great potential to support the validation and the use of simulation models. Sedlmair et al. [SHB+14] developed an abstract conceptual framework for visual parameter-space analysis problems to guide and systematize research endeavors in this area. The authors' framework covers a broad range of tools and design studies from different application fields. Their classification is based on three major components: a data-flow model abstractly describing analysis problems independent of the application domain, a set of four navigation strategies supporting the parameter-space analysis with visualization methods, and a characterization of six analysis tasks. Our work fits into this framework and fulfills the following classification criteria: it is a data-flow model with an integrated sampling step, utilizing derived measures. The navigation strategy is global-to-local. The application area is engineering and the analysis tasks are optimization, partitioning, and sensitivity investigation.

Another related work in the field of visual parameter-space analysis was done by Piringer et al. [PBK10], who use multiple 2D and 3D projections of an n-dimensional

Die approbierte gedruckte Originalversion dieser Dissertation ist an der TU Wien Bibliothek verfügbar.
The approved original version of this doctoral thesis is available in print at TU Wien Bibliothek.
TU Bibliothek Your knowledge hub WIEN

space for regression-model simulations in car engine design. Their approach compares known and predicted results, as well as results of multiple models, analyzes regions with a bad fit, and assesses the physical plausibility of models. Berger et al. [BPFG11] extend this work for uncertainty-aware exploration of continuous parameter spaces. They guide the user to potentially interesting parameter regions and visualize the model predictions' uncertainty in 2D scatter plots and parallel coordinates plots. Coffey et al. [CLEK13] utilize a local-to-global approach for exploring large design spaces in simulation-based engineering, the design of visual effects, and other tasks that require tuning parameters of computationally intensive simulations. Pretorius et al. developed Paramorama [PBCR11], a plug-in for the CellProfiler biomedical image-analysis framework that regularly samples continuous parameters of an image processing pipeline. Their visual analysis tool is used to study relationships between the input parameter-space and image-based outcomes. Results are hierarchically clustered based on the parameter values and can be queried and laid-out side-by-side for a visual comparison. Bergner et al. [BSM+13] introduced ParaGlide, a visualization system for a systematic interactive exploration of parameter spaces of multi-dimensional simulation models.

The Tuner system by Torsney-Weir et al. [TWSM+11] is somewhat similar to *Porosity Analyzer* and also addresses the problem of parameter finding in image segmentation algorithms and finding optimal algorithm presets. The parameter space of the evaluated algorithm is parsed, and off-line computations are performed. Dice-coefficients are utilized to evaluate the quality of the segmentation results compared to the ground-truth segmentations. Finally, a Pareto panel and HyperSlice [vWvL93] views are used for the visual analysis and navigation. In comparison to Tuner, there is a list of important differences that sets our work apart. First, the potential users of Tuner are segmentation-algorithm developers, i.e., people who are familiar with all the implementation details and inner workings of segmentation algorithms. *PorosityAnalyzer's* main users are domain experts, i.e., segmentation-algorithm consumers, who are required to solve specific tasks involving segmentation algorithms. Second, the goal of Tuner is to find optimal parameter settings for one segmentation algorithm. The main goal of *PorosityAnalyzer* is to evaluate and compare many different segmentation pipelines in order to find the optimal pipeline and preset. Third, optimizations in Tuner are based on a ground-truth segmentation mask. We are mainly interested in evaluating segmentation pipelines based on porosity as an domain specific criterion. In addition, we consider the reference-segmentation mask and runtime of the algorithm. The reference-segmentation mask is considered as ground truth. Fourth, Tuner is designed to work with one algorithm and one dataset at a time with the possibility to switch datasets sequentially. One important design principle of *PorosityAnalyzer* is to provide offline computations and visual analysis for multiple segmentation pipelines and multiple datasets at once. Fifth, there is a clear distinction in how the sensitivity analysis is performed. Tuner is using uncertainty/gain values provided by a Gaussian process model. Interactive sensitivity analysis is performed in the following way: as the user changes a particular parameter value all plots dependent on it change interactively, which reflects the algorithm's sensitivity to this parameter. *PorosityAnalyzer* mainly uses boxplots, histograms, statistical contours for porosity

Die approbierte gedruckte Originalversion dieser Dissertation ist an der TU Wien Bibliothek verfügbar.
The approved original version of this doctoral thesis is available in print at TU Wien Bibliothek.
TU Bibliothek WIEN Your knowledge hub

segmentations, and parameter-range sliders (PRSs) to evaluate a segmentation-pipeline's sensitivity and robustness. Finally, in the investigation phase we are utilizing a SPLOM in the analysis module, while Tuner is relying on the HyperSlice visualization.

3.3 Dataset Description

Our domain experts mainly deal with fiber-reinforced polymers (FRPs). In this work we use seven carbon fiber-reinforced polymer (CFRP) specimens, which were measured with a GE phoenix|X-Ray Nanotom 180 NF XCT device. Due to the different methods for reference porosity determination, we categorized the datasets into two classes. In the subsequent sections, we will refer to these classes as: *aeronautic industry* and *wet-chemical analysis* scans. The specimens are named accordingly: *Ex_* and *WChem_low*. In addition, we investigated the *PorePhantom* dataset, where the pores were artificially included by the domain experts using an in-house built XCT simulation software called *SimCT*, which has been developed by Reiter et. al. [RMH+09]. The simulation parameters for the virtual X-ray source and detector were chosen to be identical with respect to real-world XCT scans. Table 3.1 provides an overview of the used datasets. Figure 3.2 shows a dataset representative of each category.

Dataset Name	xyz-Dimensions (Voxels)	Resolution	Reference Porosity
E3_low	749×304×1396	10.0 µm	0.965%
E4_low	711×302×1423	10.0 µm	0.394%
E5_high	756×262×1472	10.0 µm	6.668%
E6_high	835×298×1653	11.5 µm	6.819%
E7_high	842×288×1706	11.5 µm	8.657%
WChem_low	1365×421×1674	10.0 µm	0.501%
PorePhantom	173×230×140	11.0 µm	6.123%

Table 3.1: Characteristics of the FRP datasets used in the work of *PorosityAnalyzer*.

Die approbierte gedruckte Originalversion dieser Dissertation ist an der TU Wien Bibliothek verfügbar.
The approved original version of this doctoral thesis is available in print at TU Wien Bibliothek.
TU Bibliothek Your knowledge hub WIEN

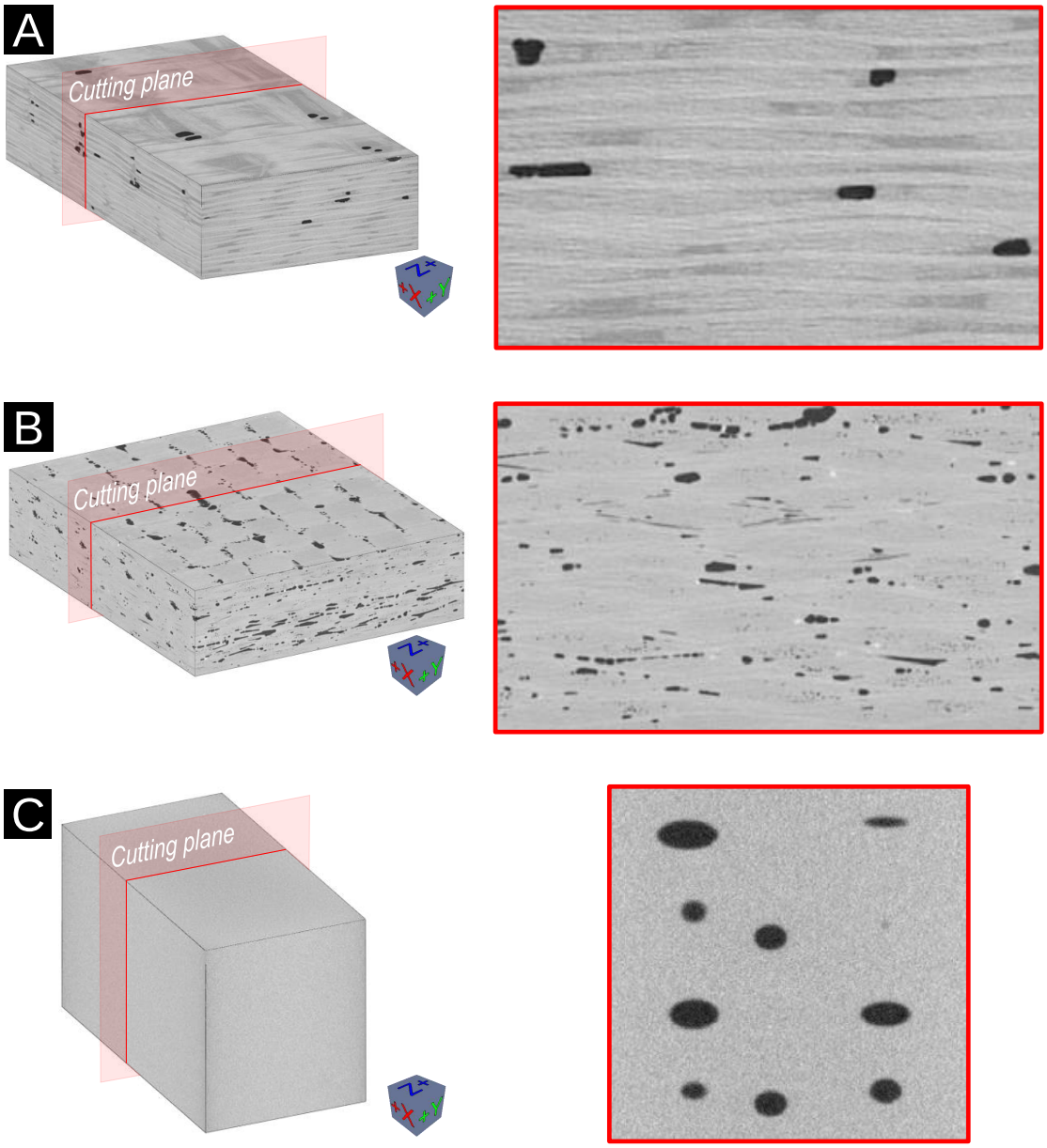

Figure 3.2: (A) *Aeronautic industry* dataset E5_high. (B) *Wet-chemical analysis* dataset WChem_low. (C) *Simulated XCT* dataset PorePhantom.

Die approbierte gedruckte Originalversion dieser Dissertation ist an der TU Wien Bibliothek verfügbar.
The approved original version of this doctoral thesis is available in print at TU Wien Bibliothek.
TU Bibliothek Your knowledge hub WIEN

3.4 Setup of Segmentation Pipelines

According to the domain-specific requirement, to be able to batch-process various segmentation pipelines (see Task 1, Section 3.1), we designed a computation module, which provides a GUI for connecting segmentation-pipeline filters within the user-defined parameter spaces in a simple way. The core of the computation module is the batch-processing of the created segmentation pipelines and the data storing of the calculated results. Starting from an identical database (XCT datasets of the FRP specimens), the module can be run on different computers simultaneously, in order to distribute the computation load. For this purpose, we designed a file and folder structure for storing the results of the individual computers in a shared folder (see Figure 3.3).

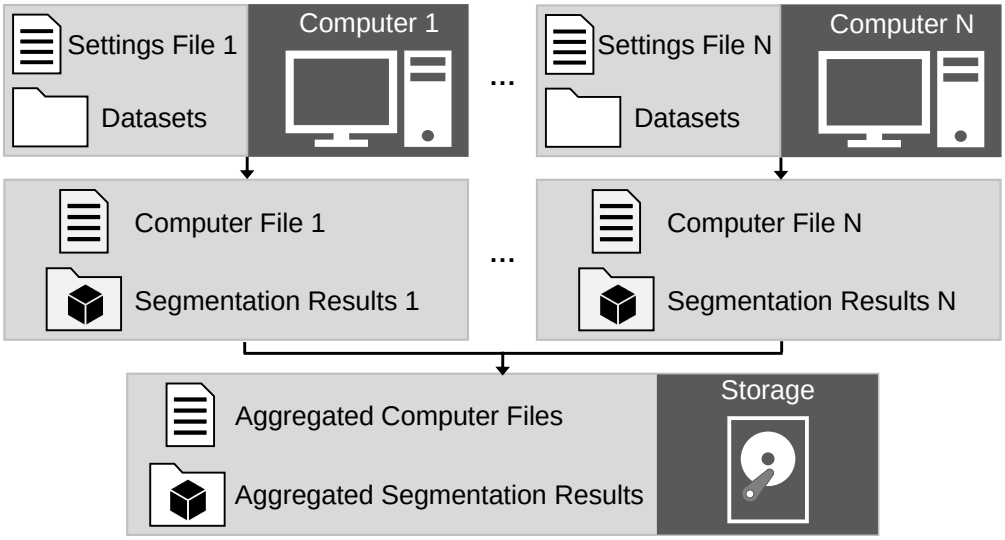

Figure 3.3: Underlying file and folder structure of the *PorosityAnalyzer* prototype.

Each segmentation-pipeline run of the batch process stores the information about the used computer (e.g., CPU type and speed), the assembled segmentation pipeline and its parameters, the calculated results (e.g., runtime, the porosity value), and the binary-segmentation masks. In the background, this module takes care of the proper filter linkage by setting the necessary intermediate connection steps (e.g., ensuring correct data types). Thus, the required user-input is kept very small. To set up a batch computation, the user has to specify the locations where the data are stored. The batch-computation settings-file (see Figure 3.4 A) contains all the previously investigated pipelines. The pipelines in the file will be automatically loaded to the segmentation-pipeline batch-table (see Figure 3.4 B). Once the paths and the folders are specified, the different segmentation pipelines can be created (see Figure 3.4 C). In addition, the log view provides information about the current progress and the created files (see Figure 3.4 D).

Die approbierte gedruckte Originalversion dieser Dissertation ist an der TU Wien Bibliothek verfügbar.
The approved original version of this doctoral thesis is available in print at TU Wien Bibliothek.
TU Bibliothek Your knowledge hub WIEN

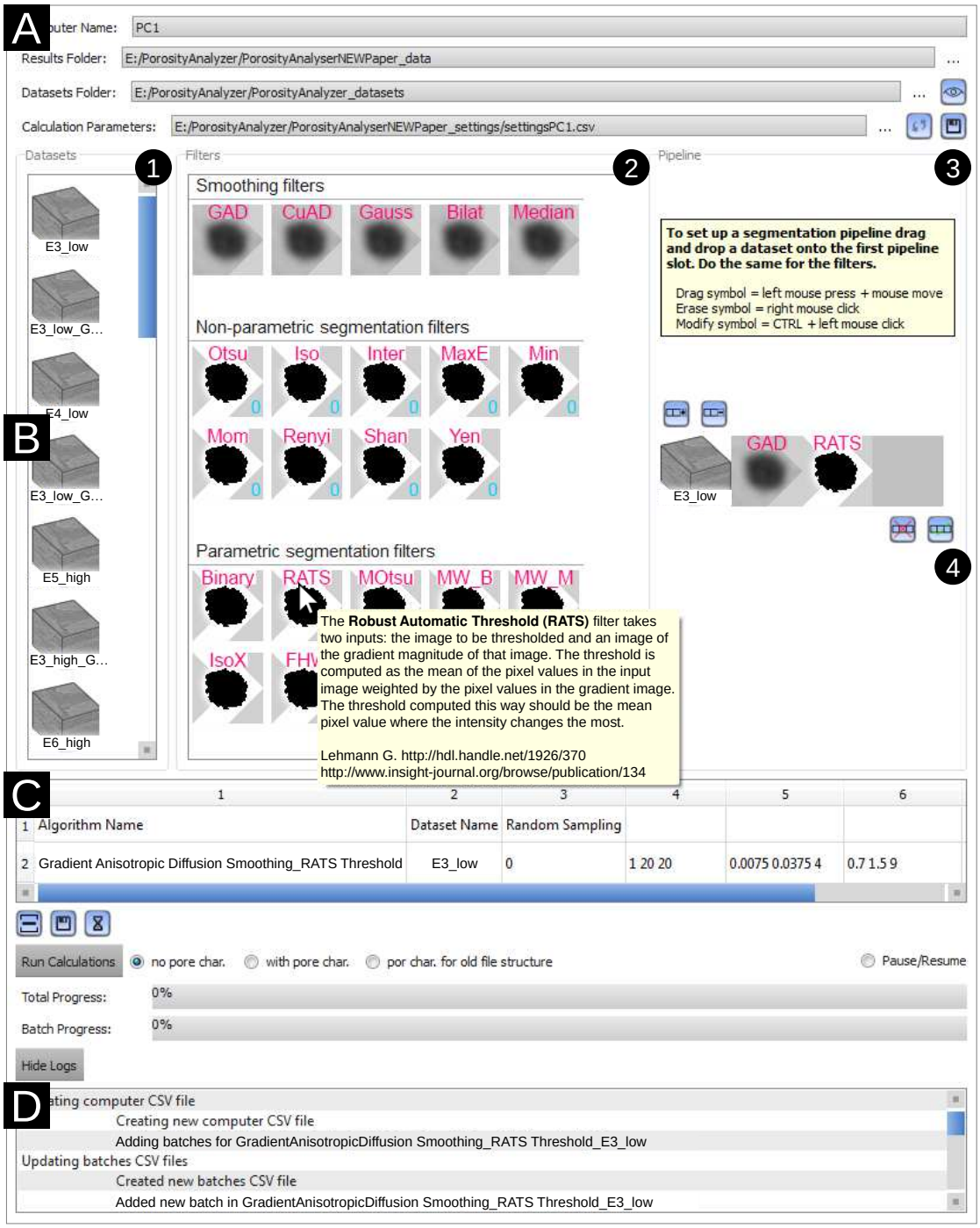

Figure 3.4: The computation module to set up and batch-process segmentation pipelines. (A) Folder and file paths to load and save the data. (B) Drag and drop area to assemble a segmentation pipeline (datasets (1), filters (2), pipeline (3)). (C) The accepted pipelines (4) are shown in the batch table. (D) The log view to inform the user.

Die approbierte gedruckte Originalversion dieser Dissertation ist an der TU Wien Bibliothek verfügbar.
The approved original version of this doctoral thesis is available in print at TU Wien Bibliothek.
TU Bibliothek Your knowledge hub WIEN

We initially pursued a text-based approach to create a segmentation pipeline. The individual filters of a pipeline and their parameter ranges were manually entered in the columns of the batch table. The involved experts criticized this approach because of the cumbersome, complicated, and error-prone data entry. In order to overcome these problems, we opted for a drag-and-drop interface to set up the segmentation pipelines (see Figure 3.4). A segmentation pipeline may consist of any number of steps. To set up a pipeline, a dataset icon from the dataset list (1) is selected and positioned into the first slot of the pipeline (3). This drag and drop process is repeated for the desired number of filters/steps (2) to build a functional segmentation pipeline.
After the pipeline assembly is completed, the parameter-space sampling is specified for each filter. For this purpose the filter icons in the pipeline can be clicked and the corresponding parameter-space sampling dialog (PSD) opens (see Figure 3.5). Here, the sampling method (regular sampling or random sampling) for each step and the corresponding parameter ranges are specified. In the case of regular sampling, the user defines the n-dimensional grid granularity by simply specifying the range and the number of samples of each filter parameter. n is the number of input parameters, which is in the range from zero to seven for the pipelines we tested. This causes the parameter step-size to be fixed to the ratio between the parameter range and the number of samples minus one. In the case of random sampling, the samples are selected arbitrarily inside a user-defined parameter range.
The first version of the PSD was designed as a simple input interface for defining the parameter ranges of a filter. However, this dialog was not well accepted by the domain experts with the argumentation that it does not preserve the context of the pipeline's dataset, which makes the parameter-range specification difficult. Therefore, we equipped the PSD with an xy-slice of the dataset, additional dataset information (e.g., dimension, resolution), the corresponding gray-value histogram (with labeled pore and material peaks), and a filter description. Finally, the created pipeline (see Figure 3.4 B (4)) with the defined parameter-space sampling can be added to the segmentation-pipeline batch-table (see Figure 3.4 D).

Die approbierte gedruckte Originalversion dieser Dissertation ist an der TU Wien Bibliothek verfügbar.
The approved original version of this doctoral thesis is available in print at TU Wien Bibliothek.
TU Bibliothek WIEN Your knowledge hub

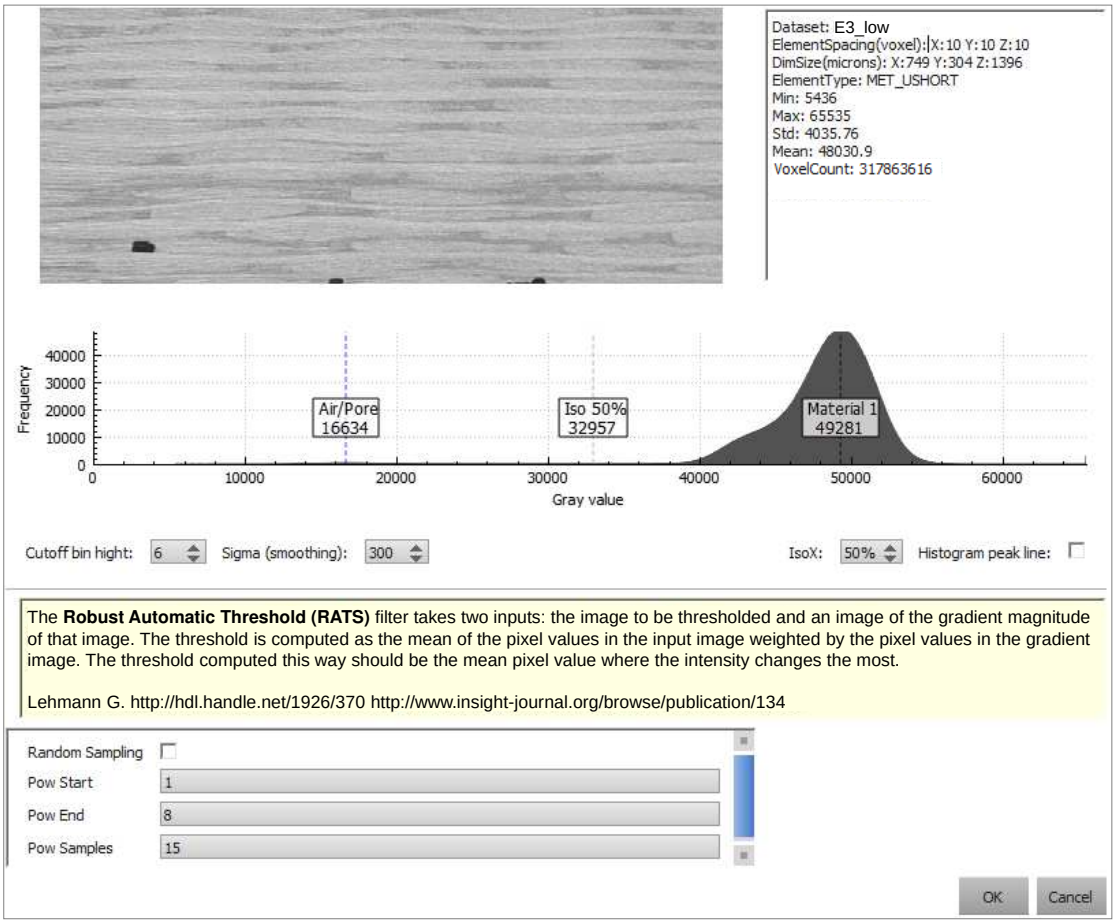

Figure 3.5: The parameter-space sampling dialog (PSD) of the Robust Automatic Threshold Selection segmentation (RATS) filter (see Table 3.2) as an example.

Pressing the *Run Calculations* button executes the defined segmentation pipelines on the machine. As presented in Figure 3.3, the computation results of the batch-processes will be stored in an aggregated computer file and an aggregated segmentation-results folder. In detail, the aggregated computer file contains the following meta information: computer name, CPU type, CPU speed, and segmentation pipeline. The aggregated segmentation-results folder contains the run files and segmentation masks for every computed segmentation-pipeline run. The masks are saved to disk as a 3D binary dataset where the segmented pores have a value of one. The run file of each computed segmentation pipeline stores the information of each single run as follows: start and elapsed time, the porosity value, the segmentation-mask file-name, the false positive/negative error based on the Dice-coefficients, and the pipeline parameter-values. By repeating the segmentation pipeline setup-process on other machines, the calculation of different segmentation pipelines can be distributed. The calculated results from the different batch-processed segmentation pipelines serve as input for the analysis module (see Section 3.5).

Die approbierte gedruckte Originalversion dieser Dissertation ist an der TU Wien Bibliothek verfügbar.
The approved original version of this doctoral thesis is available in print at TU Wien Bibliothek.
TU Bibliothek Your knowledge hub WIEN

The *PorosityAnalyzer* primarily uses the Insight Segmentation and Registration Toolkit (ITK) 4.6 [JMIC15] and its filter implementations. In our demonstrator framework we use five smoothing filters, nine non-parametric segmentation filters [Bea11], and ten parametric segmentation filters. A detailed list of the implemented filters is presented in Table 3.2.

Filter Name	**Abbreviation**	**Reference**
Smoothing filters		
Gradient Anisotropic Diffusion	GAD	[JMIC15]
Curvature Anisotropic Diffusion	CAD	[JMIC15]
Recursive Gaussian	Gauss	[JMIC15]
Bilateral	Bilat	[JMIC15]
Median	Median	[JMIC15]
Non-parametric segmentation filters		
Otsu Threshold	Otsu	[Bea11]
IsoData Threshold	Iso	[Bea11]
Intermodes Threshold	Inter	[Bea11]
Maximum Entropy Threshold	MaxE	[Bea11]
Minimum Threshold	Min	[Bea11]
Moments Threshold	Mom	[Bea11]
Renyi Threshold	Renyi	[Bea11]
Shanbhag Threshold	Shan	[Bea11]
Yen Threshold	Yen	[Bea11]
Parametric segmentation filters		
Binary Threshold	Binary	[JMIC15]
Robust Automatic Threshold Selection	RATS	[Leh06]
Multiple Otsu	MOtsu	[Ng04]
Watershed (Beucher)	MW_B	[BL06]
Watershed (Meyer)	MW_M	[BL06]
Confidence Connected	Confi	[JMIC15]
Connected Threshold	Conn	[JMIC15]
Neighborhood Connected	Neigh	[JMIC15]
IsoX Threshold	IsoX	–
Maximum Distance	Fhw	[KPSS10]

Table 3.2: Available smoothing and segmentation filters in the *PorosityAnalyzer*.

Die approbierte gedruckte Originalversion dieser Dissertation ist an der TU Wien Bibliothek verfügbar.
The approved original version of this doctoral thesis is available in print at TU Wien Bibliothek.
TU Bibliothek Your knowledge hub WIEN

3.5 Visual Analysis and Evaluation of Pore Segmentation-Pipelines

The analysis module provides exploration and analysis methods for the large number of results generated by applying multiple segmentation pipelines with varying presets to a set of different datasets. The overall purpose of this module is to provide the functionality needed by the domain experts to efficiently and conveniently perform their analysis.

In order to enable an intuitive visual-analysis workflow for segmentation data, we follow the *"overview first, zoom and filter, then details-on-demand"* design mantra by Ben Shneiderman [Shn96]. The data are analyzed on four levels-of-detail: tree view (prefiltering stage), Overview Comparative Matrix (overview stage), SPLOM and PRSs (analysis stage), and comparative visualizations using 2D slice views and 3D rendering views (visual examination stage). Figure 3.6 depicts the four data representation stages. In each stage, a portion of the data can be selected. First, the user loads all generated segmentation data and prefilters particular segmentation pipelines and datasets if necessary (see Section 3.5.1). The Overview Comparative Matrix shows the deviations of the segmentation-pipelines' porosity values from the porosity values of the reference methods (see Section 3.5.2). Here, the user selects a pipeline/dataset combination and analyzes it on the level of the individual segmentation runs (see Section 3.5.3). Finally, the user visually verifies and compares the selected segmentation runs side-by-side by means of 2D slice views and 3D views (see Section 3.5.4). By using the interconnected data representation stages, the requirements of the domain experts, i.e., *analysis, evaluation and comparison of the candidate pipelines* as well as *segmentation-pipeline parameter trade-off analysis* are met (see Task 2 and Task 3, Section 3.1).
Initially, the individual views of each stage were displayed hierarchically in tab views. With the separation into the tab views, the domain experts experienced problems as the context to the previously selected data is lost. Therefore, we decided to present all views of the individual stages at the same time. When selecting data in one view, the data in all other views are automatically updated. All views can be positioned and resized individually. In the following subsections, we describe each data representation stage of the analysis module.

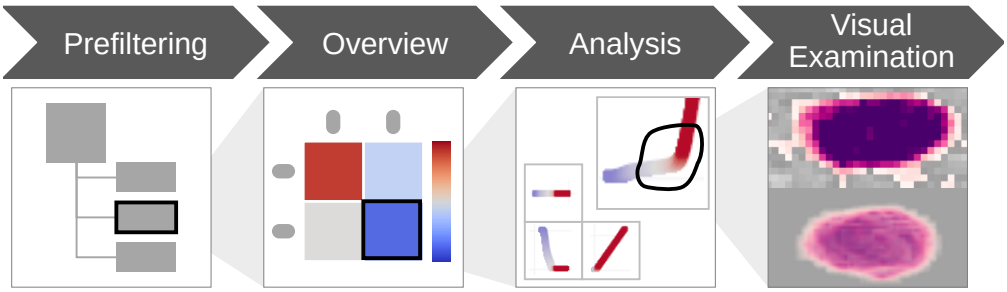

Figure 3.6: Data representation stages of the analysis module.

Die approbierte gedruckte Originalversion dieser Dissertation ist an der TU Wien Bibliothek verfügbar.
The approved original version of this doctoral thesis is available in print at TU Wien Bibliothek.

3.5.1 Prefiltering Stage

After loading the segmentation data into the analysis module we provide a collapsible and expandable side-panel for prefiltering the data. The GUI for the prefiltering segmentation data is shown in Figure 3.7. The loaded segmentation data are presented in the tree view (1). Here, the top-level tree-items can be grouped either by the segmentation pipeline or by the dataset. The grouping is selected using a combo box (2). The user can then expand top-level items. If the top-level items are grouped by dataset, the second-level items will be grouped by segmentation pipeline and vice-versa. Expanding the second-level tree-items reveals all the available information about the individual runs for the chosen segmentation pipeline/dataset combination. The filtering options (3) can be hidden using the corresponding button (4). The user can prefilter the data by selecting the segmentation pipelines or datasets. The contents of the tree view and the Overview Comparative Matrix (see Section 3.5.2) are dynamically updated whenever the filter settings are modified.

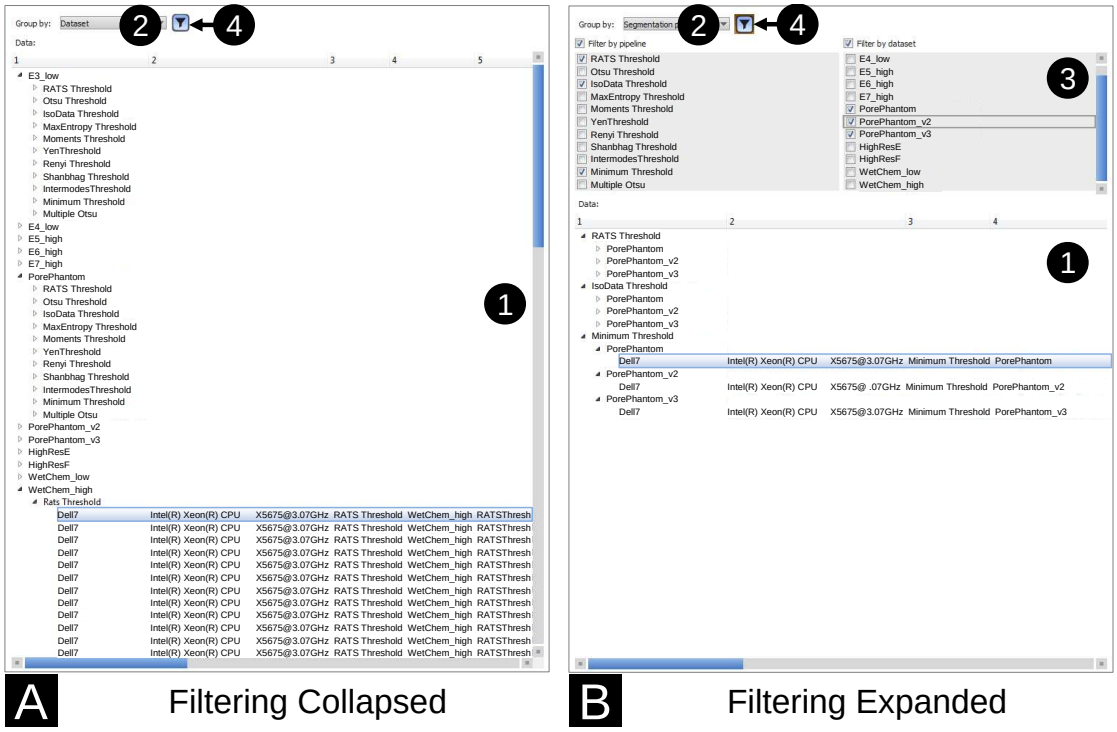

Figure 3.7: The GUI of the optionally (A) collapsed or (B) expanded prefiltering stage. The segmentation data are organized in a tree view (1), which can be grouped by segmentation-pipeline or dataset (2). The filtering options (3) may be collapsed or expanded using the button (4).

Die approbierte gedruckte Originalversion dieser Dissertation ist an der TU Wien Bibliothek verfügbar.
The approved original version of this doctoral thesis is available in print at TU Wien Bibliothek.
TU Bibliothek Your knowledge hub WIEN

3.5.2 Overview Stage

Since the domain experts are primarily interested in the porosity value of a dataset, we first calculate statistical information for the resulting porosity values of all runs of each segmentation pipeline/dataset combination and their deviations from the reference porosity values. Based on these statistical values, we provide a high-level overview visualization, to allow domain experts a first judgment concerning the robustness of the porosity values (delivered by the evaluated segmentation pipelines) and concerning the accuracy of the resulting porosities.

The segmentation data from the prefiltering stage are visualized in the Overview Comparative Matrix, which shows segmentation pipelines in columns and datasets in rows (see Figure 3.8 A (1)). The Overview Comparative Matrix provides three visualization modes: *deviation*, *boxplot*, and *histogram*. The deviation mode color-codes the median porosity deviations (in %) of each segmentation pipeline/dataset combination to the reference porosity values by using a diverging cool-to-warm perceptually-uniform color map (2) as proposed by Kenneth Moreland [Mor09]. The columns of the Overview Comparative Matrix can be expanded to fit to the lengths of the segmentation-pipeline names or collapsed (see Figure 3.8 B). In addition to the deviation mode, we want to show more details on the distribution of the porosity values. Therefore, the box-plot mode was designed to render a matrix of box plots. For example, Figure 3.8 C shows a box plot for the *RATS Threshold* applied to the WChem_low dataset. A box plot shows the statistical properties (lower and upper whisker, first and third quartiles, median, and outliers) of the porosity values of a segmentation pipeline. The reference porosity value is indicated with a vertical red dashed line and outliers are depicted with blue circles. Similarly, the histogram mode depicts one porosity-value histogram per segmentation pipeline inside a matrix cell. Figure 3.8 D shows a histogram for the *RATS Threshold* applied to the WChem_low dataset. In the Overview Comparative Matrix, a cell, a column, or a row may be selected. Figure 3.8 B shows a selected column of the *IsoData Threshold*. After the selection is made, the segmentation data are forwarded to the analysis stage where they are presented through a SPLOM and PRSs (see Section 3.5.3).

Die approbierte gedruckte Originalversion dieser Dissertation ist an der TU Wien Bibliothek verfügbar.
The approved original version of this doctoral thesis is available in print at TU Wien Bibliothek.

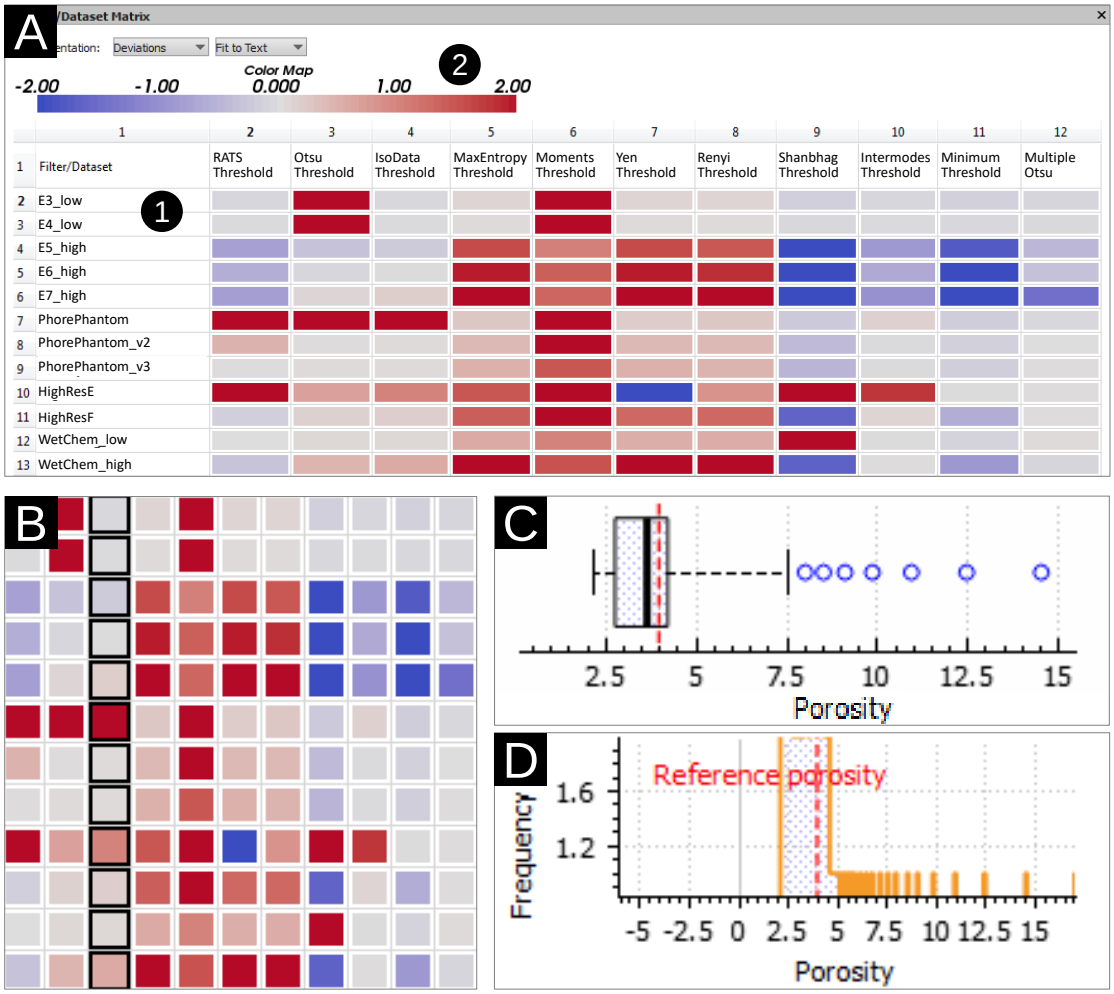

Figure 3.8: (A) The Overview Comparative Matrix in (1) *deviation* mode with the (2) diverging cool-to-warm perceptually-uniform color map, which indicates the median porosity deviation (in %) of each segmentation-pipeline/dataset combination to the reference porosity value. (B) Collapsed deviation comparative matrix with selected *IsoData Threshold* column, (C) boxplot visualization, and (D) histogram visualization.

3.5.3 Analysis Stage

The analysis stage is designed to provide techniques and methods for a detailed visual analysis of the segmentation-pipeline runs. Figure 3.9 shows the user interface for the visual analysis of segmentation data. Here, the central view is a SPLOM (1), which visualizes all the input and output parameters of each segmentation-pipeline run. To assist the visual analysis, any of these parameters can be color-coded using a perceptually-uniform color-map (2). Furthermore, a trade-off analysis is facilitated by the SPLOM.

Die approbierte gedruckte Originalversion dieser Dissertation ist an der TU Wien Bibliothek verfügbar.
The approved original version of this doctoral thesis is available in print at TU Wien Bibliothek.
TU Bibliothek Your knowledge hub WIEN

The reasons why a SPLOM was implemented are: a SPLOM is often used to make correlations, trends, and outliers visible in multi-dimensional data [Mun14] and our experts are familiar with this visual representation. When we presented the SPLOM to the experts, they mentioned that it is difficult to interpret the data points without seeing the underlaying segmentation data. In order to increase the understanding of the segmented data and their parameters, we present the segmentation result in a popup preview if the user hovers over a data point in the SPLOM. The popup preview shows the original data superimposed with the segmentation result. A region of interest (ROI) widget (7) is connected to the popup preview and shows the corresponding dataset slice-wise. By specifying a rectangular region in the ROI widget, cutouts in a dataset slice are defined and displayed in the popup preview. To compare the segmentation results of two data points in the SPLOM, one data point can be fixed. When hovering over another one, the differences in pore regions are displayed color-coded in the popup preview. Figure 3.9 depicts a dark-blue fixed data point (5) and a light blue compared data point (6). The popup preview shows a ROI of the dataset E3_low. The yellow overlay indicates that those voxels are the same in both segmentations (fixed data point (5) and compared data point (6)). The red overlay marks voxels that were segmented in the compared data point (6) segmentation but are not included in the fixed data point (5) segmentation. A blue overlay marks voxels that were segmented in the fixed data point (5) segmentation but are not present in the compared data point (6) segmentation.

Domain experts consider it as important to assess the sensitivity of variations in input parameters when evaluating a segmentation pipeline. Therefore, the PRSs, were implemented. They operate on the histogram plots of the output parameters (porosity/porosity deviations) and the input parameters of the corresponding segmentation pipeline. By selecting a range in the output-parameter histogram in Figure 3.9 (3), the corresponding range of the input-parameter histogram (4) is highlighted (yellow). Mean or median values may be chosen by the user in the input-parameter histogram. These values are calculated by keeping an input parameter constant and accumulating porosity or porosity deviation values for all combinations of the remaining input parameters. The expert can select a subset of pipeline runs by using either the SPLOM through specifying an arbitrary selection polygon in one of the scatter plots or the PRSs by specifying parameter ranges using two handles on each slider. The selection made in the PRSs is interactively synchronized with the SPLOM.

Die approbierte gedruckte Originalversion dieser Dissertation ist an der TU Wien Bibliothek verfügbar.
The approved original version of this doctoral thesis is available in print at TU Wien Bibliothek.
TU Bibliothek WIEN Your knowledge hub

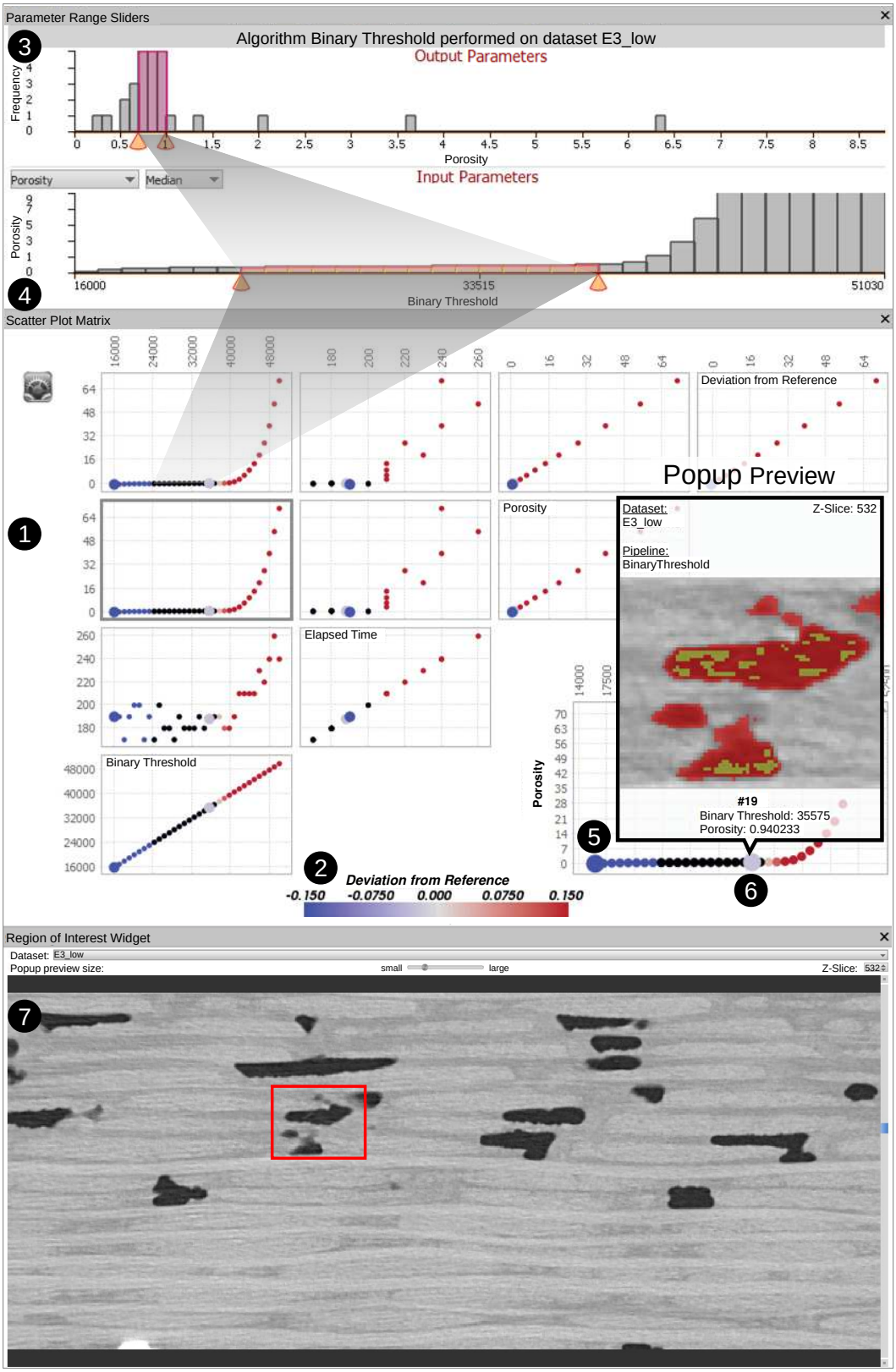

Figure 3.9: (1) The SPLOM with the different input and output parameters of a segmentation pipeline. A parameter of choice (*Deviation from Reference*) is color-coded using a (2) diverging cool-to-warm perceptually-uniform color map. (3) The porosity-frequency histogram with a selected porosity range. (4) The parameter-range slider with a selected range of the parameter *Binary Threshold*. The popup preview in the SPLOM allows the user to compare two different segmentation results (5) and (6). (7) The ROI widget with a user-specified ROI, which is used in the popup preview.

Die approbierte gedruckte Originalversion dieser Dissertation ist an der TU Wien Bibliothek verfügbar.
The approved original version of this doctoral thesis is available in print at TU Wien Bibliothek.
TU Bibliothek Your knowledge hub WIEN

Multiple selections can be managed and organized using a selections view (see Figure 3.10). Every selection from a list (1) can be chosen and dynamically loaded at any time (4). When a selection is loaded, prefiltering, overview, and analysis views automatically restore the state they had when the selection was made. This makes it easy to go back to a previous point in time during the analysis workflow. The selections view appears as a side-panel on the right, when the button (7) is toggled. The user can visually examine each selection's segmentation masks (5), or compare segmentation masks of multiple selections (6) with 2D slices views and 3D rendering views (see Section 3.5.4).

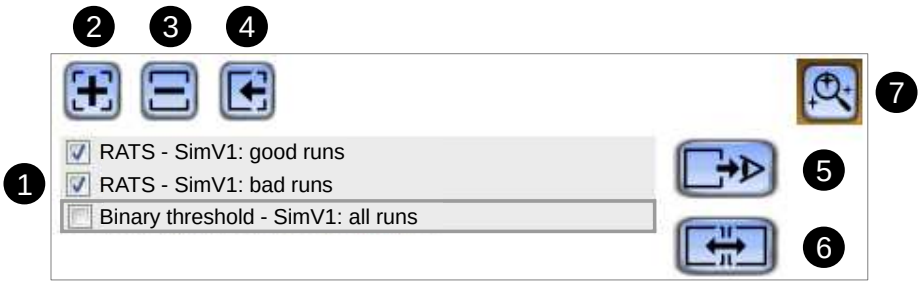

Figure 3.10: GUI of the selections view. (1) List of selections. (2) Adding or (3) removing a selection. (4) Loading a selection to the analysis stage. (5) Visualizing a single selection or (6) comparing multiple selections in the visual examination stage. Selections view visibility switch (7).

3.5.4 Visual Examination Stage

Usually, our domain experts visually examine the result of a segmentation algorithm by going through the volume and randomly investigating some 2D slices with specific features. We provide the visual examination stage to compare the segmentation results of multiple selections using 2D slice views and 3D rendering views. If a comparison of multiple selections is performed, the corresponding 2D slice view and 3D rendering view for each selection are placed side-by-side (see Figure 3.11). If the user interacts with a 2D slice views (e.g., zooming, panning) or a 3D rendering views (e.g., zooming, translation, or rotation) of one selection, the interaction results will automatically synchronize with the views of the other selections. This approach of linked views ensures that the ROIs for all the selection views under examination remain the same. Thus, the comparison of the segmentation results is facilitated.

The different visual representations of the selected data in the 2D slice view are depicted in Figure 3.12. The raw XCT data (see Figure 3.12 A) is shown in the 2D slice view to provide the proper context for the visualizations of the segmentation data. In order to convey an overview on how the selected pipeline runs segment the pores, we show an aggregated segmentation-masks overlay with adjustable opacity (Figure 3.12 B). For each voxel we calculate how many segmentation masks classify this specific voxel as a pore. Then we encode the number of masks for each voxel, using a perceptually-uniform, colorblind-safe color map chosen with ColorBrewer [HB03]. Such a representation indicates the

Die approbierte gedruckte Originalversion dieser Dissertation ist an der TU Wien Bibliothek verfügbar.
The approved original version of this doctoral thesis is available in print at TU Wien Bibliothek.
TU Bibliothek WIEN Your knowledge hub

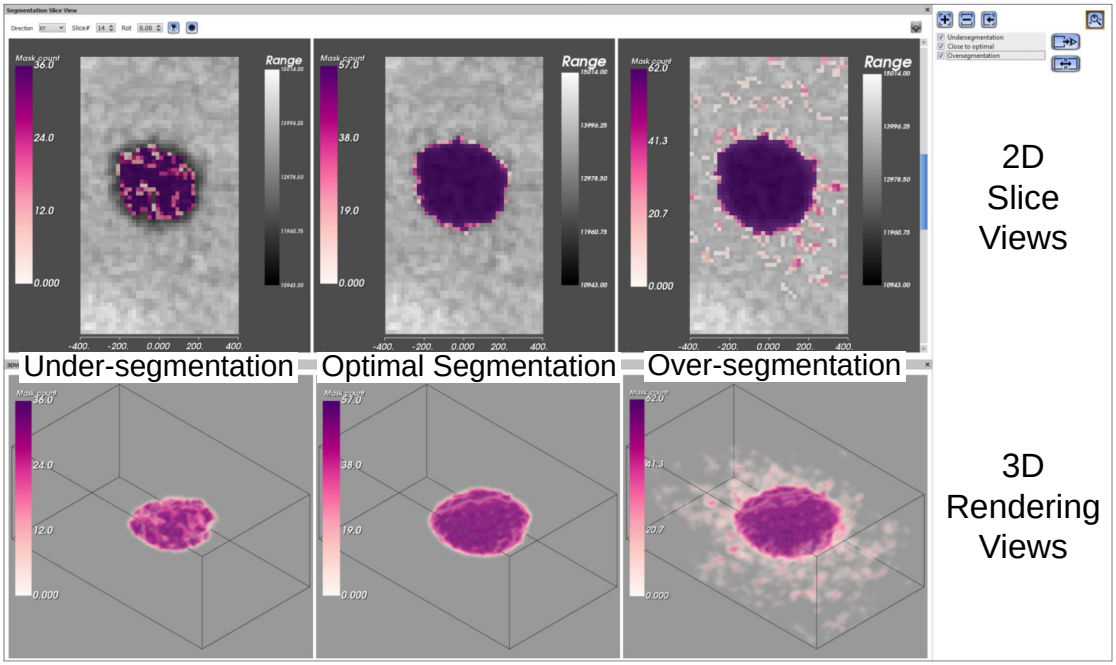

Figure 3.11: Side-by-side comparing of three different selections of aggregated segmentation masks with 2D slice views and 3D rendering views (left: under-segmentation, middle: close to optimal segmentation, right: over-segmentation).

segmented areas, and how many runs segment these areas as pores. Additional context and reference are provided by overlaying the aggregated segmentation-masks with the mask of the reference segmentation (see Figure 3.12 C). The opacity of the reference segmentation-mask overlay (yellow) can be changed by the user from transparent to opaque.

However, the segmentation masks are not capable to show exactly where the segmentation contours are. Displaying each segmentation contour for each run in the selection would result in an excessively cluttered visualization that is difficult to interpret even for experienced domain experts. Therefore, only contours are shown for three representative segmentation runs (see statistical contours in Figure 3.12 D), i.e., the runs with minimum (blue), median (black), and maximum (red) porosity values. This allows the domain experts to evaluate the potential extent of the selected runs' segmentations. The colors for the statistical contours were selected in such a way that they do not overlap with the colors from the reference and aggregated segmentation masks. Every visualization layer can be toggled on/off and displayed on top of each other, allowing the user to effectively combine the various depictions (Figure 3.12 E). For the visual-analysis scenarios where the perception of the pore shape is crucial, but 2D does not provide enough context, a 3D view is provided to the user. Aggregated segmentation masks can be rendered in 3D using volume rendering (see Figure 3.11, 3D rendering views).

Die approbierte gedruckte Originalversion dieser Dissertation ist an der TU Wien Bibliothek verfügbar.
The approved original version of this doctoral thesis is available in print at TU Wien Bibliothek.
TU Bibliothek Your knowledge hub WIEN

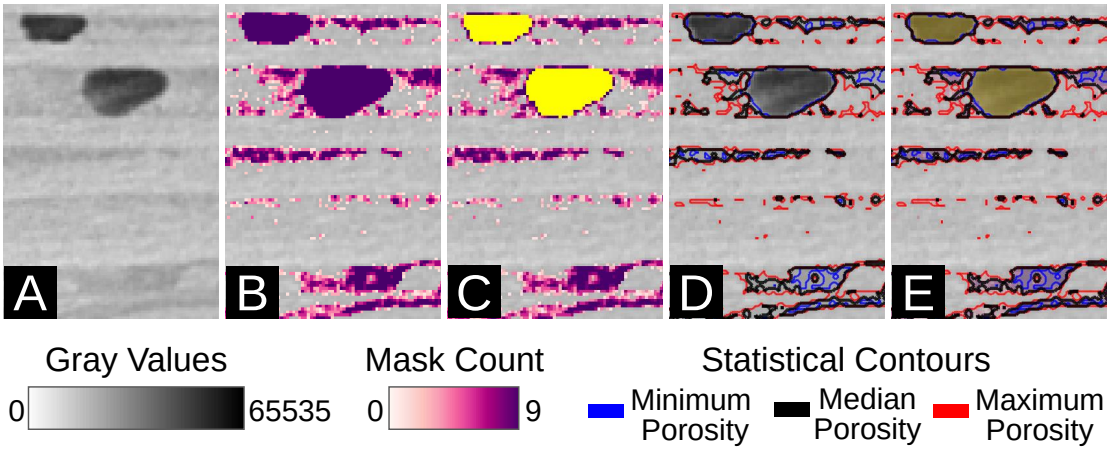

Figure 3.12: The different overlays of selected data (over-segmentation) in the 2D slice view. (A) Raw XCT data, (B) aggregated segmentation masks, (C) aggregated segmentation masks with a yellow reference-segmentation mask, (D) statistical contours, and (E) all features in combination.

3.6 Evaluation and Domain Feedback

The *PorosityAnalyzer* system was developed over a period of 16 months. During this time, we closely worked together with the domain experts. To evaluate the research prototype, a questionnaire with respect to the domain-specific tasks was compiled. The evaluation questionnaire uses a five-point Likert scale to rate the techniques and concepts. The scale ranges from one (poor) to five (excellent) respectively. In total, ten domain experts participated. Most of them work with XCT data on a daily basis, have a good knowledge of fiber-reinforced polymers (FRPs), and are well acquainted with porosity determination for FRPs. The experience of the participants in the field of XCT ranges from one year up to eleven years, in the field of FRPs from one year up to 13 years, and in the field of porosity determination of FRPs from one year up to eight years. Figure 3.13 presents the results of the evaluation questionnaire. First, the questionnaire determined how suitable the computation module and the PSD are for setting up the segmentation pipelines by showing videos of the workflow. Overall, we got a good feedback from the domain specialists in this respect. It was mentioned that the segmentation-pipeline setup by drag and drop is convenient and the automatic loading of the relevant dataset file is very comfortable. Locating the desired dataset among many others often takes a long time in commercial software. The domain experts noted that a selection of predefined segmentation pipelines (material dependent) would be helpful. The batch processing of the segmentation pipelines was lauded. With the currently used software this is only tediously possible by instantiating the program several times, setting up the different segmentation pipelines, and processing them.

To evaluate the overview visualizations of the analysis module, the domain experts had

Die approbierte gedruckte Originalversion dieser Dissertation ist an der TU Wien Bibliothek verfügbar.
The approved original version of this doctoral thesis is available in print at TU Wien Bibliothek.
TU Bibliothek Your knowledge hub WIEN

to solve domain related tasks, like comparing and rating the pipelines with respect to the reference one. Overall they performed very well, except in the case of the Overview Comparative Matrix in boxplot mode, where they could not identify the correct pipeline. One feature that may have caused confusion was the use of different plot scales. We then checked the concept of the PRSs for selecting suitable parameter ranges. Concerning the SPLOM for selecting parameters and allowing the experts a trade-off analysis, we got quite good feedback. Especially, the SPLOM popup preview to preserve the context of the segmentation results and the ROI widget were perceived as beneficial. We got excellent feedback on the 2D slice views for comparing segmentation results and overlaying those slice views with aggregated segmentation masks, reference mask, and statistical contours. The representation of aggregated segmentation masks as 3D renderings was generally received well by the domain experts, however some prefer the 2D slice views.

In addition to the questionnaire, we conducted an independent qualitative interview with two domain experts who are familiar with porosity determination of XCT scanned FRP specimens. In this interview we explained and discussed the computation and analysis module of the *PorosityAnalyzer* tool. Each module was then tested by the domain experts themselves. They created different segmentation pipelines in the computation module and evaluated previously calculated segmentation results by using the different data representation stages of the analysis module. In general, both experts pointed out that the *PorosityAnalyzer* simplifies their work significantly, (e.g., by keeping track of the segmentation results) and makes the porosity determination of FRPs more efficient (see Section 3.7, case studies). Furthermore, it provides analysis possibilities, which are hard to achieve with the currently used commercial software (e.g., comparing segmentation pipelines with color-coded 2D slice view overlays).

Die approbierte gedruckte Originalversion dieser Dissertation ist an der TU Wien Bibliothek verfügbar.
The approved original version of this doctoral thesis is available in print at TU Wien Bibliothek.
TU Bibliothek WIEN Your knowledge hub

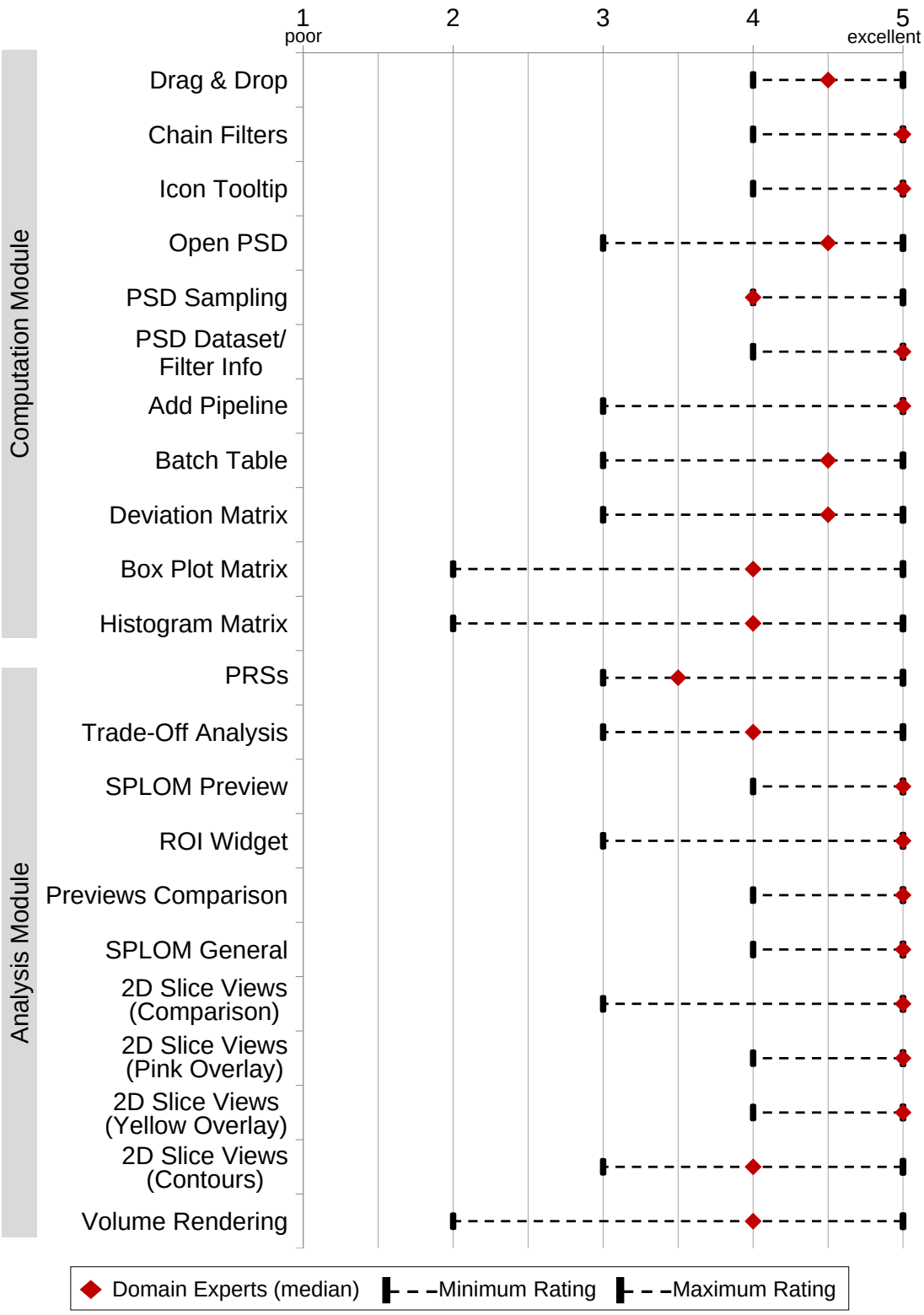

Figure 3.13: Results of the evaluation questionnaire with a five-point Likert scale ranging from one to five respectively, i.e., from poor to excellent.

Die approbierte gedruckte Originalversion dieser Dissertation ist an der TU Wien Bibliothek verfügbar.
The approved original version of this doctoral thesis is available in print at TU Wien Bibliothek.

3.7 Case Studies

In this section we present two case studies that reflect the domain-specific requirements and present the capabilities of our research prototype. First, we conduct a porosity determination with non-parametric segmentation-pipelines (see Section 3.7.1) and second, we focus on the influence of edge-preserving smoothing when determining the porosity (see Section 3.7.2).

3.7.1 Porosity Determination with Non-Parametric Segmentation Pipelines

Our domain experts often use a non-parametric segmentation algorithm called *Otsu Threshold*, because it is fast and has no parameters to specify. Our experts found out that the *Otsu Threshold* sometimes fails or provides unsatisfying results. We included into the *PorosityAnalyzer* eight other non-parametric segmentation algorithms and compared those to the *Otsu Threshold*. Figure 3.14 A shows the Overview Comparative Matrix in deviation mode (see Section 3.5.2) for the *aeronautic industry* datasets E3_low–E7_high (see Table 3.1). The datasets E3_low and E4_low have a low porosity, datasets E5_high–E7_high have a much higher porosity. All algorithms segmented the datasets E3_low and E4_low in approximately five seconds. The Overview Comparative Matrix in deviation mode shows that the *Otsu Threshold* has a high deviation for the low-porosity datasets. This relationship is illustrated in Figure 3.14 B and 3.14 C. All other segmentation pipelines except *Moments Threshold* have a low deviation from the reference for the low-porosity cases. The overview comparative matrix in deviation mode shows that the *IsoData Threshold* works for both kinds of datasets, i.e., with low and high porosity. Table 3.3 shows the results.
From the domain-specific perspective the *IsoData Threshold* is most suitable for the *aeronautic industry* datasets E3_low–E7_high as it delivers robust, accurate, and fast results for these dataset types (see Task 4, Section 3.1). Assembling and analyzing the 45 tested pipelines with the *PorosityAnalyzer* tool takes about 20 minutes compared to the conventional method of the domain experts, which takes about three and a half hours.

		Dataset Name	
Algorithm Name	**Output Parameter**	E3_low	E4_low
Isodata Threshold	Deviation from Reference	-0.0554%	-0.0224%
	Elapsed Time	4846 ms	4842 ms
Otsu Threshold	Deviation from Reference	21.03%	66.65%
	Elapsed Time	4976 ms	5073 ms

Table 3.3: Elapsed time and accuracy results, i.e., deviations from the reference porosity value in %, for the *Isodata Threshold* and the *Otsu Threshold* performed on the datasets E3_low and E4_low.

Die approbierte gedruckte Originalversion dieser Dissertation ist an der TU Wien Bibliothek verfügbar.
The approved original version of this doctoral thesis is available in print at TU Wien Bibliothek.
TU Bibliothek WIEN Your knowledge hub

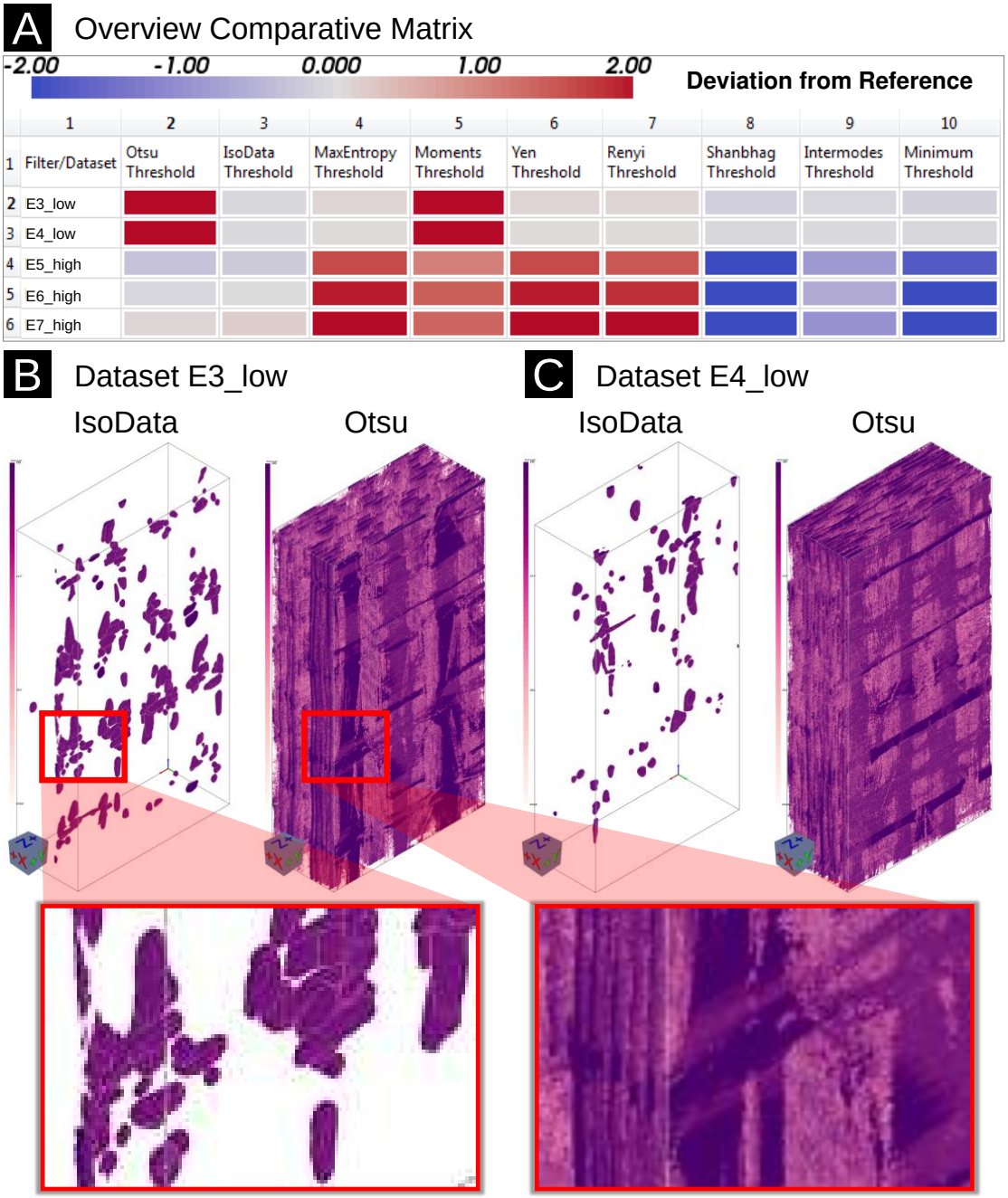

Figure 3.14: (A) The *Overview Comparative Matrix* in deviation mode presents the porosity deviations from the reference porosity value of the individual segmentation algorithms for the *aeronautic-industry* datasets. The comparison of the (pinkish) aggregated segmentation masks in 3D of *IsoData Threshold* and *Otsu Threshold* for the datasets (B) E3_low and (C) E4_low reveals that the *Otsu Threshold* has a high deviation from the reference porosity value, because it massively over-segments the pores.

Die approbierte gedruckte Originalversion dieser Dissertation ist an der TU Wien Bibliothek verfügbar.
The approved original version of this doctoral thesis is available in print at TU Wien Bibliothek.
TU Bibliothek Your knowledge hub WIEN

3.7.2 Influence of Edge-Preserving Smoothing on Porosity Determination

In order to determine the porosity of an FRP specimen, the domain experts apply a global threshold to the raw XCT data [SKO+11]. In their daily work, domain experts typically do not use smoothing filters. However, the use of global methods without smoothing has the disadvantage that noise is segmented as well. Therefore, the domain experts wanted to know, how the pore segmentation behaves if smoothing filters are used to eliminate noise. To show the effect of smoothing filters, we have assembled two segmentation pipelines, which operate on the PorePhantom dataset (see Section 3.3). The gray values of this 16-bit dataset lie between 0 and 65535. One pipeline uses gradient anisotropic diffusion (GAD), an edge-preserving smoothing method, the other pipeline does not. Both pipelines use the *Binary Threshold* (see Table 3.2) to segment the pores. For a moderate smoothing of the data, we used the following GAD filter parameters: iterations=30, timestep=0.6874, and conductance=1. The parameter range of the *Binary Threshold* filter was set to 20000–45000 with a step size of 1000 gray values. This parameter range includes all the relevant gray values between pore gray values and material gray values.

Figure 3.15 A presents the resulting porosities of the individual segmentation runs for the pipeline without GAD smoothing (upper points) and with GAD smoothing (lower points). The porosities without GAD smoothing rise faster with increasing *Binary Threshold* values than the porosities with GAD smoothing. A detailed look at both porosity values, close to the reference segmentation (the reference porosity is 6.123%), shows that the porosity difference is very small (porosity without GAD is 6.122%, with GAD it is 6.0931%). The popup preview visualizes this difference. The data point without GAD was fixed and compared to the data point with GAD (see Figure 3.15 B, popup preview). Identical segmentation areas are color-coded in yellow, different ones in blue. The blue difference voxels are not included in the segmentation with GAD (compared point). The domain experts would not classify the "lengthy" blue region as a pore. They would classify it rather as noise. Additionally in Figure 3.16 A, B, and C, we superimposed the segmentation masks without GAD and with GAD (purple voxels and black median contour) with the reference segmentation (yellow voxels) and compared them in a 2D slice view. The segmentation without GAD almost matches the reference segmentation except for a very few voxels (see Figure 3.16 B). The segmentation with GAD is largely identical to the reference segmentation, but does not segment the noisy voxels (see Figure 3.16 C). The influence of the noise is illustrated in the 3D views (see Figures 3.16 D and E). Therefore, we conclude that the used reference segmentation method is not optimal, as it contains noise.

Die approbierte gedruckte Originalversion dieser Dissertation ist an der TU Wien Bibliothek verfügbar.
The approved original version of this doctoral thesis is available in print at TU Wien Bibliothek.
TU WIEN Bibliothek Your knowledge hub

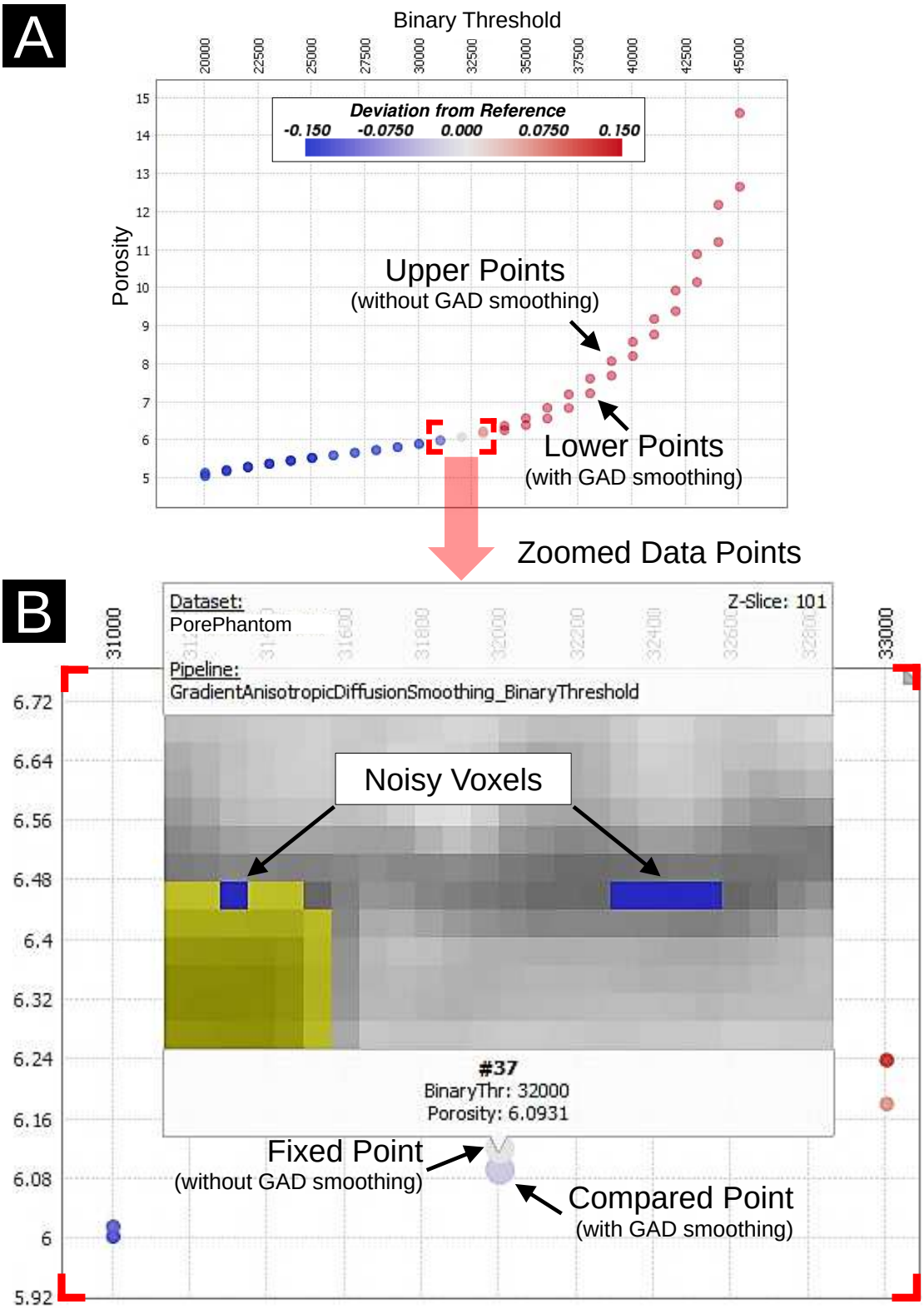

Figure 3.15: Comparison of the segmentation pipelines with GAD smoothing filter and without. (A) Resulting porosities and sampled thresholds. (B) Popup preview with blue color-coded segmentation differences (noisy voxels).

Die approbierte gedruckte Originalversion dieser Dissertation ist an der TU Wien Bibliothek verfügbar.
The approved original version of this doctoral thesis is available in print at TU Wien Bibliothek.
TU Bibliothek Your knowledge hub WIEN

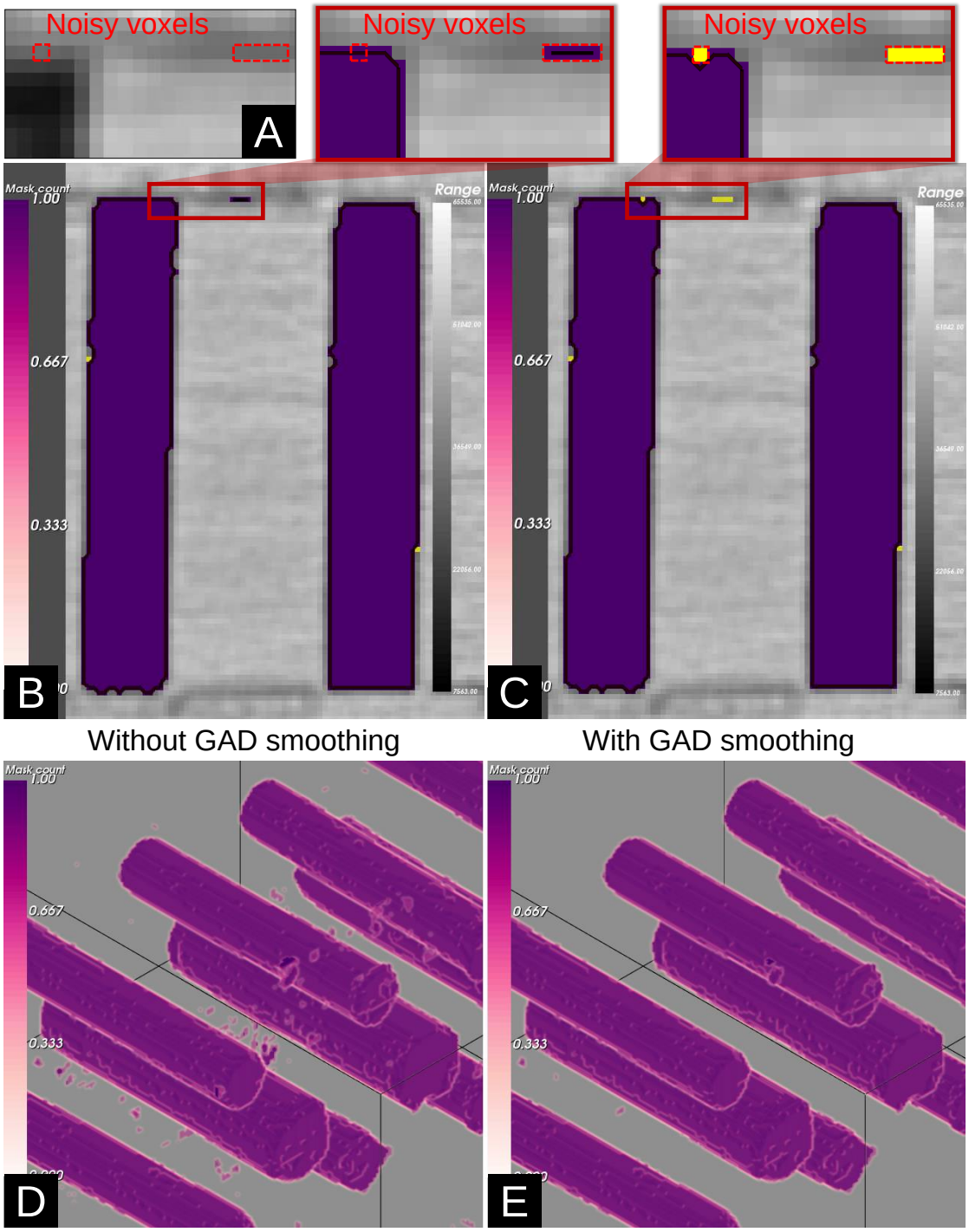

Figure 3.16: (A) Cutout of the raw XCT data. 2D slice (B, C) and 3D rendering (D, E) view comparison of the segmentation masks without GAD and with GAD smoothing (the yellow noisy voxels result from the reference).

Die approbierte gedruckte Originalversion dieser Dissertation ist an der TU Wien Bibliothek verfügbar.
The approved original version of this doctoral thesis is available in print at TU Wien Bibliothek.
TU Bibliothek Your knowledge hub WIEN

To find an optimal parameter set for the *GADSmoothing_BinaryThreshold* segmentation pipeline, we sampled the input parameter space of the GAD filter as follows: iterations 10–80, step size 10; timestep 0.6874; conductance 0.6–2.0, step size 0.1. The *Binary Threshold* was set to 32011, the same threshold value as for the reference segmentation. For an initial selection of the input parameters, we used the PRSs. We selected the porosity bin with the highest segmentation frequency in the output parameter histogram (porosity range 6–6.1%). The PRSs automatically marked the corresponding input parameter ranges (iterations 40–80; conductance 0.9–1.4 and 1.6–2.0) with yellow (see Figure 3.17 A). These ranges were selected, saved to the selections view, and loaded to the SPLOM. The scatter plot in Figure 3.17 B shows the selected ranges. The aggregated segmentation masks of these segmentation classes are illustrated in the 3D rendering view. The comparison of the two classes in 3D shows that the segmentations with conductance 0.9–1.4 contain noise, while the segmentations with conductance 1.6–2.0 do not (see Figure 3.17 B, 3D details).
Therefore, we focused on the segmentation class with conductance 1.6–2.0. To analyze the lower and upper end of this segmentation class, we divided it into two classes, one with conductance 1.6–1.7 and one with conductance 1.9–2.0 (see Figure 3.17 C, scatter plot). When examining the 2D slices of the aggregated segmentation masks, we found that the segmentations with conductance 1.9–2.0 start under-segmenting the data (see Figure 3.17 C, exemplary 2D slices). We discarded the segmentations with conductance 1.9–2.0 and further investigated the remaining class with conductance 1.6–1.7 (see Figure 3.17 D, scatter plot). By using the popup preview, we were able to compare the differences of the individual segmentations. All the segmentations start to under-segment the data except one segmentation with a conductance of 1.6 and 40 iterations (see Figure 3.17 D1, exemplary 2D slices). Figure 3.17 D2 compares the segmentation with conductance 1.6 and iterations 40 with all other segmentations with conductance 1.6-1.7. Only the pixels highlighted in yellow are segmented by the segmentations with conductance 1.6-1.7 without iterations 40. This would lead to a under-segmentation (see Figure 3.17 D2, red marked pixels in the reference segmentation). The segmentation with conductance 1.6 and iterations 40 contains in addition to the yellow marked pixels the blue marked pixels and thus causes a lower under-segmentation respectively is closer to the reference segmentation. When comparing the reference segmentation (porosity value of 6.123%) with the segmentation found (porosity value of 6.0715%), it can be seen that the reference method over-segments the data, since at least the two pixels in the upper row can be evaluated as outliers/noise (see Figure D2, red marked pixels in the reference segmentation).
For this specimen type, we propose a data preprocessing with the GAD filter (iterations=40, timestep=0.6874, conductance=1.6), for a precise porosity determination (see Task 3, Section 3.1). Assembling and analyzing the 120 segmentations of the *GADSmoothing_BinaryThreshold* segmentation pipeline takes about one hour with the *PorosityAnalyzer* tool. With traditional methods a systematic evaluation of this number of segmentation masks would not be possible within reasonable time.

Die approbierte gedruckte Originalversion dieser Dissertation ist an der TU Wien Bibliothek verfügbar.
The approved original version of this doctoral thesis is available in print at TU Wien Bibliothek.
TU Bibliothek WIEN Your knowledge hub

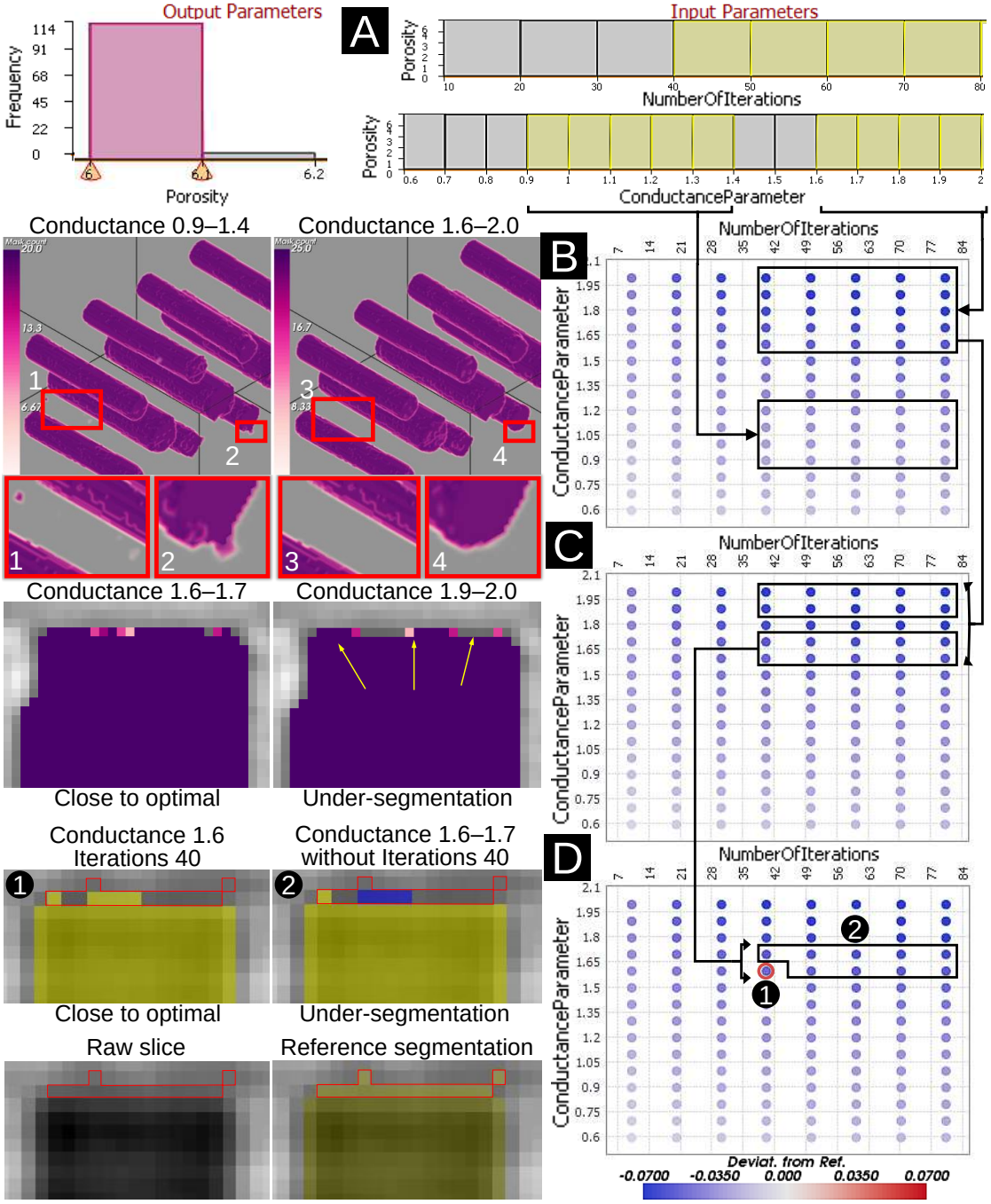

Figure 3.17: Finding the optimal parameter set for the *GADSmoothing_BinaryThreshold* segmentation pipeline. (A) PRSs with a selected bin of the output parameter *porosity* and the proposed GAD filter input parameters *iterations* and *conductance*. (B) Comparison of the 3D rendered aggregated segmentation masks. (C) 2D slice comparison. (D) Popup preview comparison.

Die approbierte gedruckte Originalversion dieser Dissertation ist an der TU Wien Bibliothek verfügbar.
The approved original version of this doctoral thesis is available in print at TU Wien Bibliothek.

3.8 Implementation

PorosityAnalyzer was implemented in C++. The experiments were performed on a desktop machine with an Intel(R) Core(TM) i7-3770 CPU, 32 GB RAM and an NVIDIA GeForce GTX 1080 GPU with 8 GB RAM. ITK 4.9 [JMIC15] was used to load the datasets, to perform basic image processing, and to segment the pores (see Table 3.2). The 3D rendering views and the 2D slice views were calculated with VTK 7.0 [SML06]. The GUI was implemented in Qt 5.8 [Gro]. The research prototype is available in the open source framework *open_iA* [FWS+19].

3.9 Summary and Conclusion

In this chapter we present the *PorosityAnalyzer*, a tool for the detailed evaluation and visual analysis of pore segmentation-pipelines in fiber-reinforced polymers. The computation module was developed to conveniently set up and execute distributed off-line computations. The analysis module is used for examining the resulting data. We demonstrate how a number of visualization techniques can be applied for the visual analysis of data on multiple levels-of-detail. These visualizations include the Overview Comparative Matrix, the SPLOM with the popup preview, the PRSs, 2D slice views with overlays, and 3D rendering views. The techniques allow the domain experts to improve their workflow, obtain important insights into pore segmentation-pipelines, and automate tedious manual operations. We present two use cases, indicating how *PorosityAnalyzer* can be employed to compare, analyze, and obtain insights into segmentation pipelines applied to a range of different datasets. We evaluate the research prototype with a questionnaire and a qualitative interview to get feedback from the domain experts. The feedback shows that our techniques make it easier to compare established as well as new segmentation techniques and reduces the required time to compare various segmentation algorithms.

Die approbierte gedruckte Originalversion dieser Dissertation ist an der TU Wien Bibliothek verfügbar.
The approved original version of this doctoral thesis is available in print at TU Wien Bibliothek.
TU Bibliothek WIEN Your knowledge hub

Die approbierte gedruckte Originalversion dieser Dissertation ist an der TU Wien Bibliothek verfügbar.
The approved original version of this doctoral thesis is available in print at TU Wien Bibliothek.

CHAPTER 4

Dynamic Volume Lines: Visual Comparison of 3D Volumes through Space-filling Curves

This chapter is based on the following publication:

J. Weissenböck, B. Fröhler, E. Gröller, J. Kastner, C. Heinzl. Dynamic Volume Lines: Visual Comparison of 3D Volumes through Space-filling Curves. *IEEE Transactions on Visualization and Computer Graphics*, Vol. 25, No. 1, pp. 1040–1049, 2019. doi: 10.1109/TVCG.2018.2864510

Follow-up publications:

J. Weissenböck, B. Fröhler, E. Gröller, J. Sanctorum, J. De Beenhouwer, J. Sijbers, S. Karunakaran, H. Hoeller, J. Kastner, C. Heinzl. An Interactive Visual Comparison Tool for 3D Volume Datasets represented by Nonlinearly Scaled 1D Line Plots through Space-filling Curves. *Proceedings of the 9th International Conference on Industrial Computed Tomography (iCT 2019)*, Padova, Italy, 2019.

In this chapter, we introduce *Dynamic Volume Lines* for the interactive visual analysis and comparison of sets of 3D volumes. Each volume is linearized along a Hilbert space-filling curve into a 1D Hilbert line plot, which depicts the intensities over the Hilbert indices. We present a nonlinear scaling of these 1D Hilbert line plots based on the intensity variations in the ensemble of 3D volumes, which enables a more effective use of the available screen space. The nonlinear scaling builds the basis for our interactive visualization techniques. An interactive histogram heatmap of the intensity frequencies serves as overview visualization. When zooming in, the frequencies are replaced by detailed 1D Hilbert line plots and optional Functional Boxplots. To focus on important regions of the volume ensemble, nonlinear scaling is incorporated into the plots. An interactive scaling widget depicts the local ensemble variations. Our brushing and linking interface reveals, for example, regions with a high ensemble variation by showing the affected voxels in a 3D spatial view. We show the applicability of our concepts using two case studies on ensembles of 3D volumes, resulting from tomographic reconstruction. In the first case study, we evaluate an artificial specimen from simulated industrial 3D X-ray computed tomography (XCT). In the second case study, a real-world Talbot-Lau grating interferometer (TLGI) XCT foam specimen is investigated. Our results indicate that *Dynamic Volume Lines* can identify regions with high local intensity variations, allowing the user to draw conclusions, for example, about the choice of reconstruction parameters. Furthermore, it is possible to detect ring artifacts in reconstructions volumes.

4.1 Introduction

A major challenge in three-dimensional material characterization with conventional industrial 3D X-ray computed tomography (XCT) systems are low densities and thin cell walls, especially at low physical resolutions. One method that overcomes these challenges is Talbot-Lau grating interferometer XCT (TLGI-XCT) [SPK+17]. It is a non-destructive testing method, which fully delivers 3D volume information of the scanned specimen at a high resolution to precisely capture external and internal structures (e.g., cracks) in a single scan. TLGI-XCT is one of the most important X-ray technology innovations in the past ten years [PKBD07]. This method provides three complementary modalities in one scan of the specimen: (1) the attenuation contrast (AC), (2) the differential phase contrast (DPC), and (3) the dark-field contrast (DFC).

Currently, it is common practice to reconstruct the data of the three modalities separately, without simultaneously using the given and instructive complementary information. To reconstruct the data from the three modalities, the conventional filtered back-projection algorithm by Feldkamp, Davis, and Kress (FDK) is used [FDK84]. This reconstruction algorithm is well suited for XCT data from the AC modality, as it is a fast and accurate method. However, for the DPC and DFC modalities, the FDK reconstruction is not optimal because the prior knowledge and the inherent physical effects of the different

Die approbierte gedruckte Originalversion dieser Dissertation ist an der TU Wien Bibliothek verfügbar.
The approved original version of this doctoral thesis is available in print at TU Wien Bibliothek.
TU Bibliothek WIEN Your knowledge hub

modalities are not considered [JRS+11, SJdD+17]. Experts in the field of computed tomography reconstruction are therefore developing new algorithms based on appropriate mathematical models. These correspond to the physical characteristics of the DFC and DPC modalities in order to achieve satisfying reconstruction results with regard to conventional methods.

The domain specialists compare the results of the different reconstruction algorithms and their parameterizations with each other and with a reference reconstruction. Regions in the volume with a high ensemble variation of the intensities (e.g., feature edges on interfaces) are of great interest to the experts, as the behavior of the reconstruction algorithm can be deduced through changing specific parameters. The comparison is typically done visually. It is based on 2D gray value slices through the volumes arranged side-by-side. Experts perform this comparison on a case-by-case basis. They try to determine promising algorithms and suitable parameters, for instance, by checking for noise and artifact suppression. The intensity differences between the various volumetric reconstructions are typically rather small. Therefore it is difficult for an expert to judge whether a particular algorithm or parameter set provides better results (e.g., sharper edges) than another one. This problem gets even worse if several or even many different reconstruction results of an algorithm are compared (e.g., due to parameter variations).

Due to a close collaboration with reconstruction specialists, we were able to analyze their workflow and identify the following tasks when comparing many volumes with specific regions of minor intensity differences:

- **Task 1:** Compare several reconstruction volumes with each other
- **Task 2:** Identify interesting spatial regions based on high local intensity variations
- **Task 3:** Reveal repeating patterns in the spatial domain, which are of high variance among all ensemble members
- **Task 4:** Find the most suitable volume in the ensemble

To address domain-specific requirements, we introduce *Dynamic Volume Lines* for the interactive visual analysis and comparison of 3D volumes using nonlinearly scaled 1D Hilbert line plots. We build upon the work of Demir et al. [DDW14], who also use the Hilbert linearization to analyze 3D data. As space-filling curve the Hilbert curve traverses the entire 3D volume. For the line plot the space-filling curve is straightened along the horizontal axis. On the vertical axis the intensities at the specific volume positions are shown. We extend the approach of Demir et al. by an adaptive, automatic, and dynamic nonlinear scaling of the horizontal axis, which allows the user to focus on interesting regions in the volumes. The nonlinear scaling highlights regions of high variation in the ensemble and optionally hides uninteresting background regions. Abstracting and reformatting 3D volumes as line plots is chosen because the domain experts are familiar with line graphs, which they use on a daily basis. The workflow of *Dynamic Volume Lines*

Die approbierte gedruckte Originalversion dieser Dissertation ist an der TU Wien Bibliothek verfügbar.
The approved original version of this doctoral thesis is available in print at TU Wien Bibliothek.
TU Bibliothek WIEN Your knowledge hub

starts with the extraction of a region of interest (ROI), which is for each volume analyzed at the same position and of the same size (see Figure 4.1 A). A Hilbert space-filling curve for the extracted ensemble volumes is generated by mapping voxel coordinates and the corresponding intensities in 3D to 1D Hilbert indices (see Figure 4.1 B). The nonlinear scaling of a Hilbert line plot is built by summing up the local ensemble variations to formulate a cumulative importance function (see Figure 4.1 C), which serves as basis for the interactive visualization techniques (see Figure 4.1 D–F). Our main contributions are:

- **Design and development of *Dynamic Volume Lines*, to compare ensembles of 3D volumes, including the following key features**:
  - Nonlinear scaling of the 1D Hilbert line plot, which is built from a cumulative importance function (see Section 4.4.2)
  - Interactive nonlinearly scaled histogram heatmap, which encodes the intensity frequencies (see Section 4.4.3.1)
  - Interactive nonlinearly scaled 1D Hilbert line plots of the individual volumes in the ensemble (see Section 4.4.3.2)
  - Interactive scaling widget, which illustrates the locally varying scaling factor (see Section 4.4.3.3)
- **Evaluation of the tool based on two case studies from the XCT domain**

In the subsequent Section 4.2, we review the related work on comparative and ensemble visualization. Section 4.3 describes the data acquisition and the used datasets. In Section 4.4 we explain *Dynamic Volume Lines*, which includes the Hilbert curve generation, the nonlinear scaling based on a cumulative importance function, and the interactive visualization techniques. Section 4.5 presents the evaluation of the developed tool based on two case studies. We conclude and point out potential future work in Section 4.6.

Die approbierte gedruckte Originalversion dieser Dissertation ist an der TU Wien Bibliothek verfügbar.
The approved original version of this doctoral thesis is available in print at TU Wien Bibliothek.
TU Bibliothek WIEN Your knowledge hub

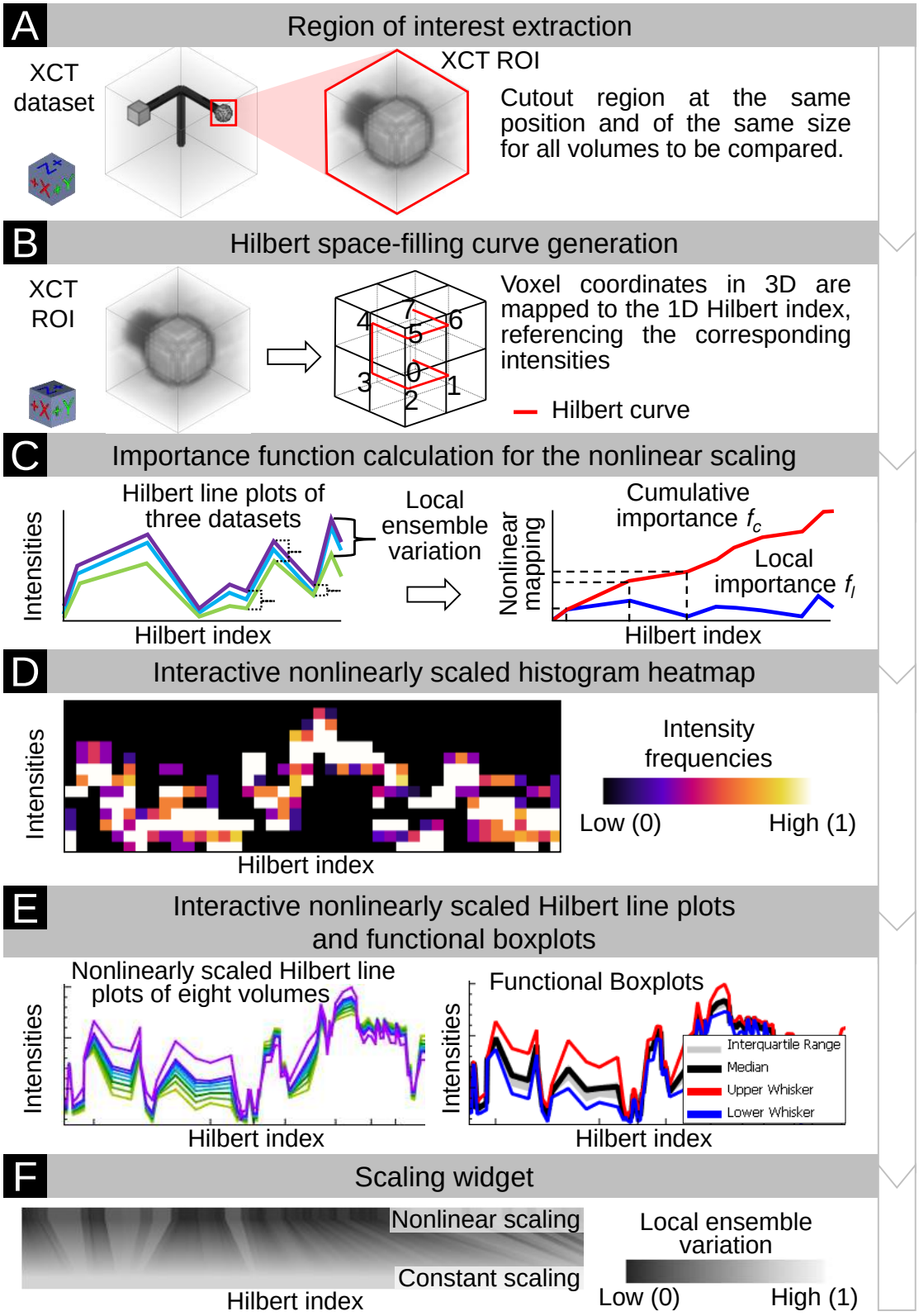

Figure 4.1: The *Dynamic Volume Lines* workflow: (A) extraction of interesting regions, (B) generation of a space-filling Hilbert curve, (C) nonlinear scaling of the Hilbert line plots, (D) interactive nonlinearly scaled histogram heatmap, (E) interactive nonlinearly scaled 1D Hilbert line plots, (F) and interactive scaling widget.

Die approbierte gedruckte Originalversion dieser Dissertation ist an der TU Wien Bibliothek verfügbar.
The approved original version of this doctoral thesis is available in print at TU Wien Bibliothek.
TU WIEN Bibliothek Your knowledge hub

4.2 Related Work

The related work is mainly in the areas of comparative and ensemble visualization, but also in the fields of visual parameter space analysis and interactive visual analysis. Gleicher et al. [GAW+11] provide a taxonomy to group comparative visual designs into one of three basic categories: juxtaposition, superposition, and explicit encoding. In the work of Malik et al. [MHG10], slices from different volumes are compared in a hexagonal arrangement. This visual representation works only for a rather small number of datasets to be compared. Schmidt et al. [SPA+14] present a tool for the comparative visual analysis of 3D meshes, which enables the simultaneous comparison of several meshes and the interactive exploration of their differences. In an earlier work [SGB13], they present a method for visualizing differences and similarities in large sets of images. The technique preserves contextual information, but also allows the user to perform a detailed analysis of subtle variations. Based on magnetic resonance cartilage-imaging techniques, Mlejnek et al. [MEV+05] propose 3D glyphs, called *Profile Flags*, for the probing of sets of underlying curve data. Weissenböck et al. [WAG+16] introduce a system to evaluate the porosity in 3D volumes. They provide 2D slice views and 3D renderings views to compare different pore segmentation results due to varying segmentation parameters. Many of the ensembles investigated in these works result from analyzing the parameter space of some algorithm, for which Sedlmair et al. [SHB+14] present a conceptual framework to guide and systematize research endeavors.

Ensemble visualization often uses statistical summaries for the comparison of many similar datasets. *Ensemble-vis* by Potter et al. [PWB+09] is a framework consisting of an interactively linked overview and statistical displays for the discovery and evaluation of simulated meteorology outcomes. Jarema et al. [JDKW15] provide a visual-analysis user-interface with multiple linked views to support the comparative exploration of 2D vector-valued ensemble fields. Fröhler et al. [FMH16] present an interactive tool for exploring and analyzing the parameter space of multi-channel segmentation algorithms and the corresponding ensemble of segmentation results. Several works have been published, which embed descriptive statistic measures such as minimum, median, and maximum in Functional Boxplots [SG11], Contour Boxplots [WMK13], and Curved Boxplots [MWK14]. Genton et al. [GJP+14] developed Surface Boxplots for the visualization and exploratory analysis of samples of images to detect potential outliers. They use the notion of volume depth to order the viewed images, which are interpreted as hightfields. Raj et al. [RMP+16] examine the effectiveness of Contour Boxplots in the medical domain of brain atlas analysis. They extend Contour Boxplots to 3D to visualize and interact with ensembles of 3D isosurfaces. Demir et al. [DJW16] determine the most central shape from a given set, to quantify a region-wise centrality, and to compute the locally most representative shape. Konyha et al. [KLM+12] and Matkovic et al. [MGKH09] focus on the interactive visual analysis of ensembles of curves called *families of curves* or *families of surfaces* using data aggregation and attribute derivation. Piringer et al. [PPBT12] extend the work on feature-preserving downsampling of 2D functions. They discuss a design study of an interactive approach for the comparative visual analysis of

Die approbierte gedruckte Originalversion dieser Dissertation ist an der TU Wien Bibliothek verfügbar.
The approved original version of this doctoral thesis is available in print at TU Wien Bibliothek.
TU Bibliothek WIEN Your knowledge hub

2D function ensembles.

In the context of visual analysis, the state-of-the-art report by Heinzl and Stappen [HS17] closes a gap between visual computing and material science. Torsney-Weir et al. [TWSM17] propose *Sliceplorer* to visually examine multi-dimensional continuous scalar functions with 1D slices. Their technique combines the benefits of topological views, i.e., screen space efficiency, with those of slices, that are a close resemblance of the underlying function. Another work of Demir et al. [DDW14], presents *Multi-Charts*, an interface to visually analyze 3D scalar ensemble fields by linearizing the 3D data points along a space-filling curve. Our approach is similar to *Multi-Charts*, as we also use the Hilbert space-filling curve to linearize 3D volumes and represent the volumes as 1D line plots. Demir et al. represent the individual ensemble members as multiple stacked and combined bar and line charts at different levels of detail. For analyzing such regions the user has to zoom in and out. This leads to a loss of context. A significant difference in our work is the computation of a nonlinear scaling of the horizontal axis based on local ensemble variations. The nonlinear scaling allows us to depict all 3D volumes as 1D line plots, which can be presented in one visualization. As a result, uninteresting regions (with low ensemble variance) are compressed in the line plots, and interesting regions (with high ensemble variance) are expanded. Thereby, we can optimally use the available screen space and no zooming is necessary in the first place, as we provide insight into the interesting regions from the initial overview state. The individual line plots of the corresponding 3D volumes can be aggregated using Functional Boxplots. Thus, we provide a statistical overview of the ensemble. In addition, the scaling widget indicates the nonlinear scaling of the data. Finally, we support an importance-driven selection by defining ranges based on a cumulative importance function.

4.3 Datasets

This section briefly explains how the Talbot-Lau grating interferometer (TLGI) industrial 3D X-ray computed tomography (XCT) data is acquired (see Section 4.3.1) and which datasets are used (see Section 4.3.2).

4.3.1 Data Acquisition

In contrast to conventional XCT (see Section 1.2), TLGI-XCT delivers three complementary modalities, i.e., attenuation contrast (AC), differential phase contrast (DPC), and dark-field contrast (DFC) in a single scan. The three modalities are perfectly registered to each other. AC provides information on the attenuation of the X-ray beam intensity and thus is equivalent to conventional X-ray imaging. DPC is related to the index of refraction and image contrast, which is achieved by the local deflection of the X-ray beam. DFC reflects the total amount of radiation scattered at small angles, e.g., caused by microscopic structures in the sample like particles, pores, fibers, struts, or cracks. In addition, the DFC modality produces a strong signal and a high contrast at interfaces and reveals information that is undetected by AC and DPC imaging.

Die approbierte gedruckte Originalversion dieser Dissertation ist an der TU Wien Bibliothek verfügbar.
The approved original version of this doctoral thesis is available in print at TU Wien Bibliothek.
TU WIEN Bibliothek Your knowledge hub

4.3.2 Dataset Description

The first ensemble consists of 3D reconstruction datasets of an artificial specimen from simulated XCT [REK+16] of the AC modality with intensities between 0 and 65535. The size of each dataset is $128 \times 128 \times 128$ voxels and the data type is unsigned short (see Figure 4.2 A). The artificial projection images are generated by calculating penetration lengths of primary monochromatic X-rays through the specimen. The specimen is represented by surface models of three cylinders, one sphere, and one cube. Attenuations are calculated by applying Lambert-Beer's law. The X-ray scatter and the blurring effects were disabled for the simulation. The virtual projection images are processed using the FDK reconstruction algorithm. We applied a Gaussian filter with increasing smoothing effect to generate five additional volumes. No smoothing was applied to the first dataset. The individual variances of the Gaussian smoothing in the range [0.2, 1.0] are increased by a step of 0.2. In a preprocessing stage, a user-defined ROI is selected and applied to all ensemble volumes (see Figure 4.2 B). The resolution of the ROI cutouts are $16 \times 16 \times 16$ voxels. Figure 4.2 C depicts an xy-slice of the dataset with no smoothing. Figures 4.2 D–H show xy-slices of the different results from the Gaussian smoothing filter.

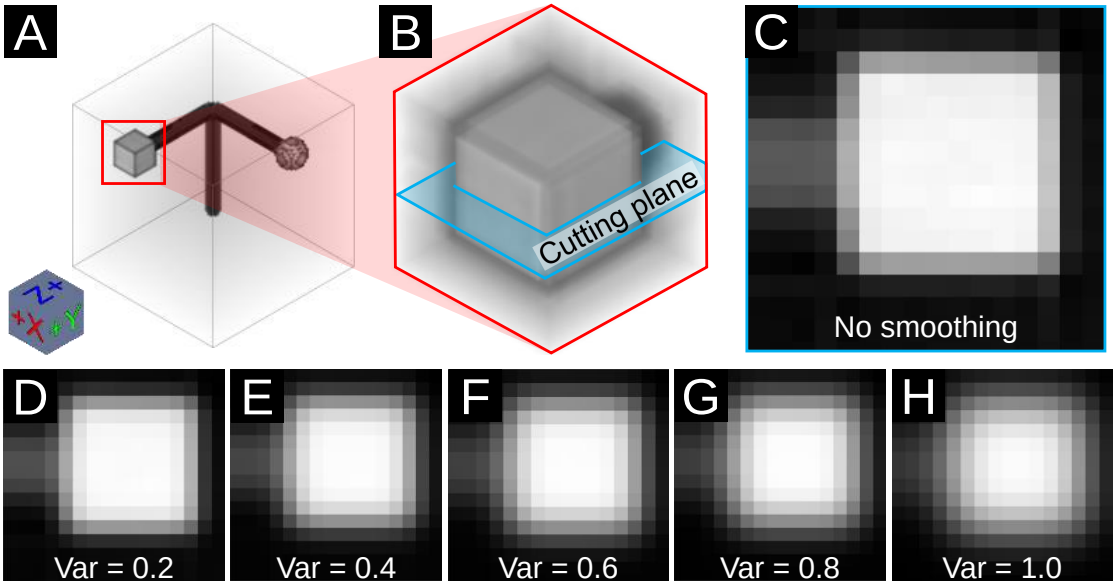

Figure 4.2: (A) 3D reconstruction dataset of the artificial specimen from simulated XCT of the AC modality, (B) with an ROI cutout of a cube. (C) shows an xy-slice view of the dataset without Gaussian smoothing. (D–H) depict the xy-slice views of the five datasets with an increasing variance of the Gaussian smoothing between 0.2 and 1.0.

The second ensemble consists of 16 datasets from a real-world open-cell polyurethane foam specimen, which was scanned with a Bruker Skyscan 1294 TLGI-XCT device at a resolution of 11.4 microns. The size of each dataset is $550 \times 550 \times 250$ voxels and the

Die approbierte gedruckte Originalversion dieser Dissertation ist an der TU Wien Bibliothek verfügbar.
The approved original version of this doctoral thesis is available in print at TU Wien Bibliothek.
TU Bibliothek Your knowledge hub WIEN

data type is unsigned short. To compare the individual datasets, we normalized the intensities (itk::NormalizeImageFilter [JMIC15]) by setting the mean to zero and the variance to one. We then rescale the intensities between 0 and 65535. Figure 4.3 A shows the thin cell walls of the foam specimen, which are revealed by the DFC modality. In the middle of the foam specimen we cut out an ROI of $64 \times 64 \times 64$ voxels (see Figure 4.3 B). Figure 4.3 C depicts an xy-slice of the cutout reference dataset, which was reconstructed from 900 projections using the FDK algorithm. The center of Figure 4.3 C exhibits ring artifacts. The other 15 datasets were reconstructed using the simultaneous iterative reconstruction technique (SIRT) [GB08] with 900 projections and the following increasing iteration parameters: 10, 50, 100, 150,...,700. Figures 4.3 D–M present the SIRT volumes with increasing iteration parameters.

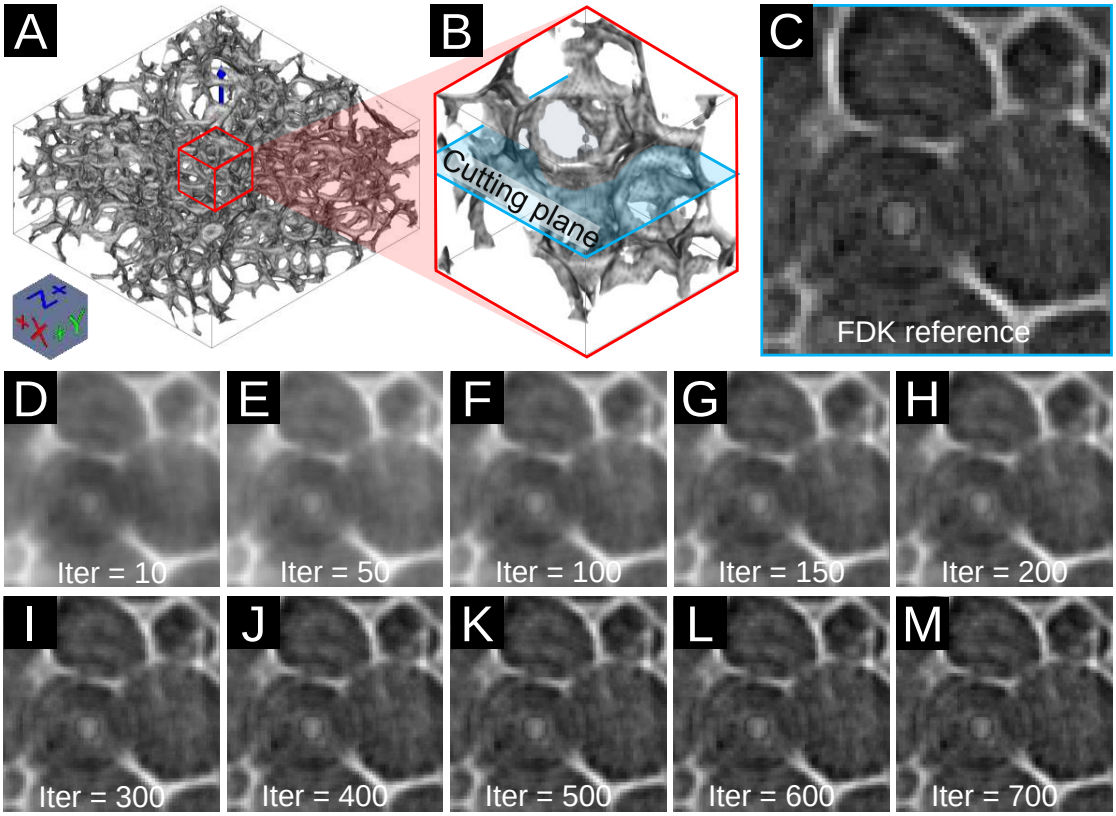

Figure 4.3: (A) 3D reconstruction dataset of a real-world TLGI-XCT foam specimen of the DFC modality, (B) an ROI cutout. (C) shows an xy-slice view of the FDK reconstructed reference dataset with ring artifacts in the center. (D–M) depict the xy-slice views of the SIRT datasets with iteration parameters increasing from 10 to 700 exemplarily.

Die approbierte gedruckte Originalversion dieser Dissertation ist an der TU Wien Bibliothek verfügbar.
The approved original version of this doctoral thesis is available in print at TU Wien Bibliothek.
TU Bibliothek Your knowledge hub WIEN

4.4 Dynamic Volume Lines

In this section we explain the generation of the Hilbert curve based on the 3D voxel intensities and compare the line plots of the Hilbert curve with the line plots of the scan line curve (see Section 4.4.1). Furthermore, we describe the nonlinear scaling of the Hilbert line plots based on local ensemble variations (see Section 4.4.2).

The basic motivation of *Dynamic Volume Lines* is to linearize 3D volumes along a space-filling curve. The resulting line plots are a familiar representation to engineers. Without occlusion, many volumes can be compared through their line plots. A comparison of many volumes in their original 3D space that differ only slightly from each other turns out to be difficult with traditional methods. For example, a direct volume visualization of many datasets is plagued by severe clutter and occlusion problems. This effect is further reinforced by the increasing number of volumes to compare. The same is true for 2D slice views. Arranging two or four slice views of different volumes side-by-side would be feasible, but with an increasing number of volumes to compare it is nearly impossible to find regions where the volumes differ. For example, if individual voxels differ by 5000 intensities, this difference is difficult to perceive as brightness difference, even for an expert. For a line plot in a range of 65000 intensities on the vertical axis, this amplitude drop would be 7% and thus easier to recognize as positional difference. A positional encoding is much more effective than color coding to indicate subtle differences. Comparing intensities is much easier through line plots, in contrast to having first to match them in two or more 2D (or 3D) views and then comparing their color encoding. One could apply statistical aggregation to determine a volume where the voxels contain the local ensemble variances. But even in such a reduced data, rendering is affected by clutter and occlusion. For example, to make differences visible in the interior of the volume, the opacity must be set to a low value. However, larger differences are then only vaguely recognizable. Small differences will be lost. In addition, statistical aggregation volumes provide only a summary or overview and would require additional detailed visualizations to compare specific members in an ROI. In our approach the differences between the individual members can easily be inspected by comparing line plots.

A drawback of linearizing volumes is the loss of spatial coherency. Among the many possibilities of space-filling curves we decided for one which is preserving the spatial coherency as much as possible. The wigglyness of the Hilbert curve ensures that very often neighboring voxels in the 3D volumes are mapped to nearby locations in the straightened Hilbert line plot. We compare the spatial coherence of the Hilbert curve with respect to another simple volume linearization, i.e., the scan line curve where the volume is traversed slice by slice and scan line by scan line within a slice. Switching scan lines or slices introduce large spatial incoherences. Such incoherences appear with Hilbert curves as well, but much less.

Die approbierte gedruckte Originalversion dieser Dissertation ist an der TU Wien Bibliothek verfügbar.
The approved original version of this doctoral thesis is available in print at TU Wien Bibliothek.
TU Bibliothek WIEN Your knowledge hub

4.4.1 Hilbert Space-Filling Curve Generation

In general, with space-filling curves, n-dimensional regular grids can be completely traversed and the grid points can be brought into a one-dimensional linear order. In this sense volumes are three-dimensional regular grids. There are many different space-filling curves such as the Hilbert curve, the Peano curve, or the Z-curve. An obvious approach to linearize the intensities of a 3D volume is to traverse the voxels in z-, y-, and x-axis order along a scan line curve, line by line and slice by slice (see Figure 4.4 A). The disadvantage of this approach is that there are large jumps in the scan line curve between the last voxel of the previous row and the first voxel of the current row and the last voxel of the previous slice and the first voxel of the current slice, respectively. In contrast, the Hilbert space-filling curve traverses every point of a square, a cube, or more generally, an n-dimensional hypercube, by preserving locality much better. Points close to each other in the n-dimensional space are very often close in their order along the Hilbert curve and vice versa [GL94]. This results in fewer large jumps. Therefore in this work, we focus on the Hilbert curve, as it preserves the locality best [MJFS01].

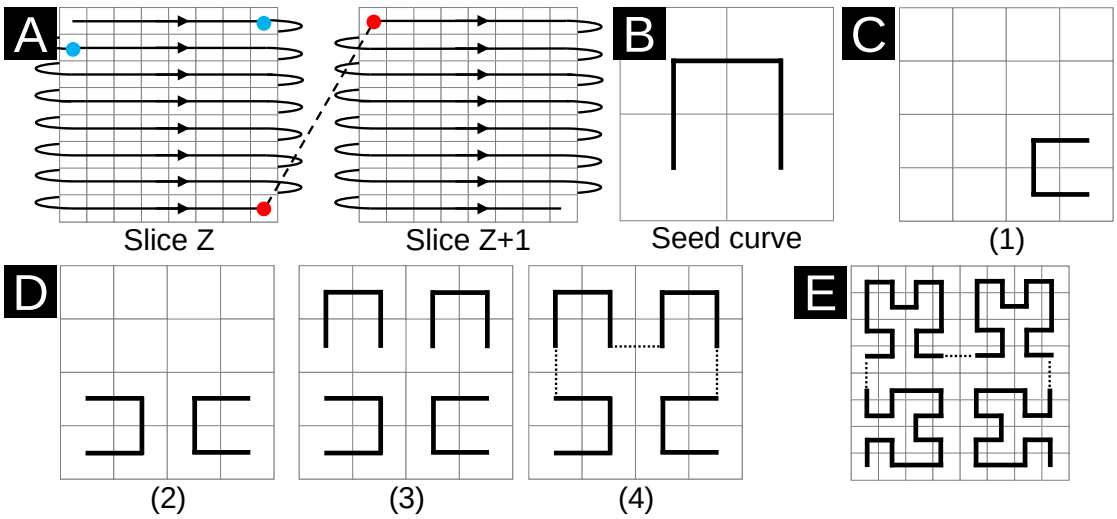

Figure 4.4: (A) shows the scan line curve of a 3D volume by traversing the voxels along their appearance. The blue dots mark a large jump due to a line change and the red dots mark a large jump due to a slice change. (B) depicts the Hilbert curve of order one (initial seed curve). (C–D) illustrate the individual steps to generate a Hilbert curve of order two in 2D space. (E) shows the Hilbert curve of order three.

In the following, we describe the generation of the space-filling Hilbert curve exemplarily in 2D space [HRC07]. Consider the initial seed curve defined on a 2×2 grid as shown in Figure 4.4 B. It is called order one Hilbert curve. Based on an order k Hilbert curve defined on a $2^k \times 2^k$ grid, we define the order *k+1* Hilbert curve on a $2^{k+1} \times 2^{k+1}$ grid according to four steps (see Figures 4.4 C–D):

Die approbierte gedruckte Originalversion dieser Dissertation ist an der TU Wien Bibliothek verfügbar.
The approved original version of this doctoral thesis is available in print at TU Wien Bibliothek.
TU WIEN Bibliothek Your knowledge hub

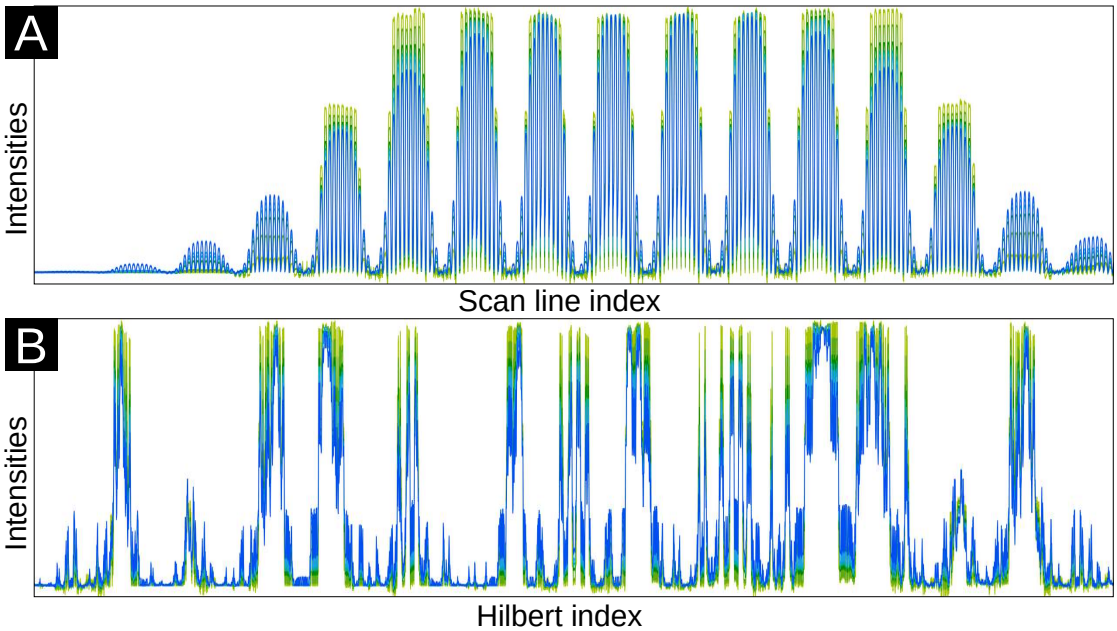

Figure 4.5: Difference between the scan line curve and the Hilbert curve due to large jumps and different locality preservations. The six datasets of the artificial specimen (see Section 4.3.2) are represented by color-coded line plots (from light-green to blue). The line plots are based on the (A) scan line curve and on the (B) Hilbert curve.

1. Place a copy of the curve in the lower right cell and rotate it 90° counter-clockwise.
2. Place a copy of the curve in the lower left cell and rotate it 90° clockwise.
3. Place a copy of the curve in each of the upper cells.
4. Connect the curves with each other.

The resulting space-filling curve visits every voxel exactly once and assigns it a scalar index resulting from the traversal order (Hilbert index). The Figures 4.4 B, D(4), and E show the Hilbert curves of order one, two, and three in 2D space. Figure 4.1 B (on the right) shows the Hilbert curve of order one in 3D space.

In the case of *Dynamic Volume Lines*, all 3D volume datasets are linearized using the implementation of Hamilton and Rau-Chaplin [HRC08]. It generates a Hilbert space-filling curve where the volumes do not need to have the same number of voxels along the x-, y-, and z-axis. The resolution along the individual axes also need not be a power of two. Figure 4.5 illustrates the difference between linearizing along the Hilbert curve and the scan line curve. It depicts the six volumes of the artificial specimen (see Section 4.3.2), each represented by a color-coded line plot (from light-green to blue). The scan line plots in Figure 4.5 A fluctuate more, due to less spatial coherence, as compared to the Hilbert line plots (in Figure 4.5 B).

Die approbierte gedruckte Originalversion dieser Dissertation ist an der TU Wien Bibliothek verfügbar.
The approved original version of this doctoral thesis is available in print at TU Wien Bibliothek.
TU Bibliothek Your knowledge hub WIEN

4.4.2 Nonlinear Scaling of the Hilbert Line Plots

When generating the Hilbert curve for a dataset of $16 \times 16 \times 16$ voxels in size, 4096 Hilbert indices are created. Currently the horizontal screen resolution of a standard PC monitor is typically between 2000 and 3000 pixels. If one wants to display all the 4096 Hilbert indices as points in a 1D Hilbert line plot on the monitor, it turns out, that the horizontal screen resolution is not sufficient to assign each Hilbert index to its own pixel column. This problem becomes even more severe with increasing volume size. Linearizing a volume reduces it to a simple line plot, but with a tremendous horizontal resolution, i.e., number of voxels. This requires automatic scaling along the horizontal axis so that important regions get the screen space they need. Unimportant regions like background can be drastically reduced in their screen space or even removed. To counteract the problem of the limited screen space, we apply a nonlinear scaling to the Hilbert line plot. Since the domain experts are interested in those regions of the dataset where the variation of the intensities is high, we compute the maximum local ensemble variation V_h for every Hilbert index as follows:

$$V_{\mathrm{h}} = \max_{\forall m \in M_h} Intensity_h(m) - \min_{\forall m \in M_h} Intensity_h(m) \tag{4.1}$$

m defines an ensemble member of a local ensemble M_h at a discrete Hilbert index h, $Intensity_h$ defines the intensity at Hilbert index h for member m.

Inspired by the work of Mindek et al. [MMGB17] and Lindow et al. [LBH12], we formulate the discrete local importance function f_l based on the maximum local ensemble variation V_h:

$$f_l(h) = \left(\frac{V_h}{\max V_h} \right)^p \tag{4.2}$$

To be able to filter for a specific importance value, we do a normalization by the maximally occurring local ensemble variation. To influence the nonlinear scaling, we introduce an exponent p, which can be adapted by the user. Setting this parameter to zero means equal importance for all Hilbert indices, setting it higher than zero increases the importance value for Hilbert indices with a high variance in the ensemble. Exponent p can be adapted by the user to fine-tune the importance value according to the individual application scenario. By summing the local importance-function values, we define the cumulative importance function f_c as follows:

$$f_c(h) = \sum_{i=0}^{h} f_l(i) \tag{4.3}$$

The cumulative importance-function values serve as a nonlinear mapping to compress the distances between the Hilbert indices (on the horizontal axis). Figure 4.1 C illustrates the

Die approbierte gedruckte Originalversion dieser Dissertation ist an der TU Wien Bibliothek verfügbar.
The approved original version of this doctoral thesis is available in print at TU Wien Bibliothek.
TU Bibliothek Your knowledge hub WIEN

calculation of the nonlinear mapping. Figure 4.6 illustrates the effect of nonlinearly scaling the Hilbert line plots. The regions indicated with red in Figure 4.6 B are compressed (respectively uncompressed in Figure 4.6 A) by the nonlinear scaling because of the low ensemble variation in these regions. In addition, we allow the user to set a threshold for intensities that are not of interest (e.g., areas of air in the dataset). For these background areas (see Figure 4.7) f_l is fixed to a value of 0.025. This value ensures that the background areas are still sufficiently visible, but at the same time occupy little screen space. By increasing the parameter p, the width of the background regions can be adjusted.

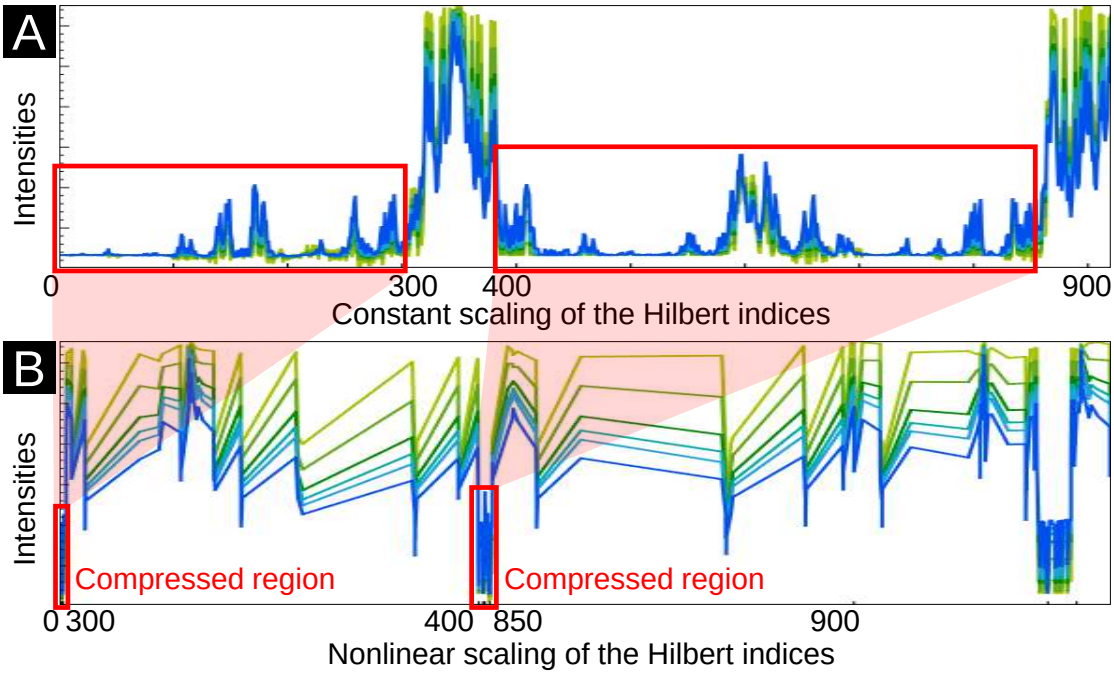

Figure 4.6: Effect of the nonlinear scaling. (A) Constantly scaled 1D Hilbert line plots of six 3D volumes. (B) Nonlinearly scaled 1D Hilbert line plots of the same six 3D volumes.

4.4.3 Visualization Techniques

Dynamic Volume Lines provides multiple linked views and follows the visual information-seeking mantra by Ben Shneiderman, *"overview first, zoom and filter, then details-on-demand"* [Shn96]. Two charts, one with nonlinear scaling and one with constant scaling, are arranged on top of each other with a scaling widget in-between. An overview is provided through the nonlinearly scaled histogram heatmap visualization. Background regions can be filtered out. If the user zooms into the chart, details for each volume are provided through the 1D Hilbert line plots. An orientation widget displays the size and position of the currently visible chart area in light-blue compared to the overall chart size, which is shown in gray (see bottom of Figures 4.7 and 4.8). In addition, we enable

Die approbierte gedruckte Originalversion dieser Dissertation ist an der TU Wien Bibliothek verfügbar.
The approved original version of this doctoral thesis is available in print at TU Wien Bibliothek.
TU Bibliothek Your knowledge hub WIEN

brushing and linking to immediately highlight the affected voxels or Hilbert indices when performing a selection in the 1D Hilbert line plots or in the 3D spatial view, respectively.

4.4.3.1 Interactive Histogram Heatmap Visualization

The histogram heatmap visualization provides an overview of the intensity distribution in the volume ensemble. To be able to fit the full volume into a chart with the width of the screen, we split the x-axis of the nonlinearly scaled chart into intervals of equal width. Due to the nonlinear scaling, the intervals may include a varying number of Hilbert indices. For each interval we then compute a single histogram of the intensities at the included Hilbert indices, over all ensemble members. The single histogram is visualized as a heatmap through a vertical bar, all histograms together form a histogram heatmap. The default width of each histogram bar is 10 pixels, and by default each histogram has 64 bins. These parameters can be adapted by the user to best fit the size and intensity distribution of the currently analyzed volumes. To improve the performance in computing the histogram heatmap, we adapt a segment tree [dBCvKO08]. A segment tree is a binary tree used for storing segments in the range $0...n-1$. Each node represents a segment and is assigned the corresponding histogram. The segment of a leave node covers only one Hilbert index (voxel), the segment of the root node covers all Hilbert indices. The segment tree partitions an arbitrary interval into a minimal set of segments (of varying sizes). With this, we avoid to compute the histogram of an interval based on single voxels. Instead we combine the histograms of the highest-level nodes, whose segments are included in the requested interval. The root node of the segment tree contains the entire segment $[0, n-1]$. A leaf node represents an elementary segment, which corresponds to one Hilbert index, i.e., one voxel. It is assigned the histogram of all the intensities at that voxel throughout the entire volume ensemble. The internal nodes merge the segments of their child nodes. The segment tree can be serialized using an array of size $2*n-1$. The internal nodes are stored in the first half of the array, the leaf nodes are stored in the second half of the array. The left child of each node at index i can be found at index $2*i+1$, the right child at index $2*i+2$. The segment tree is built bottom-up by taking the pairs of nodes with indices $(2*i+1, 2*i+2)$ and aggregating their histograms into the histogram of the parent at index i. The construction of the segment tree is performed for every ensemble and takes $O(n)$ time. In our case, each node of the segment tree contains the histogram for a segment of a certain contiguous range of Hilbert indices. A vertical bar of the histogram heatmap is created by summing up each histogram of the individual volumes. Due to the nonlinear scaling, many Hilbert indices may be covered by a vertical bar of the histogram heatmap. Without the segment tree, a histogram would have to be calculated from all these Hilbert indices. With the segment tree, a histogram for a vertical bar can be generated in $O(\log n)$ time, since only a few nodes need to be traversed. The segment tree therefore supports efficient rescaling of the charts.

In the figures in this paper, the extended black body scheme proposed by Moreland [Mor16] is used as color map for the histogram heatmap, but other predefined color maps can be

Die approbierte gedruckte Originalversion dieser Dissertation ist an der TU Wien Bibliothek verfügbar.
The approved original version of this doctoral thesis is available in print at TU Wien Bibliothek.
TU Bibliothek WIEN Your knowledge hub

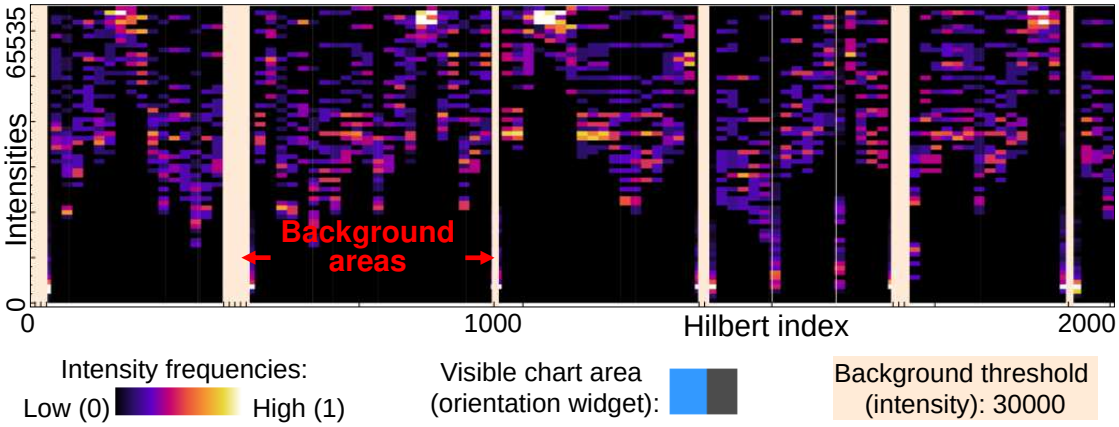

Figure 4.7: The histogram heatmap overview visualization with the extended black body color map. White areas indicate a high concentration of intensities. This is the case if all ensemble members agree on a small range of intensities, i.e., the variation in this region is low. A high variation is indicated by a broader distribution in violet, red, and yellow. Light-orange background areas hide the uninteresting intensities below an intensity of 30000. The orientation widget indicates the visible chart area in light-blue.

selected by the user. Figure 4.7 shows an example histogram heatmap. White regions denote a high concentration of intensities in a single bin. This is the case if all ensemble members agree on a small range of intensities, i.e., if the variation is low in that region. In contrast, a high variation is indicated by a broader distribution in violet, red, and yellow colors from the middle of the color map. The focus in XCT images is typically on regions containing an object, therefore areas containing only background, i.e., air, are not of interest and can be ignored for the analysis. The background areas, where the intensities of all ensemble members are below a user-defined threshold, are assigned a very low importance value and therefore are highly compressed in the nonlinear scaling. Setting the background threshold is optional, a value of zero means that the background is left out altogether. Instead of showing a histogram, these background regions are depicted by light-orange boxes. In this fashion, we can identify interesting regions, i.e., those with high local variation, which addresses Task 2 from Section 4.1.

4.4.3.2 Interactive 1D Hilbert Line Plot Visualization

In the 1D Hilbert line plots, for each volume, the intensities are plotted on the vertical axis over the Hilbert indices on the horizontal axis. Each plot is assigned a distinctive color taken from the Metro Colors scheme of Material UI [7Sp], as can be seen in Figure 4.8 A. When zooming into the histogram heatmap, the 1D Hilbert line plots are activated automatically as soon as the range of currently visible Hilbert indices fits on the screen without aggregation. The 1D Hilbert line plots can also be shown as an overlay on the histogram heatmap. Specific ensemble members can always be activated and deactivated by clicking on them in the legend. The current mouse position is highlighted by a position

Die approbierte gedruckte Originalversion dieser Dissertation ist an der TU Wien Bibliothek verfügbar.
The approved original version of this doctoral thesis is available in print at TU Wien Bibliothek.
TU Bibliothek Your knowledge hub WIEN

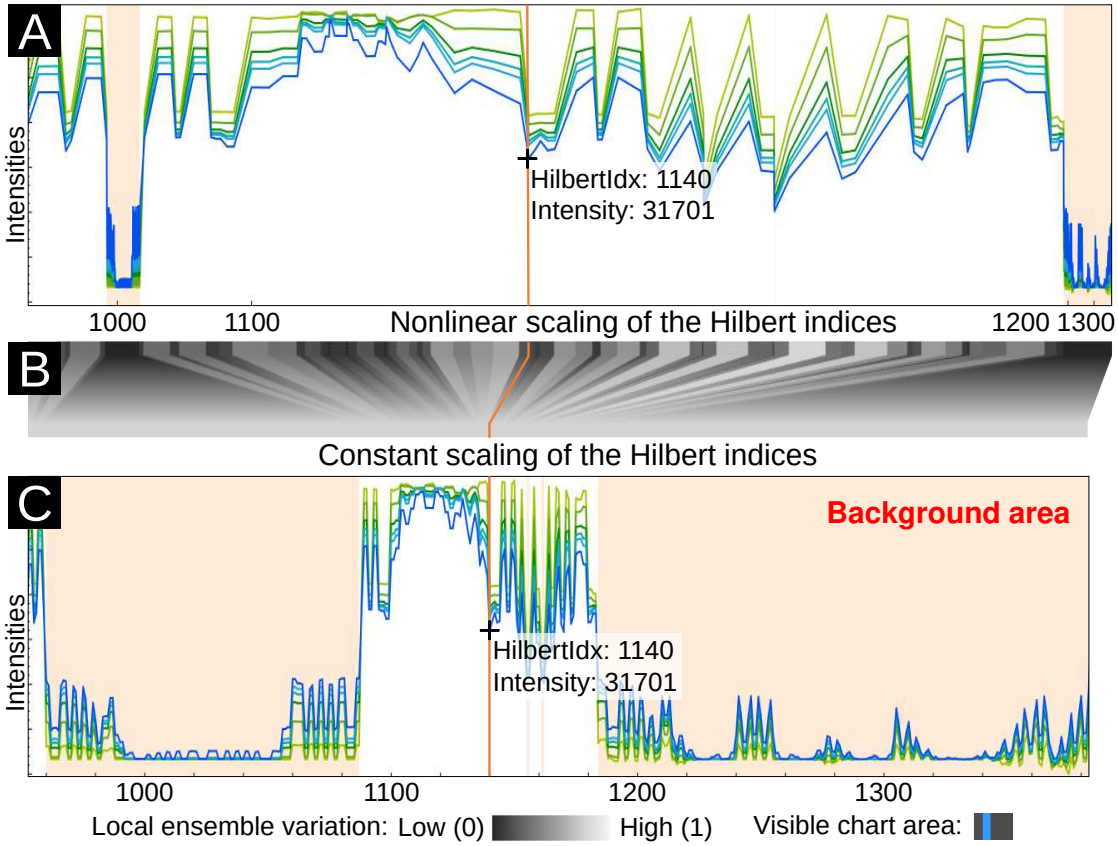

Figure 4.8: (A) The nonlinearly scaled chart shows the differently colored 1D Hilbert line plots for each volume. The intensities are plotted on the vertical axis over the Hilbert indices on the horizontal axis. The current mouse position is highlighted by an orange position marker line, which shows the Hilbert index and intensity at that position. (B) depicts the scaling widget, which emphasizes the nonlinear scaling. (C) shows the constantly scaled chart with the individual 1D Hilbert line plots.

marker line (the orange line in Figure 4.8 A and C), augmented with a tool-tip displaying the Hilbert index and intensity at that position. For better visibility and to better visually link the nonlinearly scaled and the linearly scaled chart, this line is updated simultaneously in both charts. Visualizing two or more 1D Hilbert line plots side by side enables a detailed analysis and comparison of all ensemble members, addressing Task 1 and Task 4 from Section 4.1.

Dynamic Volume Lines provides several ways to select regions of interest. The user can perform rectangular multi-selections directly in the charts. Additionally, all Hilbert indices within a specified importance range can be selected by defining upper and lower bounds. Furthermore, the user can perform a selection in the 3D spatial view, by marking a rectangular region with a dragging interaction. This selects all voxels inside of the

Die approbierte gedruckte Originalversion dieser Dissertation ist an der TU Wien Bibliothek verfügbar.
The approved original version of this doctoral thesis is available in print at TU Wien Bibliothek.
TU WIEN Bibliothek Your knowledge hub

cuboid region that is spanned by projecting the rectangle from the near plane of the viewing frustum along the viewing direction to the far plane. In either case, all intervals in the Hilbert line plot falling into the selected region are highlighted. They are emphasized in the scaling widget as well, and the respective regions in the selected ensemble members are displayed in a separate 3D visualization. As a result, different or similar areas in the ensemble of reconstruction volumes can be identified and thus repeating patterns in the data (e.g., ring artifacts) can be exposed. This addresses Task 3 from Section 4.1. Optionally, we provide an aggregated view of the individual 1D Hilbert line plots using Functional Boxplots [SG11]. The Functional Boxplots show statistics such as the lower and upper whiskers, the median, and the interquartile range (see Figure 4.10 C).

4.4.3.3 Scaling Widget Visualization

Dynamic Volume Lines depicts a nonlinearly scaled chart at the top and a constantly scaled chart at the bottom, both showing the histogram heatmap visualization as well as the Hilbert line plot visualization. Early prototypes just had those two charts on top of each other. Using those early prototypes together with the domain experts, we realized that an explicit visualization of the nonlinear scaling is necessary. For this purpose, the current design includes the scaling widget, as shown in Figure 4.8 B. Each single histogram of the histogram heatmap in the nonlinearly scaled chart is mapped to the corresponding histogram in the constantly scaled chart. If the line plots are visible, each Hilbert index in the nonlinearly scaled chart maps to the corresponding index in the constantly scaled chart, respectively. Small rectangles at the top of the scaling widget each represent a histogram or Hilbert index. Their gray values encode the local ensemble variation. Black represents a low variation, white a high variation. From these rectangles at the top, trapezoids extend to the bottom. Their color is gradually shifting to an average gray value, which represents the constant scaling applied in the lower plot. The position marker line is also shown in the scaling widget, linking the nonlinearly scaled chart at the top with the constantly scaled chart at the bottom, as shown in Figure 4.8.

4.5 Case Studies

In this section we present two case studies that reflect the domain-specific requirements and present the capabilities of *Dynamic Volume Lines*. First, we analyze reconstruction data of the artificial specimen from simulated XCT (see Section 4.5.1), and in our second case study, we analyze the real-world TLGI-XCT foam specimen (see Section 4.5.2).

4.5.1 Artificial Specimen from Simulated XCT

The specimen analyzed here is an artificial dataset from simulated XCT with three cylindrical bars orthogonal to each other (see Section 4.3.2). Two of the bars have attachments at their ends, one of which is a sphere, the other one is a cube. Different levels of smoothing produce a volume ensemble, as shown in Figure 4.2. The ROI

Die approbierte gedruckte Originalversion dieser Dissertation ist an der TU Wien Bibliothek verfügbar.
The approved original version of this doctoral thesis is available in print at TU Wien Bibliothek.
TU Bibliothek Your knowledge hub WIEN

cutout for this analysis covers the end of the bar with the attached cube, as shown in Figure 4.9 A.

The analysis goal for this dataset mainly has been to determine interesting regions, which correspond to areas where the most changes happen in the ensemble. We use a synthetic dataset in order to show the basic behavior of *Dynamic Volume Lines* under well-defined conditions. We set a filter for regions with high local variations, in this case we select an importance range between 0.5 and 1. The 3D spatial view displays the respective regions in each member, as can be seen in Figure 4.9 B. The voxels displayed there, clearly indicate that the regions with most changes are located at the edges of the cube. The selection also gets highlighted in the nonlinearly scaled Hilbert line plot and the scaling widget shown in Figure 4.9 C and 4.9 D. The scaling widget visualizes the importance through the color coding (white to light-gray for the selection) and by the trapezoidal shapes, which are much broader at the top as compared to the bottom. The background threshold is set to 30000. Intensities below this threshold correspond to air and are not of interest for this analysis. Figure 4.9 C shows these background regions, which are marked with light orange boxes. The parameter p to influence the nonlinear scaling (see Section 4.4.2, Equation (4.2)) is set to 1.4. For this dataset, this setting ensures a good balance between emphasizing regions with high variances, but still ensuring that background regions and regions with low variances remain visible.

4.5.2 Real-world TLGI-XCT Foam Specimen

We analyze the ensemble of 16 volumes from the real-world TLGI-XCT foam specimen (see Section 4.3.2) as shown in Figure 4.3. Each volume of the ensemble is represented by a Hilbert curve of length 262144. The histogram heatmap displayed in Figure 4.10 A shows that there is a broad variation in the lower intensities, indicated by the white regions. There are less intensities in the upper range, and the histogram colors indicate lower frequencies there. This implies that most of the space is occupied by voids, the remaining space is left to the cell walls.

When zooming in and viewing the 1D Hilbert line plots as shown in Figure 4.10 B, one can see at a glance that the volumes differ vastly in their local intensity variations. The ensemble member corresponding to the bottom, dark-green Hilbert line plot is nearly flat, indicating a low contrast of the intensities. The topmost, light-green plot shows highly varying intensities, revealing a high contrast. Figure 4.10 C gives the Functional Boxplots of the 1D Hilbert line plots (shown in Figure 4.10 B). The gray interquartile range covers the volumes with iteration values from 250 to 650. The volume with 500 iterations is the median. In areas of low local intensity variation, the minimum and maximum of the Functional Boxplots are very close to each other. The background threshold is set to zero, because in this analysis scenario we are interested in low intensities as well. Since there is no compression due to the background, there are more voxels competing for available screen space. The parameter p to influence the nonlinear scaling (see Section 4.4.2, Equation (4.2)) is increased to 2 in order to compress regions with low variances more and to expand interesting regions with high variances.

Die approbierte gedruckte Originalversion dieser Dissertation ist an der TU Wien Bibliothek verfügbar.
The approved original version of this doctoral thesis is available in print at TU Wien Bibliothek.
TU Bibliothek Your knowledge hub WIEN

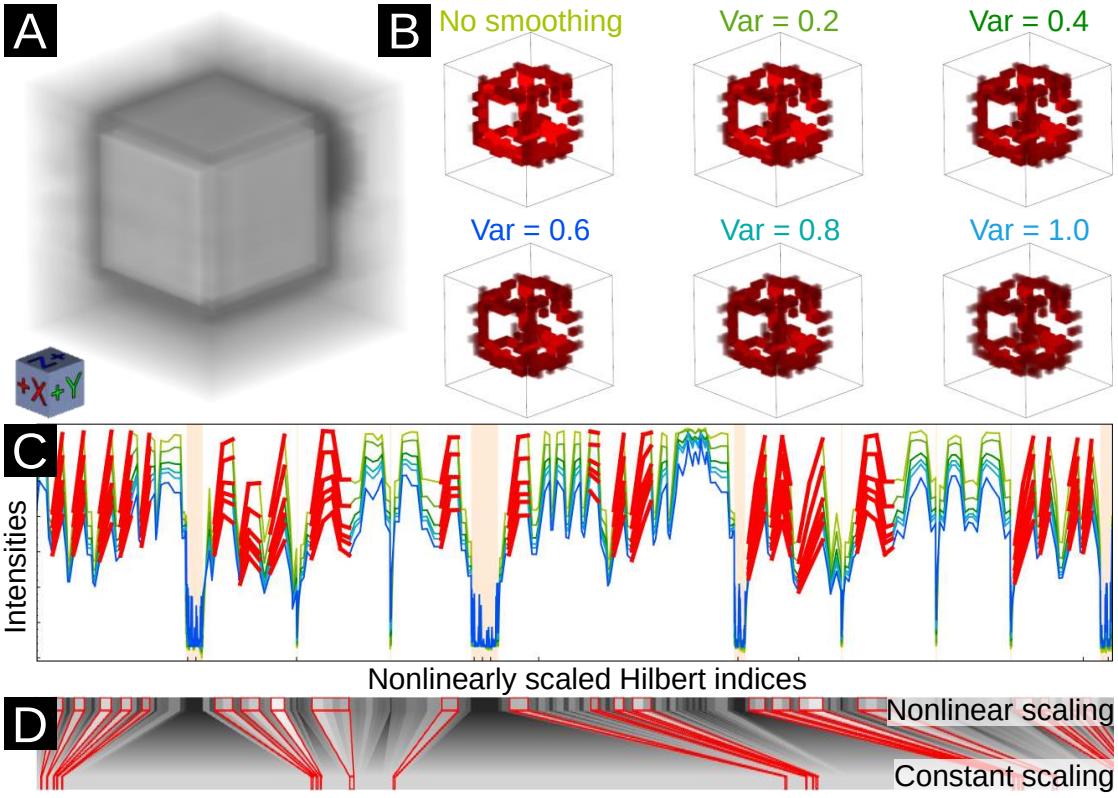

Figure 4.9: (A) 3D rendering of the volume with no smoothing. (B) 3D volume renderings of the selected voxels for all six ensemble members. (C) Corresponding Hilbert line plots with highly important regions selected. (D) Scaling widget with highlighted red selections.

We select regions with an importance value between 0.1 and 1 (high variation of the intensities). As can be seen in Figure 4.11 D, only the cell walls show such high variations. Based on the importance function, the cell walls can be separated easily. The selected indices are highlighted in the scaling widget shown in Figure 4.11 E. Inspecting the Hilbert line plots (see Figure 4.10 B) and the 3D views of the different parameter variations (see Figure 4.11 D), we can see that the volumes produced by the SIRT algorithm with less than 250 iterations result in low contrast between cell walls and voids. Starting from approximately 350 iterations, the contrast converges to the FDK reference volume. *Dynamic Volume Lines* gives a quick insight into the contrast changes in the ensemble by displaying the grey values as lines. It would be very difficult to distinguish the contrast changes without *Dynamic Volume Lines*. Since doubling the number of iterations also means doubling the required reconstruction time, we can conclude that we can stop the reconstruction at 400 iterations without a major loss of accuracy.

When selecting regions with a low importance value between 0 and 0.001 (low variation of intensities), the ring artifacts are selected, as shown in Figure 4.12 F. This indicates

Die approbierte gedruckte Originalversion dieser Dissertation ist an der TU Wien Bibliothek verfügbar.
The approved original version of this doctoral thesis is available in print at TU Wien Bibliothek.
TU Bibliothek Your knowledge hub WIEN

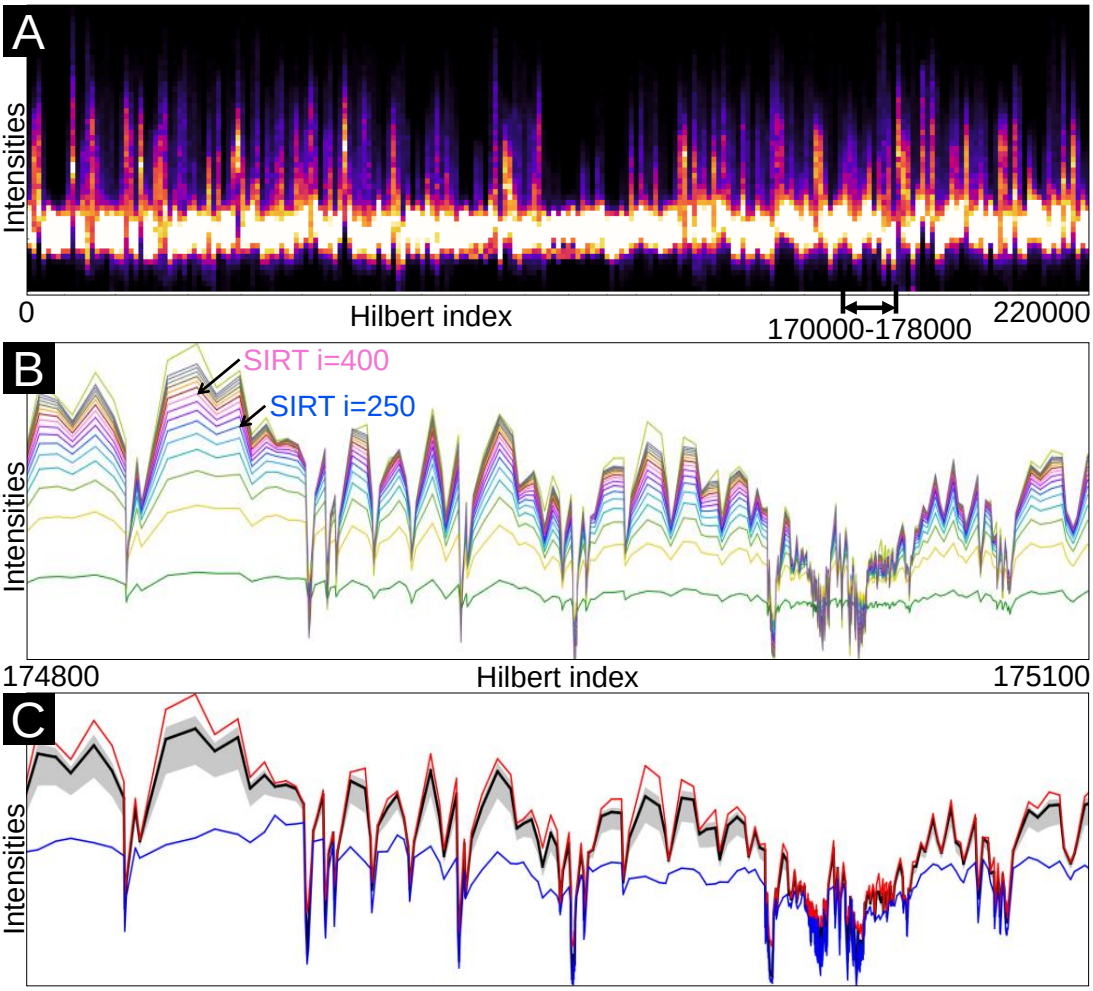

Figure 4.10: (A) Histogram heatmap of the foam volumes ensemble showing most intensities in the lower range. (B) 1D Hilbert line plots zoom-in, enabling a detailed comparison of the foam volumes, reconstructed with different SIRT *iteration* parameters. (C) Functional Boxplots of the 1D Hilbert line plots in (B).

that the SIRT iterations do not suppress the ring artifacts. Both FDK and SIRT are affected by them in exactly the same way. The importance function could therefore be used to detect such artifacts. They are the only features in the volumes, which show only little variation with different reconstruction parameters. Figure 4.12 G conveys in the Hilbert line plots that in the lower intensity range there is in general a low variation in all the volumes. There is even less variation in the highlighted regions of the ring artifacts. We therefore hypothesize that there is potential to use the local ensemble variation to develop a ring-artifact reduction algorithm for the reconstructed volumes. This is an insight that would not have been possible without the knowledge gained from the analysis with *Dynamic Volume Lines*.

Die approbierte gedruckte Originalversion dieser Dissertation ist an der TU Wien Bibliothek verfügbar.
The approved original version of this doctoral thesis is available in print at TU Wien Bibliothek.
TU WIEN Bibliothek Your knowledge hub

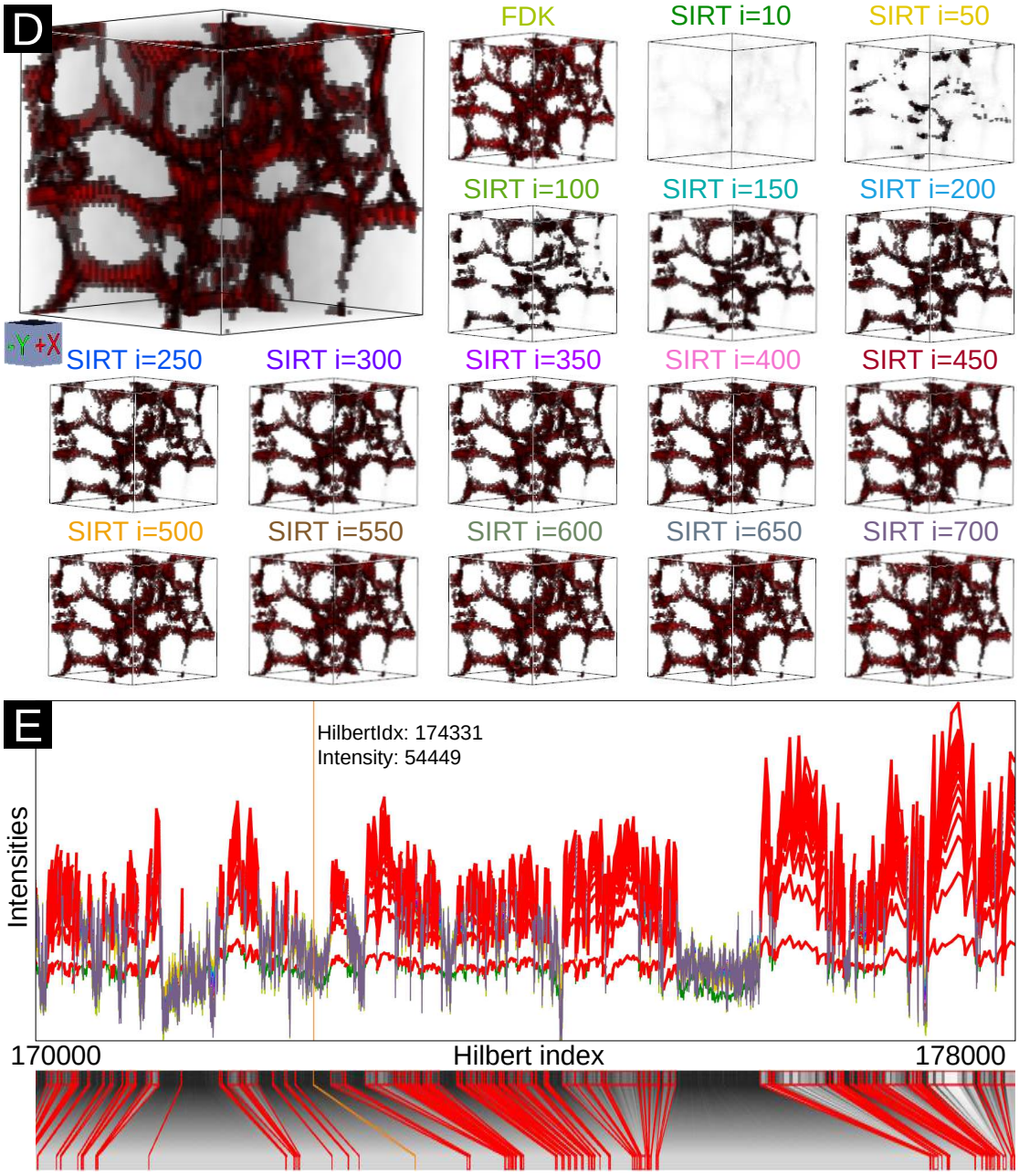

Figure 4.11: (D) 3D rendering views of regions with selected high importance, coinciding with the foam cell walls. (E) Regions of high importance as in (D), selected in the 1D Hilbert line plots.

Die approbierte gedruckte Originalversion dieser Dissertation ist an der TU Wien Bibliothek verfügbar.
The approved original version of this doctoral thesis is available in print at TU Wien Bibliothek.

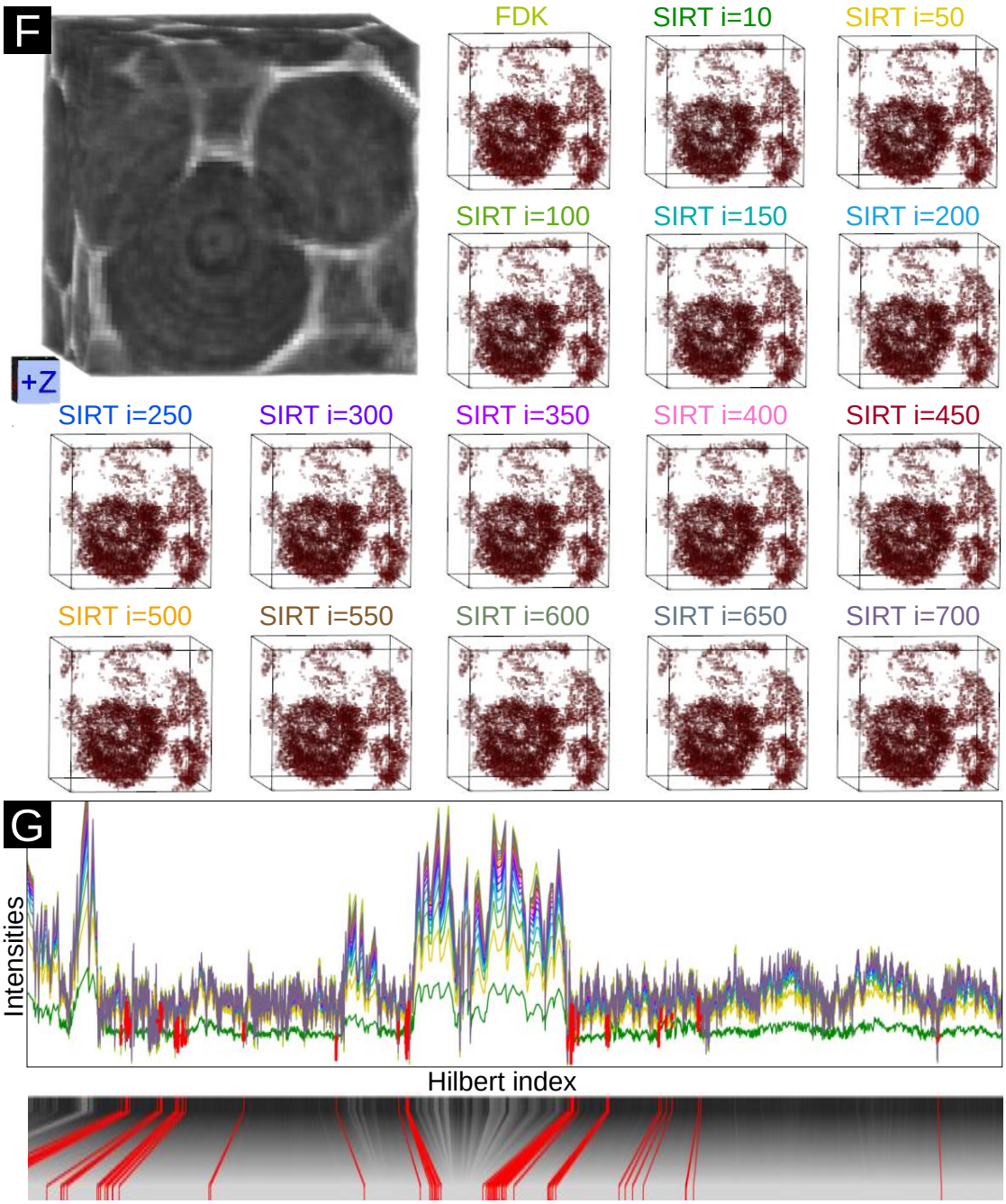

Figure 4.12: (F) 3D rendering views of regions with selected low importance, coinciding with the ring artifacts. (G) Regions of low importance as in (F), selected in the 1D Hilbert line plots.

Die approbierte gedruckte Originalversion dieser Dissertation ist an der TU Wien Bibliothek verfügbar.
The approved original version of this doctoral thesis is available in print at TU Wien Bibliothek.

4.5.3 Implementation and Performance Measurements

The experiments were performed on a desktop machine with an Intel(R) Core(TM) i7-3770 CPU, 32 GB RAM and an NVIDIA GeForce GTX 1080 GPU with 8 GB RAM. The *Dynamic Volume Lines* were implemented in C++. ITK 4.9 [JMIC15] has been used to perform basic image processing, to load the datasets, and to generate the Hilbert curves [Tus11]. The 3D rendering views were calculated with VTK 7.0 [SML06]. The histogram heatmap and the 1D Hilbert line plots were built with the QCustomPlot 2.0 library [Eic]. The scaling widget and the GUI in general were implemented in Qt 5.8 [Gro]. The calculation time scales with the size of the ensemble and the size of the individual volumes, whereby the generation of the Hilbert curve has the largest share in the calculation time. However, the generation of the Hilbert curve can be carried out before the actual analysis, so that large volumes can also be explored interactively afterwards. Computing the Hilbert curves, for example, for 16 datasets with a size of $64 \times 64 \times 64$ voxels (see Figure 4.3) takes approximately 12 seconds. This includes creating the nonlinear scaling, generating the segment tree, and the initial rendering of the charts. Dragging and zooming within the charts work in real-time. The performance of selecting 1D Hilbert line plots and rendering the corresponding 3D views depends on the number of chosen line segments and on the number of chosen volumes, but typically takes less than five seconds in our cases.

4.6 Conclusion and Future Work

In this chapter we present *Dynamic Volume Lines*, a tool for the interactive visual analysis and comparison of ensembles of 3D volumes using 1D Hilbert line plots. Volumes are linearized along a space-filling Hilbert curve. An aggregate overview visualization for volume ensembles is introduced as a histogram heatmap, which encodes the intensity frequencies. A nonlinear scaling is provided to emphasize regions with high local variations and to optimally utilize the available screen space. The scaling is illustrated in an interactive scaling widget. Using an artificial specimen from simulated XCT, we investigate the general usefulness of the tool in detecting local variations in the ensemble. On a real-world TLGI-XCT foam specimen we show that our importance function, based on local variations, can be used to detect structures such as cell walls, and to discover unwanted ring artifacts. Our domain-expert collaborators were very positive about the possibility to compare multiple volumes at once, as they previously had no comprehensive tool available to support this analysis scenario. They also positively mentioned the guidance towards interesting regions, i.e., areas with high local variations. It is important for them to be able to investigate selected regions in more detail, and to retain the relation to the spatial domain. This allows them to draw conclusions and to gain insights for adaptations in their algorithm development. In general, the concept of representing an ensemble of volumes as nonlinear 1D Hilbert line plots is not limited to 3D space, but can also be applied to (abstract) n-dimensional spaces.

Die approbierte gedruckte Originalversion dieser Dissertation ist an der TU Wien Bibliothek verfügbar.
The approved original version of this doctoral thesis is available in print at TU Wien Bibliothek.
TU Bibliothek WIEN Your knowledge hub

Die approbierte gedruckte Originalversion dieser Dissertation ist an der TU Wien Bibliothek verfügbar.
The approved original version of this doctoral thesis is available in print at TU Wien Bibliothek.

CHAPTER 5

Summary and Conclusion

Industrial 3D X-ray computed tomography is an excellent imaging technique to characterize advanced composites with respect to structural composition and defects, as it provides high-resolution images and reveals very small structures inside the specimen without destroying it. However, it also generates large amounts of data at the same time. Analyzing these data is often tedious and difficult for the experts. By using meaningful and understandable visualizations, the XCT datasets can be analyzed efficiently and profoundly. The interaction of the various internal material features (e.g., fibers, pores, inclusions) can be better understood and existing material configurations can be optimized or new ones created.

In this work, the application scenarios *fiber characterization*, *porosity-value determination*, and *feature comparison in multiple volumes* were investigated, since these are typical for the handling of advanced composite materials in the field of non-destructive testing using XCT. Three novel visual analysis methods were presented, which address the domain-specific challenges in the respective application areas. The first two visualization techniques deal with the material-specific issues of characterizing fibers and determining porosity in fiber-reinforced polymers (FRPs). The third visualization technique follows a general approach in order to compare several different volumes and their interesting features. All these visualization contributions have in common that their linked views and interaction concepts create tailored visual analysis systems for special application scenarios in material science. In this context, Heinzl and Stappen [HS17] have identified four high-level challenges of visual computing that need to be addressed for boosting research endeavors in material science. In the following, the individual visualization contributions of this thesis address the high level challenges of visual computing to support material science:

- **Interactive exploration and visual analysis of fibers in advanced composites.** An in-depth analysis of fiber characteristics, such as position, length and

orientation, is of great interest, as regularities can be derived and the material properties can be estimated. For example, these findings can then be used in finite element simulations. A research prototype, which provides a simple, detailed, and comprehensive visual analysis of FRPs based on their individual fiber characteristics and the correlations between the different characteristics, is discussed in Chapter 2. By calculating derived fiber characteristics based on the preprocessed data (e.g., fiber start and end points), overview visualizations can be realized, which support a fast and easy evaluation of fiber lengths and fiber orientations in XCT datasets. With the linked views PCP, SPLOM, Fiber Class Explorer, and 3D volume rendering of the fiber dataset, fibers can be highlighted, divided into classes according to their specific characteristics, and statistically evaluated. Thus, correlations and hidden patterns can be derived and identified among the different fiber characteristics.
The interplay of these views serves as an example of how the *Quantitative Data Visualization Challenge* can be met. In addition, the Blob and Fiber Metadata visualizations emphasize the shape of the different fiber layers and facilitates the detection of outliers in advanced composite materials. All these visualizations with their interconnected interaction possibilities, demonstrate how the *Integrated Visual Analysis Challenge* can be tackled. In contrast to standard software solutions, the presented visualization methods enable domain experts to cope with the given high information content and allows them to efficiently explore and analyze the fibers in XCT datasets.

- **Visual analysis and evaluation of porosity in fiber-reinforced polymers.** An accurate determination of the porosity value for advanced composite materials with high quality requirements is essential in order to produce as little rejects as possible. To determine the porosity value in FRP specimens scanned with XCT, suitable image processing and segmentation algorithms are required. Various combinations of image processing and segmentation algorithms and their different parameter settings may lead to several hundreds of varying segmentation results. Therefore it is difficult to find a suitable segmentation pipeline and its appropriate parameters. A visualization tool to systematically evaluate the results of different segmentation pipelines is discussed in Chapter 3. It enables the user conveniently to link and combine several image processing and segmentation filters to a pipeline by drag and drop. The behavior of the individual filters can be influenced by their parameter settings. All filter parameters of a segmentation pipeline define a parameter space that can be sampled with different granularity. As soon as the assembly of the segmentation pipelines is finished, they are processed in an automatic batch process. In addition to the segmentation masks, further derived results such as the porosity value, the segmentation pipeline runtime, and the Dice-coefficients are computed. In an intuitive visual analysis process the results can then be explored. To this end, the segmentation results are first presented with overview visualizations and only on demand with more detailed analysis visualizations. The overview visualizations allow the user to compare and preselect

Die approbierte gedruckte Originalversion dieser Dissertation ist an der TU Wien Bibliothek verfügbar.
The approved original version of this doctoral thesis is available in print at TU Wien Bibliothek.
TU Bibliothek Your knowledge hub WIEN

the data. The selected segmentation results are then transferred to a SPLOM. It allows the user to examine the results in more detail and enables trade-off analyses between the input parameters and the derived results. On an even more-detailed level, selected segmentation results can be compared with 2D and 3D comparative visualizations on a pixel/voxel level in dependence of their different parameter settings.

From the assembly of pore segmentation pipelines by drag and drop to the analysis of the results with linked views at increasing levels of detail, this visualization system tailored to pore analysis shows how the *Integrated Visual Analysis Challenge* can be met. The visualizations Overview Comparative Matrix, SPLOM with popup preview, PRSs, and the comparative 2D slice and 3D rendering views, address the *Quantitative Data Visualization Challenge*. These visual knowledge discovery methods allow domain experts to efficiently analyze and to statistically evaluate the segmentation results along with the corresponding input parameters and to classify segmentations into meaningful and correct ones. The *Visual Debugger Challenge* is partially met using the Overview Comparative Matrix (in *deviation* mode) and the SPLOM, which enable the user to quantitatively analyze the results of assembled segmentation pipelines. Both visualization techniques depict the deviation of the porosity value from the reference porosity value of the individual segmentation pipelines respectively the different parameter settings through a diverging cool-to-warm perceptually-uniform color map. Algorithms or parameterizations that lead to inappropriate or incorrect pore segmentations can be quickly discarded, but at the same time useful segmentations are indicated. Currently, there are no indications on how an analysis can be improved or suggestions which algorithms or segmentation pipelines are suitable for a specific task. The SPLOM with the popup preview and the 2D slice and 3D rendering views cover partial aspects of the *Interactive Steering Challenge*. These visualization techniques can be used to determine if the parameter space of a segmentation pipeline has been sampled with sufficient accuracy, or if the parameters need to be further refined and the results of the segmentation pipeline need to be recalculated. Information on how a specific algorithm or a certain parameterization influences the final result, e.g., already during the assembly of a segmentation pipeline, is currently not provided.

- **Visual comparison of interesting features in 3D volumes.** XCT for non-destructive testing in general, uses different reconstruction or image processing algorithms to improve the data quality, e.g., by removing artifacts or reducing noise. The different parameter settings of the algorithms generate different XCT datasets, which differ slightly in their image quality. The simultaneous comparison and evaluation of the data quality is only insufficiently achievable with conventional two-dimensional methods and varies from expert to expert. Chapter 4 discusses a visualization technique, which allows the user to compare and evaluate interesting features simultaneously in an ensemble of XCT datasets with subtle differences. For this purpose, the intensities of the 3D volumes are traversed and extracted along a space-filling Hilbert curve or a simple scan line curve and presented as 1D

Die approbierte gedruckte Originalversion dieser Dissertation ist an der TU Wien Bibliothek verfügbar.
The approved original version of this doctoral thesis is available in print at TU Wien Bibliothek.
TU WIEN Bibliothek Your knowledge hub

line plots. This ensures that each traversed voxel can be directly compared to one of its neighbor voxels and each voxel position is compared with the same voxel position in the other datasets of the ensemble. Based on the intensity variations in the ensemble, a nonlinear scaling of the 1D line plots is performed. The nonlinear scaling expands interesting regions with high intensity variations and compresses uninteresting regions with low intensity variations. The available screen space is effectively utilized and the user can concentrate on the areas with high variations in the ensemble. Based on the nonlinear scaling, the tool provides an overview visualization in the form of a histogram heatmap of the intensity frequencies, which is replaced by the detailed 1D line plots when zooming in. At each level of detail, the scaling widget emphasizes the local ensemble variations. The Functional Boxplots serve as an aggregated visualization to give a statistical view on the ensemble variations. The interaction concept of brushing and linking allows users, e.g., to select regions with high ensemble variation in the 1D line plots and to display the affected voxels in the 3D spatial context.
The interactive 2D views with the histogram heatmap, the 1D line plots with the Functional Boxplots, together with the 3D views of the volumes, provide a tailored tool for exploring and analyzing interesting features in a volume ensemble and demonstrate how to cope with the *Integrated Visual Analysis Challenge*. Due to the abstract representation of XCT volumes as 1D line plots, the intensities are quantifiable. This is because small intensity differences can be better perceived by positional encoding than by color encoding. As a result, the domain experts are able to perform a detailed and efficient analysis of interesting regions in an ensemble of XCT volumes and to find and evaluate repeating patterns in the data such as artifacts or noise. The approaches of traversing and extracting the intensities of 3D volumes along a space-filling curve and the nonlinear scaling of the 1D line plots to cluster (compress) uninteresting regions, target the *Quantitative Data Visualization Challenge*.

During the close collaboration with material experts in the field of NDT using XCT over the past seven years, it became clear that visual computing is essential for material science, e.g., in the characterization, development, and inspection process. Only with suitable visual analysis techniques, the generated XCT data can be efficiently evaluated and the questions from material science can be answered. Standard software tools for visual analysis can be used only to a limited extent, because material systems, material requirements, inspection methods, and acquisition systems are constantly evolving. For this reason, specific visual analysis tools are necessary. The increasing number of contributions to visualization and visual analysis at conferences in the field of material science such as the *Conference on Industrial Computed Tomography* [iCT] confirms that this demand is already being addressed.

The visual analysis methods of this thesis demonstrate, how the workflows of the experts are improved and supported by simple, fast, and well-grounded analysis processes to provide new insights in the field of material characterization with XCT. During the

Die approbierte gedruckte Originalversion dieser Dissertation ist an der TU Wien Bibliothek verfügbar.
The approved original version of this doctoral thesis is available in print at TU Wien Bibliothek.
TU Bibliothek Your knowledge hub WIEN

development of the presented systems it turned out that it is essential to understand the problems of the material scientists. To this end, in several cases weekly meetings with the experts were necessary, where the problems were iteratively defined and analyzed with increasing precision. It has been important to bring the terminologies from both scientific domains, i.e., visual computing and material science, closer together. During the meetings it turned out that the software solutions of the domain experts offered only a limited spectrum of visualization concepts and consequently they were not familiar with more sophisticated visualizations. In order to enable a knowledge exchange, the use of hand drawn mockups and software prototypes with basic functionalities proved to be very helpful. With them, the visualization and interaction ideas can be discussed in a target-oriented fashion. The proposed ideas were also discussed with visual computing experts, who either extended them further or rejected them completely. With the help of this multi-stage iterative design process all visualization contributions of this thesis were developed. The presented tools were integrated as software modules into the open source framework *open_iA* [FWS+19]. The achieved results were evaluated together with our project partners from the aerospace and automotive industry and the domain experts for non-destructive testing of the University of Applied Sciences Upper Austria - Wels Campus. The developed visualization techniques were tested using real-world XCT scans of advanced composites and artificial specimens generated by XCT simulation.

The numerous discussions with the material experts in the course of this work have shown, that “transparent” algorithms and visual analysis systems for finding meaningful parameter settings are of great interest for material scientists in order to optimize the data evaluation. At the beginning of this thesis, material scientists used simple pore segmentation algorithms with no or only a few parameters because they were fast and the results were easy to understand. However, as material systems became increasingly complex and the demands on the quality of material systems increased, these simple algorithms led to inaccurate or incorrect results. Therefore, complex algorithms were used more and more. The algorithms often achieve very good results, but only after the correct parameter settings have been found. This is usually time-consuming and challenging because the algorithm and its parameters must be understood in detail. Only then different parameter settings can be tested and the results evaluated. This situation indicates how important it will be in the future to provide visual analysis systems, which explain the processes in "black box" algorithms and present the results of the different parameter settings in a comprehensive way.
In the context of complex algorithms, deep learning plays an important role. This research area of machine learning has attracted a lot of attention in recent years, including material science, which aims to achieve better results in the future through neural networks than with currently used complex algorithms, e.g., in the area of object recognition/segmentation. The provision of sufficiently large training sets for the wide variety of material systems can be seen as a future challenge. At the same time, deep learning requires from visual computing to create explainable artificial intelligence systems with suitable visualization techniques. As another future area of visual computing, augmented and virtual reality applications can be identified. In these areas, suitable visual analysis

Die approbierte gedruckte Originalversion dieser Dissertation ist an der TU Wien Bibliothek verfügbar.
The approved original version of this doctoral thesis is available in print at TU Wien Bibliothek.
TU Bibliothek Your knowledge hub WIEN

systems and interaction methods have to be investigated and developed, in order to support material science, e.g., for the inspection of components. Finally, due to the increasing size of XCT datasets, the problem of clutter, occlusion, and rendering time is still considered as a future challenge in the research area of visual computing.

Die approbierte gedruckte Originalversion dieser Dissertation ist an der TU Wien Bibliothek verfügbar.
The approved original version of this doctoral thesis is available in print at TU Wien Bibliothek.

Bibliography

[7Sp] 7Span. Material UI Web Development Tools. https://www.materialui.co, (accessed on 04.11.2019).

[AAS+16] A. Amirkhanov, A. Amirkhanov, D. Salaberger, J. Kastner, E. Gröller, and C. Heinzl. Visual Analysis of Defects in Glass Fiber Reinforced Polymers for 4DCT Interrupted *In situ* Tests. *Computer Graphics Forum*, 35(3):201–210, 2016.

[AJ09] H. Altendorf and D. Jeulin. 3D Directional Mathematical Morphology for Analysis of Fiber Orientations. *Image Analysis & Stereology*, 28(3):143–153, 2009.

[Bea11] R. Beare. Histogram-based thresholding - some missing methods. *Insight Journal*, 2011. http://www.insight-journal.org/browse/publication/811, accessed on 04.11.2019.

[BL06] R. Beare and G. Lehmann. The Watershed Transform in ITK - Discussion and New Developments. *Insight Journal*, 2006. http://www.insight-journal.org/browse/publication/92, accessed on 04.11.2019.

[Bla18] S. Black. Roth filament winder to facilitate major Ariane 6 weight/cost cuts. *CompositesWorld*, 2018. https://www.compositesworld.com/articles/roth-filament-winder-to-facilitate-major-ariane-6-weightcost-cuts, accessed on 04.11.2019.

[Bli82] J. F. Blinn. A Generalization of Algebraic Surface Drawing. *ACM Transactions on Graphics (TOG)*, 1(3):235–256, 1982.

[BPFG11] W. Berger, H. Piringer, P. Filzmoser, and E. Gröller. Uncertainty-Aware Exploration of Continuous Parameter Spaces Using Multivariate Prediction. *Computer Graphics Forum*, 30(3):911–920, 2011.

[BS04] E. A. Birt and R. A. Smith. A Review of NDE Methods for Porosity Measurement in Fibre-reinforced Polymer Composites. *Insight - Journal of The British Institute of Non Destructive Testing*, 46(11):681–686, 2004.

Die approbierte gedruckte Originalversion dieser Dissertation ist an der TU Wien Bibliothek verfügbar.
The approved original version of this doctoral thesis is available in print at TU Wien Bibliothek.
TU WIEN Bibliothek Your knowledge hub

[BSM+13] S. Bergner, M. Sedlmair, T. Möller, S. Nabi-Abdolyousefi, and A. Saad. ParaGlide: Interactive Parameter Space Partitioning for Computer Simulations. *IEEE Transactions on Visualization and Computer Graphics (TVCG)*, 19(9):1499–1512, 2013.

[BW90] J. Bloomenthal and B. Wyvill. Interactive Techniques for Implicit Modeling. *ACM SIGGRAPH Computer Graphics*, 24(2):109–116, 1990.

[Che12] Q. Cheng. *Fiber Reinforced Composites*. Nova Science Publishers, 2012.

[Cie11] R. Cierniak. *X-Ray Computed Tomography in Biomedical Engineering*. Springer London, 2011.

[CKC05] P. Craig, J. Kennedy, and A. Cumming. Coordinated Parallel Views for the Exploratory Analysis of Microarray Time-course Data. In *Proceedings of the Coordinated and Multiple Views in Exploratory Visualization (CMV '05)*, pages 3–14, 2005.

[CLEK13] D. Coffey, C.-L. Lin, A. G. Erdman, and D. F. Keefe. Design by Dragging: An Interface for Creative Forward and Inverse Design with Simulation Ensembles. *IEEE Transactions on Visualization and Computer Graphics (TVCG)*, 19(12):2783–2791, 2013.

[CM88] W. C. Cleveland and M. E. McGill. *Dynamic Graphics for Statistics*. CRC Press, Inc., first edition, 1988.

[dBCvKO08] M. de Berg, O. Cheong, M. van Kreveld, and M. Overmars. *Computational Geometry: Algorithms and Applications*, chapter More Geometric Data Structures, pages 219–241. Springer-Verlag TELOS, third edition, 2008.

[DCCK+14] L. De Chiffre, S. Carmignato, J.-P. Kruth, R. Schmitt, and A. Weckenmann. Industrial Applications of Computed Tomography. *CIRP Annals*, 63(2):655–677, 2014.

[DDW14] I. Demir, C. Dick, and R. Westermann. Multi-Charts for Comparative 3D Ensemble Visualization. *IEEE Transaction on Visualization and Computer Graphics (TVCG)*, 20(12):2694–2703, 2014.

[Dic45] L. R. Dice. Measures of the Amount of Ecologic Association Between Species. *Ecology*, 26(3):297–302, 1945.

[DJW16] I. Demir, M. Jarema, and R. Westermann. Visualizing the Central Tendency of Ensembles of Shapes. In *SIGGRAPH ASIA 2016 Symposium on Visualization*, pages 3:1–3:8, 2016.

[EDF08] N. Elmqvist, P. Dragicevic, and J. Fekete. Rolling the Dice: Multidimensional Visual Exploration using Scatterplot Matrix Navigation. *IEEE Transactions on Visualization and Computer Graphics (TVCG)*, 14(6):1539–1148, 2008.

Die approbierte gedruckte Originalversion dieser Dissertation ist an der TU Wien Bibliothek verfügbar.
The approved original version of this doctoral thesis is available in print at TU Wien Bibliothek.
TU WIEN Bibliothek Your knowledge hub

[Eic] E. Eichhammer. QCustomPlot. http://www.qcustomplot.com, (accessed on 04.11.2019).

[FA13] K. Friedrich and A. A. Almajid. Manufacturing Aspects of Advanced Polymer Composites for Automotive Applications. *Applied Composite Materials*, 20(2):107–128, 2013.

[FDK84] L. A. Feldkamp, L. C. Davis, and J. W. Kress. Practical Cone-beam Algorithm. *Journal of the Optical Society of America A*, 1(6):612–619, 1984.

[FHG+09] L. Fritz, M. Hadwiger, G. Geier, G. Pittino, and E. Gröller. A Visual Approach to Efficient Analysis and Quantification of Ductile Iron and Reinforced Sprayed Concrete. *IEEE Transactions on Visualization and Computer Graphics (TVCG)*, 15(6):1343–1350, 2009.

[FL96] S.-Y. Fu and B. Lauke. Effects of Fiber Length and Fiber Orientation Distributions on the Tensile Strength of Short-fiber-reinforced Polymers. *Composites Science and Technology*, 56(10):1179–1190, 1996.

[FMH16] B. Fröhler, T. Möller, and C. Heinzl. GEMSe: Visualization-Guided Exploration of Multi-channel Segmentation Algorithms. *Computer Graphics Forum*, 35(3):191–200, 2016.

[FWS+19] B. Fröhler, J. Weissenböck, M. Schiwarth, J. Kastner, and C. Heinzl. open_iA: A Tool for Processing and Visual Analysis of Industrial Computed Tomography Datasets. *Journal of Open Source Software*, 4(35):1185, 2019.

[GAW+11] M. Gleicher, D. Albers, R. Walker, I. Jusufi, C. D. Hansen, and J. C. Roberts. Visual Comparison for Information Visualization. *Information Visualization*, 10(4):289–309, 2011.

[GB08] J. Gregor and T. Benson. Computational Analysis and Improvement of SIRT. *IEEE Transactions on Medical Imaging*, 27(7):918–924, 2008.

[Giu15] V. Giurgiutiu. *Structural Health Monitoring of Aerospace Composites*. Academic Press, 2015.

[GJP+14] M. G. Genton, C. Johnson, K. Potter, G. Stenchikov, and Y. Sun. Surface Boxplots. *Stat*, 3(1):1–11, 2014.

[GL94] C. Gotsman and M. Lindenbaum. On the Metric Properties of Discrete Space-filling Curves. In *Proceedings of the 12th IAPR International Conference on Pattern Recognition, Vol. 2 - Conference B: Computer Vision Image Processing. (Cat. No.94CH3440-5)*, volume 3, pages 98–102, 1994.

[Gmb] Volume Graphics GmbH. VGSTUDIO MAX 2.2. http://www.volumegraphics.com, (accessed on 04.11.2019).

Die approbierte gedruckte Originalversion dieser Dissertation ist an der TU Wien Bibliothek verfügbar.
The approved original version of this doctoral thesis is available in print at TU Wien Bibliothek.
TU Bibliothek WIEN Your knowledge hub

[GMG10] M. Gavrilescu, M. M. Malik, and E. Gröller. Custom Interface Elements for Improved Parameter Control in Volume Rendering. In *14th International Conference on System Theory and Control*, pages 219–224, 2010.

[Gro] Qt Group. Qt – A cross-platform development framework. `https://www.qt.io`, (accessed on 04.11.2019).

[GWW18] S. C. Garcea, Y. Wang, and P. J. Withers. X-ray Computed Tomography of Polymer Composites. *Composites Science and Technology*, 156:305–319, 2018.

[GXY11] H. Guo, H. Xiao, and X. Yuan. Multi-dimensional Transfer Function Design Based on Flexible Dimension Projection Embedded in Parallel Coordinates. In *Proceedings of IEEE Pacific Visualization Symposium (PacificVis 2011)*, pages 19–26, 2011.

[HB03] M. Harrower and C. A. Brewer. ColorBrewer.org: An Online Tool for Selecting Colour Schemes for Maps. *The Cartographic Journal*, 40(1):27–37, 2003.

[Hes14] R. B. Heslehurst. *Defects and Damage in Composite Materials and Structures*. CRC Press, 2014.

[HLRS+08] M. Hadwiger, F. Laura, C. Rezk-Salama, T. Höllt, G. Geier, and T. Pabel. Interactive Volume Exploration for Feature Detection and Quantification in Industrial CT Data. *IEEE Transactions on Visualization and Computer Graphics (TVCG)*, 14(6):1507–1514, 2008.

[HMMW03] R. Huang, K.-L. Ma, P. McCormick, and W. Ward. Visualizing Industrial CT Volume Data for Nondestructive Testing Applications. In *Proceedings of the IEEE Visualization 2003 (VIS'03)*, pages 547–554, 2003.

[HRC07] C. H. Hamilton and A. Rau-Chaplin. Compact Hilbert Indices for Multi-Dimensional Data. In *1st International Conference on Complex, Intelligent and Software Intensive Systems*, pages 139–146, 2007.

[HRC08] C. H. Hamilton and A. Rau-Chaplin. Compact Hilbert Indices: Space-filling Curves for Domains with Unequal Side Lengths. *Information Processing Letters*, 105(5):155–163, 2008.

[HS17] C. Heinzl and S. Stappen. STAR: Visual Computing in Materials Science. *Computer Graphics Forum*, 36(3):647–666, 2017.

[iCT] Conference on Industrial Computed Tomography (iCT). `http://www.3dct.at/cms2/index.php/en/welcome-4`, (accessed on 04.11.2019).

Die approbierte gedruckte Originalversion dieser Dissertation ist an der TU Wien Bibliothek verfügbar.
The approved original version of this doctoral thesis is available in print at TU Wien Bibliothek.
TU WIEN Bibliothek Your knowledge hub

[ID90] A. Inselberg and B. Dimsdale. Parallel Coordinates: A Tool for Visualizing Multi-dimensional Geometry. In *Proceedings of the IEEE Visualization 1990 (VIS '90)*, pages 361–378, 1990.

[JDKW15] M. Jarema, I. Demir, J. Kehrer, and R. Westermann. Comparative Visual Analysis of Vector Field Ensembles. In *Proceedings of IEEE Visual Analytics Science and Technology (VAST)*, pages 81–88, 2015.

[JLS+13] B. Jackson, T. Y. Lau, D. Schroeder, K. C. Toussaint, and D. F. Keefe. A Lightweight Tangible 3D Interface for Interactive Visualization of Thin Fiber Structures. *IEEE Transactions on Visualization and Computer Graphics (TVCG)*, 19(12):2802–2809, 2013.

[JMIC15] H. J. Johnson, M. M. McCormick, L. Ibáñez, and The Insight Software Consortium. *The ITK Software Guide Book 1: Introduction and Development Guidelines*. Kitware, Inc., fourth edition, 2015. `https://itk.org/ItkSoftwareGuide.pdf`, accessed on 04.11.2019.

[JRS+11] I. Jerjen, V. Revol, P. Schuetz, C. Kottler, R. Kaufmann, T. Luethi, K. Jefimovs, C. Urban, and U. Sennhauser. Reduction of Phase Artifacts in Differential Phase Contrast Computed Tomography. *Optics Express*, 19(14):13604–13611, 2011.

[Kei02] D. A. Keim. Information Visualization and Visual Data Mining. *IEEE Transactions on Visualization and Computer Graphics (TVCG)*, 8(1):1–8, 2002.

[KH18] J. Kastner and C. Heinzl. X-Ray Tomography. In N. Ida and N. Meyendorf, editors, *Handbook of Advanced Non-Destructive Evaluation*, chapter 31. Springer International Publishing, 2018.

[KLM+12] Z. Konyha, A. Lež, K. Matković, M. Jelović, and H. Hauser. Interactive Visual Analysis of Families of Curves Using Data Aggregation and Derivation. In *Proceedings of the 12th International Conference on Knowledge Management and Knowledge Technologies (i-KNOW '12)*, pages 24:1–24:8, 2012.

[KMN+02] T. Kanungo, D. M. Mount, N. S. Netanyahu, C. D. Piatko, R. Silverman, and A. Y. Wu. An Efficient k-means Clustering Algorithm: Analysis and Implementation. *IEEE Transactions on Pattern Analysis and Machine Intelligence (TPAMI)*, 24(7):881–892, 2002.

[KPR12] J. Kastner, B. Plank, and G. Requena. Non-destructive characterisation of polymers and al-alloys by polychromatic cone-beam phase contrast tomography. *Materials Characterization*, 64:79–87, 2012.

Die approbierte gedruckte Originalversion dieser Dissertation ist an der TU Wien Bibliothek verfügbar.
The approved original version of this doctoral thesis is available in print at TU Wien Bibliothek.
TU Bibliothek Your knowledge hub WIEN

[KPSS10] J. Kastner, B. Plank, D. Salaberger, and J. Sekelja. Defect and Porosity Determination of Fibre Reinforced Polymers by X-ray Computed Tomography. In *2nd International Symposium on NDT in Aerospace*, 2010.

[KZZM12] X. Kuang, H. Zhang, S. Zhao, and M. J. McGuffin. Tracing Tuples Across Dimensions: A Comparison of Scatterplots and Parallel Coordinate Plots. *Computer Graphics Forum*, 31(3pt4):1365–1374, 2012.

[LBH12] N. Lindow, D. Baum, and H.-C. Hege. Perceptually Linear Parameter Variations. *Computer Graphics Forum*, 31(2pt4):535–544, 2012.

[LC87] W. E. Lorensen and H. E. Cline. Marching Cubes: A High Resolution 3D Surface Construction Algorithm. *ACM SIGGRAPH Computer Graphics*, 21(4):163–169, 1987.

[Leh06] G. Lehmann. Robust Automatic Threshold Selection. *Insight Journal*, 2006. `http://www.insight-journal.org/browse/publication/134`, accessed on 04.11.2019.

[Lub82] G. Lubin, editor. *Handbook of Composites*. Van Nostrand Reinhold Company Inc., 1982.

[LZQ13] B. Li, X. Zhao, and H. Qin. Four-Dimensional Geometry Lens: A Novel Volumetric Magnification Approach. *Computer Graphics Forum*, 32(8):122–133, 2013.

[Mal07] P. K. Mallick. *Fiber-Reinforced Composites: Materials, Manufacturing, and Design*. CRC Press, third edition, 2007.

[Mas13] M. A. Masuelli, editor. *Fiber Reinforced Polymers*, chapter Introduction of Fibre-Reinforced Polymers – Polymers and Composites: Concepts, Properties and Processes. IntechOpen, 2013.

[MEV+05] M. Mlejnek, P. Ermes, A. Vilanova, R. van der Rijt, H. van den Bosch, F. Gerritsen, and E. Gröller. Profile Flags: A Novel Metaphor for Probing of T2 Maps. In *Proceedings of IEEE Visualization 2005 (VIS '05)*, pages 599–606, 2005.

[MGKH09] K. Matković, D. Gracanin, B. Klarin, and H. Hauser. Interactive Visual Analysis of Complex Scientific Data As Families of Data Surfaces. *IEEE Transactions on Visualization and Computer Graphics (TVCG)*, 15(6):1351–1358, 2009.

[MGVVL19] M. Mehdikhani, L. Gorbatikh, I. Verpoest, and S. V Lomov. Voids in Fiber-reinforced Polymer Composites: A Review on Their Formation, Characteristics, and Effects on Mechanical Performance. *Journal of Composite Materials*, 53(12):1579–1669, 2019.

Die approbierte gedruckte Originalversion dieser Dissertation ist an der TU Wien Bibliothek verfügbar.
The approved original version of this doctoral thesis is available in print at TU Wien Bibliothek.
TU Bibliothek WIEN Your knowledge hub

[MHG10] M. M. Malik, C. Heinzl, and E. Gröller. Comparative Visualization for Parameter Studies of Dataset Series. *IEEE Transaction on Visualization and Computer Graphics (TVCG)*, 16(5):829–840, 2010.

[Mil18] E. Milberg. SpaceX Falcon Heavy Launch Holds Promise for Carbon Fiber Composites. *Composites Manufacturing*, 2018. `http://compositesmanufacturingmagazine.com/2018/02/spacex-falcon-heavy-carbon-fiber-composites/`, accessed on 04.11.2019.

[MJFS01] B. Moon, H. V. Jagadish, C. Faloutsos, and J. H. Saltz. Analysis of the Clustering Properties of the Hilbert Space-Filling Curve. *IEEE Transactions on Knowledge and Data Engineering (TKDE)*, 13(1):124–141, 2001.

[MMGB17] P. Mindek, G. Mistelbauer, E. Gröller, and S. Bruckner. Data-sensitive Visual Navigation. *Computers and Graphics*, 67(C):77–85, 2017.

[Mor09] K. Moreland. Diverging Color Maps for Scientific Visualization. In *Advances in Visual Computing*, pages 92–103. Springer Berlin Heidelberg, 2009.

[Mor16] K. Moreland. Why We Use Bad Color Maps and What You Can Do About It. *Electronic Imaging*, 2016(16):1–6, 2016.

[MPSH11] G. Mayr, B. Plank, J. Sekelja, and G. Hendorfer. Active Thermography as a Quantitative Method for Non-destructive Evaluation of Porous Carbon Fiber Reinforced Polymers. *NDT & E International*, 44(7):537–543, 2011.

[Mun09] T. Munzner. A Nested Model for Visualization Design and Validation. *IEEE Transactions on Visualization and Computer Graphics (TVCG)*, 15(6):921–928, 2009.

[Mun14] T. Munzner. *Visualization Analysis and Design*. A K Peters/CRC Press, 2014.

[MWK14] M. Mirzargar, R. T. Whitaker, and R. M. Kirby. Curve Boxplot: Generalization of Boxplot for Ensembles of Curves. *IEEE Transactions on Visualization and Computer Graphics (TVCG)*, 20(12):2654–2663, 2014.

[Ng04] Hui-Fuang Ng. Automatic Thresholding for Defect Detection. In *IEEE 1st Symposium on Multi-Agent Security and Survivability*, pages 532–535, 2004.

[Ots79] Nobuyuki Otsu. A Threshold Selection Method from Gray-Level Histograms. *IEEE Transactions on Systems, Man and Cybernetics*, 9(1):62–66, 1979.

Die approbierte gedruckte Originalversion dieser Dissertation ist an der TU Wien Bibliothek verfügbar.
The approved original version of this doctoral thesis is available in print at TU Wien Bibliothek.
TU WIEN Bibliothek Your knowledge hub

[PBCR11] A. J. Pretorius, M.-A. Bray, A. E. Carpenter, and R. A. Ruddle. Visualization of Parameter Space for Image Analysis. *IEEE Transactions on Visualization and Computer Graphics (TVCG)*, 17(12):2402–2411, 2011.

[PBK10] H. Piringer, W. Berger, and J. Krasser. HyperMoVal: Interactive Visual Validation of Regression Models for Real-Time Simulation. *Computer Graphics Forum*, 29(3):983–992, 2010.

[PKBD07] F. Pfeiffer, C. Kottler, O. Bunk, and C. David. Hard X-Ray Phase Tomography with Low-Brilliance Sources. *Physical Review Letters*, 98(10):108105, 2007.

[PPBT12] H. Piringer, S. Pajer, W. Berger, and H. Teichmann. Comparative Visual Analysis of 2D Function Ensembles. *Computer Graphics Forum*, 31(3pt3):1195–1204, 2012.

[PWB+09] K. Potter, A. Wilson, P.-T. Bremer, D. Williams, C. Doutriaux, V. Pascucci, and C. R. Johnson. Ensemble-Vis: A Framework for the Statistical Visualization of Ensemble Data. In *IEEE International Conference on Data Mining Workshops*, pages 233–240, 2009.

[QCX+07] H. Qu, W.-Y. Chan, A. Xu, K. Chung, K. Lau, and P. Guo. Visual Analysis of the Air Pollution Problem in Hong Kong. *IEEE Transactions on Visualization and Computer Graphics (TVCG)*, 13(6):1408–1415, 2007.

[REK+16] M. Reiter, M. Erler, C. Kuhn, C. Gusenbauer, and J. Kastner. SimCT: A Simulation Tool for X-ray Imaging. In *Proceedings of the 6th Conference on Industrial Computed Tomography*, 2016.

[RGK+13] A. Reh, C. Gusenbauer, J. Kastner, E. Gröller, and C. Heinzl. MObjects – A Novel Method for the Visualization and Interactive Exploration of Defects in Industrial XCT Data. *IEEE Transactions on Visualization and Computer Graphics (TVCG)*, 19(12):2906–2915, 2013.

[RMH+09] M. Reiter, M. M. Malik, C. Heinzl, D. Salaberger, E. Gröller, H. Lettenbauer, and J. Kastner. Improvement of X-Ray Image Acquisition using a GPU based 3DCT Simulation tool. In *International Conference on Quality Control by Artificial Vision*, 2009.

[RMP+16] M. Raj, M. Mirzargar, J. S. Preston, R. M. Kirby, and R. T. Whitaker. Evaluating Shape Alignment via Ensemble Visualization. *IEEE Computer Graphics and Applications*, 36(3):60–71, 2016.

[RPK+12] A. Reh, B. Plank, J. Kastner, E. Gröller, and C. Heinzl. Porosity Maps – Interactive Exploration and Visual Analysis of Porosity in Carbon Fiber Reinforced Polymers. *Computer Graphics Forum*, 31(3):1185–1194, 2012.

Die approbierte gedruckte Originalversion dieser Dissertation ist an der TU Wien Bibliothek verfügbar.
The approved original version of this doctoral thesis is available in print at TU Wien Bibliothek.
TU Bibliothek WIEN Your knowledge hub

[RWS07] K. Robb, O. Wirjadi, and K. Schladitz. Fiber Orientation Estimation from 3D Image Data: Practical Algorithms, Visualization, and Interpretation. In *Proceedings of the 7th International Conference on Hybrid Intelligent Systems*, HIS '07, pages 320–325, 2007.

[SG11] Y. Sun and M. G. Genton. Functional Boxplots. *Journal of Computational and Graphical Statistics*, 20(2):316–334, 2011.

[SGB13] J. Schmidt, E. Gröller, and S. Bruckner. VAICo: Visual Analysis for Image Comparison. *IEEE Transactions on Visualization and Computer Graphics (TVCG)*, 19(12):2090–2099, 2013.

[SHB+14] M. Sedlmair, C. Heinzl, S. Bruckner, P. Harald, and T. Möller. Visual Parameter Space Analysis: A Conceptual Framework. *IEEE Transactions on Visualization and Computer Graphics (TVCG)*, 20(12):2161–2170, 2014.

[Shn96] B. Shneiderman. The Eyes Have It: A Task by Data Type Taxonomy for Information Visualizations. In *Proceedings of IEEE Symposium on Visual Languages (VL '96)*, pages 336–343, 1996.

[SJdD+17] J. Sanctorum, E. Janssens, A. den Dekker, S. Senck, C. Heinzl, J. De Beenhouwer, and J. Sijbers. A Workflow to Reconstruct Grating-based X-ray Phase Contrast CT Images: Application to CFRP Samples. In *Proceedings of the 4th Conference on X-ray and Neutron Phase Imaging with Gratings*, pages 139–140, 2017.

[SKK+11] D. Salaberger, K. A. Kannappan, J. Kastner, J. Reussner, and T. Auinger. Evaluation of Computed Tomography Data from Fibre Reinforced Polymers to Determine Fibre Length Distribution. *International Polymer Processing*, 26(3):283–291, 2011.

[SKO+11] R. Stoessel, D. Kiefel, R. Oster, B. Diewel, and L. Llopart Prieto. µ-Computed Tomography for 3D Porosity Evaluation in Carbon Fiber Reinforced Plastics (CFRP). *International Symposium on Digital Industrial Radiology and Computed Tomography*, 2011.

[SKW17] M. Sauer, M. Kühnel, and E. Witten. Composites Market Report 2017 – Market Developments, Trends, Outlook and Challenges. *Carbon Composites*, 2017. `https://www.carbon-composites.eu/media/2997/ccev-avk-market-report-2017.pdf`, accessed on 04.11.2019.

[SML06] W. Schroeder, K. Martin, and B. Lorensen. *The Visualization Toolkit–An Object-Oriented Approach To 3D Graphics*. Kitware, Inc., fourth edition, 2006.

[SPA+14] J. Schmidt, R. Preiner, T. Auzinger, M. Wimmer, E. Gröller, and S. Bruckner. YMCA - Your Mesh Comparison Application. In *Proceedings of IEEE Visual Analytics Science and Technology (VAST)*, 2014.

Die approbierte gedruckte Originalversion dieser Dissertation ist an der TU Wien Bibliothek verfügbar.
The approved original version of this doctoral thesis is available in print at TU Wien Bibliothek.
TU Bibliothek WIEN Your knowledge hub

[SPK+17] S. Senck, B. Plank, J. Kastner, V. Revol, K. Dobes, and M. Scheerer. Non-destructive Evaluation of Defects in Polymer Matrix Composites for Aerospace Applications using X-ray Talbot-Lau Interferometry and Micro CT. In *58th AIAA/ASCE/AHS/ASC Structures, Structural Dynamics, and Materials Conference, AIAA SciTech Forum*, pages 1–9, 2017.

[SSK11] M. Stommel, M. Stojek, and W. Korte. *FEM zur Berechnung von Kunststoff- und Elastomerbauteilen*. Carl Hanser Verlag, 2011.

[TMF+12] A. Tatu, F. Maas, I. Farber, E. Bertini, T. Schreck, T. Seidl, and D. Keim. Subspace Search and Visualization to Make Sense of Alternative Clusterings in High-dimensional Data. In *Proceedings of IEEE Visual Analytics Science and Technology (VAST)*, pages 63–72, 2012.

[TMG+10] M. Teßmann, S. Mohr, S. Gayetskyy, U. Hassler, R. Hanke, and G. Greiner. Automatic Determination of Fiber-length Distribution in Composite Material using 3D CT Data. *EURASIP Journal on Advances in Signal Processing*, 2010:1:1–1:9, 2010.

[Tus11] N. Tustison. Why Do Walks With Hilbert Seem To Take So Long? *Insight Journal*, 2011. http://hdl.handle.net/10380/3324 (accessed on 04.11.2019).

[TWSM+11] T. Torsney-Weir, A. Saad, T. Möller, H.-C. Hege, B. Weber, J. Verbavatz, and S. Bergner. Tuner: Principled Parameter Finding for Image Segmentation Algorithms using Visual Response Surface Exploration. *IEEE Transactions on Visualization and Computer Graphics (TVCG)*, 17(12):1892–1901, 2011.

[TWSM17] T. Torsney-Weir, M. Sedlmair, and T. Möller. Sliceplorer: 1D Slices for Multi-dimensional Continuous Functions. *Computer Graphics Forum*, 36(3):167–177, 2017.

[UMW+12] D. Ushizima, D. Morozov, G. H. Weber, A. G. C. Bianchi, J. A. Sethian, and E. W. Bethel. Augmented Topological Descriptors of Pore Networks for Material Science. *IEEE Transactions on Visualization and Computer Graphics (TVCG)*, 18(12):2041–2050, 2012.

[vWvL93] J. J. van Wijk and R. van Liere. HyperSlice: Visualization of Scalar Functions of Many Variables. In *Proceedings of the IEEE Visualization 1993 (VIS'93)*, pages 119–125, 1993.

[WAG+16] J. Weissenböck, A. Amirkhanov, E. Gröller, J. Kastner, and C. Heinzl. PorosityAnalyzer: Visual Analysis and Evaluation of Segmentation Pipelines to Determine the Porosity in Fiber-Reinforced Polymers. In *Proceedings of IEEE Visual Analytics Science and Technology (VAST)*, pages 101–110, 2016.

Die approbierte gedruckte Originalversion dieser Dissertation ist an der TU Wien Bibliothek verfügbar.
The approved original version of this doctoral thesis is available in print at TU Wien Bibliothek.
TU Bibliothek Your knowledge hub WIEN

[WB97] P. C. Wong and R. D. Bergeron. 30 Years of Multidimensional Multivariate Visualization. In *Scientific Visualization, Overviews, Methodologies, and Techniques*, pages 3–33, 1997.

[Wir07] O. Wirjadi. Survey of 3D Image Segmentation Methods. Technical Report 123, Fraunhofer-Institut für Techno- und Wirtschaftsmathematik (ITWM), Fraunhofer-Platz 1, 67663 Kaiserslautern, Germany, 2007.

[WMK13] R. T. Whitaker, M. Mirzargar, and R. M. Kirby. Contour Boxplots: A Method for Characterizing Uncertainty in Feature Sets from Simulation Ensembles. *IEEE Transactions on Visualization and Computer Graphics (TVCG)*, 19(12):2713–2722, 2013.

[YSW94] B. Yamrom, J. A. Sutliff, and A. P. Woodfield. Visualizing Polycrystalline Orientation Microstructures with Spherical Color Maps. In *Proceedings of the IEEE Visualization 1994 (VIS '94)*, pages 46–51, 1994.

[ZCQ+09] H. Zhou, W. Cui, H. Qu, Y. Wu, X. Yuan, and W. Zhuo. Splatting the Lines in Parallel Coordinates. *Computer Graphics Forum*, 28(3):759–766, 2009.

[ZK10] X. Zhao and A. Kaufman. Multi-dimensional Reduction and Transfer Function Design using Parallel Coordinates. In *Proceedings of the 8th IEEE/EG International Conference on Volume Graphics (VG'10)*, pages 69–76, 2010.

[Zwe06] C. Zweben. Composite Materials. In Myer Kutz, editor, *Mechanical Engineers' Handbook*, chapter 10. John Wiley & Sons, Inc., 2006.

Die approbierte gedruckte Originalversion dieser Dissertation ist an der TU Wien Bibliothek verfügbar.
The approved original version of this doctoral thesis is available in print at TU Wien Bibliothek.
TU WIEN Bibliothek Your knowledge hub

Die approbierte gedruckte Originalversion dieser Dissertation ist an der TU Wien Bibliothek verfügbar.
The approved original version of this doctoral thesis is available in print at TU Wien Bibliothek.

Appendix

In the following, the evaluation questionnaires of the research prototypes *FiberScout* (see Chapter 2) and *PorosityAnalyzer* (see Chapter 3) are listed.

Die approbierte gedruckte Originalversion dieser Dissertation ist an der TU Wien Bibliothek verfügbar.
The approved original version of this doctoral thesis is available in print at TU Wien Bibliothek.

FiberScout Evaluation Questionnaire

1 Introduction

This questionnaire is about the software prototype for interactive exploration and visual analysis of fibrous materials based on X-ray computed tomography (XCT) data. Your feedback will be part of a submission for the

XCT is the most promising method for non-destructive testing and fully three-dimensional characterization of composite components up to now. In this evaluation questionnaire we will focus on the visualization and advanced analysis of fiber reinforced polymers (FRP). Figure 1 shows an overview of the visualization tool. Details of the tool will be introduced in later sections.

By analyzing the fiber characteristics of FRP specific questions are coming up. We discussed with domain experts carefully and determined the following tasks, which also will be evaluated in this questionnaire:

- Task 1: Classification of fibers,
- Task 2: Visualization of fiber orientations,
- Task 3: Determination of fiber regions,
- Task 4: Visualization of regional information with the material characteristics.

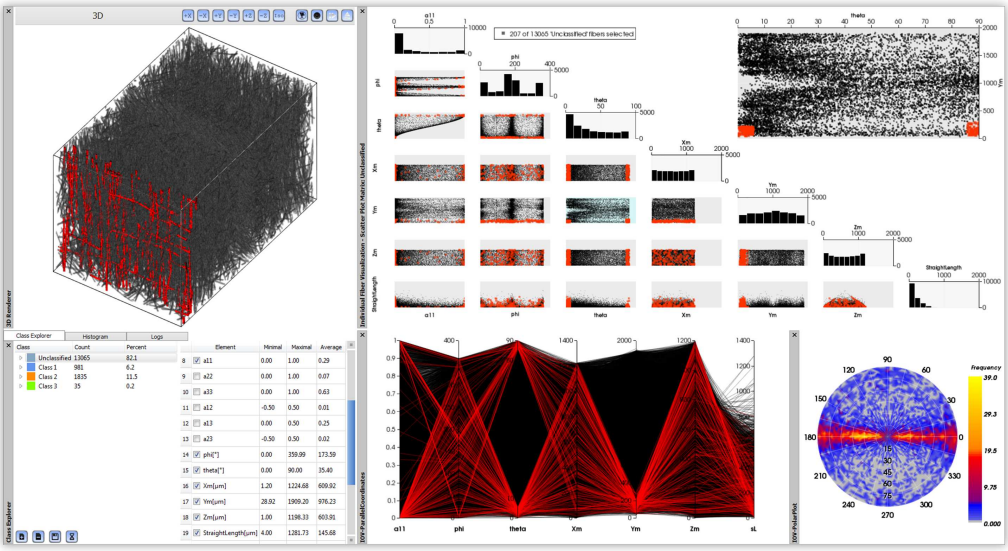

Figure 1: An overview of the visualization tool.

Die approbierte gedruckte Originalversion dieser Dissertation ist an der TU Wien Bibliothek verfügbar.
The approved original version of this doctoral thesis is available in print at TU Wien Bibliothek.
TU Bibliothek Your knowledge hub WIEN

2 General Questions

1a. How often do you work with X-ray computed tomography (XCT) data?
☐ Never ☐ Annually ☐ Monthly ☐ Weekly ☐ Daily

1b. How often do you explore XCT data using visual representations?
☐ Never ☐ Annually ☐ Monthly ☐ Weekly ☐ Daily

1c. How many years of experience do you have with XCT metrology? _____ years.

1d. Are you experienced with fiber reinforced polymers?
☐ No experience ☐ Introductory ☐ Intermediate ☐ Advanced ☐ High level

1e. How many years of experience do you have with fiber reinforced polymers? _____ years.

3 Clustering

When applying a fiber characterization pipeline (FCP) and a labeling filter to the original gray value XCT volume data (see Figure 2a) we get a label image and a csv-file with individual label identification. The corresponding fiber characteristics are given in the csv-file for each label. We then use these two datasets as input data for the visualization tool. In this section we will focus on the classification of the fibers using parallel coordinates and a scatter plot matrix.

3.1 Classification of fibers with parallel coordinates

Parallel coordinates (PC) is a visualization technique using n-dimensional geometry for the analysis of multivariate data. Unlike in the Cartesian coordinate system the axes in PC are set up parallel and equidistant to each other. A point in n-dimensional space is represented using lines crossing the n parallel axes. The position of the intersection on the ith axis corresponds to the value of the ith coordinate of the point. Finally, each multidimensional point is transformed to a polyline through the parallel axes.

In this software prototype PC are used to visualize and classify fiber characteristics. Figure 2b shows PC of 22656 fibers using the following material characteristics

- *Label* – the identification of a fiber;
- $a11$, $a22$, $a33$ – main elements of the orientation tensor of a fiber;
- $Xm[\mu m]$, $Ym[\mu m]$, $Zm[\mu m]$ – 3D Cartesian coordinates of the middle point of a fiber;
- sL $[\mu m]$ – the straight length of a fiber

as dimensional information.

The interaction technique of *brushing* and *linking* is used to explore the data set. With PC the user is able to select a range of interest for each fiber property by *brushing* through the corresponding axis (e.g., the red rectangles along the axes in Figure 2b) to define a new class. The selected fibers are then highlighted in the PC as well as in the 3D view (see Figure 2c) and in the scatter plot matrix (*linking*, see Figure 4a).

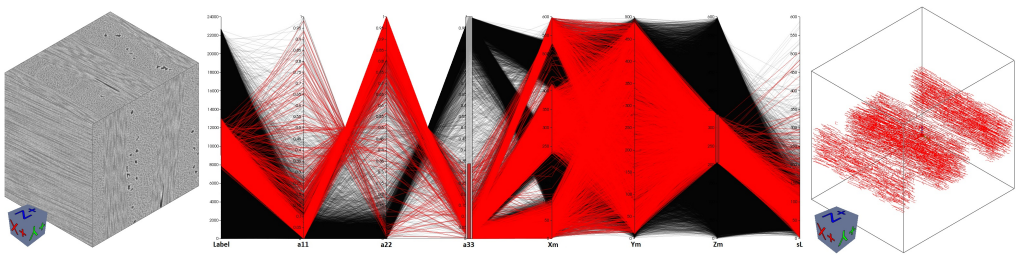

(a) (b) (c)

Figure 2: (a) 3D view of the original gray value volume image. (b) View of a parallel coordinates system. (c) View of a real-time rendering of the selected fibers.

Die approbierte gedruckte Originalversion dieser Dissertation ist an der TU Wien Bibliothek verfügbar.
The approved original version of this doctoral thesis is available in print at TU Wien Bibliothek.
TU Bibliothek WIEN Your knowledge hub

2a. How good can you identify the fiber structure in Figure 2a?
☐ poor ☐ fair ☐ average ☐ good ☐ excellent

2b. How good can you identify the fiber structure in Figure 2c?
☐ poor ☐ fair ☐ average ☐ good ☐ excellent

2c. How would you evaluate the visualization technique of *linking* and *brushing*?
☐ poor ☐ fair ☐ average ☐ good ☐ excellent

A new class will be created with the selected fibers. The user is able to specify the name and the color of the new class. The created classes are then listed in the class explorer (see Figure 3a). Additionally, the number of fibers in the class (*Count*) and the percentage of the fiber content (*Percent*) are calculated as header information. An element explorer that contains the *Minimal*, *Maximal* and *Average* value of all fiber characteristics is also computed for each class.

According to fiber orientation and the spatial position in x-direction of the fibers we manually defined 5 classes of fibers (Figure 3a). Figure 3b represents extracted statistical information from the element explorer of the fiber characteristics of *Class* 4 highlighted in Figure 3a. By clicking on a *Label* or a *Class* in the class explorer the user is able to visualize a single fiber or a cluster of fibers (Figure 3c) in the 3D view as well as in PC and in the scatter plot matrix. Figure 3d shows the 3D view of a direct volume rendering based on color transfer function of all the manually defined classes (Figure 3a).

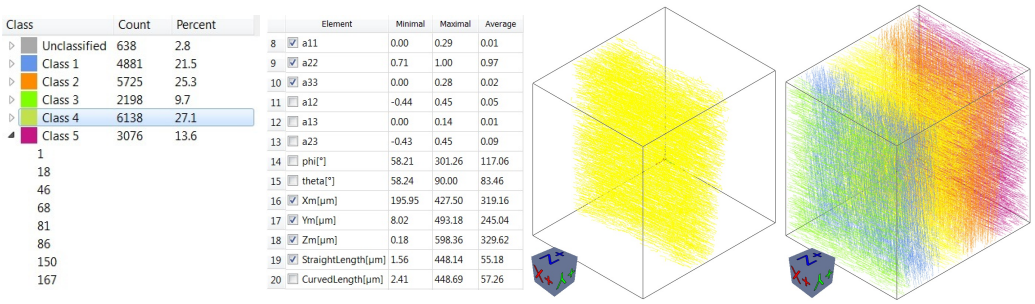

Class	Count	Percent
Unclassified	638	2.8
Class 1	4881	21.5
Class 2	5725	25.3
Class 3	2198	9.7
Class 4	6138	27.1
Class 5	3076	13.6
1		
18		
46		
68		
81		
86		
150		
167		

	Element	Minimal	Maximal	Average
8	a11	0.00	0.29	0.01
9	a22	0.71	1.00	0.97
10	a33	0.00	0.28	0.02
11	a12	-0.44	0.45	0.05
12	a13	0.00	0.14	0.01
13	a23	-0.43	0.45	0.09
14	phi[°]	58.21	301.26	117.06
15	theta[°]	58.24	90.00	83.46
16	Xm[µm]	195.95	427.50	319.16
17	Ym[µm]	8.02	493.18	245.04
18	Zm[µm]	0.18	598.36	329.62
19	StraightLength[µm]	1.56	448.14	55.18
20	CurvedLength[µm]	2.41	448.69	57.26

(a) (b) (c) (d)

Figure 3: (a) Meta information of the manually classified classes. (b) Extracted element table of the fiber characteristics of *Class* 4. (c) Direct volume rendering of the *Class* 4. (d) Direct volume rendering of all classes.

3a. How useful is the meta information in Figure 3a?
not at all ☐—☐—☐—☐—☐ very useful

3b. How useful is the statistical information in Figure 3b?
not at all ☐—☐—☐—☐—☐ very useful

3c. Can you identify the fiber classes in Figure 3d?
☐ poor ☐ fair ☐ average ☐ good ☐ excellent

3d. Remarks concerning classification with parallel coordinates (benefits/drawbacks):

_____

_____

_____

_____

3.2 Classification of fibers with scatter plot matrix

In addition to parallel coordinates we use a scatter plot matrix (SPM) to visualize and reveal relationships such as dependencies, patterns and even outliers among all of the fiber characteristics. Further the SPM serves as a

Die approbierte gedruckte Originalversion dieser Dissertation ist an der TU Wien Bibliothek verfügbar.
The approved original version of this doctoral thesis is available in print at TU Wien Bibliothek.
TU Bibliothek Your knowledge hub WIEN

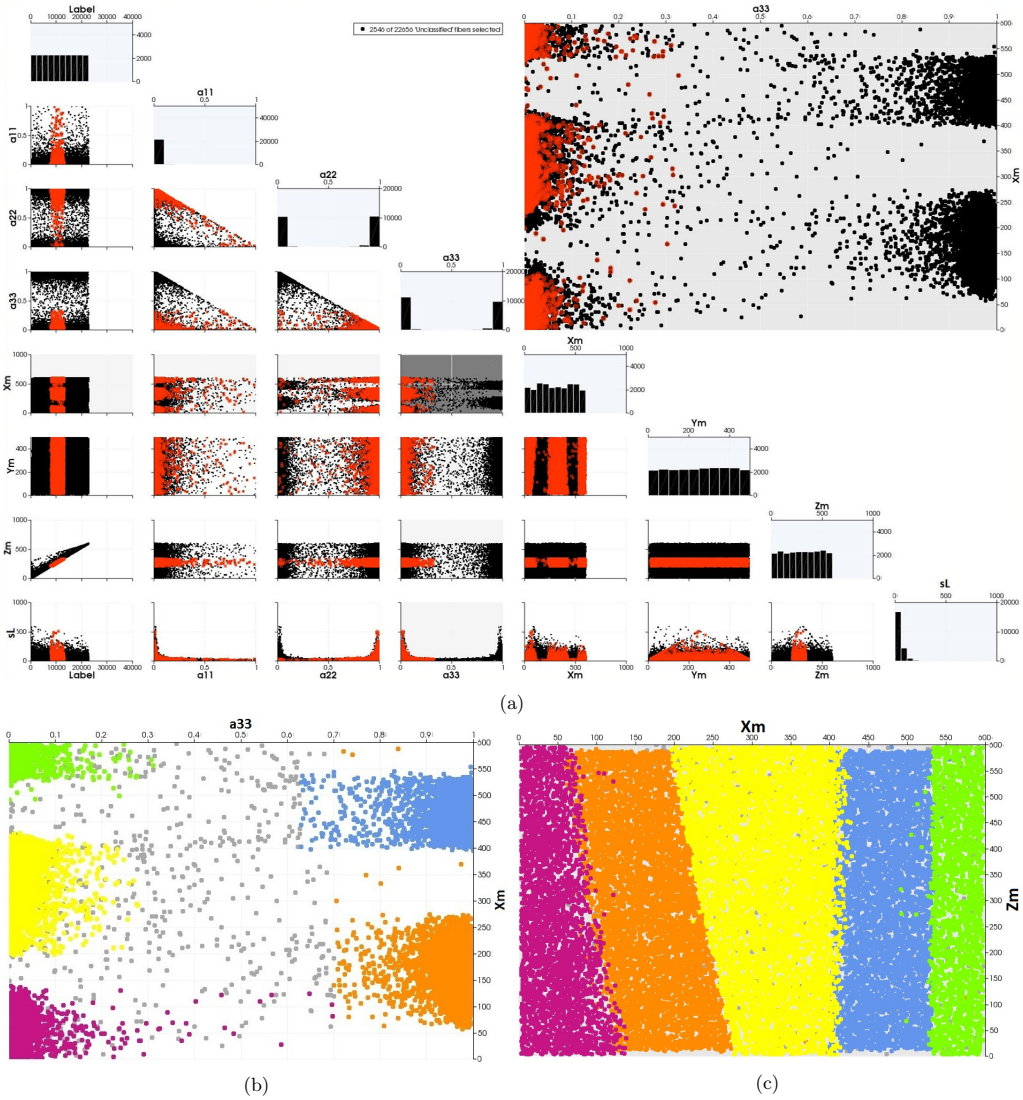

Figure 4: (a) View of a scatter plot matrix with the interaction technique *brushing* and *linking*. (b) Scatter plot of the fiber properties $a33$ and Xm. The points are color coded according to the clusters in Figure 3a. (c) Scatter plot of the fiber properties Xm and Zm color coded according to the clusters in Figure 3a.

refinement of the rough PC selection.

A SPM consists of $n(n-1)/2$ scatter plots organized as a matrix where only the part below the main diagonal is filled to avoid redundancy. A Histogram of each fiber characteristic is shown in the main diagonal. Under this main diagonal a scatter plot is drawn for each pair of the characteristics. In the upper right corner, an enlarged view of the selected scatter plot is displayed. Figure 4a shows a SPM with the same fiber characteristics as in Figure 2b. The selected small scatter plot under the main diagonal is marked in gray.

In the enlarged view and in the small charts it is possible to select the black points by drawing rectangles which will turn them into red ones (*brushing*). The selections done in the enlarged view will be applied to all other scatter plots, the PC and the 3D view (*linking*). The enlarged view in Figure 4a shows the scatter plot of

Die approbierte gedruckte Originalversion dieser Dissertation ist an der TU Wien Bibliothek verfügbar.
The approved original version of this doctoral thesis is available in print at TU Wien Bibliothek.
TU Bibliothek Your knowledge hub WIEN

the fiber characteristics: $a33$ - the orientation tensor of a fiber in z-direction and Xm - the x coordinate of the fiber middle point. The red points represent the currently selected fibers in PC. Figure 4b, 4c display the same data color coded to the manually defined classes presented in Figure 3a.

4a. Can you identify fiber classes in Figure 4a?
☐ poor ☐ fair ☐ average ☐ good ☐ excellent

4b. Can you identify fiber classes in Figure 4b?
☐ poor ☐ fair ☐ average ☐ good ☐ excellent

4c. Can you identify outliers in Figure 4b?
☐ poor ☐ fair ☐ average ☐ good ☐ excellent

4d. Can you identify dependencies between Figure 4b and Figure 4c?
☐ poor ☐ fair ☐ average ☐ good ☐ excellent

4e. How would you evaluate the method of clustering fibers with parallel coordinates?
☐ poor ☐ fair ☐ average ☐ good ☐ excellent

4f. How would you evaluate the method of clustering fibers with scatter plot matrix?
☐ poor ☐ fair ☐ average ☐ good ☐ excellent

4g. Remarks concerning classification with scatter plot matrix (benefits/drawbacks):

_____

_____

_____

_____

4 Fiber Orientation Distribution

To present the fiber orientation, spherical coordinates are used. Figure 5a shows the construction of the orientations in the Cartesian coordinates System. θ represents the polar angle measured from the zenith z-direction. The azimuth angle ϕ passes through the origin in xy-plane and is measured from the x-direction. Because of the symmetry it is possible to depict all fiber orientations on a half sphere by specifying $\theta \in [0, \pi/2]$ and $\phi \in [0, 2\pi)$. We then discretize the northern half sphere with a resolution of 3 degrees and compute the frequency for each discretized direction, which builds up the fiber orientation distribution (FOD). The azimuthal projection is later used to generate the 2D image of the FOD. Figure 5b shows the global FOD of the original data set. The annotations around the outer circle represent the azimuthal angle and the annotations inside represent the polar angle. In addition to the global FOD, an FOD may be computed for each manually defined class. For example Figure 5c displays the FOD of *Class* 4 in Figure 3a.

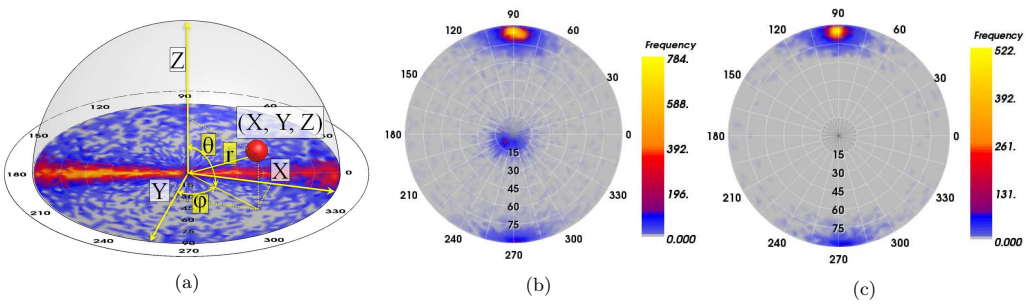

(a) (b) (c)

Figure 5: (a) Construction of the fiber orientation. (b) Global fiber orientation distribution (FOD) of all fibers. (c) FOD of *Class*4 in Figure 3a.

5a. Can you identify the main fiber orientation in Figure 5b?
☐ poor ☐ fair ☐ average ☐ good ☐ excellent

5b. Can you identify the main fiber orientation of *Class* 4 in Figure 5c?
☐ poor ☐ fair ☐ average ☐ good ☐ excellent

Die approbierte gedruckte Originalversion dieser Dissertation ist an der TU Wien Bibliothek verfügbar.
The approved original version of this doctoral thesis is available in print at TU Wien Bibliothek.
TU Bibliothek WIEN Your knowledge hub

5c. How would you evaluate the method of FOD?
☐ poor ☐ fair ☐ average ☐ good ☐ excellent

Besides the fiber orientation distribution, the visualization of the real fiber orientations in 3D is also implemented. We developed a spherical color map (see Figure 6a) that maps the 3D space orientation in every direction. Figure 6b shows you the direct volume rendering of the fibers according to fiber orientation color coded according to the spherical color map.

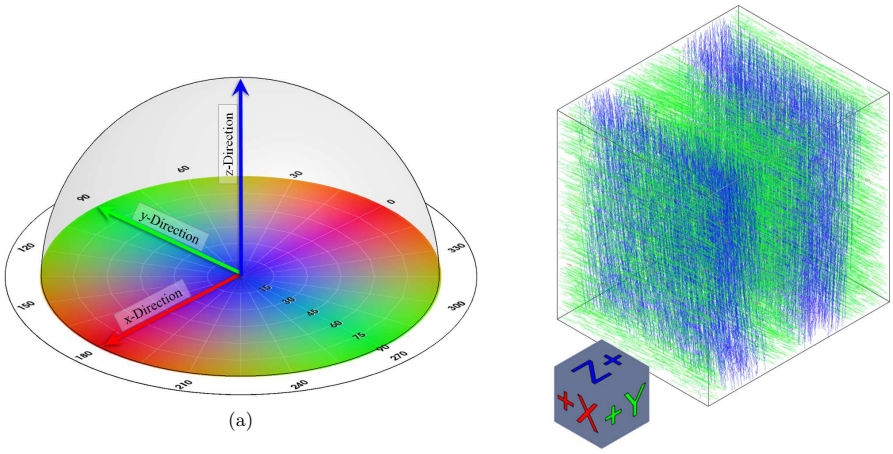

(a) (b)

Figure 6: (a) The spherical color map. (b) Direct volume rendering of the fibers according to fiber orientation color coded with the spherical color map.

6a. Can you identify the color coding of the spherical color map in Figure 6a?
☐ poor ☐ fair ☐ average ☐ good ☐ excellent

6b. Can you identify fiber orientations in Figure 6b based on the spherical color map?
☐ poor ☐ fair ☐ average ☐ good ☐ excellent

6c. Can you identify the fiber classes in Figure 6b?
☐ poor ☐ fair ☐ average ☐ good ☐ excellent

6d. Remarks concerning to fiber orientation distribution (benefits/drawbacks):

_____

_____

_____

_____

Die approbierte gedruckte Originalversion dieser Dissertation ist an der TU Wien Bibliothek verfügbar.
The approved original version of this doctoral thesis is available in print at TU Wien Bibliothek.
TU Bibliothek Your knowledge hub WIEN

5 Blob Visualization

Groups of fibers with similar characteristics - fiber classes classified with parallel coordinates and scatter plot matrix are visualized in the form of one blob or more. A blob is represented as a contoured surface surrounding all fibers of a class. The contoured surface provides an overview of the cluster and shows its spatial position in the data. If two or more blobs are drawn together it is possible to separate the clusters from each other. Figure 2a shows the original gray value volume data. Figure 7b shows the blobs according to the defined classes.

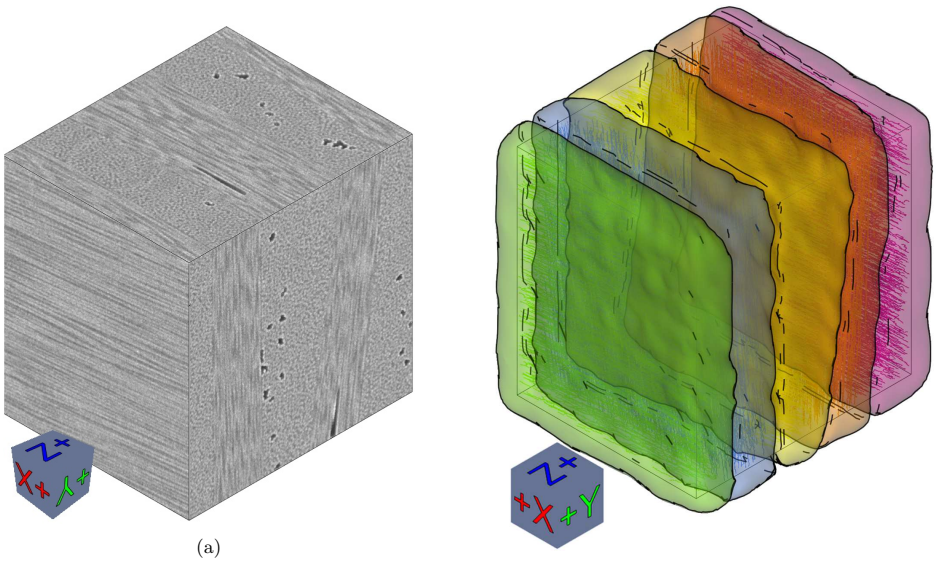

(a) (b)

Figure 7: (a)Original gray value volume data. (b) Blob visualization of the fiber classes determined by fiber orientation.

7a. Can you identify the fiber classes of Figure 7b in comparison with Figure 7a?
☐ poor ☐ fair ☐ average ☐ good ☐ excellent

7b. Remarks concerning blob visualization (benefits/drawbacks):

_____

_____

_____

_____

Die approbierte gedruckte Originalversion dieser Dissertation ist an der TU Wien Bibliothek verfügbar.
The approved original version of this doctoral thesis is available in print at TU Wien Bibliothek.
TU WIEN Bibliothek Your knowledge hub

6 Metadata Visualization

A meta-image was generated using regional information of material characteristics (fiber characteristics). We first discretize the original dataset with a user specified discretization-factor to larger cells. The average of the selected fiber characteristics is calculated for each cell for all fibers crossing through this cell. These average values are then used to generate the meta-image.

In our example the voxel size of the original dataset is $1\mu m$; the cell size we defined for the regional information is 30µm using a discretization-factor of 40. Figure 8a shows the 3D view of a meta-image overlaid on the original gray value image and color coded according to fiber orientations. Blue represents the y-direction and orange the z-direction. Figure 8b displays a slice view of the meta-image with the fiber characteristic θ being in the yz-plane.

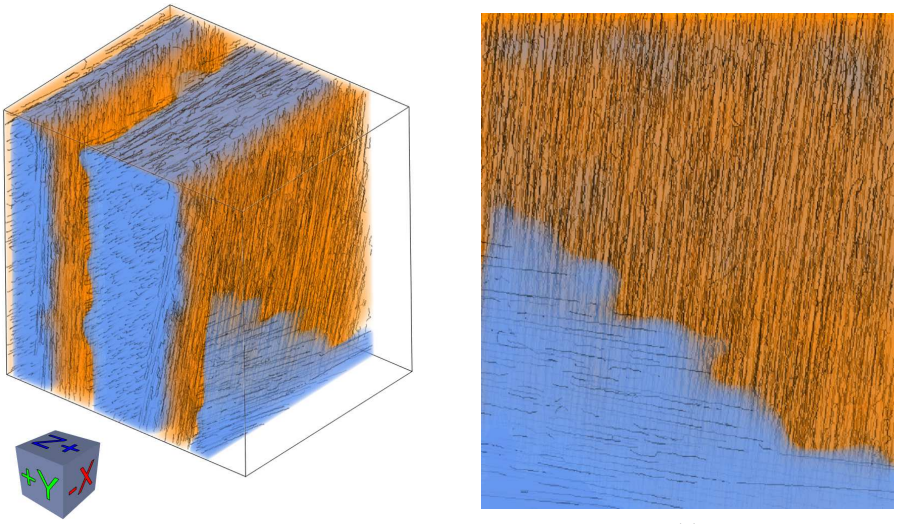

(a) (b)

Figure 8: Views of meta-image color coded according to fiber orientation. Blue represents the y-direction and orange the z-direction. (a) 3D view of the meta-volume. (b) A slice view of the meta-volume with the fiber characteristics θ being in the yz-plane.

8a. Can you identify fiber classes in Figure 8a?
☐ poor ☐ fair ☐ average ☐ good ☐ excellent

8b. Can you identify fiber orientations in Figure 8a?
☐ poor ☐ fair ☐ average ☐ good ☐ excellent

8c. Can you identify fiber orientations in Figure 8b?
☐ poor ☐ fair ☐ average ☐ good ☐ excellent

8g. Remarks concerning metadata visualization (benefits/drawbacks):

_____

_____

_____

_____

Die approbierte gedruckte Originalversion dieser Dissertation ist an der TU Wien Bibliothek verfügbar.
The approved original version of this doctoral thesis is available in print at TU Wien Bibliothek.
TU Bibliothek WIEN Your knowledge hub

PorosityAnalyzer - Evaluation Questionnaire

PorosityAnalyzer - A tool for visual analysis and evaluation of segmentation pipelines to determine the porosity in fiber-reinforced polymers

Introduction

This questionnaire aims to evaluate a software prototype for the visual analysis and exploration of segmentation pipelines to determine the porosity in fiber-reinforced polymers (FRPs).

We present several visualizations concepts to explore, analyze and evaluate many different segmentation pipelines (datasets and segmentation algorithms) according to porosity, algorithm run-time, algorithm parameters etc..
Furthermore, we will ask you to perform some simple analysis tasks using the visualizations. Please give us a feedback on these visualizations techniques.

Thanks in advance!

NOTE: there will be video materials demonstrating some interactive concepts. If there is no full-screen button on your embedded video, please open it in YouTube or use the zoom-in functionality of your browser (CTRL + or CTRL-).
If some images seem small to you, please zoom-in in your browser (CTRL + or CTRL-).

General Questions

Questions to determine your experience level in the field of X-ray computed tomography (XCT)

Your name:

Your affiliation:

How often do you work with XCT data?

- Daily
- Weekly
- Monthly
- Annually
- Never

How often do you explore XCT data using visual representations?

- Daily
- Weekly
- Monthly
- Annually
- Never

Die approbierte gedruckte Originalversion dieser Dissertation ist an der TU Wien Bibliothek verfügbar.
The approved original version of this doctoral thesis is available in print at TU Wien Bibliothek.
TU Bibliothek Your knowledge hub WIEN

How many years of experience do you have with XCT metrology?
(in years)

How experienced are you with fiber-reinforced polymers?

- High level
- Advanced
- Intermediate
- Introductory
- No experience

How many years of experience do you have with fiber-reinforced polymers?
(in years)

How experienced are you with porosity determination of fiber-reinforced polymers?

- High level
- Advanced
- Intermediate
- Introductory
- No experience

How many years of experience do you have in porosity determination of fiber-reinforced polymers?
(in years)

Die approbierte gedruckte Originalversion dieser Dissertation ist an der TU Wien Bibliothek verfügbar.
The approved original version of this doctoral thesis is available in print at TU Wien Bibliothek.
TU Bibliothek Your knowledge hub WIEN

PorosityAnalyzer - Evaluation Questionnaire

Computation Module - General Description

The computation provides a graphical user interface (see Figure 1) for chaining different segmentation pipeline filters within the user-defined parameter spaces per drag and drop. The created segmentation pipelines are batch processed. For every parameter combination within a segmentation pipeline a segmentation result is generated. In the background, this module manages the data storing of the calculated results and takes care of the proper filter linkage by setting the necessary intermediate connection steps (e.g., correct input/output data types). In addition, a log view keeps the user up to date of the current status (e.g., running batch progress, errors).

Computation Module - Dataset/Filter Drag & Drop

To set up a batch computation, the user has to specify the computer name, the input folder of the datasets, the output folder of the computation results, and the path of the batch computation settings file, which contains all the set up pipelines.

To set up a segmentation pipeline, a dataset icon from the datasets section has to be selected and positioned per drag and drop onto the first slot of the pipeline. This drag and drop process has to be repeated for the desired filters. For each icon we provide additional information with tool tips.

This described process is shown in Video 1.

Die approbierte gedruckte Originalversion dieser Dissertation ist an der TU Wien Bibliothek verfügbar.
The approved original version of this doctoral thesis is available in print at TU Wien Bibliothek.
TU Bibliothek Your knowledge hub WIEN

Figure 1: Graphical User Interface of the Computation Module.

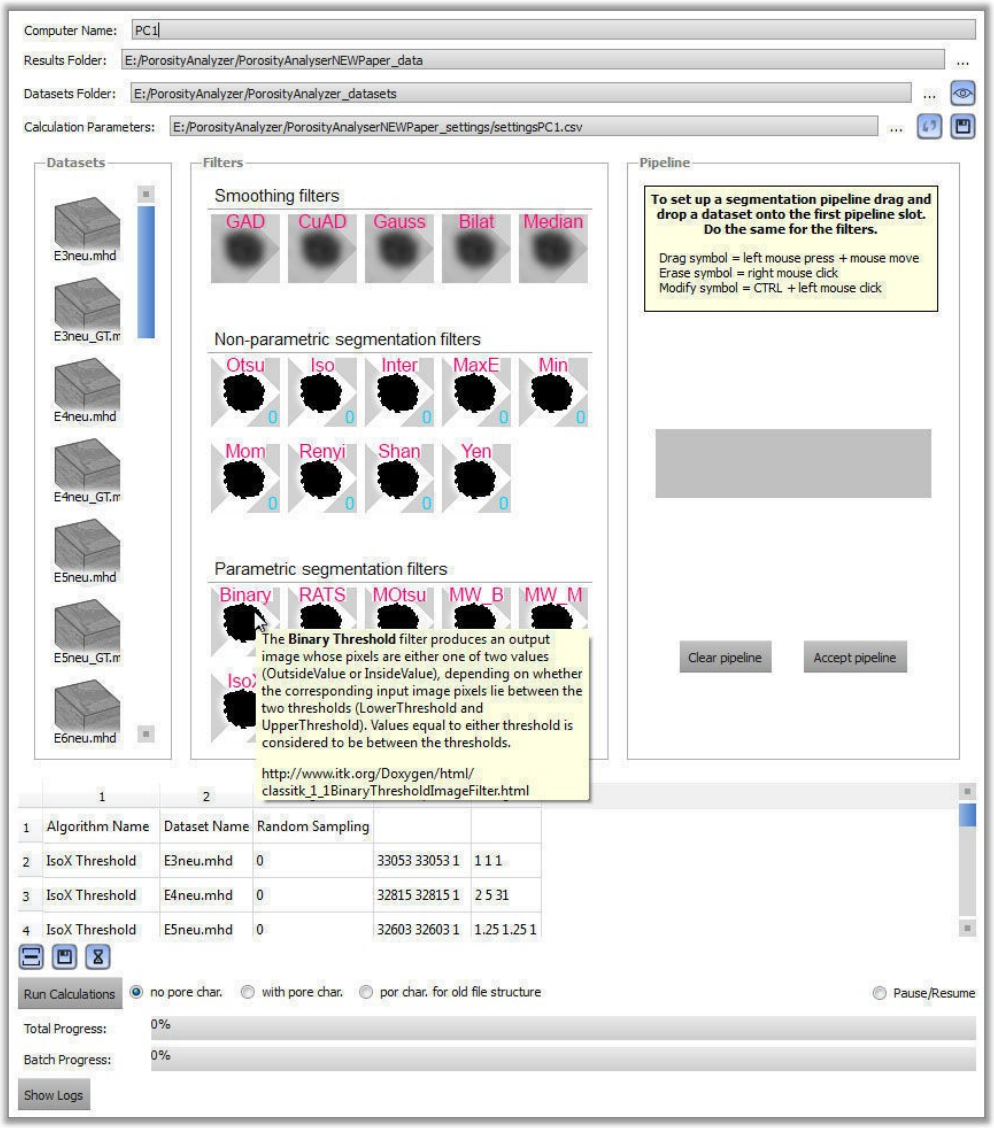

Die approbierte gedruckte Originalversion dieser Dissertation ist an der TU Wien Bibliothek verfügbar.
The approved original version of this doctoral thesis is available in print at TU Wien Bibliothek.
TU Bibliothek WIEN Your knowledge hub

Video 1: Computation Module - Dataset/Filter Drag & Drop

PA CompModule DragDrop 1

NOTE: there will be video materials demonstrating some interactive concepts. If there is no full-screen button on your embedded video, please open it in YouTube or use the zoom-in functionality of your browser

How would you evaluate the dataset/filter icon drag and drop concept to set up a segmentation pipeline?

	1	2	3	4	5	
poor	○	○	○	○	○	excellent

How intuitive is the drag and drop concept to chain filters together?

	1	2	3	4	5	
poor	○	○	○	○	○	excellent

How useful is the tooltip information when hovering over a dataset/filter icon?

	1	2	3	4	5	
poor	○	○	○	○	○	excellent

Remarks concerning the dataset/filter drag & drop (benefits/drawbacks):

Die approbierte gedruckte Originalversion dieser Dissertation ist an der TU Wien Bibliothek verfügbar.
The approved original version of this doctoral thesis is available in print at TU Wien Bibliothek.
TU Bibliothek Your knowledge hub WIEN

PorosityAnalyzer - Evaluation Questionnaire

Computation Module - Parameter Space Dialog

As shown before in Video 1 a segmentation pipeline is set up by using the concept of drag and drop.

To define the parameter space sampling of each filter, the user has to press CTRL + left mouse button on the filter icon in the pipeline. Then the parameter space dialog opens (see Figure 2) and the parameter space sampling and the individual parameter ranges (start, end) and the number of samples must be specified. Thereby, additional information about the dataset and the current filter are provided. If all the parameters for all the filters are set, the created pipeline can be added to the segmentation pipeline batch table.

This described process is shown in Video 2.

Figure 2: Parameter Space Dialog of the Computation Module.

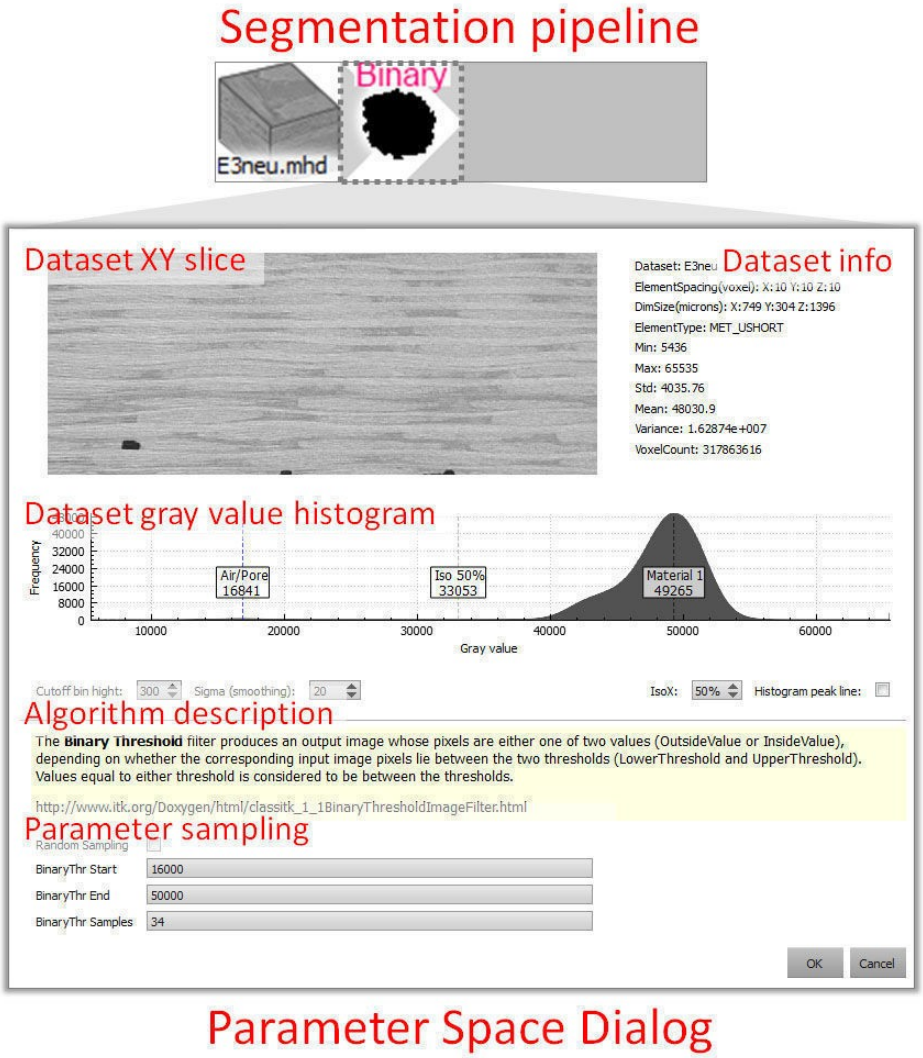

Die approbierte gedruckte Originalversion dieser Dissertation ist an der TU Wien Bibliothek verfügbar.
The approved original version of this doctoral thesis is available in print at TU Wien Bibliothek.
TU Bibliothek Your knowledge hub WIEN

Video 2: Computation Module - Parameter Space Dialog

PA CompModule ParamSpaceDialog

NOTE: there will be video materials demonstrating some interactive concepts. If there is no full-screen button on your embedded video, please open it in YouTube or use the zoom-in functionality of your browser

How intuitive/convenient is it to open the parameter space dialog with CTRL + left mouse click on the filter icon in the pipeline?

1 2 3 4 5

poor ○ ○ ○ ○ ○ excellent

How intuitive/convenient is it to define the parameter ranges, sampling etc.?

1 2 3 4 5

poor ○ ○ ○ ○ ○ excellent

How useful are the information on the dataset and current filter provided by the parameter space dialog?

1 2 3 4 5

poor ○ ○ ○ ○ ○ excellent

How intuitive/convenient is the way to add an accepted pipeline to the batch table (see Video 2, minute 0:30)?

1 2 3 4 5

poor ○ ○ ○ ○ ○ excellent

Remarks concerning the parameter space dialog (benefits/drawbacks):

Die approbierte gedruckte Originalversion dieser Dissertation ist an der TU Wien Bibliothek verfügbar.
The approved original version of this doctoral thesis is available in print at TU Wien Bibliothek.
TU Bibliothek Your knowledge hub WIEN

PorosityAnalyzer - Evaluation Questionnaire

Computation Module - Segmentation Pipeline Batch Table

As shown before in Video 2 (minute 0:30) an accepted segmentation pipeline is added to the batch table (see Figure 3). This table gives an overview of the different segmentation pipelines (filter chain, dataset, parameter ranges) which will be processed.

Once a row is added to the batch table it can be edited or removed (via context menu short cut or buttons).

Figure 3: Batch Table of the Computation Module.

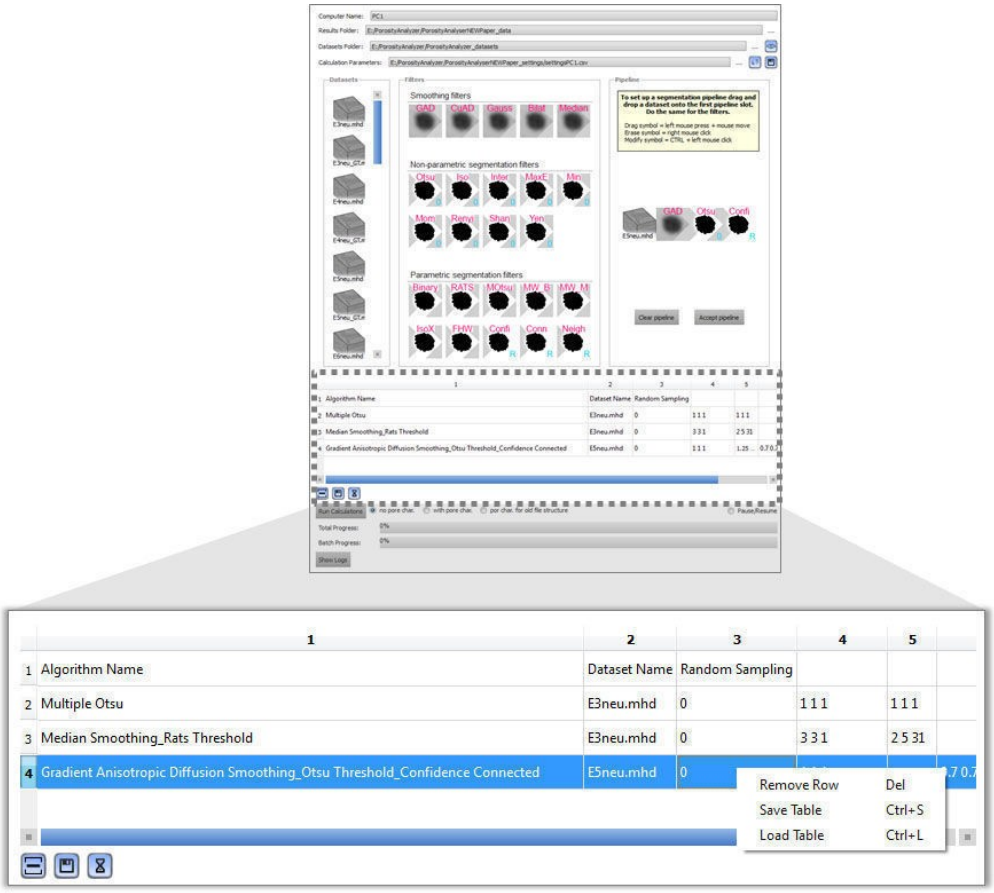

How would you evaluate the batch table for managing the segmentation pipelines?

1 2 3 4 5

poor ○ ○ ○ ○ ○ excellent

Remarks concerning the batch table (benefits/drawbacks):

Die approbierte gedruckte Originalversion dieser Dissertation ist an der TU Wien Bibliothek verfügbar.
The approved original version of this doctoral thesis is available in print at TU Wien Bibliothek.
TU Bibliothek WIEN Your knowledge hub

PorosityAnalyzer - Evaluation Questionnaire

Analysis Module - General Description

The analysis module provides navigation and analysis methods for vast amounts of data generated by applying multiple segmentation pipelines with varying presets to a set of different datasets. The overall purpose of this module is to provide functionality needed by the domain experts to efficiently and conveniently perform their analysis tasks. Therefore, we provide overview visualizations, visualizations for parameter selection and trade-off analysis and comparative visualizations.

Analysis Module - Pipeline/Dataset Matrix Overview Visualization (Deviations)

The pipeline/dataset matrix overview visualization in Figure 4 color-codes the porosity deviation in % of a segmentation pipeline (median of all the results) to a reference. The reference is provided by the user.

The rows show the individual datasets, the columns show the used segmentation pipelines (segmentation algorithms).

Figure 4: Deviation Matrix Overview Visualization

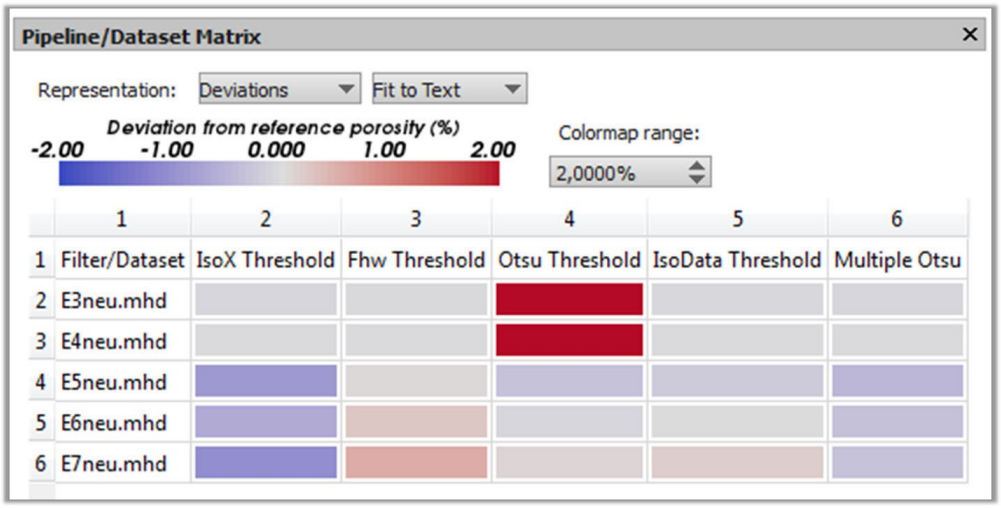

Which segmentation pipeline (algorithm) shows the minimum deviation to the reference for all the datasets?

- ○ IsoX Threshold
- ○ Fhw Threshold
- ○ Otsu Threshold
- ○ IsoData Threshold
- ○ Multiple Otsu

Die approbierte gedruckte Originalversion dieser Dissertation ist an der TU Wien Bibliothek verfügbar.
The approved original version of this doctoral thesis is available in print at TU Wien Bibliothek.
TU Bibliothek WIEN Your knowledge hub

How useful is the deviation matrix overview visualization?

1 2 3 4 5

poor ○ ○ ○ ○ ○ excellent

Remarks concerning the deviation matrix overview visualization (benefits/drawbacks):

Analysis Module - Pipeline/Dataset Matrix Overview Visualization (Box Plots)

The pipeline/dataset matrix overview visualization in Figure 6 shows a box plot for the results of a segmentation pipeline. The X-axis shows the porosity in %. The rows show the individual datasets, the columns show the used segmentation pipelines (segmentation algorithms).

Figure 5 clarifies the box plot representation.

NOTE: If some images seem small to you, please zoom-in in your browser (CTRL+ or CTRL-) or do a right-click on the image and open it in a new tab.

Figure 5: Box Plot Legend

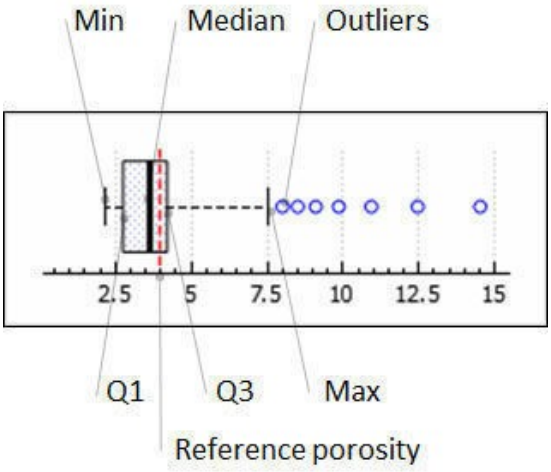

Die approbierte gedruckte Originalversion dieser Dissertation ist an der TU Wien Bibliothek verfügbar.
The approved original version of this doctoral thesis is available in print at TU Wien Bibliothek.
TU Bibliothek WIEN Your knowledge hub

Figure 6: Box Plot Matrix Overview Visualization

Same pipeline/dataset data in both views, but right view shows zoomed in data.

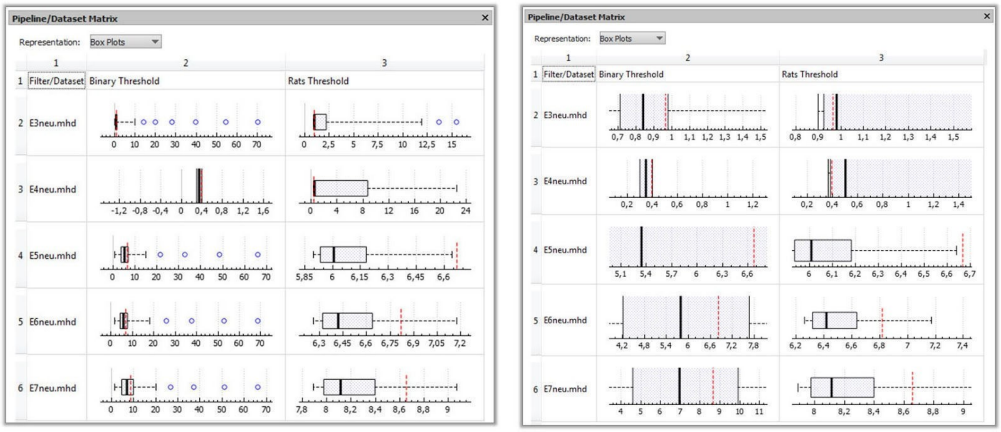

Which segmentation pipeline performs closer to the reference (red dotted line) for all the datasets?

- ◯ Binary Threshold
- ◯ Rats Threshold

How useful is the box plot matrix overview visualization?

	1	2	3	4	5	
poor	◯	◯	◯	◯	◯	excellent

Remarks concerning the box plot matrix overview visualization (benefits/drawbacks):

Analysis Module - Pipeline/Dataset Matrix Overview Visualization (Histograms)

The pipeline/dataset matrix overview visualization in Figure 7 shows the histogram generated from the results of a segmentation pipeline (frequencies of segmentation results with the same porosity in %).

The rows show the individual datasets, the columns show the used segmentation pipelines (segmentation algorithms).

Die approbierte gedruckte Originalversion dieser Dissertation ist an der TU Wien Bibliothek verfügbar.
The approved original version of this doctoral thesis is available in print at TU Wien Bibliothek.
TU Bibliothek Your knowledge hub WIEN

Figure 7: Histogram Matrix Overview Visualization

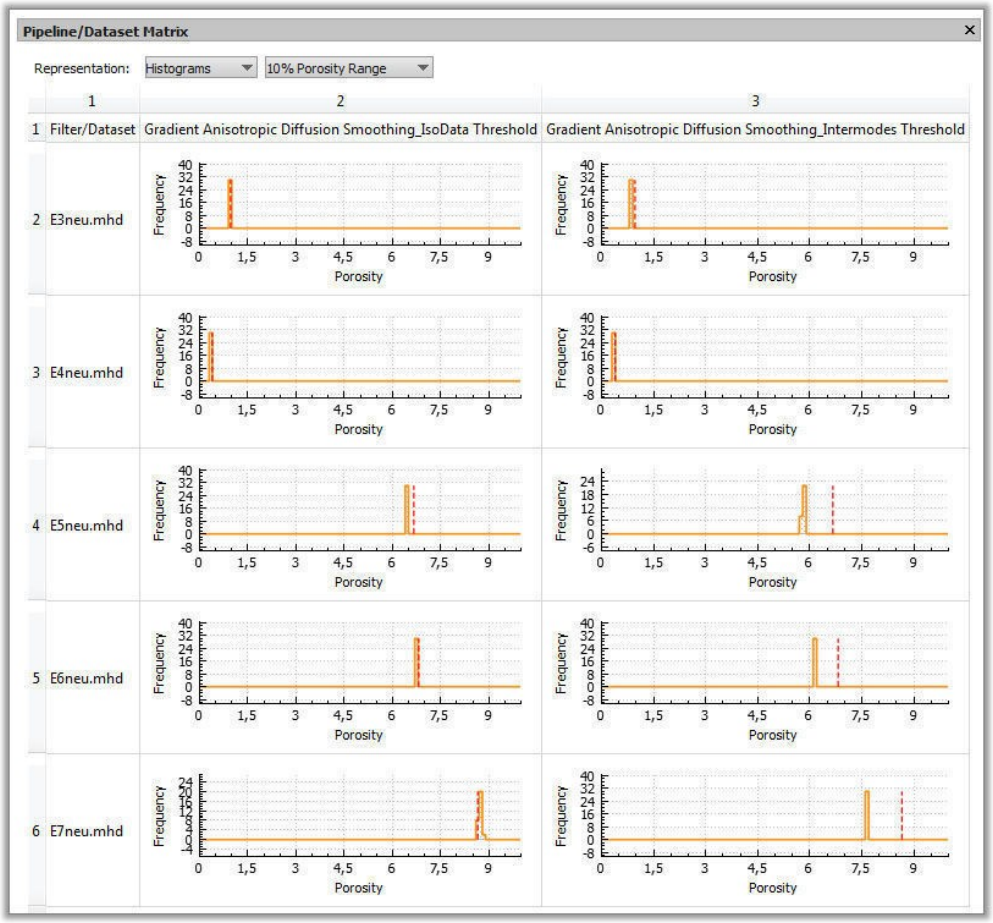

Which segmentation pipeline performs closer to the reference (red dotted line) for all the datasets?

- ◯ Gradient Anisotropic Diffusion Smoothing_IsoData Threshold
- ◯ Gradient Anisotropic Diffusion Smoothing_Intermodes Threshold

How useful is the histogram matrix overview visualization?

1 2 3 4 5

poor ◯ ◯ ◯ ◯ ◯ excellent

Remarks concerning the histogram matrix overview visualization (benefits/drawbacks):

Die approbierte gedruckte Originalversion dieser Dissertation ist an der TU Wien Bibliothek verfügbar.
The approved original version of this doctoral thesis is available in print at TU Wien Bibliothek.
TU Bibliothek Your knowledge hub WIEN

PorosityAnalyzer - Evaluation Questionnaire

Analysis Module - Parameter Range Slider

Consider you have chosen a pipeline-dataset combination (pipeline/algorithm: RATS Threshold, dataset: E4neu with ~0.4% porosity) from one of the overview visualizations (deviations, box plots, histograms) before, which you want to analyse in more detail. Therefore, we provide the parameter range slider (PRS) widget (see Figure 8) which allows finding the right parameters of a pipeline in order to get reasonable segmentation results and exploring the sensitivity of the input parameters to the output parameter (porosity).

By setting two handles one the X-axis of each slider (diagram) the corresponding pipeline's input parameter is selected by choosing from the output histogram (porosity frequencies). The selection is simultaniousley forwarded to the scatter plot matrix (will be explained on the next page).

Video 3 shows the functionality of the PRS widget.

Video 3: Parameter Range Slider

PA VisModule PRS

NOTE: there will be video materials demonstrating some interactive concepts. If there is no full-screen button on your embedded video, please open it in YouTube or use the zoom-in functionality of your browser

Die approbierte gedruckte Originalversion dieser Dissertation ist an der TU Wien Bibliothek verfügbar.
The approved original version of this doctoral thesis is available in print at TU Wien Bibliothek.
TU Bibliothek Your knowledge hub WIEN

Figure 8: Parameter Range Slider Widget

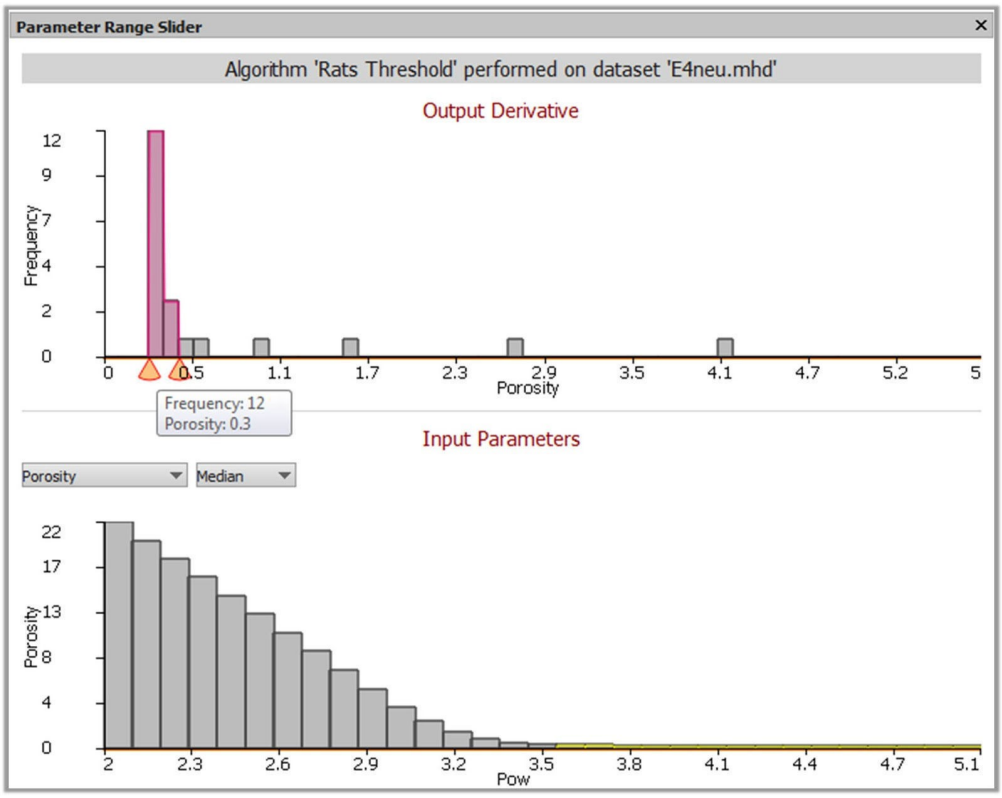

Figure 8 shows the PRS widget for the pipeline/algorithm 'RATS Threshold' and the dataset E4neu.mhd which has ~0.4% porosity (reference method). Two handles are set between the two highest histogram bins. The first bin (0.2-0.3%) contains 12 segmentations, the second (0.3-0.4%) 3 segmentations. Which 'Pow' values (input parameters) correspond to the selected porosity range (0.2-0.4%)?

- ○ 2 - 2.3
- ○ 2 - 3.5
- ○ 3.6 - 5.0
- ○ 3

How useful is the porosity range slider widget?

	1	2	3	4	5	
poor	○	○	○	○	○	excellent

Remarks concerning the PRS widget (benefits/drawbacks):

Die approbierte gedruckte Originalversion dieser Dissertation ist an der TU Wien Bibliothek verfügbar.
The approved original version of this doctoral thesis is available in print at TU Wien Bibliothek.
TU Bibliothek WIEN Your knowledge hub

PorosityAnalyzer - Evaluation Questionnaire

Analysis Module - Scatter Plot Matrix (SPLOM)

The scatter plot matrix (SPLOM) visualizes all the parameters of each run including input and output parameters of the segmentation pipeline like run time, porosity value (in %), deviation from the reference porosity (in %) and the index of the dataset. By using the SPLOM (see Figure 9) the user can select a subset of pipeline runs by drawing an arbitrary polygon in one of the scatter plots. The SPLOM allows selecting different segmentations according to their specific parameters (e.g., porosity, run-time) and performing trade-off analyses. The black colored selections done in the SPLOM can be managed and organized using the selections view.

Analysis Module - SPLOM Parameter Selection

Figure 9: Scatter Plot Matrix - Parameter Selection

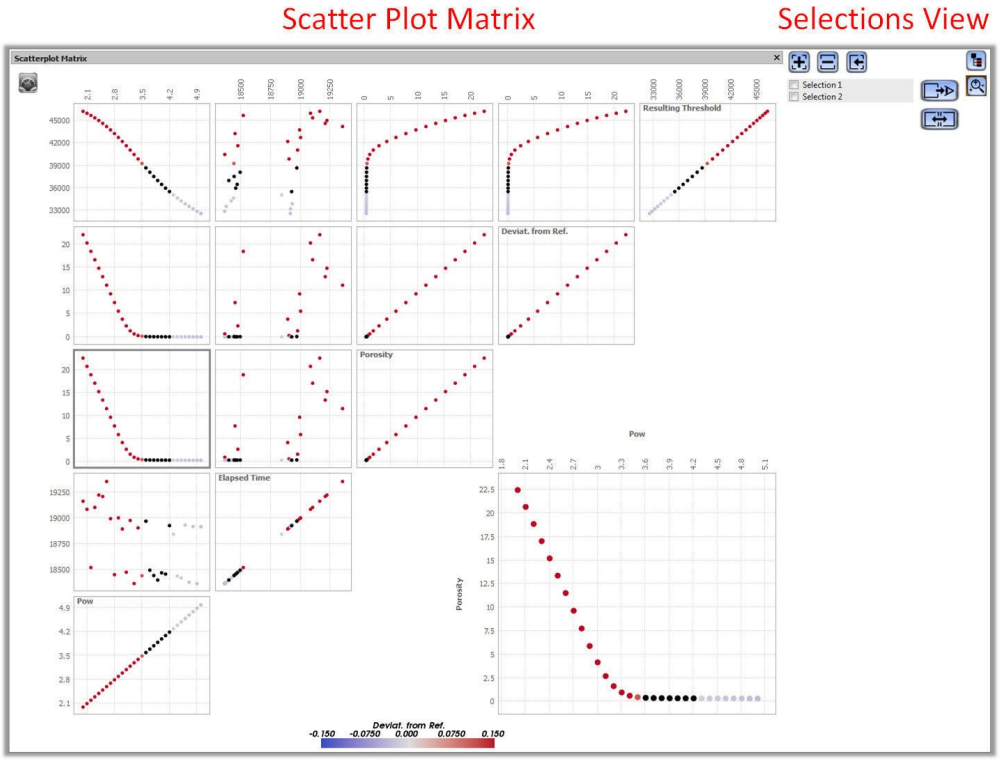

In Figure 9 the big scatter plot (bottom right) shows the resulting porosities (in %) for the different 'Pow' values (of the RATS pipeline/algorithm on dataset E4neu). 'Pow' values from 3.6 to 4.2 are selected. Can you identify the approximate range of the corresponding 'Resulting Threshold' from the scatter plot matrix?

- ○ 18500 - 19000
- ○ -0.0097 - 0.045
- ○ 35471 - 38643

Die approbierte gedruckte Originalversion dieser Dissertation ist an der TU Wien Bibliothek verfügbar.
The approved original version of this doctoral thesis is available in print at TU Wien Bibliothek.
TU Bibliothek Your knowledge hub WIEN

Analysis Module - SPLOM Trade-Off Analysis

The SPLOM allows performing trade-off analysis. Video 4 shows a RATS pipeline/algorithm trade-off analysis for suitable 'Pow' parameters (segmentation results) and the algorithm run-time.

Video 4: SPLOM Trade-Off Analysis

PA VisModule SPLOM

NOTE: there will be video materials demonstrating some interactive concepts. If there is no full-screen button on your embedded video, please open it in YouTube or use the zoom-in functionality of your browser

How would you evaluate using the SPLOM for doing a trade-off analysis?

	1	2	3	4	5	
poor	○	○	○	○	○	excellent

Die approbierte gedruckte Originalversion dieser Dissertation ist an der TU Wien Bibliothek verfügbar.
The approved original version of this doctoral thesis is available in print at TU Wien Bibliothek.
TU Bibliothek Your knowledge hub WIEN

Analysis Module - SPLOM Previews and Regio of Interest (ROI) Widget

When hovering over a data point in the SPLOM we provide the user with a preview of the corresponding segmentation result. With +/- on the keyboard the user can slide through the dataset volume. The ROI widget allows defining a region of interest within a dataset volume by spanning a rectangle to bring specific areas in the dataset into focus. The previews of two data points can be compared with each other by fixing one point and hovering over the other. The difference is color-coded.

Video 5: SPLOM Previews and ROI Widget

PA VisModule SPLOM prev

NOTE: there will be video materials demonstrating some interactive concepts. If there is no full-screen button on your embedded video, please open it in YouTube or use the zoom-in functionality of your browser

How useful are the previews of the segmentation results when hovering over a data point?

	1	2	3	4	5	
poor	○	○	○	○	○	excellent

How useful is the ROI widget?

	1	2	3	4	5	
poor	○	○	○	○	○	excellent

Die approbierte gedruckte Originalversion dieser Dissertation ist an der TU Wien Bibliothek verfügbar.
The approved original version of this doctoral thesis is available in print at TU Wien Bibliothek.
TU Bibliothek Your knowledge hub WIEN

How would you evaluate the possiblity to compare two different segmentation result previews (of two different data points) in the SPLOM?

	1	2	3	4	5	
poor	○	○	○	○	○	excellent

Remarks concerning SPLOM previews and the ROI widget (benefits/drawbacks):

In general, how would you evaluate using the SPLOM for selecting different segmentation results according to their individual input and output parameters (e.g., input parameter pow, output parameter porosity)?

	1	2	3	4	5	
poor	○	○	○	○	○	excellent

Remarks concerning SPLOM (benefits/drawbacks):

Die approbierte gedruckte Originalversion dieser Dissertation ist an der TU Wien Bibliothek verfügbar.
The approved original version of this doctoral thesis is available in print at TU Wien Bibliothek.
TU Bibliothek Your knowledge hub WIEN

PorosityAnalyzer - Evaluation Questionnaire

Analysis Module - Comparative Views for Segmentation Pipeline Results

For visual examination of one or more selections we provide 2D slice and 3D views.
In the 2D slice view we show the original CT-data which can be overlaid with the reference segmentation (yellow), the aggregated segmentation results of a selection color-coded in pink (according to the frequency of runs segmenting the same area) and the statistical contours (min, max, median) of the aggregated segmentation results.
In the 3D view the aggregated segmentations results of a selection are color-coded in pink according to the frequency of runs segmenting the same area.
When comparing multiple selections the 2D slices and 3D renderings are placed side-by-side. All views are synchronized to zooming, panning or rotation of the dataset.

Analysis Module - 2D Slice View

Video 5: 2D Slice View

PA VisModule 2DSliceView

NOTE: there will be video materials demonstrating some interactive concepts. If there is no full-screen button on your embedded video, please open it in YouTube or use the zoom-in functionality of your browser

Die approbierte gedruckte Originalversion dieser Dissertation ist an der TU Wien Bibliothek verfügbar.
The approved original version of this doctoral thesis is available in print at TU Wien Bibliothek.
TU Bibliothek Your knowledge hub WIEN

How useful is the 2D slice view for comparing selections of segmentation results?

	1	2	3	4	5	
poor	○	○	○	○	○	excellent

How useful is it to overlay the aggregated segmentation results (pinkish) onto the original CT-data?

	1	2	3	4	5	
poor	○	○	○	○	○	excellent

How useful is it to overlay the reference segmentation (yellow) onto the original CT-data/aggregated segmentation results?

	1	2	3	4	5	
poor	○	○	○	○	○	excellent

How useful is it to overlay the statistical contours of the aggregated segmentation results?

	1	2	3	4	5	
poor	○	○	○	○	○	excellent

Remarks concerning the 2D Slice View (benefits/drawbacks):

Die approbierte gedruckte Originalversion dieser Dissertation ist an der TU Wien Bibliothek verfügbar.
The approved original version of this doctoral thesis is available in print at TU Wien Bibliothek.
TU Bibliothek WIEN Your knowledge hub

Analysis Module - 3D Volume Rendering

Figure 10: 3D Volume Rendering

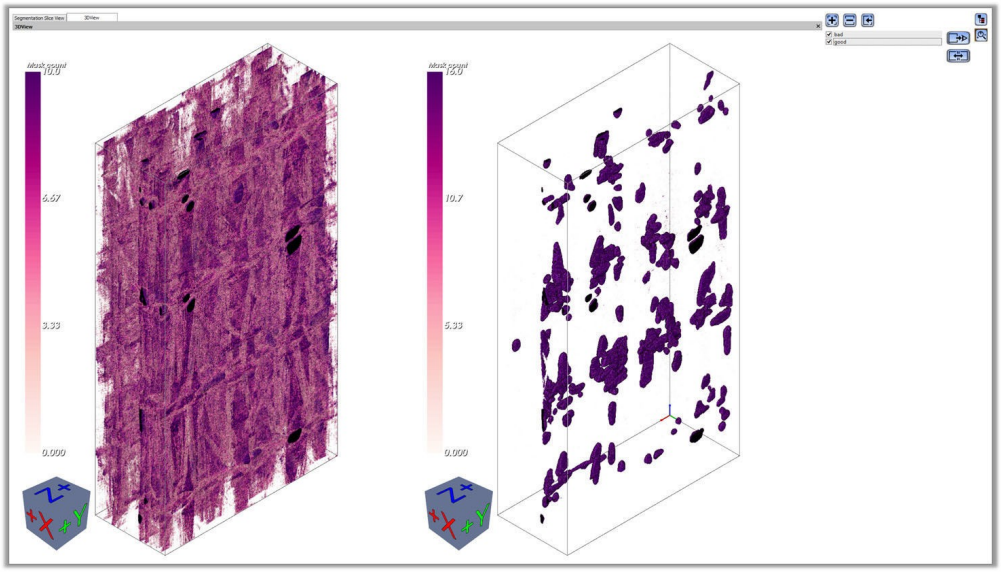

How useful is it to compare different selections of the color-coded aggregated segmentation results in the 3D rendering view?

1 2 3 4 5

poor ○ ○ ○ ○ ○ excellent

Remarks concerning the 3D Volume Rendering (benefits/drawbacks):

Die approbierte gedruckte Originalversion dieser Dissertation ist an der TU Wien Bibliothek verfügbar.
The approved original version of this doctoral thesis is available in print at TU Wien Bibliothek.
TU Bibliothek Your knowledge hub WIEN

PorosityAnalyzer - Evaluation Questionnaire

Thank you!

That's it! We would like to thank you very much for taking your time to participate in this questionnaire!

You will be able to edit your answers for at least one more day.

Have a great day!

Do you have additional comments?

If you have any additional comments, critics, or suggestions, please enter them here

Die approbierte gedruckte Originalversion dieser Dissertation ist an der TU Wien Bibliothek verfügbar.
The approved original version of this doctoral thesis is available in print at TU Wien Bibliothek.

Curriculum Vitae

Contact Information

Name Johannes Weissenböck

Date of birth 08.02.1982

Citizenship Austria

E-mail johannes.weissenboeck@gmail.com

Education

Since 2013 Doctoral program (technical sciences) at the Vienna University of Technology (TU Wien), Institute of Visual Computing and Human-Centered Technology, Research Group Computer Graphics supervised by Ao.Univ.-Prof. Dipl.-Ing. Dr.techn. Eduard Gröller and DI (FH) Dr. Christoph Heinzl (FH OÖ, Campus Wels)

2003 – 2011 Bachelor and Master program in Medical Informatics at the TU Wien:

Master of Science (Dipl.-Ing.) Master thesis at the TU Wien at the Institute of Visual Computing and Human-Centered Technology (Interactive Media Systems Working Group) supervised by Priv.-Doz. Mag. Dr. Hannes Kaufmann and Dipl.-Ing. Michael Mehling: Design eines interaktiven taktilen Shape Displays mittels Schrittmotoren und dem Bowdenzug-Konzept

Bachelor of Science (BSc). Bachelor thesis at Institute of Information Management and Image Processing (Medical University of Vienna) under Ao. Univ.-Prof. Dipl.-Ing. Dr. Ernst Schuster supervised by Dipl.-Ing. Georg Fischer: Detektieren und Verfolgen eines Laserpunktes im Zusammenhang mit Therapien am menschlichen Auge in Echtzeit

01/ 2003 – 09/2003 Military service

1997 – 2002 General qualification for university entrance: Höher Technische Bundeslehranstalt für Automatisierungstechnik und Informatik Neufelden (Abteilung Automatisierungstechnik)

Die approbierte gedruckte Originalversion dieser Dissertation ist an der TU Wien Bibliothek verfügbar.
The approved original version of this doctoral thesis is available in print at TU Wien Bibliothek.
TU WIEN Bibliothek Your knowledge hub

Work Experience

2012 – 2019	Research Associate at the University of Applied Sciences Upper Austria (FH OÖ) – Wels Campus (Research Group Computed Tomography)
2012	IT-based processing of information at KELAG
2008 – 2010	Verkehrsverbund Ost-Region
2007	Marinomed Biotechnologie GmbH
2001; 2004 – 2010	Trainee at Voest Alpine Linz
1999	Trainee at Vogt Electronic Austria
1997 – 1998; 2002	Trainee at Marktgemeinde Ottensheim

Skills

Mother tongue	▪ German
Other language	▪ English
Software design, architecture and modeling	▪ OO-design and programing ▪ Database design using the ER model ▪ Software system modeling using UML/UML2
Programing	▪ C, C++ (Qt, ITK, VTK), CMake, Java, Visual Basic ▪ R, Matlab ▪ Basics in HTML, PHP, CSS, JavaScript
Version control	▪ SVN, Git
Databases / Operating Systems	▪ MySQL, PostgreSQL ▪ Windows, Linux
Micro controller / PCB-prototypes	▪ Firmware programing Arduino (Atmel ATmega2560 micro controller) ▪ PCB design and layout with EAGLE and SMD-PCB-prototype development
CAD	▪ Autodesk AutoCAD and Inventor

Die approbierte gedruckte Originalversion dieser Dissertation ist an der TU Wien Bibliothek verfügbar.
The approved original version of this doctoral thesis is available in print at TU Wien Bibliothek.
TU WIEN Bibliothek Your knowledge hub

List of Publications

Journal Publications (fully reviewed)

B. Fröhler, T. Elberfeld, T. Möller, H.C. Hege, J. Weissenböck, J. De Beenhouwer, J. Sijbers, J. Kastner, C. Heinzl. A Visual Tool for the Analysis of Algorithms for Tomographic Fiber Reconstruction in Materials Science. *Computer Graphics Forum*, Vol. 38, No. 3, pp. 273–283. doi:10.1111/cgf.13688

J. Weissenböck, B. Fröhler, E. Gröller, J. Kastner, C. Heinzl. Dynamic Volume Lines: Visual Comparison of 3D Volumes through Space-filling Curves. *IEEE Transactions on Visualization and Computer Graphics*, Vol. 25, No. 1, pp. 1040-1049, 2019. doi: 10.1109/TVCG.2018.2864510

B. Fröhler, J. Weissenböck, M. Schiwarth, J. Kastner, C. Heinzl. open_iA: A tool for processing and visual analysis of industrial computed tomography datasets. *Journal of Open Source Software*, 4(35), 1185, 2019. doi: 10.21105/joss.01185

A. Bhattacharya, J. Weissenböck, R. Wenger, A. Amirkhanov, J. Kastner, C. Heinzl. Interactive Exploration and Visualization using MetaTracts extracted from Carbon Fiber Reinforced Composites. *IEEE Transactions on Visualization and Computer Graphics*, Vol. 23, No. 8, pp. 1988-2002, 2017. doi: 10.1109/TVCG.2016.2582158

J. Weissenböck, A. Bhattacharya, B. Plank, C. Heinzl, J. Kastner. Visual classification of braided and woven fiber bundles in X-ray computed tomography scanned carbon fiber reinforced polymer specimens. *Case Studies in Nondestructive Testing and Evaluation*, Vol. 6, Part B, pp. 39-46, 2016. doi: 10.1016/j.csndt.2016.05.006

Conference Publications (fully reviewed)

J. Weissenböck, A. Amirkhanov, E. Gröller, J. Kastner, C. Heinzl. PorosityAnalyzer: Visual Analysis and Evaluation of Segmentation Pipelines to Determine the Porosity in Fiber-Reinforced Polymers. *Proceedings of the IEEE Conference on Visual Analytics Science and Technology (VAST)*, pp. 101-110, Baltimore, United States of America, 2016. doi: 10.1109/VAST.2016.7883516

J. Weissenböck, A. Amirkhanov, W. Li, A. Reh, A. Amirkhanov, E. Gröller, J. Kastner, C. Heinzl, FiberScout: An Interactive Tool for Exploring and Analyzing Fiber Reinforced Polymers, *Proceedings of the IEEE Pacific Visualization Symposium (PacificVis)*, pp. 153-160, Yokohama, Japan, 2014. doi: 10.1109/PacificVis.2014.52

Die approbierte gedruckte Originalversion dieser Dissertation ist an der TU Wien Bibliothek verfügbar.
The approved original version of this doctoral thesis is available in print at TU Wien Bibliothek.
TU Bibliothek WIEN Your knowledge hub

Other Publications

L. Da Cunha Melo, B. Fröhler, J. Weissenböck, J. Kastner, C. Heinzl. Multimodal Transfer Functions for Talbot-Lau Grating Interferometry Data. *Proceedings of the International Symposium on Digital Industrial Radiology and Computed Tomography (DIR 2019),* Fürth, Germany, 2019. (Abstract reviewed)

J. Weissenböck, B. Fröhler, E. Gröller, J. Sanctorum, J. De Beenhouwer, J. Sijbers, S. Karunakaran, H. Hoeller, J. Kastner, C. Heinzl. An Interactive Visual Comparison Tool for 3D Volume Datasets represented by Nonlinearly Scaled 1D Line Plots through Space-filling Curves. *Proceedings of the 9th International Conference on Industrial Computed Tomography (iCT 2019)*, Padova, Italy, 2019. (Extended abstract reviewed)

F. Zanini, G. Gerardi, J. Weissenböck, C. Heinzl, J. Kastner, S. Carmignato. Experimental investigation on the accuracy of CT measurement of fiber length in fiber reinforced polymers. *Proceedings of the 9th International Conference on Industrial Computed Tomography (iCT 2019)*, Padova, Italy, 2019. (Extended abstract reviewed)

B. Fröhler, L. da Cunha Melo, J. Weissenböck, J. Kastner, T. Möller, H.-C. Hege, E. Gröller, J. Sanctorum, J. Sijbers, C. Heinzl. Tools for the Analysis of Datasets from X-Ray Computed Tomography based on Talbot-Lau Grating Interferometry. *Proceedings of the 9th International Conference on Industrial Computed Tomography (iCT 2019)*, Padova, Italy, 2019. (Extended abstract reviewed)

J. Sanctorum, J. De Beenhouwer, J. Weissenböck, C. Heinzl, J. Sijbers. Simulated grating-based x-ray phase contrast images of CFRP-like objects. *Proceedings of the 9th International Conference on Industrial Computed Tomography (iCT 2019)*, Padova, Italy, 2019. (Extended abstract reviewed)

B. Fröhler, T. Möller, J. Weissenböck, H.-C. Hege, J. Kastner, C. Heinzl. Exploring Uncertainty in Image Segmentation Ensembles. *Proceedings of the 20th EG/VGTC Conference on Visualization (EuroVis 2018, Poster)*, Brno, Czech Republic, 2018. doi:10.2312/eurp.20181123 (Abstract reviewed)

M. Schiwarth, J. Weissenböck, B. Plank, B. Fröhler, C. Heinzl, J. Kastner. Visual Analysis of Void and Reinforcement Characteristics in X-Ray Computed Tomography Dataset Series of Fiber-Reinforced Polymers. *Proceedings of 13th International Conference on Textile Composites (TexComp-13)*, Milan, Italy, 2018. doi:10.1088/1757-899X/406/1/012014 (Abstract reviewed)

B. Fröhler, C. Heinzl, J. Weissenböck, A. Amirkhanov, M. Arikan, J. Kastner. open_iA: A Framework for Analyzing Industrial Computed Tomography Data. *Proceedings of the 12th European Conference on Non-Destructive Testing (ECNDT 2018)*, Gothenburg, Sweden, 2018. (Abstract reviewed)

J. Weissenböck, M. Arikan, D. Salaberger, J. Kastner, J. Beenhouwer, J. Sijbers, S. Rauchenzauner, T. Raab-Wernig, E. Gröller, C. Heinzl. Comparative Visualization of Orientation Tensors in Fiber-Reinforced Polymers. *Proceedings of the 8th International Conference on Industrial Computed Tomography (iCT 2018)*, Wels, Austria, 2018. (Extended abstract reviewed)

Die approbierte gedruckte Originalversion dieser Dissertation ist an der TU Wien Bibliothek verfügbar.
The approved original version of this doctoral thesis is available in print at TU Wien Bibliothek.
TU WIEN Bibliothek Your knowledge hub

J. Weissenböck, S. Senck, B. Plank, C. Heinzl, J. Kastner. Porosity Evaluation of Carbon Fiber-Reinforced Polymers with Porosity Analyzer. *Proceedings of the 3rd International Conference on Tomography of Materials and Structures (Poster)*, Lund, Sweden, 2017. (Extended abstract reviewed)

C. Heinzl, J. Weissenböck, A. Reh, J. Kastner, T. Dierig, T. Günther, D. Kiefel, R. Stössel. Software tools for robust extraction, analysis and visualization of porosities in XCT scans of fiber-reinforced polymers. *Proceedings 6th International symposium for NDT in Aerospace (AeroNDT)*, Madrid, Spain, 2014. (Abstract reviewed)

J. Weissenböck, A. Reh, D. Salaberger, C. Heinzl, J. Kastner. Advanced Visualization and Exploration Techniques for Fiber Reinforced Polymers. *Proceedings of 11th European Conference on Non-Destructive Testing (ECNDT 2014)*, Prague, Czech Republic, 2014. (Abstract reviewed)

J. Weissenböck, M. Arikan, D. Salaberger, C. Heinzl, J. Kastner. Quantitative Measurement and Visualization of Fiber Orientation and Length Distribution of Glass-, Carbon- and Cellulose Fiber Reinforced Polymers using X-Ray Computed Tomography. *Proceedings of the German Society for Non-Destructive Testing Conference (DGZFP)*, Potsdam, Germany, 2014. (Abstract reviewed)

Die approbierte gedruckte Originalversion dieser Dissertation ist an der TU Wien Bibliothek verfügbar.
The approved original version of this doctoral thesis is available in print at TU Wien Bibliothek.
TU Bibliothek Your knowledge hub WIEN